Structural modification of proteins and peptides for the creation of nanomaterials

Megan Garvey

Under the joint supervision of:

Professor John Carver
Executive Deputy Dean
School of Chemistry & Physics
The University of Adelaide
Adelaide, South Australia 5005, AUSTRALIA

and

Professor Juliet A. Gerrard
School of Biological Sciences
The University of Canterbury
Christchurch, NEW ZEALAND

A dissertation submitted in January 2009 to The University of Adelaide, in collaboration with The University of Canterbury, for the degree of Doctor of Philosophy.

THE UNIVERSITY
OF ADELAIDE
AUSTRALIA

UC
UNIVERSITY OF
CANTERBURY
Te Whare Wānanga o Waitaha
CHRISTCHURCH NEW ZEALAND

Table of Contents

Table of Figures

Table of Tables

Abbreviations

AFM	Atomic force microscopy
Cryo-EM	Cryo-electron microscopy
DMSO	Dimethylsulphoxide
DTT	Dithiothreitol
EDTA	Ethylenediaminetetraacetic acid
FTIR	Fourier transform infrared spectroscopy
GdnHCl	Guanidine hydrochloride
HMW	High molecular weight
HOPG	Highly ordered pyrolytic graphite
NaD	*Nicotinia alata* defensin
NMR	Nuclear magnetic resonance
QCM-D	Quartz crystal microgravimetry with dissipation
RsAFP	*Raphanus sativus* antifungal protein/peptide
RCM	Reduced and carboxymethylated
sHSP	Small heat shock protein
SDS-PAGE	Sodium dodecyl sulphate-polyacrylamide gel electrophoresis
ThT	Thioflavin T
TEM	Transmission electron microscopy
TFE	Trifluoroethanol
XPS	X-ray photoelectron spectroscopy

Synopsis

Amyloid fibrils are highly ordered β-sheet structures that are formed from a variety of proteins *in vivo*, where they may have biological roles or, more commonly, are found associated with a broad range of diseases (known as amyloidoses). Due to the role of amyloid fibrils in disease and their potential as bionanomaterials, formation of amyloid and amyloid-like fibrils *in vitro* are exciting areas of research activity. This thesis explores the formation and characterisation of nanofibre structures, including amyloid and amyloid-like fibrils, from diverse peptides and proteins.

The growing interest in protein nanofibres in the bionanotechnology industry has led to research into new nanofibre forming target peptides and proteins. In this thesis, *Raphanus sativus* antifungal peptide 19mer (RsAFP-19) and a mutant of β2-microglobulin where the 3rd arginine was replaced with an alanine (R3A β2-microglobulin), were examined for their amyloiogenicity and nanofibre-forming propensity. Generation of nanofibre structures was successful for both, and the characteristics of formation, fibril structure and morphology were explored *via* thioflavin t binding (ThT), transmission electron microscopy (TEM), atomic force microscopy (AFM) and X-ray fibre diffraction. Nanofibre formation was also further characterised for mammalian lens crystallin proteins. Their ability to form protein nanofibres from semi-pure and crude protein mixtures was established, and the resulting fibrils characterised, including for their amyloid-like characteristics. This work demonstrates the ability of crystallin proteins to form inexpensive base materials for use in the bionanotechnology industry.

Inhibition of amyloid fibril formation is an area of current research activity for therapeutic purposes (against amyloidoses). α-Crystallin is a well-known molecular chaperone which traps intermediately structured target proteins, preventing them from both amorphous and ordered (amyloid fibril) aggregation. Like other crystallin proteins, α-crystallin can itself form amyloid fibrils under mildly denaturing conditions. The chaperone activity of αT- and αB-crystallin, in native, amorphously aggregated and fibrillar forms were assessed. Amyloid fibrils

and amorphous aggregates derived from αT and αB-crystallin acted as chaperones, although with modified activity to their native (non-fibrillar) structures. αB-Crystallin fibrils displayed enhanced chaperone activity, compared to native αB-crystallin. The chaperone activity of αB-crystallin was also assessed after its immobilisation onto solid surfaces. Protein immobilisation of the chaperone αB-crystallin was achieved using plasma generated aldehyde polymerisation and Schiff-based covalent bonding of the proteins. Immobilisation was characterised using X-ray photoelectron spectroscopy, AFM and quartz crystal micrography. Immobilised αB-crystallin was shown to act 100-fold to 5000-fold more effectively as a chaperone than native solution αB-crystallin (dependent upon target protein and the type of stress it was exposed to). This research has established that αT- and αB-crystallin can retain chaperone activity, or may even show enhanced activity, under conditions of extreme structural perturbation.

This thesis explores both the induction and inhibition of amyloid fibril, amyloid-like fibril and nanofibre formation, using a range of peptides and proteins, both pure and in crude mixtures. These protein nanofibre structures were characterised, to establish potential future use in bionanotechnology, kinetics and activity of amyloid and amyloid-like fibril formation and assessment of amyloid fibril inhibitors. This work further deliniated aspects of αT- and αB-crystallin chaperone ability, highlighting these proteins' ability to act as effective chaperones under a broad range of conditions.

Declaration

This work contains no material which has been accepted for the award of any other degree or diploma in any university or other tertiary institution and, to the best of my knowledge and belief, contains no material previously published or written by another person, except where due reference has been made in the text.

I give consent to this copy of my thesis, when deposited in the University Library, being made available for loan and photocopying, subject to current copyright laws (Copyright Act, 1968).

Megan Garvey

Adelaide
2009

Acknowledgements

Over the course of this PhD I have had help, advice, assistance and encouragement from many wonderful people. I would primarily like to thank my two supervisors, John Carver and Juliet Gerrard, who have been fantastic in their support, guidance and leadership. John and Juliet provided intresting and successful projects, insight when I was lost, encouragement to follow my own ideas, understanding when things went wrong and good wine with loud laughter at my parties. They have my heartfelt gratitude.

I would also like to thank numerous people who I worked under or with, including: Hans Griesser, Stefani Griesser and Benjamin Thierry, who's assistance and guidance made the immobilised chaperone project very successful and equally fun; Sally Gras who introduced me to XRD and was a joy to work with; Heath Ecroyd and Sarah Meehan, who both taught me so much, especially the glories of α-crystallin and the beauty of amyloid; Grant Pearce and Suzie Meade who provided knowledge and insight into amyloid fibrils and great company for lunch; Matt Nussio, Joe Shapter, Paula Brooksby, Leanne Britcher, Lyn Waterhouse, Daniel Bilusich, Phil Clements and Manfred Ingerfeld, who all provided much needed expertise in a range of highly skilled fields.

I have had the privilege of working as part of two great research groups over the past few years. I'd like to thank everyone who was part of Lab 7 or The Purple Bubble in that time. In particular (other than those already mentioned): Chris Brockwell who kept things real; David Thorn who is my angel; Scott Buckley for all the walks home; Tom Kouldelka for mass spec and tea breaks; Danielle Williams for making me smile so often; Yanqin Liu for so many lovely meals; Francis Dehle and Sean Hudson for being such good fun in very different ways; Shiva Rao for our fibril work; Sean Devenish and Ren Dobson for providing entertainment and advice; and Jackie Healy for looking after me in the lab.

Much of the last few years have been spent thinking and talking about work even when I shouldn't. For their understanding in such matters I'd like to thank all my friends, particularly: Christabel Hough who insipired me; Keina Tiaon for those Melbourne visits; Owen Powell who is always there for me; Thivanka Dedigama, Cat Hyndman, Gajan Tyagarajah and Kim Hynes for drinks and tasty brunches; Mike Maclean and the CMC for scotch and understanding; Kate Langdon for Grace-ful moments; Bruce May for everything except the stalking; Jess 'Sugar' Young for many fanciful tales; Simone Haigh and her ambulances; Steven Poon for all those small joys; Jens Kroeske for all the music and sunny days; Joel Rathus for ukeles and debates; Amy O'Loughlin for the laughter and the puppies; Justin Williams for tea-chats and understanding; Yallana Burgess who makes life shine; Simon Grealy for some champagne moments; and Markus Pietsch with whom each day is brighter and happier than the last.

Finally, I could never have done anything like this if not for my family: my brothers and their wives (Adam, Amor, Nathan and Tara) who are all wonderful and inspirational people; but especially my parents, Ian and Janet Garvey – their love, friendship, advice and support has been strong and constant, through this PhD and for all of my life. I am grateful in so many ways to them all and proud to be part of their family and able to share their lives.

CHAPTER 1

INTRODUCTION AND LITERATURE REVIEW

Protein unfolding and aggregation, particularly into the aggregated form known as amyloid fibrils, are areas of very active research interest. This thesis explores the formation and characterisation of amyloid fibril and other nanofibre structures formed from a variety of peptides and proteins. Further, it explores how such protein aggregation can be inhibited, *via* the action of α-crystallin, a molecular chaperone protein. In this chapter, the concepts of protein aggregation, amyloid and amyloid-like fibrils and the lens crystallin protein family will be introduced and the relevant literature reviewed.

1.1 Protein folding

Protein folding is the ability of polypeptide chains to fold into specific and complex structures. Successful protein folding occurs when the polypeptide chain extruded by the ribosome undergoes a rapid, energetically favourable transition to the designated native state. This process, known as on-pathway folding (Figure 1.1, light grey region), is now thought to rely upon a small number of initial interactions between 'key residues' of the polypeptide chain, and to involve the presence of intermediate structures (Dobson, C. M. 2003; Jahn, T. R. and Radford, S. E. 2008). It may also involve the assistance of other proteins, such as molecular chaperones, to guide the structure to the correct folding end-product (native state) (Hartl, F. U. and Hayer-Hartl, M. 2002). Through a variety of mechanisms, discussed more fully below, proteins enter an off-pathway folding. This occurs either during the folding process or through fluctuations in their intermediate or native states. Protein off-pathway folding (Figure 1.1, dark grey region) may lead to a number of misfolded protein structures, including amorphous aggregates, oligomers, ordered aggregates and amyloid fibrils (Gsponer, J. and Vendruscolo, M. 2006; Jahn, T. R. and Radford, S. E. 2008). Off-pathway protein folding may be inhibited by the action of aforementioned molecular chaperones, dealt with *via* protein quality control mechanisms or, more rarely, may lead to a wide range of diseases known collectively as protein misfolding disorders (Thomas, P. J. *et al.* 1995).

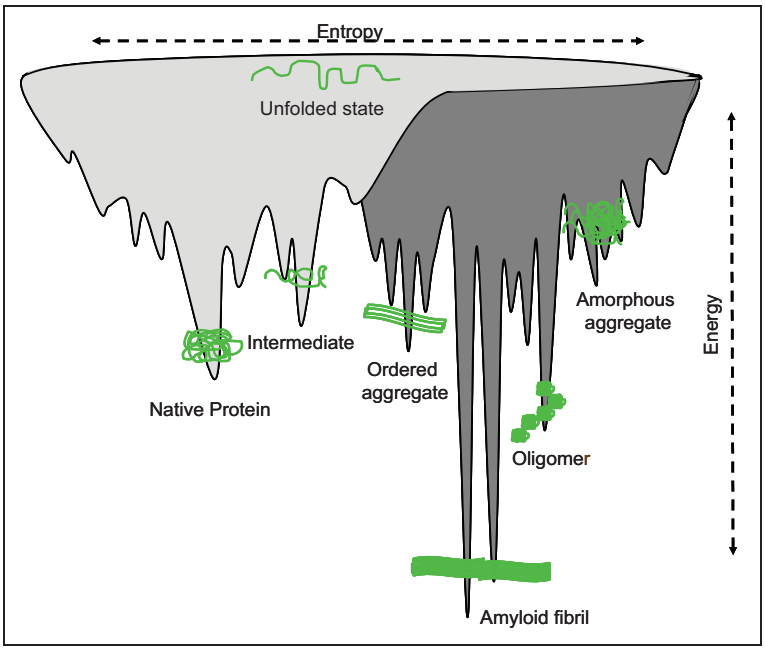

Figure 1.1: Energy landscape of protein folding (adapted from Jahn, T. R. and Radford, S. E. 2008)[1] showing the on- and off-pathway folding (light and dark grey, respectively) and the conformational states common to each. The ruggedness of the energy landscape simulates the areas in which protein undergoing folding must cross energetic barriers on the pathway to a stable folded state.

1.2 Protein aggregation

Proteins are one of the fundamental units of all living tissue. The human body contains more than 50,000 different proteins, which together instigate and regulate all our chemical processes (Chiti, F. and Dobson, C. M. 2006). The maintenance of proteins in their optimal functional state is thus a challenge of primary importance for all cells. Many factors affect protein folding and the stability of the native state. Proteins are specifically engineered by the body to fold to a specific structure and to remain stable and perform their individual functions even under highly crowded cellular conditions (Anfinsen, C. B. 1973; Dobson, C. M. 2003). It can take only slight disturbances to the normal state of homoeostasis to upset the stable native state of many proteins and lead to formation of intermediate species which populate the off-pathway folding (Gsponer, J. and Vendruscolo, M. 2006). Figure 1.2 outlines the normal on- and off-pathway protein folding, as well as indicating some of the factors which may lead to destabilisation of a protein's native structure and areas in which intervention to protect against protein misfolding can occur.

[1] Reprinted with permission from Elsevier.

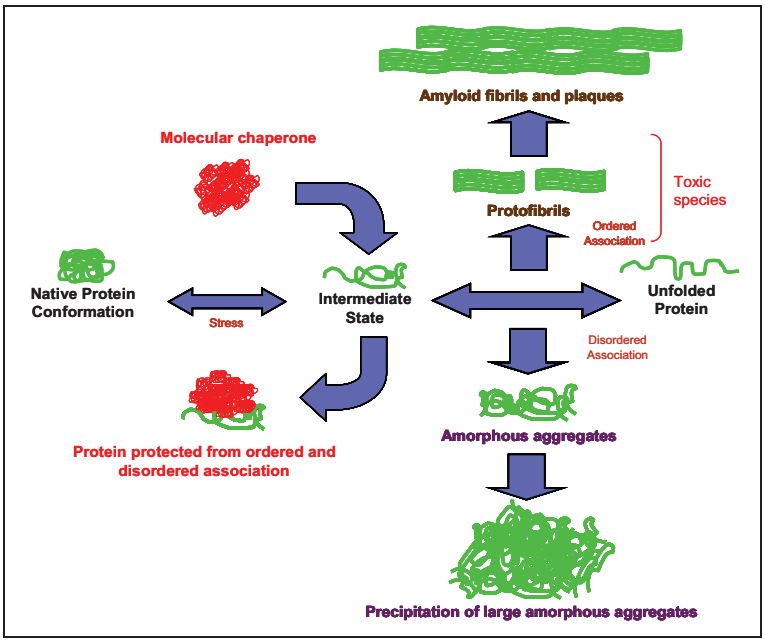

Figure 1.2: Diagram of protein folding and off-pathway folding, highlighting causes of destabilisation and points of protective intervention (adapted from Ecroyd, H. and Carver, J. A. 2008a).

Protein misfolding (Figure 1.2) leads to two major forms of aggregates: disordered aggregation which leads to the formation of amorphous aggregates, and a much more rigid, ordered form known as amyloid fibrillar aggregation (Ecroyd, H. and Carver, J. A. 2008c). The difference in the formation, characteristics and effects of these aggregation types has significant impact on the roles they play *in vivo* in a range of disease processes. Aggregation of proteins can lead to damage or disease in a variety of ways. These include the loss of protein function (*via* damage to the active site, prevention of the protein reaching its optimal environmental position, or blocking biologically important interactions with other proteins), the formation of toxic species, or the formation of large aggregates (either amorphous or, more frequently, containing amyloid fibrils) (Barral, J. M. *et al.* 2004). This third mechanism of protein misfolding disease, the formation of large protein aggregates, is of primary importance to this thesis and is discussed in detail below (§ 1.2.1 and § 1.2.2).

1.2.1 Amorphous protein aggregation

Disordered protein aggregation is usually termed amorphous aggregation, after the irregular non-crystalline nature of the protein aggregates produced (Ecroyd, H. and Carver, J. A. 2008c). Amorphous aggregation occurs as a result of destabilisation of the basic structure of the protein. This may occur at many stages

of the protein's lifespan, from protein synthesis, where intrinsic destabilisation arises due to mutation or problems with necessary interactions between the key folding residues, through to perturbation of the folded native protein due to the effects of pH, temperature, chemical influences and post-translational modifications (Dobson, C. M. 2006).

Once proteins become destabilised, they can follow the protein off-pathway folding (§ 1.1). Protein destabilisation leads to the externalisation of normally hidden regions of the protein, such as hydrophobic residues and regions of the polypeptide backbone. These partially folded or unfolded structures may then associate together through hydrophobic self association and, once large enough, precipitate out of solution as aggregates of varied size and structure (hence their amorphous state) (Hartl, F. U. and Hayer-Hartl, M. 2002). These species can be removed prior to aggregation (i.e. when misfolded and still in cellular or extracellular circulation) *via* tagging with ubiquitin which marks them for destruction by proteasomal mechanisms (McClellan, A. J. *et al.* 2005).

1.2.1.1 Amorphous aggregation related disease processes

Amorphous aggregation has been associated with a number of mammalian and human disease processes. These disorders arise when aggregation occurs on such a scale that it prevents the normal function of that protein (Barral, J. M. *et al.* 2004) or there is a failure in the breakdown of amorphous aggregates (Ecroyd, H. and Carver, J. A. 2008a). One important amorphous aggregation disorder is cataract[2]. Cataract affects an estimated 8 million people, making it the most common ocular disease worldwide (Lucas, R. M. *et al.* 2008; WHO 2001). Cataract is characterised by a clouding of the eye lens, as shown in Figure 1.3, a result of protein aggregation after destabilisation and misfolding. Refraction of light is highly dependent on the supramolecular organisation of a family of proteins known as the crystallins, which are present in the lens in high concentration. These proteins are associated with cataract, due to their presence within the aggregates characteristically found with the disease (Slingsby, C. and Clout, N. J. 1999). Furthermore, a number of forms of cataract have been

[2] Specific strains of cataract have been recognised which are associated with fibril formation or crystallisation, only those forms associated with amorphous aggregation will be discussed here.

discovered which are linked to genetic mutation of one or more crystallin proteins (Bloemendal, H. *et al.* 2004). The role of the crystallin proteins in cataract is complex and will be discussed in greater detail below (§ 1.3).

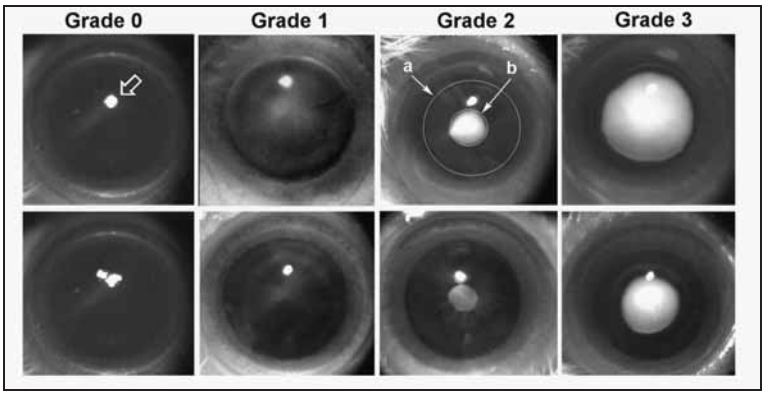

Figure 1.3: Cataract grades for selenium-induced murine cataract, containing aggregated crystallin proteins, demonstrating increasing opacity as protein precipitation occurs (open arrow shows the slit lamp flash, a: border of lens area, and b: nuclear opacity border) (Muranov, K. *et al.* 2004)[3].

1.2.2 Ordered protein aggregation (amyloid fibril formation)

In ordered protein misfolding the native protein becomes rearranged into highly ordered β-sheet nanofibre structures known as amyloid fibrils (Uversky, V. N. and Fink, A. L. 2004). Amyloid fibrils are associated with cellular damage in the tissues they are formed in, due to the formation of toxic precursors and the deposition of large conglomerates composed primarily of amyloid fibrils, known as amyloid plaques (Dobson, C. M. 2006). Amyloid fibrils are thought to be a structure accessible to all proteins, and have been formed *in vitro* from many proteins not currently associated with disease (Chiti, F. and Dobson, C. M. 2006). The formation, characteristics and effects of amyloid fibrils are of intense research interest, due to both their role in a wide range of disease states and their possible nanotechnological uses (Waterhouse, S. H. and Gerrard, J. A. 2004; Gras, S. L. 2007; Hamley, I. W. 2007; Cherny, I. and Gazit, E. 2008). In addition, a number of biologically active amyloid species (known as amyloidin, Table 1.1) have recently been shown to exist, including curlin protein amyloid in *Escherichia coli* which assist in surface binding, and Pmel 17 protein amyloid in melanosomes in humans (and other species) which provide surfaces that enable small molecule conversion into melanin (Chapman, M. R. *et al.* 2002; Fowler, D. M. *et al.* 2006).

[3] Reprinted with permission from Springer Science + Business Media.

Table 1.1: Recognised forms of amyloidin: amyloid fibril and amyloid-like fibril structures with specific biological (non-pathological) functions (adapted from Chiti, F. and Dobson, C. M. 2006; Gras, S. L. 2007).

Protein	Organism/s	Function
Amyloid fibrils		
Curlin	*Escherichia coli*	Component of bacterial biofilm
Pmel17	Eukaryotes	Surface for melanin granule formation
Amyloid-like fibrils		
Chaplins	*Streptomyces coelicolor*	Lower water surface tension (hyphae development)
Hydrophobin EAS	*Neurospora crassa*	As above
Chorion proteins	*Bombyx mori*	Protect the oocyte
Spidroin	*Nephila edulis*	Form silk fibres
Prions: Ure2p and Sup35p	*Saccharomyces cerevisiae*	Promote nitrogen uptake and confer new phenotypes
Prion: HET-s	*Podospora anserina*	Trigger cell death
Prion: Neuronal CPEB	*Aplisia californica*	Promote synaptic maintenance

1.2.2.1 Disease relationship

The amyloid hypothesis states that amyloid fibril formation is the causative factor of amyloid disease, due to its situation within this range of "distinct maladies associated with the aberrant self assembly of any one of twenty non-homologous human proteins" (Kelly, J. W. 2002). Amyloid deposits[4], have been found in at least 40 disease processes, involving 20 different globular proteins, as specified in Table 1.2 (Uversky, V. N. and Fink, A. L. 2004; Chiti, F. and Dobson, C. M. 2006). The term amyloid-like fibril has been used to define those structures which contain most characteristics of amyloid fibrils, but where no known link with disease has been observed (Gras, S. L. 2007).

Amyloid deposit composition from *ex vivo* sources, as well as amyloid and amyloid-like fibril formation *in vitro* and in animal models has been extensively studied. This is particularly true for disease related proteins and peptides, in an attempt to increase understanding of the disease processes and to find areas for therapeutic intervention. Such high-interest peptides and proteins include those responsible for Alzheimer's disease (Nordstedt, C. *et al.* 1994; Tjernberg, L. O. *et al.* 1999), type II diabetes (Munishkina, L. A. and Fink, A. L. 2007), dialysis-related amyloidosis (Esposito, G. *et al.* 2000; Jahn, T. R. *et al.* 2006), Parkinson's disease (Rekas, A. *et al.* 2004) and systemic amyloidoses (Sunde, M. *et al.* 1997; Serpell, L. C. *et al.* 2000). The *in vitro* studies have established that while the

[4] Used in this thesis to include both extracellular amyloid plaques and intracellular inclusions with amyloid-like characteristics.

Table 1.2: Amyloid diseases and associated proteins and peptides (adapted from Chiti, F. and Dobson, C. M. 2006).

NOTE:
This table is included on page 8
of the print copy of the thesis held in
the University of Adelaide Library.

* May be classified as non-amyloid protein misfolding disorders by some researchers (Westermark, P. *et al.* 2007).

** with PolyQ expansion

fully formed amyloid fibril is biologically inert, the early species of many amyloid fibril structures have toxicity and can lead to cellular oxidation, degradation and death (Bucciantini, M. *et al.* 2002). However, the mechanism/s by which this occurs is still unclear (Barral, J. M. *et al.* 2004; Ecroyd, H. and Carver, J. A. 2008c) as is the role of such toxicity in various amyloid diseases (Kelly, J. W. 2002; Dobson, C. M. 2006). The stages of amyloid formation are more fully delineated below (§ 1.2.2.3).

The amyloid hypothesis was developed due firstly to the presence of amyloid fibrils and deposits within multiple disease processes, but also to the recognition of characteristic structural features of amyloid fibrils derived from varied source proteins. All amyloid fibrils contain a highly ordered β-sheeted structure, a feature that is constant, despite fibrils being formed from various different native proteins and peptides (Rochet, J. C. and Lansbury, P. T., Jr. 2000). As well as being highly ordered, amyloid and amyloid-like fibrils are extremely thermodynamically stable and exhibit resistance to proteolysis, dehydration and extremes of pH, temperature or pressure (Dobson, C. M. 2003; Gsponer, J. and Vendruscolo, M. 2006; Gras, S. L. 2007).

The kinetic and thermodynamic stability, together with the protease resistance of amyloid fibrils contribute to the occurrence of amyloid-related diseases (Dobson, C. M. 2003). Protease resistance confers immunity to normal protein aggregate removal mechanisms (i.e. the ubiquitin proteosomal degradation systems), leading to the formation of deposits of aggregated proteins (Nordstedt, C. *et al.* 1994). In amyloid disease states, these deposits, known as amyloid plaques, are used as diagnostic of individual amyloid diseases (often post-mortem), dependent on the tissues involved and the protein composition of the plaques (Bely, M. and Apathy, A. 2000). Most amyloid plaques contain not just the amyloid-forming protein but also a wide range of co-localised proteins. In fact, nearly 500 different proteins have been found present in the amyloid plaques of Alzheimer's Disease (Liao, L. *et al.* 2004). Certain factors are now acknowledged to be characteristically found in all amyloid deposits, including glycosaminoglycans and serum amyloid P (Westermark, P. *et al.* 2007); it has been argued that these are related to the formation and stability of the deposits (Jahn, T. R. *et al.* 2008). Chaperone

proteins are also commonly seen associated with amyloid deposits, although whether their role is protective or causes aggravation of the disease is still under debate (Barral, J. M. *et al.* 2004). The presence of molecular chaperone proteins within amyloid plaques is taken as an indication that regulation of protein misfolding is still undertaken by the body, even when normal (degradation) mechanisms have failed (Sherman, M. Y. and Goldberg, A. L. 2001).

1.2.2.1.1 Dialysis-related amyloidosis

Dialysis-related amyloidosis (DRA) is an amyloid disease of particular relevance to research undertaken in this thesis. DRA is a treatment-caused (iatrogenic) disease that occurs as a direct result of long term haemodialysis, a treatment used in severe kidney failure. The amyloid deposits within DRA are found in the musculoskeletal system (Trinh, C. H. *et al.* 2002). These deposits are characterised by the presence of β2-microglobulin, a protein which plays a role in the human leukocyte antigen (HLA) complex in the immune system (Bellotti, V. *et al.* 1998). β2-Microglobulin levels are significantly raised in patients with renal failure and by up to fifty-fold in those undergoing haemodialysis treatment (Stone, M. J. 1990; Farrell, J. and Bastani, B. 1997). β2-Microglobulin has been demonstrated to form into amyloid fibrils *in vitro*, from both recombinant protein and using *ex vivo* fibril seeds isolated from DRA sufferers (Naiki, H. *et al.* 1997). β2-Microglobulin nanofibre formation forms the basis of § 4, and detailed information about the formation and characteristics, including the amyloid-like features, of β2-microglobulin nanofibres formed is provided there.

1.2.2.2 Amyloid and amyloid-like fibril structure

Amyloid and amyloid-like fibrils all contain similar characteristics, regardless of which native protein they are derived from (Hoang, T. X. *et al.* 2006). They are typically long, filament-like structures, which are unbranched, 6 to 12 nm in diameter (larger for more complex multi-fibril structures), may extend up to microns in length, are resistant to proteolysis and feature a characteristic 'cross-β' fibril core (Serpell, L. C. *et al.* 2000; Carulla, N. *et al.* 2005; Nelson, R. *et al* 2005; Knowles, T. P. *et al.* 2007). Aspects of fibril structure have been investigated by a variety of techniques over the last decades, including dye binding, microscopy, spectroscopy and X-ray fibre diffraction (§ 3.3, Nielsen, L.

et al. 2001). At present, many of these techniques are limited in the samples they are able to analyse, thus resulting in much research to date being conducted on small nanofibre forming peptides (particularly NMR and X-ray based techniques), with the findings extrapolated to encompass fibril formation of entire proteins. As a result, there is a process of continual refinement of nanofibre investigative tools, allowing us to explore and understand more about the structure of all amyloid and amyloid-like fibrils, particularly those of relevance to disease (Chiti, F. and Dobson, C. M. 2006).

The intrinsic structure of all amyloid and amyloid-like fibrils has two major features: β-strands which lie perpendicular to the fibril axis, formed by polypeptide backbones folding upon themselves at a distance of 4.7 – 4.8 Å; and β-sheet filaments, running parallel to the fibril axis, which are composed of interweaving β-strands at a distance of 8 – 10 Å apart (dependent upon protofilament number) (Sunde, M. *et al.* 1997; Serpell, L. C. *et al.* 2000; Chiti, F. and Dobson, C. M. 2006). Each amyloid or amyloid-like fibril contains a number of protofilaments, generally between 4 and 6, which are wound together to form the complete fibril assembly (Lashuel, H. A. *et al.* 2000; Serpell, L. C. *et al.* 2000; Jimenez, J. L. *et al.* 2002). Figure 1.4 demonstrates one model, based on an amyloid fibril forming peptide, of how the β-strand, β-sheet and protofilament structures associate to form nanofibres.

Some regions, particularly of longer proteins, are not incorporated into the β-strands. These may be flexible loops and turns (unstructured regions of the protein) which are so securely associated with the fibrillar assemblies that they are resistant to proteolysis. Such regions are deemed to be part of the fibrillar core, or the essential β-sheet structure of the fibril (Fandrich, M. and Dobson, C. M. 2002). Others regions of the native protein may remain un-associated with the fibril structure, being external to the β-strands and β-sheets and thus able to be proteolytically degraded (Zurdo, J. *et al.* 2001). The position of the side chains and any amino acids not incorporated into the β-strands vary depending on the native protein structure, but it appears likely that these may lie either externally or in the internal cavity of the fibril (Petkova, A. T. 2002; Tycko, R. 2006).

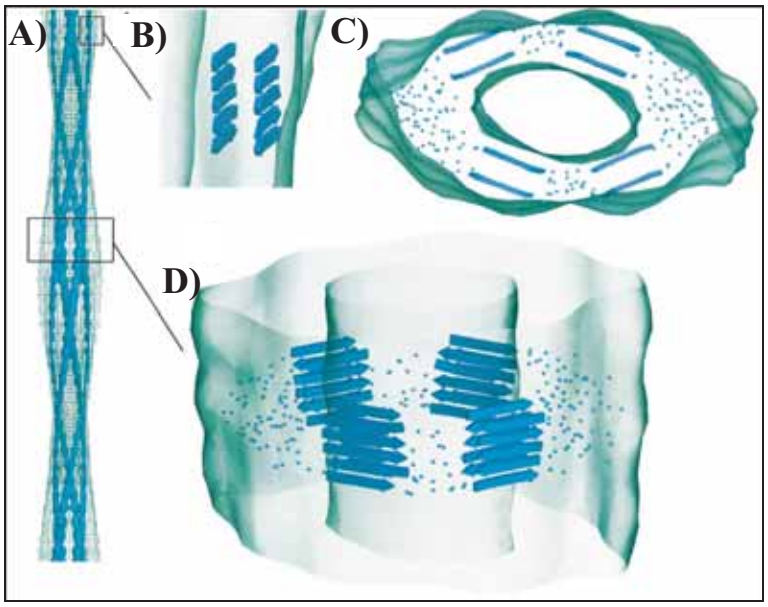

Figure 1.4: Diagram of the packing of an amyloid fibril structure, based on research from an SH3 domain amyloid fibril by Jiménez and co-workers (1999)[5] showing: A) the complete fibril with protofilaments in solid blue; B) a single protofilament revealing β-strands; with C and D) sections of complete fibril from top and side views (respectively) showing how β-sheets are situated around the central core of the fibril.

The length of the native protein chain, or of those sections of native protein not incorporated into the fibrillar core, has been demonstrated to play a role in the stiffness of the nanofibre produced (Gras, S. L. 2007; Knowles, T. P. *et al.* 2007). Knowles, Fitzpatrick *et al.* (2007) established that while the majority of amyloid and amyloid-like fibrils have a single relatively rigid stabilised structure, a number of amyloid fibril systems characteristically show more flexibility. The latter structures appear to be stabilised by different types of intermolecular interactions than the more commonly observed rigid (straight) amyloid or amyloid-like fibrils. These differences may suggest that the flexible (curly) amyloid or amyloid-like fibrillar structures are actually a late-stage protofibrillar structure, to which they correlate morphologically, rather than complete nanofibres. Further support for this hypothesis is provided by FTIR differences observed between straight and curly fibrils derived (*via* different formation conditions) from β2-microglobulin (Jahn, T. R. *et al.* 2008). The different morphological properties of amyloid and amyloid-like fibrils, while of uncertain disease relevance, has a large role to play in the nanobiotechnological potential of these structures (Gras, S. L. 2007), as is discussed below (§ 1.2.2.4).

[5] Reprinted with permission from the National Academy of Sciences, USA.

1.2.2.3 Amyloid fibril formation

Formation of amyloid fibrils involves a significant rearrangement of native protein structure. For this to occur, ordered proteins must undergo a structural destabilisation, similar to that for disordered aggregation (Dobson, C. M. 2002). This may be triggered *in vivo* or *in vitro* by physiological stress factors such as altered pH, increased temperature and breakage of disulfide linkages, or by alterations such as truncation, destabilising mutations or post-translational modifications (Dobson, C. M. 2006). Irrespective of the cause, the destabilisation leads to the partial unfolding of the protein or, in the case of natively unfolded proteins, partial folding of the protein.

For amyloid or amyloid-like fibrils to be formed, protein misfolding must allow for the production of stable intermediate structures. These structures interact in a specific manner, in contrast to amorphous aggregation, leading to the stacking of the amino acid backbones of the proteins into β-sheet structures (Uversky, V. N. and Fink, A. L. 2004). Even in cases where the protein exists natively unfolded, the production of a stable intermediate structure is still thought to be necessary for the formation of these nanofibres (Ecroyd, H. *et al.* 2008). This stable intermediate forms the basis of the fibril nucleus, or seed fibril. Fibril formation *in vitro* can be instigated or increased (both in rate and total yield) by the addition of amyloid fibril seeds from the same, or an extremely highly homologous, protein or peptide (O'nuallain, B. *et al.* 2004; Lundmark, K. *et al.* 2005; Ohhashi, Y. *et al.* 2005; Gsponer, J. and Vendruscolo, M. 2006). Figure 1.5 depicts the stages of amyloid formation.

1.2.2.4 Nanobiotechnological potential

Amyloid and amyloid-like fibrils have recently generated interest in a new field, that of nanotechnology. Amyloid-like fibrils have a number of desirable characteristics that could make them of great use in this growing field, including their ability to self assemble, similarity in size to currently used nanofibres (such as carbon nanotubes), access to a variety of morphological traits, and the ability to host attached functional molecules (Gras, S. L. 2007). Protein nanofibres share these traits, but may be lacking some of the intrinsic structure of amyloid and amyloid-like fibrils (e.g. the cross-β core or packing that confers protease

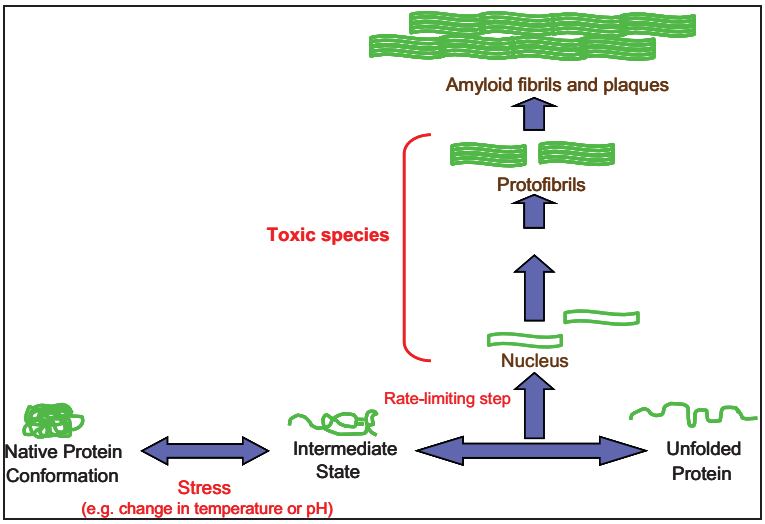

Figure 1.5: Stages of amyloid fibril formation, indicating the presence of toxic species (modified from Barral, J. M. *et al.* 2004; Ecroyd, H. and Carver, J. A. 2008a).

resistance) and/or the intrinsic structure have yet to be determined. Self assembly is a highly desirable trait in the nanotechnological field, due to the difficulties in manipulating nanometre-sized products. There are constraints upon the ability to effectively and efficiently manipulate larger materials into smaller ones (Hamada, D. *et al.* 2004). The self association of small molecules, such as proteins, into ordered assemblies removes these constraining factors and would allow for simpler large scale production of the desired nanomaterials, such as nanotubes or nanofibres which could be used in drug delivery systems, protein scaffolds, and electronic devices (Rajagopal, K. and Schneider, J. P. 2004).

The self assembling characteristic of amyloid and amyloid-like fibrils has an additional benefit for a nanotechnological component, since it affords the potential to form into different morphological forms (Zhang, S. 2003). Amyloid-like fibrils have been observed to occur in a range of alternative structures, including the classic straight fibrils, twisted fibrils, linear assemblies (such as ribbon structures), curled fibrils, ring structures and spherulites (Gras, S. L. 2007), as displayed in Figure 1.6. In some cases, multiple structures may be produced from one base protein, simply by changing the fibril formation conditions, such as by altering pH (Jahn, T. R. *et al.* 2008) or the addition of modifying substances (Griffin, M. D. *et al.* 2008). In other cases, it has been observed that a range of fibril structures may occur in a single sample (Jimenez, J. L. *et al.* 2002). The discovery that amyloid-like fibrils are a conformation accessible to many,

arguably all, proteins and peptides has led to the development of a range of peptides designed specifically for their ability to form fibrils, and thus potentially be used as nanofibres (Fezoui, Y. *et al.* 2000; Lashuel, H. A. *et al.* 2000; Hamada, D. *et al.* 2004; Deechongkit, S. *et al.* 2005; Baldwin, A. J. *et al.* 2006). The production of reliable, reproducible structures remains one of the challenges in the field of bionanomaterials, and is an area in which designed or specifically selected peptides hold much promise (Zhang, S. 2003).

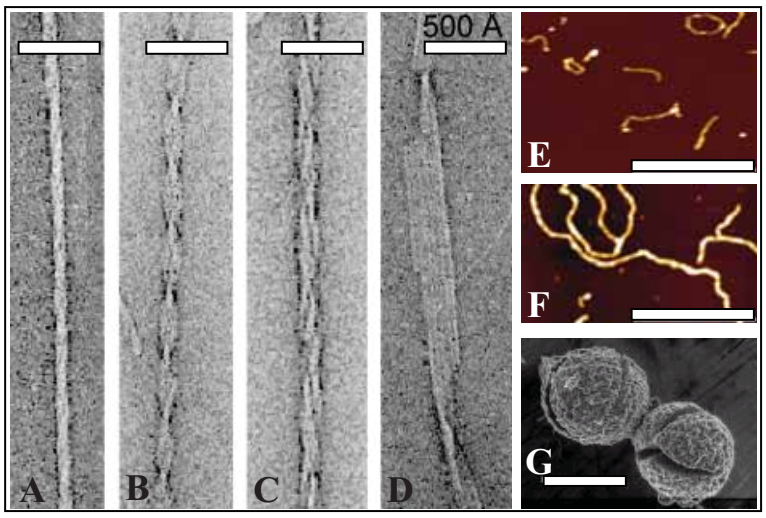

Figure 1.6: Morphological variation of protein nanomaterials made from amyloid and amyloid-like fibrils, including A) straight; B and C) twisted or intertwined; D) linear assemblies; E) curly; F) loop; and G) spherulite assemblies. Structures are composed of: insulin (A, B, C and D), images by Jiménez *et al.* (2002)[6], scale bars 50 nm; αB-crystallin (E and F) images by Meehan *et al.* (2007)[7], scale bars 500 nm; and insulin (G) image by Krebs *et al.* (2004)[8], scale bar is 50 µm.

The ability to easily attach enzymes, drugs or other functional molecules to protein nanostructures is one reason that amyloid-like fibrils have such great potential for nanotechnological uses (Waterhouse, S. H. and Gerrard, J. A. 2004). This research is based, in part, on the recognition of amyloidin, amyloid-like fibrils with native biofunctionality, as well as folded and functional domains within a number of designed amyloid and amyloid-like fibril structures (Fowler, D. M. *et al.* 2006; Gras, S. L. 2007; Sackewitz, M. *et al.* 2008). Designed peptides have since been used to create nanofibres with functional fluorphores, enzymes or ligand binders incorporated (Gras, S. L. *et al.* 2008), showing that specific functionalisation of the end-product nanomaterial is possible when using amyloid-like fibrils. Further, it has been demonstrated that conversion into the nanofibre

[6] Reprinted with permission from Macmillian Publishers Ltd.
[7] Reprinted with permission from Elsevier.
[8] Reprinted with permission from the National Academy of Sciences, USA.

structure increased the stability and longevity of such functional elements (Yu, L. *et al.* 2005; Gras, S. L. *et al.* 2008). Together with the ability to self assemble into a variety of morphological species, this ability to be biofunctionalised greatly enhances the potential use for amyloid-like fibrils as protein nanomaterials.

1.3 Crystallin proteins

One family of proteins which have the potential to be of use in the creation of protein nanomaterials are the crystallin proteins, the predominant proteins of the vertebrate eye lens (Tardieu, A. 1988; Bloemendal, H. *et al.* 2004). Of this family, which are highly conserved (across species and time), the α-, β- and γ-crystallins are found in mammalian eye lenses (Harding, J. J. and Dilley, K. J. 1976). The functions and aggregation characteristics of these proteins form the basis for much of the research described in this thesis. The β/γ-crystallin proteins are well known for their highly ordered structures, from which the protein family name is derived (from crystalline). These proteins, together with α-crystallin, at high density create a supramolecular, liquid-like matrix which is designed to allow light to be transmitted through the eye lens to the retina with minimal scattering (Tardieu, A. 1988). Disruption to the native arrangement of crystallin proteins leads to aggregation and may result in the development of cataract, the leading cause of blindness worldwide (Bloemendal, H. *et al.* 2004). Crystallin proteins have been demonstrated to be able to aggregate both amorphously and into amyloid fibrils *in vitro* and, it is argued, *in vivo* (Sandilands, A. *et al.* 2002; Meehan, S. *et al.* 2004), making the structure and protein misfolding kinetics of this family of proteins one of great relevance. Further, α-crystallin has been recognised as a member of the small Heat Shock Protein (sHSP) family, a ubiquitous class of intracellular molecular chaperones (Horwitz, J. *et al.* 1998; Hartl, F. U. and Hayer-Hartl, M. 2002). As such, α-crystallin acts as a molecular chaperone to prevent protein aggregation and precipitation, both within the eye lens and extralenticularly *via* one subunit αB-crystallin (Augusteyn, R. C. *et al.* 2002; Horwitz, J. 2003). Thus, the crystallin proteins have an interesting role within the protein folding landscape, being capable of disease-related disordered and ordered protein aggregations (§ 5 & § 6), whilst also containing a chaperone component which may be used to prevent such forms of aggregation by these and a range of other proteins (§ 6 & § 7, Ecroyd, H. and Carver, J. A. 2008a).

1.3.1 The eye lens

The vertebrate eye lens is responsible for the refraction of light, which occurs prior to focussing on the retina, and thus is essential for vision. The eye lens is composed of a dense nucleus, surrounded by a cortex, both of which consist of closely packed lens fibre cells, and finally an outermost layer of epithelial cells, where the crystallin proteins are synthesised and which form the underlayer of the lens capsule (Figure 1.7). One feature of lens fibres is their very high protein concentration, composed almost entirely of crystallin protein, estimated to be between 0.2 and 0.4 g/mL (Delaye, M. and Tardieu, A. 1983; Veretout, F. *et al.* 1989; Bloemendal, H. *et al.* 2004). The fibres rely upon the maintenance of a highly ordered structure between those proteins for the successful refraction of light (Benedek, G. B. 1971). As a result, there is little genetic diversity between the protein compositions of eye lenses, even between evolutionary distinct mammalian species (Chiou, S. H. *et al.* 1988).

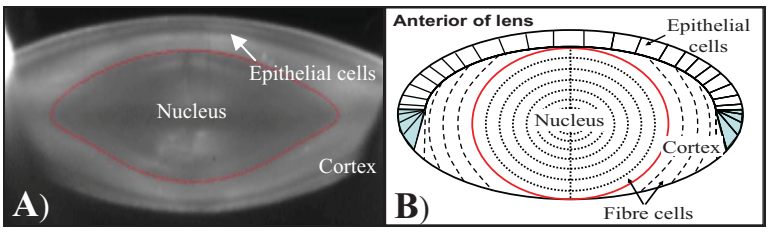

Figure 1.7: Structure of the eye lens, showing nucleus, cortex and epithelial cell layer: A) with nucleus (in red) geometrically defined (adapted from Hermans, E. *et al.* 2007)[9]; and B) diagram showing positioning of lens cells, with nucleus defined in red and regions of cellular differentiation in blue (adapted from Bloemendal, H. *et al.* 2004)[10].

A number of crystallin proteins are expressed during foetal development and are important for lens formation, whilst others are only expressed after birth (Bloemendal, H. *et al.* 2004). Lens fibre cell differentiation begins during early embryonic development. These cells are derived from cells in the epithelial layer, which differentiate (including loss of their cell nuclei and mitochondria) to form lens fibre cells (Figure 1.7B, blue regions). As lens fibre cells age, they migrate from the periphery of the lens (the cortex) towards the nucleus, with new lens fibre cells being produced in the cortex throughout life. Lens fibre cells are not degraded, so the nucleus of the lens will contain fibres developed in prenatal stages, and the proteins within those fibres, throughout life (Andley U. P. 2007).

[9] Reproduced with permission from the Association for Research in Vision and Ophthalmology (ARVO).
[10] Reproduced with permission from Elsiver.

1.3.2 Nomenclature of crystallin proteins

The crystallin proteins make up 90 % of the dry weight of the mammalian eye lens. They are separated into classes based on properties such as their molecular weight and charge, a classification system that has remained valid post-gene sequence recognition (Bloemendal, H. *et al.* 1989). The α- and β-crystallins are ubiquitous, although varying in proportion, within vertebrate lenses. The γ-crystallins are the third major component of mammalian lens proteins, being replaced by δ-crystallins in avian species. There is also a small number of rare crystallins found within individual species (Bloemendal, H. *et al.* 2004). The mammalian crystallin proteins and some characteristics of each subgroup are outlined in Table 1.3.

Table 1.3: Human crystallin proteins and their characteristics, (collated from Siezen, R. J. and Argos, P. 1983; Bloemendal, H. *et al.* 2004; Ecroyd, H. and Carver, J. A. 2008a).

Protein	Number of Residues	Mass (Da)	Mass of bovine homologue (Da)	β-sheet (%)	Arrangement
α-crystallins					
αA-	173	19 909		69	Heterogenous oligomers of ~28 subunits
αB-	175	20 159		67	
β-crystallins					
βA1-	198	23 191		61 – 68	Heterogenous oligomers (dimers to octamers)
βA2-	196	21 964			
βA3-	215	25 150			
βA4-	195	22 243			
βB1-	251	27 892			
βB2-	204	23 249	23 250		
βB3-	211	24 230			
γ-crystallins					
γS-	177	20 785	20 796	~68	Monomeric
γA-	173	20 761	-		
γB-	174	20 776	20 965		
γC-	173	20 747	-		
γD-	173	20 607	20 735		
γE-	*	-	21 008		
γF-	*	-	20 955		

* Genes in humans inactive due to nonsense mutation

1.3.3 Characteristics of lens crystallin proteins

The structure of crystallin proteins are intrinsically linked to their functions. Importantly, the α-crystallins have regions of extreme flexibility to act as highly effective molecular chaperones and yet, along with the β- and γ-crystallins are able to pack tightly and act cohesively as a stable highly ordered array (Tardieu,

A. 1988; Carver, J. A. *et al.* 1992a; Ecroyd, H. and Carver, J. A. 2008a). The structures and functions of the crystallin proteins are outlined below.

1.3.3.1 α-Crystallin

αT-Crystallin is the predominant lens protein, making up 47 % of the eye lens proteins (Delaye, M. and Tardieu, A. 1983). αT-Crystallin is composed of two subunits, labelled αA- and αB-crystallin, named originally for their acidic and basic natures, which form into large oligomeric species in a ratio of 3:1, respectively (Tardieu, A. 1988). Although no crystal structure has been ascertained for these proteins, either separately or together, the structure of αT-crystallin and its subunits has been extensively studied *via* a number of techniques, including nuclear magnetic resonance (NMR), mass spectrometry (MS) and cryo-electron microscopy (cryo EM) (Lindner, R. A. *et al.* 1998; Carver, J. A. 1999; Haley, D. A. *et al.* 2000; Aquilina, J. A. *et al.* 2003; Peterson, J. J. *et al.* 2004). For ease of reference, throughout this thesis the individual subunits of α-crystallin are referred to by their correct names (αA- and αB-crystallin); the term αT-crystallin is used to refer to these subunits in a ratio of 3:1 respectively, as isolated from the bovine lens; and the term α-crystallin is used to refer to any solution composed of α-crystallin subunits (i.e. when refering to similar characteristics in the activity of both αT-crystallin and αB-crystallin solutions).

1.3.3.1.1 Structure of α-crystallin

The composition and features of α-crystallin oligomers have been an area of much debate over the last decade. Early separation techniques showed wide variation in the size of the αT-crystallin proteins isolated from bovine lenses. Over time, the major variations observed by the different research groups were seen to be attributable to changes in isolation techniques and buffers, with αT-crystallin oligomers associating in different ways for each condition (Augusteyn, R. C. 2004a). This subunit dynamism and exchangeability are now recognised to be the hallmark characteristics of α-crystallin oligomers. It is thought to be related to αT-crystallin's role as a molecular chaperone which, in the specialised system of the eye lens, requires a high degree of flexibility and adaptability to counter the

effects of molecular crowding and limited protein degradation found within that tissue (Tardieu, A. 1988; Carver, J. A. and Lindner, R. A. 1998; Ecroyd, H. and Carver, J. A. 2008a).

αA- and αB-Crystallin are 173 and 175 residues in length, respectively (Table 1.3) and feature 57 % sequence similarity, both having a high proportion of β-sheet content (Siezen, R. J. and Argos, P. 1983; Groenen, P. J. *et al.* 1994). In the early 1980s, it was recognised that α-crystallin shares structural similarity with small Heat Shock Proteins (sHSPs), and both subunits are now recognised as belonging to this class of molecular chaperones (Ingolia, T. D. and Craig, E. A. 1982; Horwitz, J. *et al.* 2004). In common with other sHSPs, α-crystallin subunits contain a conserved 'α-crystallin domain': a region featuring seven β-sheet strands. This is flanked by an N-terminal domain and a highly flexible C-terminal extension, which have little sequence conservation between species. The sequence of α-crystallin, showing postulated structural figures, is given in Figure 1.8. The structural characteristics of α-crystallin proteins are covered in § 6 and § 7.

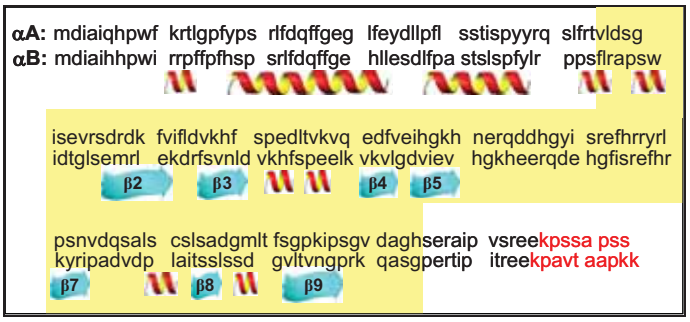

Figure 1.8: Primary sequences of bovine αA- and αB-crystallin (Ouderaa, F. J. *et al.* 1973; Ouderaa, F. J. *et al.* 1974), with the crystallin domain highlighted in yellow and flexible C-terminal extension regions labeled in red (Carver, J. A. *et al.* 1992). Putative secondary features (based on the X-ray crystal structure of two non-mammalian sHSPs, wheat HSP 16.9 and *Methanococcus jannaschi* HSP 16.5) are indicated with α-helices in red/yellow and β-strands in blue (Ghosh, J. G. and Clark, J. I. 2005).

It is not simply the structure of the α-crystallin monomeric units that provides a challenge to structural biologists, but also how they interact together to form heterogenous multimers. The overall structure of the αT-crystallin oligomer remains unknown, due to limitations in current technology and the inability to crystallise such a flexible protein assembly. Augusteyn (2004a) established that

models of αT-crystallin oligomers must allow for: no specific arrangement of either αA or αB subunits in the aggregate; the ability of the subunits to exist in multiple physical orientations with regard to each other; and the ability for such a structure to accommodate large variations in subunit numbers. NMR experiments investigating structural alterations in α-crystallin assemblies during chaperone function indicate that the retention of protein flexibility is also essential, particularly of the C-terminal extension which appears to act in the solubilisation of the αB-crystallin assemblies and its complex with target proteins under stress conditions (Carver, J. A. *et al.* 1992; Lindner, R. A. *et al.* 1998; Carver, J. A. 1999). The most comprehensive data on the quaternary structure of α-crystallin has been provided by Hayley and co-workers, who used cryo electron microscopy to compile three-dimensional images of both αT-crystallin and αB-crystallin assemblies (Haley, D. A. *et al.* 1998; Haley, D. A. *et al.* 2000). This work firmly established the presence of a large central cavity in the α-crystallin oligomer, a feature of our earlier model (Carver, J. A. *et al.* 1994), as well as providing further evidence for the variable monomer packing within these assemblies by revealing that there is no specific packing of subunits within the protein shell.

While αA-crystallin, and thus the αT-crystallin oligomer, is found only within the lens tissue, αB-crystallin is found in many tissues throughout the body, e.g. brain, lung, cardiac and skeletal muscle tissue (Kato, K. 1991). In these tissues, αB-crystallin also forms into oligomeric assemblies, retaining many of the characteristics of αT-crystallin oligomers (Abgar, S. *et al.* 2000). A combination of size exclusion chromatography followed by multi-angle light scattering showed the average mass of the αB-crystallin oligomer is 585 kDa, with a range of 533 to 684 kDa (Horwitz, J. 2003). As αB-crystallin has a monomeric molecular mass of ~20 kDa (Table 1.3), the assemblies consist of between 26 to 34 subunits. Mass spectrometry of αB-crystallin assemblies by Aquilina, Benesch *et al.* (2003) showed that the oligomers generally containing between 24 and 33 subunits, that other oligomers are present outside of this distribution (minimum of 10 and maximum of 40 subunits) and that the most common assembly consisted of 28 monomers. Both αT-crystallin and αB-crystallin form highly dynamic oligomeric

species, a crucial feature for their effective function as molecular chaperones in the eye lens and throughout the body, respectively.

1.3.3.1.2 Function of α-crystallin

The molecular chaperone function of α-crystallin species has been extensively studied since it was first recognised in the early 1990s (Horwitz, J. 1992). In recent years, it has been established that αT and αB-crystallin work to protect not only other lenticular proteins from aggregation (including its own subunits), but that they have the capacity to act as molecular chaperones against a wide range of amorphous and amyloid fibril forming target proteins (Ecroyd, H. and Carver, J. A. 2008a).

The chaperone activity of sHSPs is one of the first defences against protein misfolding in the body. As the name implies, these proteins are upregulated during the stress response (such as may be triggered due to fluctuations in temperature within the cell) (Feder, M. E. and Hofmann, G. E. 1999). This response acts to both lower the production of unstable proteins (those affected by stress) and to provide protection for the destablilised proteins already present in the cell. By associating with unfolding or misfolding proteins (those undergoing an off-pathway folding), sHSPs stop self association of those proteins and the potential of amorphous aggregation or amyloid fibril formation. Further, sHSPs provide a reservoir of partly folded proteins which may then be refolded by other, generally ATP-driven, chaperone proteins, such as HSP70 (MacRae, T. H. 2000).

αT-Crystallin acts within the eye lens to chaperone misfolding and aggregating proteins (particularly the crystallin proteins) and limit or prevent their precipitation. Various forms of cataract may be related to the misfolding of lens proteins (Bloemendal, H. *et al.* 2004). Gene knock-out mouse models have examined the loss of αA-, αB- and αT-crystallin and thus, by default, the areas in which they act *in vivo*. As expected, loss of both α-crystallin subunits leads to gross abnormalities in lens fibres of knock-out mice. Of the two subunits, αA-crystallin (the major component of α-crystallin oligomers) showed the most marked phenotypic damage when lost, resulting in cataracts, cytoplasmic inclusions and also inhibition of normal lens development (Brady J. P., *et al.*

1997). Knockout mice without αB-crystallin exhibited minimal eye lens damage, presumably because the αT-crystallin multimer exists as a ratio of 3:1 αA- to αB-crystallin and thus the majority of protein remains operational within the lens. However, a progressive muscular dystrophy was observed in αB-knockout mice, highlighting αB-crystallin's importance as an extralenticular protein (Brady J. P. *et al.* 2001). Further work has been done *in vitro* to understand chaperone activities of α-crystallin species with lens proteins and in particular with other aggregating proteins (Ecroyd, H. and Carver, J. A. 2008a). These studies will be discussed in detail in § 6 and § 7.

1.3.3.2 β/γ-Crystallin family

The β- and γ-crystallin proteins are commonly referred to as the β/γ-crystallin family, due to their similar functions and structural features. As seen in Table 1.3, there are six β-crystallins and seven γ-crystallins common to mammalian lenses. The β/γ-crystallin proteins contain two domains of very similar structure (Figure 1.9). Each domain has eight β-sheets arranged into two Greek Key motifs (Ecroyd, H. and Carver, J. A. 2008a).

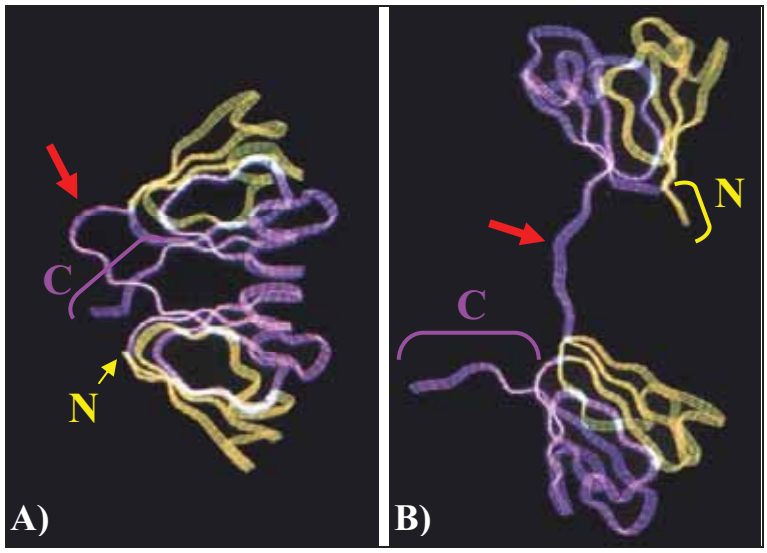

Figure 1.9: Structural similarity of β- and γ-crystallin monomeric units, A) γB-crystallin monomer, and B) βB2-crystallin monomer when part of the βB2-crystallin dimer. Red arrows indicate the connecting peptides, N and C indicate the N-termini and C-termini, respectively with brackets indicating extension regions (where relevant). Image adapted from crystal structures derived by Bax and co-workers (1990)[11].

[11] Reprinted by permission from Macmillan Publishers Ltd: Nature, Bax *et al.* 1990

The β-crystallin proteins are separated into basic (βB1-3) and acidic (βA1-3) subunits, which differ in that the basic proteins have unstructured and flexible N- and C-terminal extensions (as shown for βB2-crystallin, Figure 1.9B) and the acidic proteins only feature the N-terminal extension (Carver, J. A. 1999; Ecroyd, H. and Carver, J. A. 2008a). They range from 21 to 28 kDa in mass, feature sequence similarity of 45 - 60 % and exist as oligomers of 50 – 200 kDa in mass (Bloemendal, H. *et al.* 2004; Ecroyd, H. and Carver, J. A. 2008a). Their main role in the body is acting within the aforementioned supramolecular, liquid-like matrix within the lens; however, some β-crystallin proteins have been found extralenticularly, implying further roles for these proteins. These may include calcium binding and roles in the oxidative stress response, due to the Maf Response Element in promoter regions of the β-crystallin genes (this element can be activated by binding of Maf transcription factors, which are involved in the response to various kinds of stress) (Andley, U. P. 2007; Jobby, M. K. and Sharma, Y. 2007).

Of the β-crystallins, βB2 is the most common subunit found in mammalian lens tissues, making up ~50 % of the β-crystallins (Slingsby, C. and Bateman, O. A. 1990) and thus over 20 % of total lens protein. βB2-crystallin also features a high heat tolerance, making it unique amongst the crystallin proteins in that it will remain in solution (although unfolded) at temperatures of up to 100 °C (Horwitz, J. *et al.* 1986; McFalngai, M. *et al.* 1986). The β-crystallins all exist within oligomers, ranging from dimers to octamers (Cooper, P. G. *et al.* 1993), composed of intermixed subunits in which the N-terminus is buried (Bloemendal, H. *et al.* 2004). They feature an extended peptide linker between the two Greek key motifs, the major point of difference from the otherwise highly similar monomeric γ-crystallins (in which the peptide linker is bent, see red arrows in Figure 1.9).

The γ-crystallin proteins all exist as monomeric species of ~20 kDa in size. γ-Crystallins play a similar role to β-crystallins, with which they feature 30 % homology, a similar Maf region and an equivalent extralenticular dispersal pattern. As a result, they are thought to have the same functional roles as β-crystallins, i.e. primarily a structural role in lenticular tissue (Andley, U. P. 2007).

The major point of difference to the β-crystallins are that γ-crystallins feature a bent peptide linker joining the domains within the dual Greek key (Bloemendal, H. *et al.* 2004). There are seven recognised γ-crystallins, of which γS- (formerly βS-crystallin), γC- and γD- are the predominant species expressed. In the human eye lens, the remaining γ-crystallins exist in negligible amounts, if at all (Hanson, S. R. *et al.* 1998). After crystallin extraction from the mammalian lens, separation and purification of the individual crystallin subunits involves a combination of size exclusion and ion-exchange chromatography.

1.4 Conclusion

This thesis comprises further investigation into the formation and characteristics of amyloid fibril structures, both in relation to their role in disease processes and as potential bionanomaterials. This includes work on amyloidogenic peptides and proteins (§ 3 & § 4), but primarily centres on the role of crystallin proteins, firstly in their ability to form amyloid fibril structures (§ 5 & § 6) and also the capability of α-crystallin to inhibit protein aggregation, of both amorphous and amyloid fibril aggregates (§ 6 & § 7).

CHAPTER 2

EXPERIMENTAL PROCEDURES

2.1 Materials

Bovine serum albumin (BSA), κ-casein, catalase, insulin, pepsin and trypsin were obtained from Sigma Chemical Co. (U.S.A.). 1,4 Dithiothreitol (DTT), β-mercaptoethanol and thioflavin T (ThT), were also purchased from Sigma. All chemical reagents were purchased from AJAX Finechem (Australia). Clear and μClear 96 well plates were obtained from Greiner Bio-One (Germany). ThinSeal was purchased from Excel Scientific (U.S.A.). Supor (0.2 μm) syringe filters and Macropep 10kDa spin tubes were obtained from Pall Life Sciences (U.S.A.). Formvar and carbon coated nickel electron microscopy grids were purchased from Pro Sci Tech (Australia).

Cow, sheep and deer eye lenses were supplied by local abattoirs (T & R Ptd. Ltd., Murray Bridge, Australia; CMP Canterbury Ltd, Ashburton, New Zealand). *Eschericia coli* containing the plasmid vector pET20b(+) with the human wild type αB-crystallin gene previously inserted was obtained from W. de Jong and W. Boelens at the University of Nijmegen, Netherlands. RsAFP-19 and NaD1-19 peptides were a gift from Professor D. Craik, University of Queensland and Professor M. Anderssen, La Trobe University. Freeze-dried samples of β2-microglobulin and the mutant R3A β2-microglobulin proteins were gifts from Doctor S. Giorgetti and Professor V. Bellotti at the University of Pavia, Italy.

2.2 Basic protein purification techniques

2.2.1 *Ex vivo* mammalian protein sources

2.2.1.1 Mammalian crystallin protein extraction

Bovine (cow), ovine (sheep) and cervine (deer) crystallin proteins were extracted using standard methods, adapted from Carver, J. A. *et al.* (1996). Multiple lenses (from a single species) were homogenised in 3 mL buffer per lens, with the buffer containing 50 mM Tris pH 7.2, 1 mM dithiothreitol (DTT) and 0.04 % NaN_3. For 3 lenses or less, a manual homogeniser was used, or an electric homogeniser for larger volumes. The homogenate was centrifuged at 13,000 *g* for 30 minutes at room temperature. The supernatant, or crude crystallin stock, was removed and stored at $^{-}$20 °C.

2.2.1.2 Mammalian crystallin separation

Extracted crystallin proteins were separated using size exclusion chromatography (SEC). Separation was performed using an AKTA FPLC (Amersham Biosciences, Sweden). Aliquots of homogenate (1 mL) were run over either a Superdex 200 Highload 16/60 column (§ 5, Amersham Biosciences) or a Sephacryl 300 Highprep 26/60 column (§ 6 and § 7, Amersham Biosciences). Stock solutions were prepared as either semi-purified stocks (containing multiple proteins, loosely classified together), purified stocks (containing one or two proteins with close sequence similarity) or heat-treated stocks (containing those proteins which remain in solution after heat treatment).

Pure bovine crystallin stock solutions (§ 5.2.2, § 5.2.3) were extracted using an equilibration and elution buffer of 50 mM Tris and 0.04 % NaN_3, pH 7.4. Fractions of 10 mL were collected and two fractions from each peak combined. Buffer fractions (i.e. those between peaks which may contain some of both peak proteins) were discarded to limit contamination by adjacent peaks. Buffer was removed and proteins concentrated by four repeated washes in deionised H_2O using a Macrosep 10K Dalton Omega ultrafiltration membrane (Pall Life Sciences). The composition of semi-purified and pure crystallin stocks was assessed using SDS-PAGE gel electrophoresis (§ 2.2.4) with a wide range marker (Sigma) and only non-contaminated samples used for further assays.

Semi-pure bovine crystallin stock solutions (§ 5.2.4) were extracted using an equilibration and elution buffer of 50 mM Tris, 1 mM EDTA and 0.04 % NaN_3, pH 8. Fractions of 50 mL were collected, each containing multiple peaks equating to the αT-, βT- or γT-crystallin elution regions (e.g. the βT-crystallin fraction incorporated both βH and βL peaks). Slight cross-over of peaks between regions occurred during sample collection, due to the lack of intermediate buffer fractions (i.e. those discarded when producing pure crystalline stocks). Samples were used immediately after SEC, and were neither concentrated nor dialysed before use in further assays.

Heat treated stocks were prepared following the method of Horwitz J. *et al.* (1986). Crude crystallin stock solutions and pure bovine βL-crystallin stock solutions were heated in 1mM DTT, 50 mM Tris, 1 mM EDTA and 0.04 % NaN_3, pH 8 at 75°C for 20 minutes. Solutions were centrifuged at 13,000 *g* for 30 minutes at room temperature to remove precipated protein. The supernatant, or heat-treated crystallin stock, was removed for use in further assays.

2.2.2 Recombinant protein sources

2.2.2.1 Human wild type αB-crystallin expression

Protein expression, following the methods of Horwitz (1998), was begun by plating and streaking out a small amount of thawed vector-containing *E. coli* onto an ampicillin imbued agar plate. Ampicillin resistance was the selectable marker for this plasmid, thus only *E. coli* featuring the wild type αB-crystallin gene could grow on an ampicillin containing media. The culture plate was incubated at 37 °C overnight to allow colonies to develop. Once colonies over the size of 2 mM were present, the plate was placed to 4 °C and stored for up to 2 weeks. Only individual colonies were selected for further culture and large scale protein expression.

Large scale protein expression, also following the methods of Horwitz (1998), involved the transfer of an individual *E. coli* colony (containing the plasmid vector) to 50 mL LB media with ampicillin (50 ng ampicillin:1 mL), culture was then grown at 37 °C with shaking overnight. The cultured media was then distributed between 2 L of LB media (without ampicillin) and culturing at 37 °C with shaking continued. Once the *E. coli* had grown adequately, with an OD_{600} between 0.6 and 1.0, protein expression was induced by the addition of 0.25 mM iso-propyl-thio-galactosine (IPTG). The *E. coli* was incubated for a further 3 – 4 hours (as above) to allow protein expression to occur. Cultures were then removed and the cells centrifuged at 7,000 rpm for 20 minutes to form a cell pellet. The supernatant was discarded and the cell pellet collected, weighed and stored at -20 °C until cell lysis and protein purification (a maximum of 1 month).

Cell lysis is performed to remove the majority of cellular components from the cell pellet prior to protein purification. The *E. coli* cell pellet was defrosted by

resuspension in an ice-cold buffer of 50 mM Tris and 100 mM NaCl at pH 8, using 3 mL of buffer per gram of cell pellet (per gcp). To this was added phenyl-methyl-sulfonyl-fluoride (PMSF, 2 μL of 0.5 M stock per gcp), lysozyme (0.8 mg per gcp) and deoxycholic acid (4 mg per gcp). The cell lysis mixture was then placed at room temperature and gently shaken for 45 minutes. DNA was broken down by addition of DNAse I (2 μL of a 10mg/ml stock per gcp) with shaking at room temperature until the mixture lost viscosity. Metals were removed by the addition of EDTA (8 μL of 250 mM stock per gcp) and the waste components removed by centrifugation at 14,000 rpm for 30 minutes at 4°C. The unpurified protein fraction, contained in the supernatant, was collected.

2.2.2.2 Human wild type αB-crystallin purification

Purification of recombinant human wild type αB-crystallin (hereafter referred to as αB-crystallin) from the cell lysis supernatant was achieved using two techniques over the course of this research: anion exchange chromatography (AEC) and modified-AEC. Both techniques produced pure αB-crystallin, as observed by SDS-PAGE electrophoresis (§ 2.2.4).

AEC and modified-AEC feature a reduction and an excess DNA binding step. Five mg of dithiothreitol (DTT) and 36 μL of polyetheleneimine (PEI) per gcp were added to the cell lysis supernatant and incubated at room temperature with constant mixing for 20 minutes. Waste proteins were removed by centrifugation at 14,000 rpm for 30 minutes at 4°C, with the αB-crystallin containing supernatant collected for further purification.

For AEC, the supernatant was loaded onto a DEAE column (XK 26, packed with Sepharose Fast Flow gel, Amersham Biosciences) which had been equilibrated with 3 column volumes of 20 mM Tris, 1 mM EDTA at pH 8. αB-Crystallin and all contaminant protein were then removed *via* a salt gradient using a buffer of 20 mM Tris, 1 mM EDTA and 1 M NaCl. The major peaks were assessed by SDS-PAGE (§ 2.2.4), αB-crystallin was the primary peak eluted, removed by a salt concentration of approximately 10 %, containing a pure band of an approximately 20,000 kDa protein.

For modified-AEC the DEAE column (above) was equilibrated using 3 column volumes of 0.1 M sodium phosphate at pH 7.4. The supernatant containing impure αB-crystallin (post DTT and PEI treatment) was then loaded. αB-crystallin eluted as the primary peak in the void volume, as it did not bind to the column under these conditions. SDS-PAGE analysis identified a pure band of an approximately 20,000 kDa protein. Remaining proteins were eluted by flushing the column with 0.1 M sodium phosphate, 1 M NaCl at pH 7.4 (no gradient used).

2.2.3 Reduction and carboxymethylation of κ-casein

κ-Casein was reduced and carboxymethylated according to the method from Schechter *et al*. (1973). κ-Casein was reconstituted in 1M Tris, 8M urea buffer (pH 8.0) containing 0.01 % EDTA. DTT was added at a ratio of 5:3, protein to DTT, and the reduction proceeded for 1 hr at room temperature. An excess of iotoacedic acid (3 times the original protein concentration) was added to the stirred reaction mixture and after 20 min the mixture was subjected to gel filtration on a Sephadex G-25 column (2 x 45 cm) and eluted using 0.05 M ammonium bicarbonate. RCMκ-Casein was identified using SDS-PAGE (§ 2.2.4), freeze dried and stored at -20 °C.

2.2.4 SDS-PAGE Protocol

The purity of isolated proteins, or composition of protein mixtures, was examined using sodium dodecyl sulfate polyacrylamide gel electrophoresis (SDS-PAGE), following the method of Laemmli (1970). Gels containing 3.6 % (stacking gel) and 15 % (resolving gel) acrylamide were prepared from a stock solution of 30 %/w acrylamide and 0.8 %/w N,N'-*bis*-methylene acrylamide. Final gel concentration was: 375 mM Tris-HCl, and 0.1 % SDS. Gels were polymerized chemically by the addition of 0.025 %/v of tetramethyl-ethylenediamine (TEMED) and ammonium persulphate. Resolving gels of 5 by 10 cm were poured between glass plates, after polymerisation stacking gels of 1 by 10 cm were poured and polymerised in the same way. The electrode buffer contained 0.025 M Tris base, 0.192 M glycine and 0.1 % SDS. Sample loading buffer contained 0.5 M Tris-HCl at pH 6.8, 25 % glycerol, 2 % SDS, 1 % Bromophenol blue and 5 % mercaptoethanol. Samples were boiled at 90 °C for 10 minutes prior to loading

and 15 μL/well was loaded. Gels were run at 150 V for approximately 1 hour (or until dye-front had run off the base of the gel). Gels were stained for 1 to 4 hours in Coomassie brilliant blue solution (0.025 % w/v coomassie blue, 40 % v/v methanol, 0.5 % v/v acetic acid) and destained overnight in a solution of 40 % v/v methanol, 0.5 % v/v acetic acid.

2.3 Protein aggregation monitoring

2.3.1 Amorphous protein aggregation

2.3.1.1 Induction of amorphous aggregation

Amorphous aggregation of the protein to be chaperoned (or target protein) was induced in two ways, by either temperature destabilisation or by the reduction of disulfide bonds (Farahbakhsh, Z. T. *et al.* 1995; Ecroyd, H. and Carver, J. A. 2008b). Protein precipitation increases the turbidity of solutions. This turbidity can be measured by the amount of light scatter created at a wavelength of 340 nm (Ecroyd, H. and Carver, J. A. 2008b). Measurements were taken using a Fluostar Optima plate reader (BMG Lab technologies, Australia). For § 6, all proteins (target and chaperone) were prepared in 0.1 M sodium phosphate at pH 7.4 and filtered with 0.2 μm filter immediately prior to further sample preparation (i.e. formation into amorphous or fibrillar aggregates). Assays were run in clear 96-microwell plates, using a sample volume of 200 μL/well. No agitation of solutions was used. For § 7, all chaperone proteins were prepared at the time of protein immobilisation (1 day prior to chaperone assay) and stored at 4 °C till use. Assays were run in clear 96-microwell plates, using a sample volume of 100 μL/well. Linear agitation of solutions (115 rpm) was used to assist interaction between target proteins and immobilised chaperone proteins (§ 7.2.3).

2.3.1.1.1 Light scatter assessment of thermally induced amorphous aggregation

Catalase was used to assess temperature destabilised amorphous aggregation, at temperatures ranging from 55 °C to 60 °C (dependent on chaperone protein qualities being assessed, § 6.2 and § 7.3). Assay samples included: buffer alone (0.1 M sodium phosphate at pH 7.4); catalase in buffer; chaperone protein in buffer; and catalase and chaperone protein in buffer. All samples were run in duplicate, and the activity of each chaperone protein assessed over three to six

separate experiments. Aggregation was determined as maximum change in light scatter at 340 nm ± 10 nm between the initial time-point and the final time-point. Final time-points were determined by a plateau in light scatter (i.e. completion of protein precipitation by catalase at 40 minutes (§ 6.2) or 50 minutes (§ 7.3), depending upon assay conditions). Results displayed in each case are mean ± standard error (SE) for all replicates.

2.3.1.1.2 Light scatter assessment of disulfide-bond reduction induced amorphous aggregation

Insulin was used as a disulfide-bond reduction induced amorphously aggregating target protein, in assays at 37 °C. Assay samples included: buffer with DTT (0.1 M sodium phosphate at pH 7.4, 20 mM DTT); insulin in buffer with DTT; chaperone protein in buffer with DTT; and insulin and chaperone protein in buffer with DTT. All samples were run and aggregation assessed as per catalase aggregation (§ 2.3.1.1.1), with plateaus in light scatter monitored at 40 minutes for all assays (§ 6.2 and § 7.3). Results displayed in each case are mean ± standard error (SE) for all replicates.

2.3.1.1.3 Refolded aggregate formation for use as chaperones

αT- and αB-Crystallin refolded aggregates were formed to examine their molecular chaperone qualities (§ 6.2.3 and § 6.2.4). 3 mg/mL of each protein was reconstituted into 0.1 M sodium phosphate, 1 M GdnHCl and incubated at 4°C for 2 hrs. To allow refolding of aggregates the removal of GdnHCl was achieved as outlined in § 2.3.4.

2.3.1.1.4 Amorphous aggregate formation for use as chaperones

αT-Crystallin, αB-crystallin and aldehyde dehydrogenase (ADH) amorphous aggregates were formed to examine their molecular chaperone qualities (§ 6.2.3 and § 6.2.4). 3 mg/mL of each protein was reconstituted into 0.1 M sodium phosphate, 1 M GdnHCl and incubated at 90°C for 2 hrs. Where required, samples were treated using the method for removal of GdnHCl (§ 2.3.4.) to produce equivalent conditions and thus allow for comparison of samples.

2.3.2 Fibrillar protein aggregation

2.3.2.1 Aggregation induction

Protein nanofibres were formed under different conditions dependant on the peptide or protein involved and the desired fibril morphology. All fibril formation experiments were repeated at least three times and assessment for amyloid-like characteristics was made by at least two methods (as outlined in § 3.1.2).

2.3.2.1.1 Nanofibre formation by RsAFP-19

Nanofibres were formed from RsAFP-19, reconstituted at 3 mg/mL in H_2O (approximately pH 7), in two ways: by incubation at 60 °C for 20 hours (§ 3.2.3.1) without shaking and with aliquots removed every 2 hours for ThT and TEM assessment; and by sequential freeze thaw cycles (§ 3.2.3.2), where the reconstituted solution was frozen at -20 °C for 6 to 12 hours, followed by thawing to room temperature for 2 hours, and the cycle repeated three times.

2.3.2.1.2 Nanofibre formation by R3A β2-microglobulin

R3A β2-microglobulin was reconstituted into 0.1 M sodium phosphate, pH 7.4, nanofibres were formed upon incubation at 37 °C with orbital shaking at 700 rpm for up to 16 days in the presence or absence of 10 μM ThT (§ 4.3 and § 7.3.4). R3A β2-microglobulin fibril seeds were formed from nanofibre samples taken after 16 days incubation. These were stabilised against pH unwinding by the addition of 20 % TFE, then sonicated for 10 minutes to produce short seed fibrils.

2.3.2.1.3 Nanofibre formation by seeded β2-microglobulin

β2-microglobulin was reconstituted into 0.1 M sodium phosphate, pH 7.4, nanofibres were formed upon seeding with seed fibrils of R3A β2-microglobulin (20 %), followed by incubation at 37 °C with orbital shaking at 700 rpm for up to 16 days in the presence or absence of 10 μM ThT (§ 4.3).

2.3.2.1.4 Nanofibre formation by pure crystallin solutions

Pure bovine crystallin nanofibres (§ 5.2.3) were formed from 6 mg/mL solutions of each crystallin protein (α, βL, or γL, § 2.21.2 and βH, § 6.2.3) in deionised H_2O, using methods adapted from Meehan, S. (2004). These were adjusted to pH 2 with HCl and 10 % (v/v) trifluoroethanol (TFE) was added, samples were then incubated at 60 °C for 18 hrs.

2.3.2.1.5 Nanofibre formation by semi-pure crystallin mixtures

Semi-pure bovine crystallin amyloid fibrils (§ 5.2.4) were formed using methods adapted from Meehan, S. *et al.* (2004). TFE (10 %) was added to the semi-purified bovine crystallin proteins in SEC buffer (0.02 M Tris, 1 mM EDTA, 0.04 % NaN_3) after adjustment to pH 2 with HCl. Samples were then incubated at 60 °C for 18 hrs.

2.3.2.1.6 Nanofibre formation by crude crystallin mixtures

Crude crystallin nanofibres were initially produced (§ 5.2.5.1) by diluting crude crystallin stock (crystallin homogenate, § 2.2.1.1) 1:10 into a solution of 50 mM Tris, 0.04 % NaN_3 at pH 2 (adjusted with HCl). To this mixture, 10 % TFE was added and the solution was incubated at 60 °C for 18 hrs. The final formation conditions for crude crystallin amyloid fibrils (§ 5.2.5.2) were to dilute crude crystallin stock 1:10 into a solution of 50 mM Tris, 1 mM EDTA, 0.04 % NaN_3 at pH 2, add 10 % TFE and incubate at 60 °C for 18 hours. Crystallin mixtures from cow, sheep, deer, a mixture of all three (stock preparation given in § 2.2.1.2) and heat-treated cow stocks (§ 2.2.1.2.1) were used for crude nanofibre formation.

2.3.2.1.7 Nanofibre formation by α-crystallin using GdnHCl

αT- and αB-Crystallin amyloid fibrils (§ 6.2.1 and § 6.2.4) were formed using methods adapted from Meehan, S. *et al.* (2004). 3 mg/mL of each protein was reconstituted into 0.1 M sodium phosphate, 1 M GdnHCl and incubated at 60 °C for 2 hrs. Where required, samples were treated using the method for removal of GdnHCl (§ 2.3.4.) to produce equivalent conditions and thus allow for comparison of samples.

2.3.2.1.8 Nanofibre formation by RCM κ-casein

RCM κ-casein was reconstituted into 0.1 M sodium phosphate and 10 μM ThT, pH 7.4, amyloid fibrils were formed upon incubation at 37 °C with linear shaking at 115 rpm for up to 20 hours (§ 7.3.3), following the method of Thorn *et al*. (2005).

2.3.2.2 Assessment of amyloid characteristics of nanofibre formation

2.3.2.2.1 Thioflavin t

ThT assays were performed *in situ* by a method adapted from Nielsen, Khurana et al. (2001). Samples were incubated with 10 μM ThT in μClear 96-microwell plates using a sample volume of 100 – 200 μl per well. Plates were sealed with ThinSeal TM to prevent evaporation, and incubated at 37 °C with or without shaking. Fluorescence was measured at regular intervals using Fluostar Optima plate reader (BMG Lab technologies, Australia) with a 440/490 nm excitation/emission filter set (± 10 nm) until a plateau in fluorescence was obtained (different for each target protein). For § 6, all proteins (target and chaperone) were prepared in 0.1 M sodium phosphate at pH 7.4 and filtered with 0.2 μm filter immediately prior to use (i.e. prior to formation into potential chaperone structures). Sample volume was 200 μL/well and no agitation of solutions was used. For § 7, all chaperone proteins were prepared at the time of protein immobilisation (1 day prior to chaperone assay) and stored at 4 °C till use. Sample volume was 100 μL/well and agitation of solutions (linear at 115 rpm for RCM κ-casein and orbital at 700 rpm for R3A β2-microglobulin) was used to assist interaction between target proteins and immobilised chaperone proteins (§ 7.3). To allow comparison between increases in ThT fluorescence, each curve was normalised relative to the initial fluorescence intensity (change in fluorescence) to eliminate artefacts resulting from the ThT binding propensity of the native target peptide or protein. Maximum change in fluorescence (between the initial time-point and the final time-point) was used for all further calculations, and mean ± SE of three replicates was used for all statistics and graphs.

Non-*in situ* fibril formation was assessed on pre-formed nanofibre samples, in a method adapted from Thorn *et al*. (2005). Using a 50 mM Glycine-NaOH buffer, at pH 9 with 5 μM ThT. Fibril solutions were formed independently (at 37 °C or 60 °C) and aliquots from selected time points removed and frozen to halt fibril formation. Amyloid fibril formation was judged complete when a peak or plateau in fluorescence was observed (individual to each protein or peptide: § 3.2.3; § 3.3.2; § 4.3; § 7.3.3 and § 7.3.4). ThT fluorescence was read and normalised as above. Maximum change in fluorescence (between the initial time-point and the final time-point) was used for all further calculations, and mean ± SE of three replicates was used for all statistics and graphs.

2.3.2.2.2 Transmission electron microscopy

Transmission electron microscopy (TEM) was performed as described by Thorn *et al*. (2005). Samples were prepared on formvar and carbon coated nickel electron microscopy grids. Protein samples were diluted to 0.5 or 1 mg/mL and 2 μL was deposited on each grid. The grid was rinsed 3 times with 10 μL of H_2O, negatively stained with 10 μL of uranyl acetate (2 % w/v) and dried with filter paper. Samples were analysed under magnifications of 20,000 to 130,000 x, using an excitation voltage of 120 kV on a Philips Technai 100 transmission electron microscope. For all samples multiple regions (at least three) on the grid were examined to assess structure dispersal. For initial nanofibre assessment at least three separate samples were examined. For monitoring of chaperone activity against known amyloid or amyloid-like fibril forming proteins, TEM assessment was performed on target protein alone and target protein in the presence of chaperone for three separate experiments.

2.3.2.2.3 Atomic force microscopy

Atomic force microscopy (AFM) was used to examine nanofibres formed from a range of peptides and proteins, following the methods of Chamberlain *et al.* (2000). Samples were prepared as described above (§2.3.2.1), diluted to ~1 mg/mL and 5 μL pipetted onto freshly resurfaced highly ordered pyrolytic graphite (HOPG). Topographical measurements were obtained using a silicon cantilever (NSC 15 model, Ultrasharp) in ambient air on an AFM from Digital Instruments Dimension 3100, with images collected at 512 samples per line and a scan rate of 0.5 Hz. For all samples multiple regions (at least three) on the surface were examined to assess structure dispersal. For initial nanofibre assessment at least three separate samples were examined. Topographical and height analysis of samples was performed using Nanoscope software (Version 5).

2.3.2.2.4 Protease treatment

Assessment for protease resistance of potential amyloid and amyloid-like fibrils was achieved with pepsin or trypsin (for fibrils formed at pH 2 and pH 7, respectively), following the method of Zurdo, Guijarro and Dobson (2001). The protease was applied to the protein solution, containing pre-formed nanofibres or native protein, at a ratio of 1:200 (protease:substrate protein). Solutions were incubated for 3 hours at 37 °C and then frozen to halt the proteolytic activity.

Protease treated samples and control samples were then examined with TEM (§ 2.3.2.2.2) to assess for the presence or absence of nanofibres.

2.3.2.2.5 X-ray fibre diffraction

X-ray fibre diffraction (XRD), also known as Wide Angle X-ray Scattering (WAXS), was performed using a R-AXIS-IV Rigaku MSC (at CSIRO, Melbourne), following the method of Squires *et al.* (2006). Samples were prepared by suspending aliquots of native or potentially fibrillar protein solutions (12-20 μL) between two wax-filled capillary ends, which were slowly separated to enhance fibril alignment while the sample air-dried. Production of cloudy stalks has been observed to diffract in a manner showing misalignment of the sample (personal communication, Dr. S. Gras), thus only clear protein stalks were used for further analysis. The small stalk of protein obtained was placed in an X-ray beam and diffraction data were obtained at a wavelength of 1.542 Å with a sample to detector distance of 300 mm and exposure times of 10 – 20 minutes. Single samples were analysed for each specimen, with all data analysed using FIT2D (Hammersley, A. P. 1995).

2.3.3 Chaperone activity quantification

Chaperone activity was determined from the light scatter and ThT variables measured as described above (§ 2.3.1.1 and § 2.3.2.2.1). The percentage of protection provided by a given chaperone is derived from the difference between the maximum change in light scatter or ThT fluorescence for the target protein alone and in the presence of the chaperone, i.e. the maximum change in light scatter or ThT fluorescence for the target protein is judged to be 100 % aggregated (or 0 % protected), upon addition of an active chaperone to the target protein a drop in maximum light scatter or ThT fluorescence would be observed, this equates to less target protein aggregated (and thus a percentage has been protected from aggregation). The following equation (Eq. 1) was used to quantify the protection given by each chaperone (Ecroyd, H. and Carver, J. A. 2008b):

$$\text{Percentage Protection} = \left(\frac{Max_{\text{Target Protein}} - Max_{\text{Target Protein + Chaperone}}}{Max_{\text{Target Protein}}} \right) \text{x } 100 \qquad \textbf{Eq. 1}$$

Where *Max* is the maximal change observed in light scatter or ThT fluorescence between the initial time-point and end time-point of the assay. All statistical analysis of percent protection results was performed on the mean percent protection value of three to six replicates.

2.3.4 Removal of GdnHCl from α-crystallin samples for use as molecular chaperones

To remove GdnHCl from solutions of α-crystallin aggregate species: native protein (GdnHCl-free control), GdnHCl unfolded protein (§ 2.3.1.1.3), amorphous aggregates (§ 2.3.1.1.4) or amyloid fibrils (§ 2.3.2.1.7) were spun at 14 000 *g* in Macropep 10 kDa spin tubes for three consecutive 30 minute washes (with 0.1 M sodium phosphate buffer, pH 7.4) and then resuspended into an equivalent volume of 0.1 M sodium phosphate buffer, pH 7.4. As noted above, to ensure equality of all potential chaperone samples (for statistical analysis) both those formed in the presence of GdnHCL and those formed in buffer alone were treated using this method.

2.4 Protein immobilisation techniques

2.4.1 Protein immobilisation

2.4.1.1 Plasma generated aldehyde polymerisation onto solid supports

Solid supports were cleaned prior to use by sequential washing and sonication in acetone, methanol and ethanol. Plasma immobilisation was induced by radio frequency plasma glow discharge, performed under vacuum, following the method of Blättler *et al.* (2006), using a capacitively coupled glow discharge plasma instrument controlled using a radio frequency power generator (13.56 MHz; RFX-600, Advanced Energy). An initial vacuum of 2.5 x 10^{-2} mbar was achieved before manual flooding with propionaldehyde vapour. Radio frequency power was then applied to initiate a plasma, resulting in the polymerisation of aldehydes onto the surfaces within the chamber. For all substrates, plasma treatment proceeded at 50 Watts for 2 minutes, followed by treatment at 20 Watts for a further 2 minutes. This polymerisation technique has been observed to produce reliable plasma polymers, over 10 nm thick and with the specific interfacial properties desired (free, easily accessible aldehyde groups for Schiff-based chemistry) (Vermette, P. *et al.* 2003). Covalent immobilisation of proteins

directly followed polymerisation. Polymerisation was repeated over six separate experiments. For each experiment, alydehyde polymerisation was assessed using X-ray photoelectron spectroscopy (XPS, § 2.4.2.1), and for three experiments it was further analysed *via* AFM (§ 2.4.2.2).

2.4.1.2 Covalent immobilisation of proteins to aldehyde polymer coated surfaces

For covalent immobilisation, the protein to be immobilised (αB-crystallin or BSA) was dissolved in 100 mM sodium phosphate buffer at pH 7.4 and mixed with sodium cyanoborohydrate (1 mg/mL protein: 3 mg/mL $NaBH_3CN$). Aldehyde coated FEP and silicon wafer were immersed in this solution overnight at 4 °C, allowing enough time for reductive deamination to covalently link exposed lysine residues on the proteins to the polymerised aldehydes on the solid substrate. Aldehyde-coated QCM-D crystals underwent protein covalent immobilisation during QCM experiments (§ 2.4.2.3). The success of protein immobilisation, pre and post chaperone assays, was further characterised by XPS (§ 2.4.2.1) and AFM (§ 2.4.2.2).

2.4.2 Plasma polymer and protein immobilisation assessment

2.4.2.1 X-ray photoelectron spectroscopy

XPS data was obtained using a Kratos AXIS Ultra DLD XPS, with a monochromatic A1 Kα X-ray source and a hemispherical analyser. The pass energy was 20 eV with a resolution of 0.3 eV for high resolution spectra. Spectra were collected at a photoelectron takeoff angle of 90 °C. Binding energies were referenced to the C1s hydrocarbon carbon peak at 285.0 eV to compensate for surface charging effects. Component fitting of the high resolution spectra was performed using CasaXPS version 2.3.12 software.

XPS nitrogen (N) signals from multiple integrated spectra were used to estimate the quantity of immobilised protein with minimal random error. Protein compositions were determined *via* calculation of changes in fluorine (F) signals (present in FEP) and concomitant changes in N signals (present in the immobilised protein), achieved using multilayer XPS algorithm software, as described by Chatelier, R. C. *et al.* (1997). XPS spectral examination was

obtained for FEP samples of: aldehyde polymer, aldehyde polymer with immobilised chaperone, and aldehyde polymer with immobilised chaperone post-chaperone protection of RCM κ-casein. Data was obtained for between three to six separate immobilisation experiments (dependent on sample assessed). Values of protein composition are given as mean ± SE of all experiments.

2.4.2.2 Liquid phase atomic force microscopy

Liquid phase tapping mode AFM was used to image aldehyde coating or surface immobilised αB-crystallin on silicon wafer, following the methods of Chamberlain, A. K. *et al.* (2000). Experiments were conducted using a commercial AFM (Nanoscope IV, Digital Instruments, Santa Barbara, CA) with triangular silicon cantilevers (OTR-4) and a spring constant of 0.08 N/m. Surface topography of silicon wafer coated with aldehydes or with surface immobilised αB-crystallin was examined in 0.1 M sodium phosphate buffer, pH 7.4 at room temperature for at least 3 replicates. Grain analysis was performed on 2 x 2 μm micrographs, using Nanoscope software (Version 5). Analysis was performed for 3 separate immobilisation experiments, on all particles present for images with less than 5 % surface particle coverage or on 100 discrete particles per image where particles constituted more that 5 % of the image.

2.4.2.3 Quartz Crystal Microgravimetry

QCM with dissipation measurements were perfomed on an E4 QCM (Q-sense AB, Göteborg, Sweden), based on the methods of Thierry, B. *et al.* (2008). All measurements were performed at 25 °C using gold coated QCM AT-cut quartz crystal sensors (Q-sense) with a fundamental frequency of 4.95 mHz. Sensors were plasma cleaned for 10 minutes prior to use. Plasma treatment, as described above (§ 2.4.1.1), was used to coat the gold surface of the sensor with a thin polymerised layer with reactive aldehyde groups. The 3^{rd}, 5^{th}, 7^{th}, 9^{th} and 11^{th} overtone response in frequency and dissipation were continuously recorded and provided information about the adsorbed mass and viscoelastic properties. QCM-D equilibration was achieved first in H_2O then in 100 mM sodium phosphate buffer, pH 7.4 at a flow rate of 100 μL/min and left to stabilise 20 minutes. Crystals were then treated either with buffer or protein immobilisation solution (1 mg/mL αB-crystallin and 3 mg/mL sodium cyanoborohydrate) at a flow rate of 50

μL/min again until stabilisation (45 minutes). Data analysis was performed on normalised data from the seventh harmonic (35 MHz). In a first approximation, changes in frequency (ΔF) were converted into wet adsorbed mass using the Sauerbrey equation as described by Fleming *et al.* (2008) using Equation 2:

$$\Delta m = -C\Delta f_N \qquad \textbf{Eq. 2}$$

Where Δm is mass change, C is a constant based on the properties of the crystal QCM chip (Q-sense gold coated AT cut quartz crystal sensors: C = 17.7 ng/cm^2) and Δf_N is the change in frequency (overtone-normalised by Q-sense software). All QCM-D experiments were repeated three times and statistics and graphs are based on the mean ± SE of these results.

CHAPTER 3

SYNTHETIC PEPTIDES FOR NANOFIBRE FORMATION

As discussed in § 1, the formation of amyloid and amyloid-like fibrils is an area of continuing research interest, due to the multiple foci of their role within disease, their role as functional biological structures and their potential uses in nanotechnology (§ 1.2.2, Lashuel, H. A. *et al.* 2000; Chiti, F. and Dobson, C. M. 2006; Gras, S. L. 2007). The possibility of altering a protein or peptide's off-pathway folding trajectory towards or away from amyloid fibril formation is thus an area of great significance. Certain peptides and proteins have a high propensity to misfold into intermediate structures which tend to ordered aggregation after minimal destabilisation (such as a slight increase in temperature). Increasingly peptides are being designed with amyloid-like fibril forming propensities, to facilitate the *in vitro* study of amyloid fibril formation under physiological temperature and pH conditions (Hamley, I. W. 2007). In this research, two peptides originally derived from plant defensin proteins, designed for their antifungal properties (Lay, F. T. and Anderson, M. A. 2005), were tested to examine amyloid-like fibril forming propensities under temperature destabilisation.

3.1 Nanofibre forming peptide systems

Amyloid-like fibril forming peptides feature the useful traits of a short amino acid sequence and easily understood folding behaviour (Kammerer, R. A. *et al.* 2004). As a result, peptides have been used over the past decade to study aspects of amyloid fibril formation in detail, from the protofilament level to higher order assemblies (Fezoui, Y. *et al.* 2000; Kammerer, R. A. *et al.* 2004; Rajagopal, K. and Schneider, J. P. 2004; Elgersma, R. C. *et al.* 2006). Small amyloid and amyloid-like fibril-forming peptides have contributed greatly to knowledge of amyloid fibril structural characteristics, as they are able to be examined *via* solid-state NMR and X-ray diffraction techniques to a much closer degree than larger peptides or proteins (§ 1.2.2.2, Chiti, F. and Dobson, C. M. 2006). Amyloid-like fibril-forming peptides, including designed peptides, have been used in the production of nanomaterials with specific morphology or structural characteristics (Fezoui, Y. *et al.* 2000; Lashuel, H. A. *et al.* 2000; Deechongkit, S. *et al.* 2005; Elgersma, R. C. *et al.* 2006). They have also been used to explore specific interactions occurring within the amyloid fibril formation process, such as molecule-molecule interactions (MacPhee, C. E. and Dobson, C. M. 2000;

Takahashi, Y. *et al.* 2002) and surface-molecule interactions (Yang, H. *et al.* 2007). In addition, many nanofibre-forming peptides display rapid aggregation kinetics and may therefore be used for *in vitro* assays into potential inhibitors of amyloid fibril formation (Kammerer, R. A. *et al.* 2004; Ecroyd, H. and Carver, J. A. 2008b). Finally, peptides have been used to explore the addition of biological function to amyloid-like fibrils, either through the incorporation of functional domains (Channon, K. J. *et al.* 2008; Sackewitz, M. *et al.* 2008) or *via* attachment of biologically active molecules to previously formed peptide-based nanofibres (Kodoma, H. *et al.* 2004).

3.2 Plant defensin proteins and peptides

Plant defensins are proteins produced in seeds, flowers and pathogen-stressed leaves. Their role is to provide protection for the plant against a variety of potentially damaging agents, such as fungal and bacterial pathogens. Plant defensins are small proteins, 45 – 54 amino acids in length, which are rich in cysteine residues and include four intramolecular disulfide bonds (De Samblanx, G. W. *et al.* 1997). These intramolecular bonds lead to a specific conformational structure, known as the 'cysteine stabilised alpha beta' (CSαβ), a region where three disulfide bridges stabilise a triple-stranded antiparallel β-sheet associated on one strand with an α-helix (§ 3.4.2: Figure 3.1, disulfide bonds highlighted in red). The CSαβ region is common to many insect and plant defensins and may act as a scaffold to host a range of the important functional regions of these proteins (Cornet, B. *et al.* 1995; Lay, F. T. *et al.* 2003a; Lay, F. T. *et al.* 2003b).

Defensins have a range of commercial applications, including roles as antifungals, antimicrobials and enzyme inhibitors (Lay, F. T. *et al.* 2003b). This is true for both the native proteins; and particularly for small enzymatically active peptide regions of those proteins. RsAFP-19, derived from *Raphanus sativus* (radish seed) Antifungal Protein (RsAFP1 or 2), is one such bioactive plant defensin region. RsAFP-19 has been synthesised to examine the effect of disulfide-mediated stability on native protein function, as disulfide linkages play an integral role in the stability of the native RsAFP proteins, and as a potential commercial antifungal peptide (Schaaper, W. M. *et al.* 2001). A second plant defensin peptide derived from ornamental tobacco plant *Nicotinia alata* defensin protein, is NaD1-

19 (Lay, F. T. *et al.* 2003b). NaD1-19 has a similar sequence and biological activity to RsAFP-19, both being bioactive peptides which work primarily as antifungal agents and have potential use in the agricultural industry. Investigations into the structure and stability of these short peptide sequences revealed a tendency for gel formation by RsAFP-19, initiating investigation into the amyloidogenicity of these peptides. To this end, a range of destabilisation techniques and fibril forming conditions were examined for each peptide and the resulting structures characterised (§ 3.2.3; § 3.3.2).

3.3 Assessment of nanofibre formation

Protein aggregation can be monitored by a variety of techniques. As proteins aggregate, whether amorphously or amyloidogenically, they often clump together to form insoluble aggregates which precipitate out of solution. Techniques such as measurement of light scatter within a solution are used to follow this precipitation, particularly when monitoring amorphous (disordered) protein aggregation. Monitoring amyloid-like fibril formation (ordered aggregation) involves techniques which specifically recognise the characteristic properties of amyloid and amyloid-like fibrils, and thus discriminate between amorphous or fibrillar aggregate structures. Techniques to assess amyloid and amyloid-like fibril formation include the binding of β-sheet specific dyes, such as thioflavin t (ThT) and Congo red, microscopy techniques capable of imaging in the nano-scale, including transmission electron microscopy (TEM) and atomic force microscopy (AFM), assessment of protease resistance and X-ray fibre diffraction (Chiti, F. and Dobson, C. M. 2006). Due to the complex nature of amyloid and amyloid-like fibril structures (because of the variability introduced by the different peptide or protein bases) multiple techniques are required to initially confirm the formation of amyloid-like fibril species from a peptide or protein (Nilsson, M. R. 2004). Once amyloid or amyloid-like fibril formation is established, individual techniques, such as measurement of ThT fluorescence or (less commonly) light scattering, may be used to determine the kinetics of formation and to assess potential inhibitors fibril formation (Raman, B. *et al.* 2005; Ecroyd, H. and Carver, J. A. 2008b).

ThT is a β-sheet specific fluorescent dye that is frequently used to assess target protein amyloid and amyloid-like fibril formation (Groenning, M. *et al.* 2007). It is most effectively used as a way of monitoring fibril formation in peptides and proteins already proved to be amyloidogenic, as these fibrils contain high amounts of β-sheet (§ 1.2.2.2). For target peptides and proteins that have been proven to misfold into amyloid or amyloid-like fibrils, ThT binding assays, in conjunction with TEM imaging, can be used to examine the kinetics of fibril formation and the activity of chaperone molecules (Ecroyd, H. and Carver, J. A. 2008b).

TEM is a technique used to image in the nano-scale (nanometres to microns). It is based on electron scattering properties and utilises a high voltage electron source to image coated surfaces. Enhanced resolution can be gained by the addition of a negative stain, such as uranyl acetate (Nilsson, M. R. 2004). TEM provides information on two planes and is a commonly used tool for investigating the length and width features of nanofibres, whether amyloid-like or non β-sheet based, in some cases even revealing aspects of protofibrillar structure (Jimenez, J. L. *et al.* 2002).

AFM is a form of scanning microscopy, which can be used to provide high quality information in the nanoscale on the length and height of surface-attached structures. AFM uses a sharp nano-sized tip on the end of a cantilever to scan the chosen surface. The changes in force encountered are measured and extrapolated into an image of surface topography (Binnig, G. *et al.* 1986). AFM can also provide information about the viscoelastic properties of surface, indicating where there are differences in the viscosity or elasticity of the surface material encountered, *via* phase contrast and amplitude imaging (respectively) (Shao, Z. *et al.* 1995; Marchant, R. E. *et al.* 2002). For nanofibre imaging, dry surface tapping mode AFM is often employed (Kad, N. M. *et al.* 2003). This technique involves 'tapping' the tip (using short touches) across the surface, as opposed to the tip being continuously on the surface, and is a more accurate technique for the imaging of 'soft' structures such as proteins and protein nanofibres (Vinckier, A. *et al.* 1998).

XRD is used to determine molecular structure from the scattering pattern instigated by an X-ray beam. As discussed in § 1.2.2.2, amyloid and amyloid-like fibrils all contain a fibrillar core structure of β-strands and β-sheets, arranged perpendicular and parallel to the fibrillar axis, respectively (Jimenez, J. L. *et al.* 2002). Together these diffract into a characteristic cross-β structure (Sunde, M. *et al.* 1997). XRD can determine whether these characteristic interactions (found in the core of all amyloid and amyloid-like fibrils) are present in a sample, and is thus judged to be the most definitive technique for differentiating amyloid and amyloid-like fibril structures from other nanofibrillar structures (Makin, O. S. and Serpell, L. C. 2005).

3.4 Fibril formation by Raphanus sativus Antifungal Peptide (RsAFP-19)

3.4.1 RsAFP-19 Structure

The RsAFP-19 peptide is 19 amino acids in length and is derived from the double β-barrel region of RsAFP proteins (Figure 3.1), as determined by solution NMR spectroscopy (Fant, F. *et al.* 1998). It includes one of two regions important for the antifungal activity exhibited by both RsAFP1 and 2 (De Samblanx, G. W. *et al.* 1997), which spans from amino acid 38 to 46. The synthesised peptide has been further modified to have no cysteine residues (replaced by α-aminobutyric acid) in order to avoid uncontrolled disulfide bridge formation between the three cysteine residues initially in the peptide region (Schaaper, W. M. *et al.* 2001).

3.4.2 RsAFP-19 Amyloidogenicity

Preliminary investigations into the structure of RsAFP-19 peptide revealed a high gel forming propensity. Upon undertaking NMR characterisation of the peptide, the sample, over a period of three months, formed a highly stable gel in the NMR tube (H. Schirra, unpublished data). Examination of this gel showed classical amyloid-like fibril characteristics, including ThT binding attributes and long thin nanofibre structures when examined by TEM (§ 3.4.3.3: Figure 3.7B, S. Meehan, unpublished data). These findings indicated that RsAFP-19 may have the potential to form amyloid-like fibril structures.

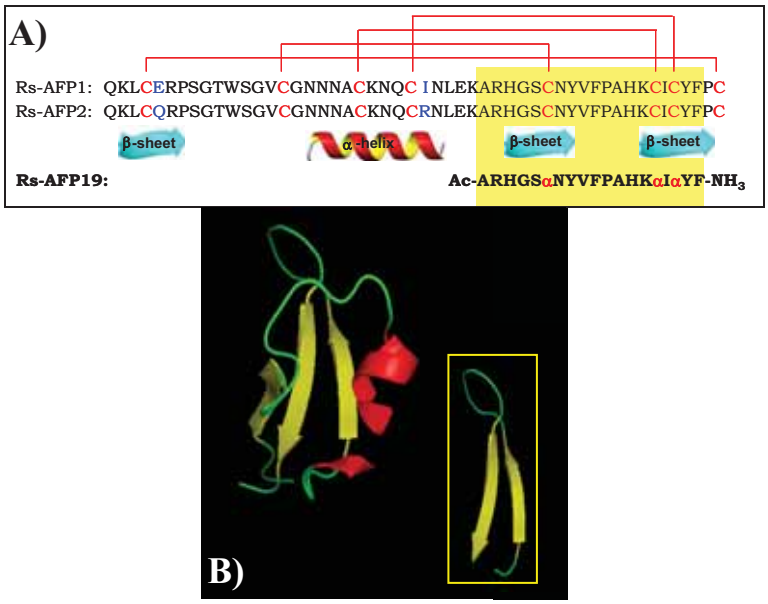

Figure 3.1: Structure of RsAFP proteins and peptide, showing A) sequence similarity of RsAFP1 and 2, cysteines and disulfide linkages are indicated in red and sequence differences in blue (adapted from Fant, F. *et al.* 1998; Thomma, B. P. *et al.* 2002). The RsAFP-19 region is highlighted in yellow, with the specific sequence given in bold, where Ac is an acetyl group, NH_3 is an amino group and α are α-aminobutyric acids, used to replace cysteines (Schaaper, W. M. *et al.* 2001); and B) 3D structure of RsAFP1 determined *via* NMR, with inset (yellow edged box) of RsAFP-19 region, images drawn using PyMOL (Delano, W. L. 2002: www.pymol.org) from sequences derived from Pubmed for molecule: 1AYJ_A (Fant, F. *et al.* 1998).

Increasingly, over the previous decade, protein prediction algorithms have been used to analyse the amyloid fibril forming propensity of different peptides and proteins. TANGO (Fernandez-Escamilla, A. M. *et al.* 2004, http://tango.crg.es) is one such statistical mechanics algorithm which incorporates the amino acid sequence of the peptide or protein (though not the polypeptide's structure) and also such physico-chemical parameters as concentration, pH, ionic strength and the effect of adding a destabiling agent (such as trifluoroethanol). To examine their β-sheet aggregation propensities, RsAFP1 and RsAFP-19 were analysed using TANGO. As discussed above (§ 3.4.1) all cysteine residues in the RsAFP-19 peptide were mutated, so as to avoid variation due to uncontrolled cross-linking. For more detailed examination of the importance of disulfide linkages in the β-sheet aggregation propensity of these molecules, RsAFP1 and RsAFP-19 were further analysed using TANGO after mutation of all cysteine residues. Use of α-aminobutyric acid is incompatible with the TANGO algorithm, so for these computations the RsAFP mutant structures have cysteine residues replaced by alanine (rather than α-aminobutyric acid) residues. Alanine was selected as the

closest amino acid to α-aminobutyric acid, due to the similarity in structure between the two aliphatic α-amino acids, with alanine featuring a methyl side chain and α-aminobutyric acid an ethyl side chain (Cocinero, E. J. *et al.* 2006).

TANGO assessment of RsAFP1 and RsAFP-19, with cysteine residues or with alanine residues replacing cysteine residues, was run using the parameters: 25°C in H_2O at pH 7 with an ionic strength of 0.02, no protection for the termini and a protein stability of -10 (with ionic strength selected for potential remnants from peptide synthesis and protein stability chosen as being a neutral situation). The TANGO results showed a change in the predicted aggregation propensity between the native RsAFP1 and the modified structures (Figure 3.2).

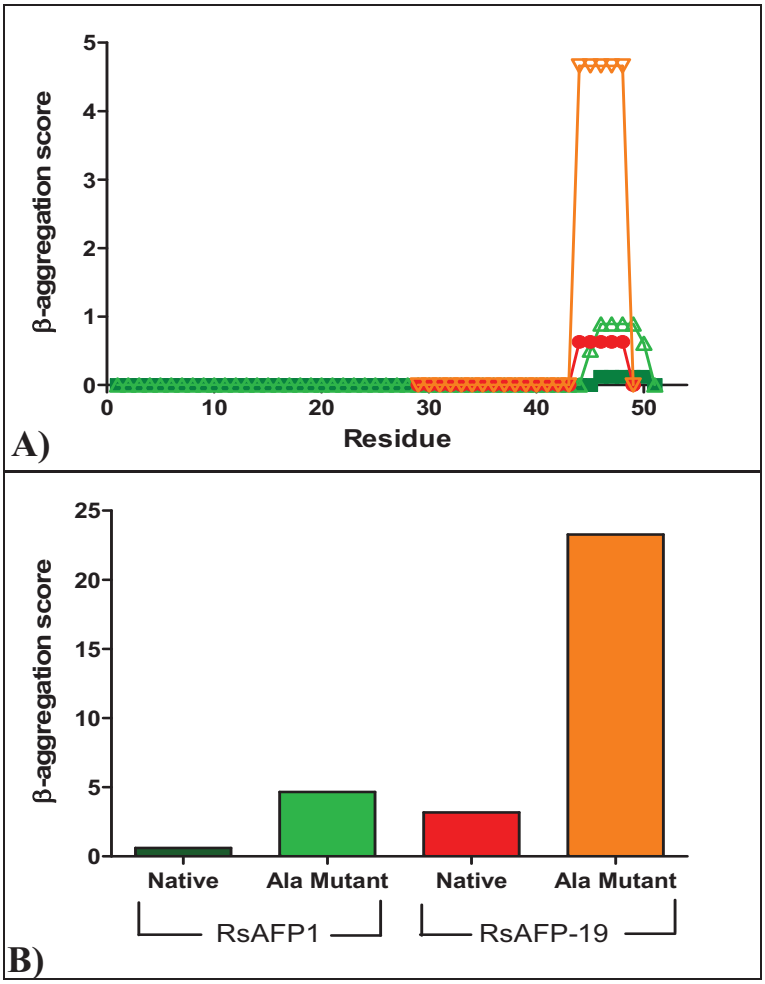

Figure 3.2: TANGO β-aggregation scores for RsAFP proteins and peptides, where native species have cysteine residues in place and Ala mutant species have cysteine residues replaced by alanine residues for the TANGO computations, showing A) aggregation propensity for each residue (■ Native RsAFP1, △ Ala mutant of RsAFP1, ● Native RsAFP-19, ▽ Ala mutant of RsAFP-19); and B) total aggregation propensity for that protein or peptide.

RsAFP1 featured some aggregation propensity, with a TANGO score for aggregation of 0.6, a similar score to some known amyloidogenic proteins, such as transthyretin or the F571 mutant of lysozyme (Fernandez-Escamilla, A. M. *et al.* 2004). Removal of the disulfide linkages, by replacement of cysteine residues with alanines, leads to an increase in predicted aggregation propensity (to a score of 4.7). Native RsAFP-19 showed a higher propensity for β-aggregation than the native full length protein, with an aggregation score of 3.2. Figure 3.2A shows the predicted aggregation propensity of each residue of the tested proteins and peptides. Once the cysteine residues, and thus any stabilising disulfide bonds, were removed by mutation, the aggregation score of RsAFP-19 (ala RsAFP-19) becomes 23.3, an increase of over thirty-fold from the native protein and over 5-fold from the wild-type RsAFP-19 peptide. This indicates a very high prospect of β-sheet aggregation, potentially amyloid-like fibril formation, from this modified peptide (Figure 3.2B). Both native and mutant RsAFP1 showed aggregation regions in the RsAFP-19 peptide region, explaining why the shorter peptide is more aggregation prone.

3.4.3 Characterisation of nanofibre formation by RsAFP-19

3.4.3.1 Thermally induced nanofibre formation of RsAFP-19

Lyophilised solutions of RsAFP2-19 were reconstituted in deionised H_2O at 4 mg/ml and the pH measured to be approximately pH 7. Solutions were then incubated at 60^{o}C for 24 hours, with aliquots taken every 2 hours and fibril formation monitored using ThT fluorescence. ThT fluorescence remained steady at a low value over the first 10 hours of RsAFP-19 incubation. ThT fluorescence then increased sharply at 12 hours (Figure 3.3). The decrease in ThT after 14 hours is most likely attributed to higher order aggregated formation, where nanofibres associate together, blocking ThT binding sites and potentially precipitating out of solution.

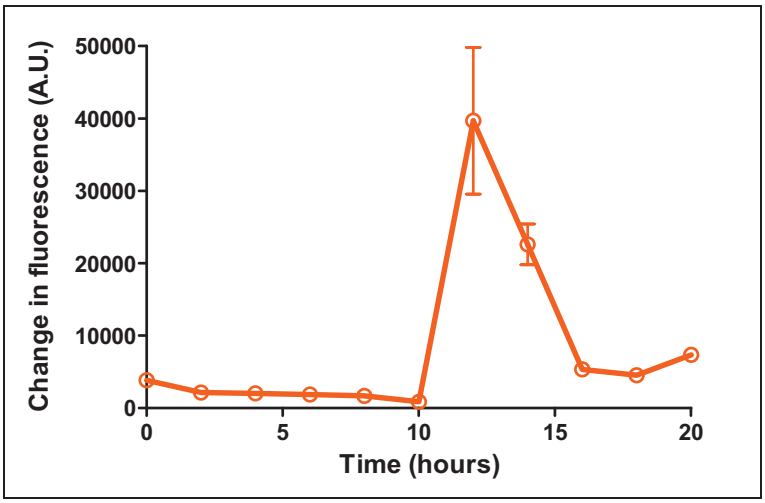

Figure 3.3: ThT fluorescence of RsAFP-19 after incubation at 4 mg/mL in H_20, pH 8 at 60°C over 20 hours (error bars show SEM of *n*=3).

RsAFP-19 nanofibre formation was also monitored by TEM, which revealed a more gradual fibril formation process than was indicated by ThT (Figures 3.4 and 3.5). At the initiation of fibril formation (zero hours) there were no fibrillar aggregates present (Figure 3.4A). After 4 hours incubation at 60 °C, there were a number of fibril structures present, of approximately 10 nm in diameter and varying between 30 and 300 nm in length (Figure 3.4B). After 8 hours incubation, these RsAFP-19 fibrils were of a similar diameter but had increased in length to 500 nm (Figure 3.4C), though ThT still showed no increase in fluorescence (Figure 3.3). After 12 hours, the fibrils were up to 1 µm in length (Figure 3.5A), and by 14 hours they were observed to be longer than can be measured at high magnification, i.e. over 1.2 µm in length (Figure 3.5B). After incubation for 20 hours, long fibrils were still present, but higher sample dilution was required to obtain TEM images without overloading the sample grid (Figure 3.5C), implying an increased yield of nanofibres. In 4 and 8 hour samples, TEM showed the presence of nanofibres, while there was no concurrent increase in ThT. These results indicate that ThT is only able to recognise RsAFP-19 fibril structures at higher concentrations. This, in conjunction with the drop in fluorescence observed upon the formation of higher aggregate structures (§ 3.4.3.5) leads to the conclusion that ThT is unreliable way to monitor nanofibre formation by this peptide.

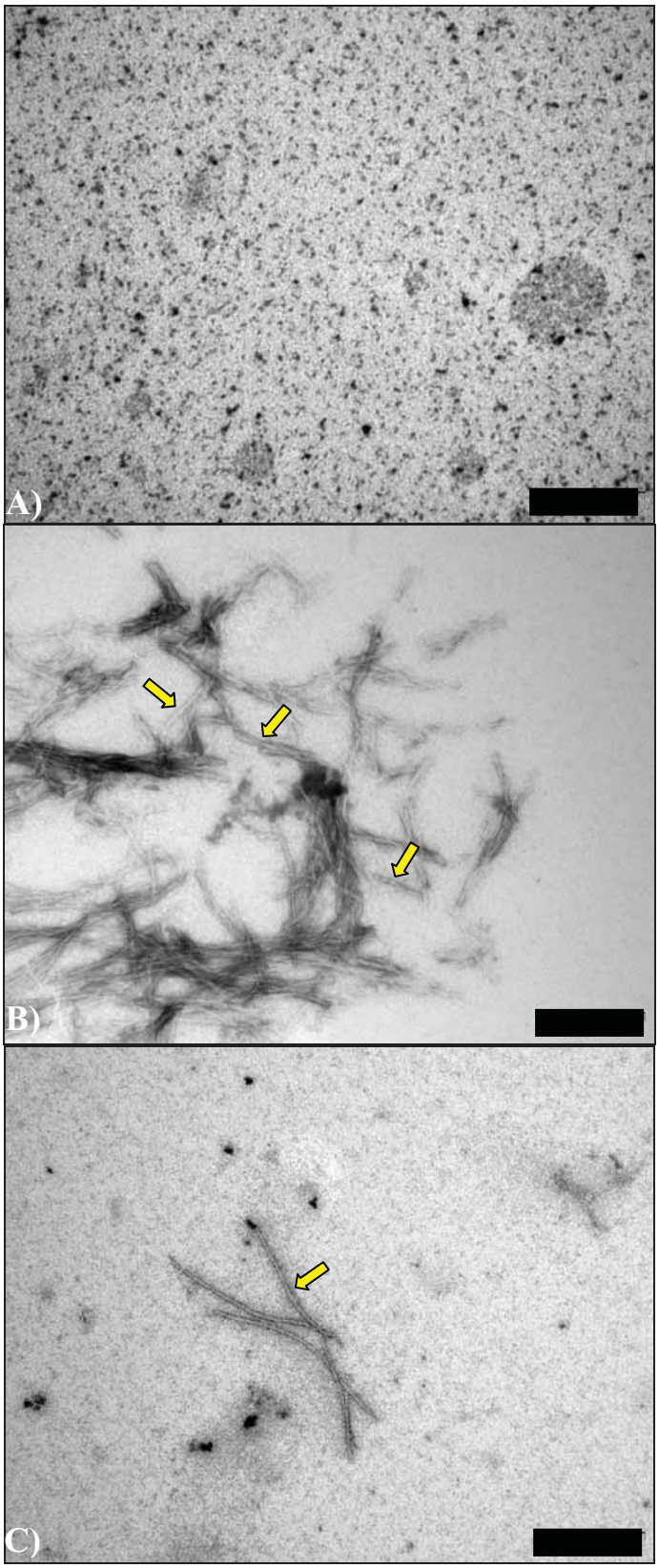

Figure 3.4: TEM images of RsAFP-19 nanofibres formed at 4 mg/mL in H_2O, pH 8 after incubation at 60°C for: A) 0 hours, B) 4 hours, C) 8 hours. Yellow arrows highlight individual fibrils; scale bars are 200 nm.

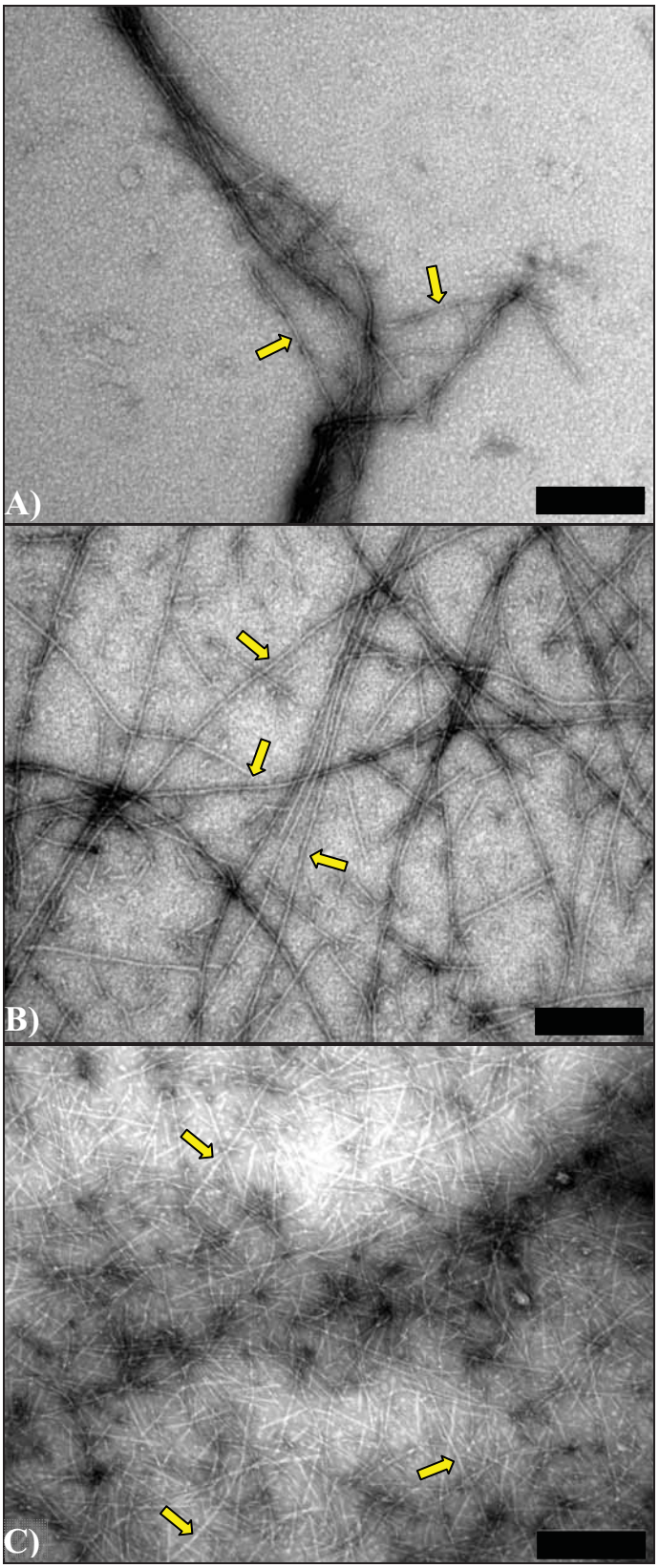

Figure 3.5: TEM images of RsAFP-19 nanofibres formed at 4 mg/mL in H_2O, pH 8 after incubation at 60°C for: A) 12 hours, B) 14 hours and C) 20 hours. Yellow arrows highlight individual fibrils; scale bars are 200 nm.

3.4.3.2 Freeze-thaw induced nanofibre formation of RsAFP-19

Further examination of fibril formation by RsAFP-19 involved subjecting duplicate solutions of RsAFP-19 (reconstituted in H_2O at 4 mg/mL, as above) to sequential freeze-thaw cycles. This was achieved by freezing the solution at -20 °C for 6 to 12 hours, followed by thawing to room temperature for 2 hours, a process that was repeated 3 times. Nanofibre formation by this technique was a serindipidous finding following the examination of frozen and thawed control samples from previous experiments. The fibril structures thus formed were examined by TEM and AFM (Figure 3.6) and observed to be approximately 10 nm in diameter and up to 200 nm in length. AFM was used to examine the characteristics of protofilaments and complete fibril structures, and was performed by Dr. Paula Brooksby (University of Canterbury, New Zealand).

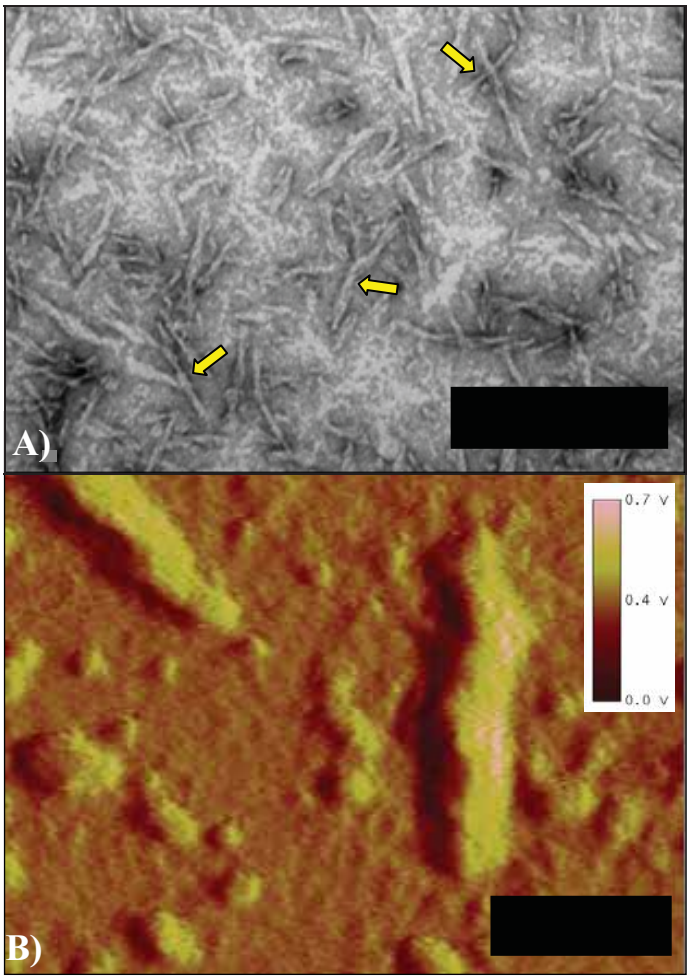

Figure 3.6: RsAFP-19 nanofibres formed by 3 cycles of freeze-thawing at 4 mg/mL in H_2O at pH 8: A) TEM image of fibrils formed, yellow arrows indicate individual fibrils and B) AFM of same sample at higher resolution (scale bars are 200 nm and 125 nm, respectively).

3.4.3.3 X-ray fibre diffraction analysis of RsAFP-19 nanofibres

XRD analysis was performed on nanofibres formed from RsAFP-19 protein which had been used for NMR examination and formed fibrils under the conditions used in sample preparation. For this, RsAFP-19 was reconstituted in H_2O at high concentration (~10 mg/mL) then heated to high temperatures (~90 °C) and left at room temperature for over three months. This treatment of RsAFP-19 resulted in a firm gel solution and nanofibres with the characteristic appearance of amyloid-like fibrils as observed by TEM and AFM, performed for this sample only by Dr. Sarah Meehan (Figures 3.7A and B, respectively). The alignment of fibrils observed by TEM is potentially due to the high temperature or other NMR preparation techniques used on the sample. XRD on this sample was performed by Drs Glyn Devlin and Sarah Meehan (University of Monash, Aust.; and Cambridge, U.K., respectively).

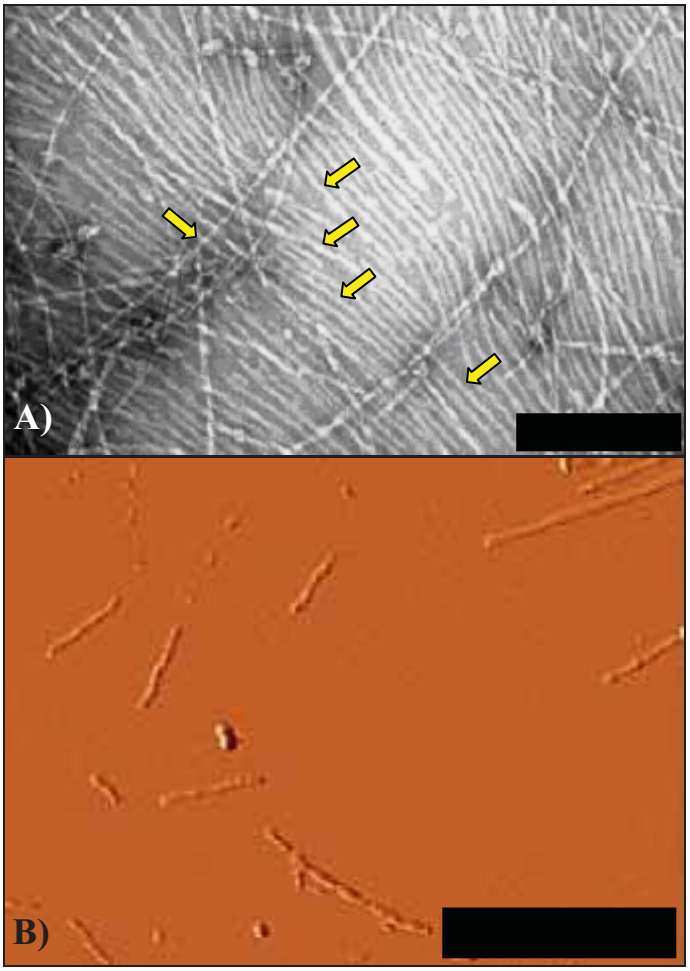

Figure 3.7: RsAFP-19 nanofibres formed at high concentration and temperature, imaged by A) TEM (yellow arrows indicate individual fibrils, scale bar 200 nm) and B) AFM (scale bar 600 nm).

Figure 3.8A shows a characteristic XRD cross-β pattern common to amyloid fibrils (Sunde, M. *et al.* 1997) with meridional and equatorial reflections shown at 4.7 and 10.9 Å respectively. A further isotropic peak was observed at 4.1 Å, which has been commonly observed in high power X-ray diffraction of amyloid fibril samples. It is thought to be related to sample contamination and thus does not arise from the fibrillar structure (Sunde, M. *et al.* 1997). These peaks are further elucidated in Figure 3.8B, which provides the 1-D patterns of Fit2D analysis of this sample, highlighting the relevant peaks. Data analysis was performed by Dr. Sally Gras (University of Melbourne, Australia).

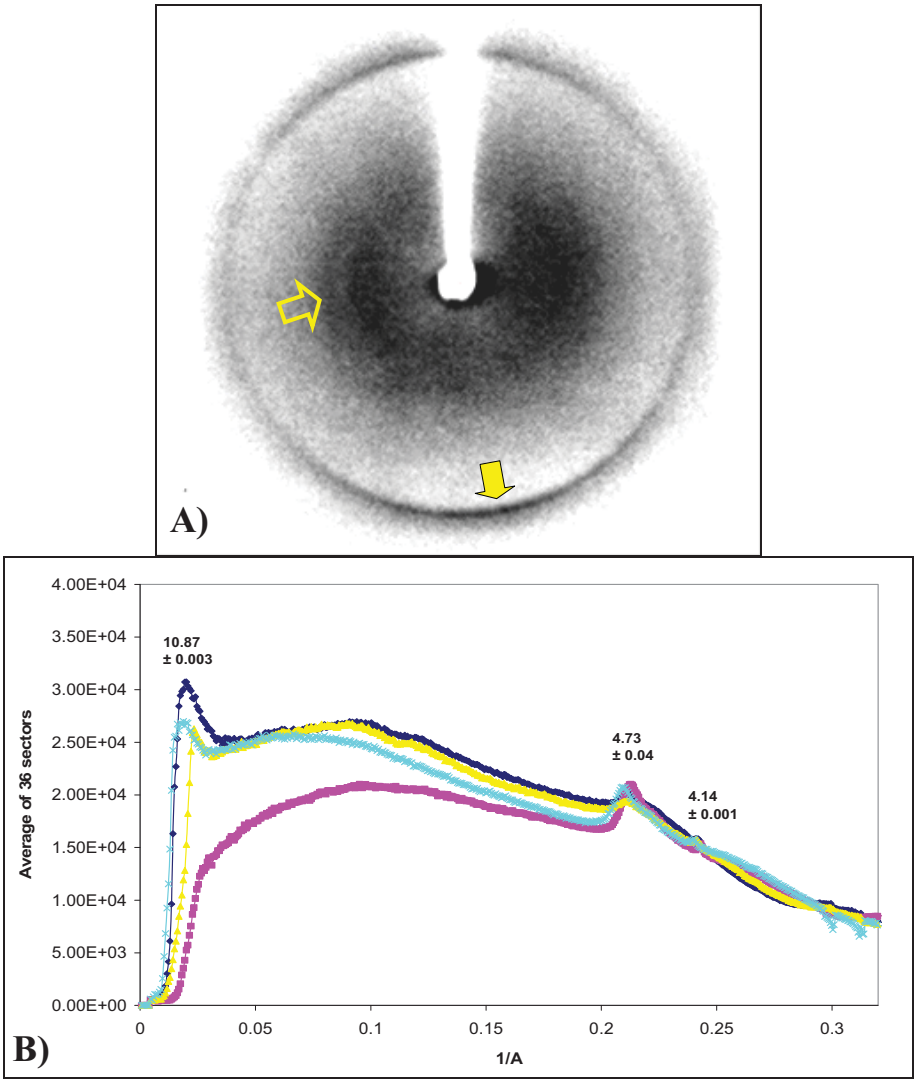

Figure 3.8: RsAFP-19 nanofibres formed at high concentration and temperature, imaged by A) X-ray fibre diffraction (closed arrow indicates the equatorial reflection at 10.9 Å and the open arrow the meridional reflection at 4.7 Å) with B) 1-D pattern analysis of peaks, indicating their associated Å distance.

3.4.3.4 Examination of RsAFP-19 nanofibres

High magnification TEM and AFM of RsAFP-19 nanofibres, produced by either thermal or freeze-thaw induction (Figures 3.9A and B, respectively) revealed the twining of protofilaments which is characteristically seen in many amyloid fibrils (Serpell, L. C. *et al.* 2000). AFM data capture was performed by Dr. Paula Brooksby to assess the height of protofilaments and complete fibrils. AFM showed that protofilaments of RsAFP-19 (closed arrows) have a height of ~4 nm, whilst the complete fibrils (open arrows) were ~8 nm high.

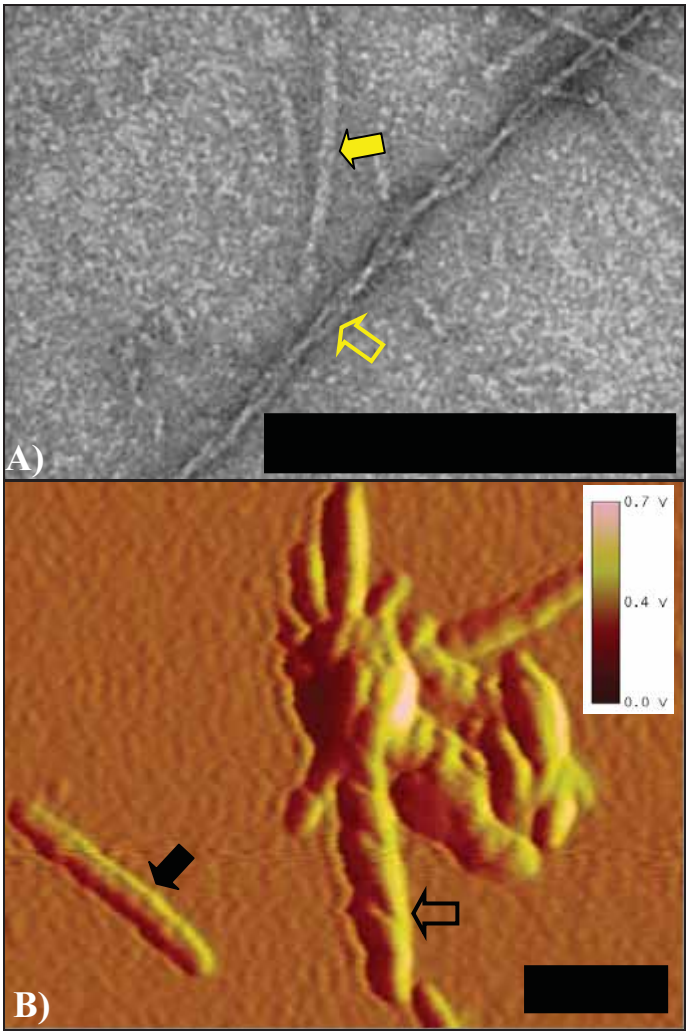

Figure 3.9: RsAFP-19 nanofibres formed at 4 mg/mL in H_2O at pH 8, showing protofilament twisting: A) TEM image of fibrils formed after incubation at 60°C for 14 hours and B) AFM of fibrils formed after 3 cycles of freeze thawing. Arrows indicate examples of single protofilaments (filled arrows) and complete fibrils, with protofilament twists clearly visible (open arrows). Scale bars are 200 nm and 250 nm, respectively.

These results are within the normal amyloid and amyloid-like fibril range, which has a protofilament size of between 2 and 5 nm, with a complete amyloid fibril structure, composed of twisted protofilaments, between 7 and 13 nm in width (Chiti, F. and Dobson, C. M. 2006). This procedure, the intertwining of protofilament structures, is an important step in the self-assembly process of amyloid and amyloid-like fibrils. In a number of peptide and protein systems it has been observed that self association of complete amyloid and amyloid-like fibril structures may continue, leading to the formation of higher order structures, such as peptide ribbons (Lashuel, H. A. *et al.* 2000; Krebs, M. R. *et al.* 2004; Hamley, I. W. 2007).

3.5 Nicotinia alata Defensin 1 modified peptide (NaD1-19)

3.5.1 NaD1-19 Structure

RsAFP-19 and NaD1-19 have a high sequence similarity. They both contain a number of key residues conserved within the entire plant defensin family and the CSαβ region (Lay, F. T. *et al.* 2003b). Figure 3.10 shows the primary sequences of both full peptides (RsAFP1 and NaD1), with the cysteines (all of which are conserved) and disulfide bonds in red, other conserved residues in blue and synthesised peptide regions highlighted in yellow. NaD1-19 is an extended version of a previously designed peptide, NaD1-17. The original bioactive peptide designed from the NaD1 sequence (NaD1-17) differed significantly from RsAFP-19 in that it lacked the proline and the adjoining alanine situated in the loop joining the two β-barrels (residues 41 and 42 in RsAFP native proteins). During investigations into the structural characteristics of both RsAFP-19 and NaD1-17 peptides, a second designed peptide of 19 residues (NaD1-19) which incorporated this proline-alanine segment was synthesised. Both NaD1-17 and NaD1-19 sequences are given in bold in Figure 3.10. As with RsAFP-19, the cysteine residues in these peptides have been replaced with α-aminobutyric acids to avoid uncontrolled disulfide bond formation.

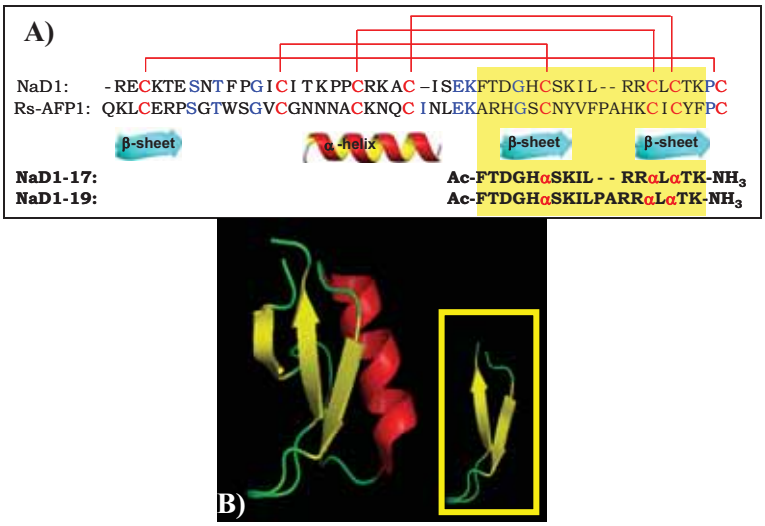

Figure 3.10: A) Sequence similarity of RsAFP2 and NaD1 (adapted from Lay, F. T. *et al.* 2003b). Peptide structures are shown in the yellow box, with the mutated NaD1-17 and NaD1-19 peptides below in bold, including the synthetically added proline and alanine segment and the α-aminobutyric acids in place of native cysteine residues, and B) Structure of NaD1, determined by solution NMR with inset (yellow edged box) of NaD1-19 region, images drawn using PyMOL (Delano, W. L. 2002: www.pymol.org) from sequences derived from Pubmed sequence: Q8GTM0 (Lay, F. T. *et al.* 2003a; Lay, F. T. *et al.* 2003b).

Similarities in both structure and function have been demonstrated between many antifungal proteins, including between NaD1 and RsAFP1 (Lay, F. T. *et al.* 2003b; Lay, F. T. and Anderson, M. A. 2005). Analysis using a statistical mechanics algorithm (TANGO) revealed inherent differences in the predicted β-aggregation propensity of these proteins, and of the synthesised peptides of each used in this research. As with RsAFP1 (§ 3.2.2), NaD1 was analysed both in native state and where all cysteine residues had been replaced by alanine residues. Two mutants were also examined, NaD-17 and NaD-19 (Figure 3.10), also in both native and alanine mutant forms. In all six cases, no aggregation propensity was observed (TANGO aggregation score of 0.0), under the same conditions used for RsAFP1 and RsAFP-19 (§ 3.4.2). Under these conditions all RsAFP proteins and peptides showed some aggregation propensity, with the alanine mutant of RsAFP-19 showing a very high level of β-aggregation propensity (TANGO score of 23.3). This indicates that the inherent structure of NaD1 is less amyloidogenic than RsAFP proteins and peptides. This difference may be due to variations between NaD1 proteins and peptides in the specific region identified as having a high amyloid propensity in RsAFP1 and RsAFP-19 (Figure 3.2A). In this region, both NaD1 and RsAFP1 feature two β-sheet segments, however the only conserved residues are the two cysteine residues (not present in the peptides) used

internal bonding, with the remainder of the β-sheets being composed of different residues for each of the peptides. For further research, the 19mer peptide was chosen (of the two NaD1 derived peptides), due to the increased amyloidogenicity traditionally associated with the flexibility conferred by proline-centred loops (Dubay, K. F. *et al.* 2004).

3.5.2 NaD1-19 Amyloidogenicity

Lyophilised solutions of NaD1-19 were reconstituted in deionised H_2O, pH 8 to a concentration of 4 mg/ml. Solutions were then incubated at 60 ^{o}C for 36 hours, with aliquots removed at intervals and fibril formation monitored using ThT fluorescence. In contrast to the RsAFP-19 peptide, no increase in ThT fluorescence was observed after incubation of NaD1 for up to 36 hours, in fact a slight decrease in fluorescence was observed over that period (Figure 3.11). Further, no nanofibre structures were observed under TEM at any time-point (data not shown). No fibril structures were obtained from NaD1-19 under these conditions. These results correlate with the aggregation propensity score given by TANGO, which showed NaD1-19 had no predicted aggregation propensity (with or without disulfide bonding). Together, these results indicate that the fibril forming propensity of RsAFP-19 is specific to that peptide alone and may be a result of the particular sequence within that peptide. There is no evidence to suggest that amyloid-like fibril formation is a common characteristic of synthesized antifungal peptides, nor is it likely to be related to the activity of these peptides (as similar biological activites are observed for RsAFP-19 and NaD1).

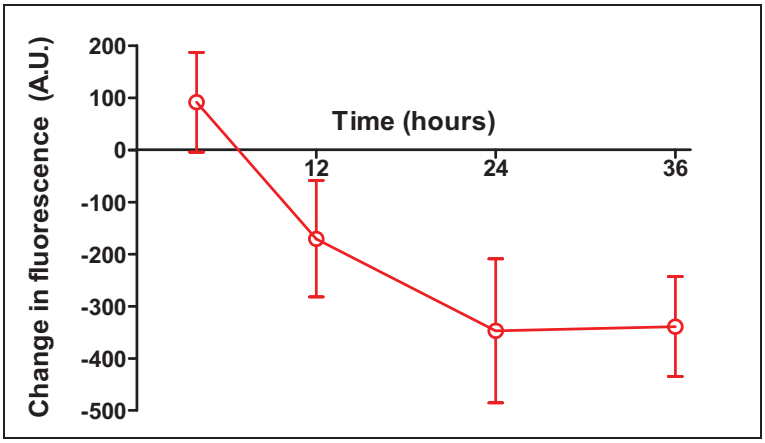

Figure 3.11: ThT fluorescence of NaD1-19 incubated at 60°C over 36 hours.

3.6 Discussion of nanofibre formation by RsAFP-19 and NaD1-19

Amyloid-like fibrils were successfully prepared from antifungal peptide RsAFP-19. Formation of amyloid-like fibrils from new sources is an area of continuing research and development, due to the importance of these protein structures in human disease and the potential use of such protein nanofibres as bionanomaterials (Ecroyd, H. and Carver, J. A. 2008a). Many aspects of the formation and structure of amyloid and amyloid-like fibrils still remain to be determined. In the previous decade, much progress has been achieved in these areas through the use of short amyloid fibril forming peptides (Chiti, F. and Dobson, C. M. 2006; Cherny, I. and Gazit, E. 2008). RsAFP-19 is an amyloid-like fibril forming peptide that has the potential for multiple uses, including in rapid *in vitro* assays of amyloid fibril inhibitors; as a source of long, straight nanofibre structures; and, potentially, as a peptide to which functional domains could be incorporated.

This research has shown that in addition to its antifungal properties, the peptide RsAFP-19 is highly amyloidogenic, displaying a sequence with high amyloid fibril forming propensity and forming nanofibres in H_2O under thermal stress (60 °C) and freeze-thaw stress (3 cycles). RsAFP-19 nanofibres contain all the classical amyloid fibril characteristics, including narrow protofilaments which twist together to form long, straight, non-branching fibrils. The fibrils elongated over time, bind the β-sheet associated fluorophore ThT and show a cross β-pattern under X-ray fibre diffraction characteristic of amyloid-like structures. RsAFP-19's amyloidogenicity is unlikely to be a generic feature of antifungal peptides, despite the high similarity of sequence and bioactivity in these peptides. This conclusion is drawn from the fact that NaD1-19, a second antifungal peptide, exhibited no amyloid fibril forming propensity by sequence analysis or under laboratory experimental conditions which initiate fibril formation in RsAFP-19. The length of RsAFP-19 amyloid-like fibrils produced was observed to alter size depending upon the formation conditions (high temperature vs. freeze-thaw cycling) and the length of incubation. Straight, aligned fibrils were observed under certain formation conditions (high temperature for a short period followed by three months incubation at room temperature). These variations in morphology

indicate that RsAFP-19 may be easily morphologically controlled, a desirable property in base nanomaterials (Rajagopal, K. and Schneider, J. P. 2004; Gras, S. L. 2007; Griffin, M. D. *et al.* 2008). RsAFP-19 is thus an amyloid-like fibril forming peptide, with the potential for use in amyloid fibril formation elucidation or within the wider bionanotechnological industry.

CHAPTER 4

Nanofibre formation from disease-associated mutant protein variants

β2-Microglobulin is the primary protein found in dialysis-related amyloidosis (DRA) amyloid fibrillar deposits (§ 1.2.2.1, Bellotti, V. *et al.* 1998), and thus fibril formation by this protein is an important research area. Difficulties in forming amyloid fibrils from β2-microglobulin *in vitro* under physiological conditions led to the utilisation of destabilised mutant varieties of this protein, such as the N-terminal truncation mutant ΔN6 β2-microglobulin (Esposito, G. *et al.* 2000). Protein aggregation characteristics of such mutants, particularly their nanofibre forming propensity, are of interest for two major reasons: in the search for models to further understand the *in vivo* amyloid formation process of the native protein; and to create *in vitro* systems for testing potential amyloid formation inhibitor molecules.

Ordered aggregation, such as into amyloid fibrils, is a considerably more complex process than that of disordered or amorphous aggregation. As discussed in §1.2.2.3, specific intermediate structures are required for a target protein to misfold into amyloid fibrils (Dobson, C. M. 2004). Induction of amyloid fibril protein aggregates thus involves techniques which are specific to the protein or proteins being destabilised. Furthermore, specific monitoring of the aggregation process and the end products is required to ascertain whether amyloid or amyloid-like fibrils are present (§ 3.3), as alteration in the destabilisation technique may shift the off-pathway folding to an amorphous rather than fibrillar outcome (Uversky, V. N. and Fink, A. L. 2004). Investigations into specific circumstances for amyloid fibril formation by individual disease-related proteins have led to the production of therapeutic treatments for certain amyloid diseases, e.g. use of metal ionophores and chelators to modulate copper and zinc metabolism and potentially prevent amyloid formation in Alzheimer's disease (Bush, A. I. 2008). Thus, much may be gained from investigations into the specific protein aggregation characteristics for each disease-related amyloid fibril forming protein or peptide.

Identification of potential therapeutic molecules is of equal or greater importance as understanding the amyloid fibril forming pathway. For accurate testing of potential amyloid fibril formation inhibitors, *in vitro* amyloid fibril forming systems must be designed. Testing in this manner may be undertaken in two ways;

against the general amyloid-like fibril formation process, or against a specific (disease-related) amyloid fibril forming protein. To be of use in the investigation into amyloid fibril formation modifiers, the amyloid aggregation system must be rapid, reproducible and easily assessable. With this aim, amyloid-like fibrils were formed from R3A β2-microglobulin at physiological pH and temperature. Experiments of other researchers to form β2-microglobulin amyloid fibrils were repeated, but induced using R3A β2-microglobulin seed fibrils as opposed to *ex vivo* sourced or other native β2-microglobulin fibril seeds (Myers, S. L. *et al.* 2006; Jahn, T. R. *et al.* 2008).

4.1 Structure and function of β2-microglobulin

The major histocompatibility complex class one antigens (MHC-1) are found on most human cell surfaces, as well as in a range of physiological fluids (Becker, J. W. and Reeke, G. N. 1985). β2-Microglobulin, when biologically active in its native state is known as human leukocyte antigen (HLA) light chain. It is a 99 residue protein which forms part of the MHC-1, associating with the heavy chain part of the HLA complex and acting in the assembling process and stabilisation of this antigen (Massa, M. *et al.* 2000). As part of its role in human immunity, β2-microglobulin is continuously shed from cell surfaces and transported through the serum for removal *via* the kidneys. In renal failure, β2-microglobulin degradation and excretion is impaired, due to damage in the proximal tubules leading to inefficient catabolism of this protein (Musialik, D. 1989; Floege, J. *et al.* 2001). Further problems arise with the inability of current haemodialysis membranes to remove β2-microglobulin from urine (Ohhashi, Y. *et al.* 2005).

In contrast to its primary role in the MHC system, β2-microglobulin has also been found associated with DRA, an iatrogenic disease associated with haemodialyis treatment (§ 1.2.2.1.1). β2-Microglobulin native and truncated proteins are the major component of DRA amyloid plaques, which are primarily found in osteoarticular sites (Bellotti, V. *et al.* 1998). The characteristics of β2-microglobulin amyloid fibril formation are a target for research, due to the greater opportunities for therapeutic intervention (or prevention *via* alterations to current therapeutic procedures) in treatment-caused diseases such as this.

β2-Microglobulin exhibits the typical β-barrel immunoglobulin fold that is characteristic of the immunoglobulin 'superfamily' of proteins (Becker, J. W. and Reeke, G. N. 1985). Human β2-microglobulin primarily exists, and is most stable, as part of the HLA complex. Early work on β2-microglobulin structure was undertaken by solution-state NMR studies and by comparison with crystal structures of the entire HLA complex (including β2-microglobulin associated with HLA heavy chain protein) (Esposito, G. *et al.* 2000). The solution-structure data determined by NMR spectroscopy, and that of complexed β2-microglobulin, differ from the recently elucidated crystal structure of uncomplexed β2-microglobulin (i.e. not associated with the HLA heavy chain protein, Figure 4.1). The β2-microglobulin crystal state has no 'bulge' evident in the D strand (also known as Strand V) (Trinh, C. H. *et al.* 2002; Corazza, A. *et al.* 2004). The observed differences are argued to be due to the structural characteristics of the crystalline form of β2-microglobulin. It is thought that the D bulge is the native solution structure for this region (Corazza, A. *et al.* 2004), and it is postulated that the form of β2-microglobulin without a bulge (i.e. that seen in the crystal structure) may be an amyloid fibril precursor state (Trinh, C. H. *et al.* 2002).

Figure 4.1: Crystal structures of human β2-microglobulin by Trinh *et al.* (2002), derived from crystal structures of β2-microglobulin when in two interacting conditions, showing A) the complete uncomplexed structure (i.e. β2-microglobulin alone), B) a detailed view of the D strand from uncomplexed β2-microglobulin and c) a detailed view of the D strand of β2-microglobulin as part of the HLA-β2-microglobulin complex showing the D strand bulge.

4.1.1 Structure of mutant R3A β2-microglobulin

The mutant R3A β2-microglobulin protein, one of a range of mutants developed to examine wild-type β2-microglobulin stability, is inherently more unstable than the wild-type protein (Corazza, A. *et al.* 2004). R3A β2-microglobulin remains essentially similar to β2-microglobulin, having only a slightly lowered midpoint of denaturation (4.3 and 4.7 molar units of urea, respectively) and an almost identical *m*-value (derived from the alteration in protein stability upon adding urea) of 3.4 and 3.5, respectively (Smith, D. P. *et al.* 2003). There is a small change in isoelectric point upon mutation, with the pI lowering from 6.07 for β2-microglobulin to 5.73 for R3A β2-microglobulin. Further, R3A β2-microglobulin has a slightly lowered thermodynamic stability compared to the wild type protein (5.9 ± 0.2 and 6.3 ± 0.2 kcal/mol, respectively) (Corazza, A. *et al.* 2004). R3A β2-microglobulin also displays a strong similarity to the wild type solution NMR structure (Esposito, G. *et al.* 2005).

4.2 Amyloidogenicity of β2-microglobulin and R3A β2-microglobulin

Many techniques have been used for the formation of amyloid fibrils *in vitro* from β2-microglobulin, from both *de novo* and *ex vivo* sourced protein (Trinh, C. H. *et al.* 2002). Fibril formation at physiological pH and temperature has been observed to be extremely difficult, and mutation, seeding or other non-physiological influences have generally been used to initiate the fibril formation process (Trinh, C. H. *et al.* 2002; Ma, B. and Nussinov, R. 2003; Naiki, H. *et al.* 2005; Ohhashi, Y. *et al.* 2005; Raman, B. *et al.* 2005; Jahn, T. R. *et al.* 2006; Jahn, T. R. *et al.* 2008) Trinh and co-workers (2002) used detailed NMR analysis of β2-microglobulin and a mutant (P32G β2-microglobulin) to establish a potential native physiological intermediate structure that may be responsible for fibril formation *in vivo*. Another possible fibril initiation process is *via* the presence of amyloid fibrils from a truncated form of β2-microglobulin, ΔN6 β2-microglobulin. These have been observed to constitute approximately 30 % of amyloid plaques within DRA (Bellotti, V. *et al.* 1998). Esposito and co-workers (2000) demonstrated *in vitro* that ΔN6 β2-microglobulin has a much higher amyloidogenicity than the wild-type protein. Further, they were able to extend the length of *ex vivo* DRA amyloid fibrils (the composition of which was unstated)

using both β2-microglobulin and the truncated ΔN6 β2-microglobulin, making the latter form of the protein a strong candidate for *in vivo* enhancement of amyloid fibril formation by the full length protein.

Amyloid fibril formation is a process which can be highly variable in its kinetics. Changes in temperature, buffer salt concentration, pH conditions and agitation rates can lead to marked differences in the rate and extent of fibril formation, and may even affect the morphology of the end product (Trinh, C. H. *et al.* 2002). The variations apparent in amyloid fibril formation by β2-microglobulin include differences in both kinetics and morphology due to changes in pH (Jahn, T. R. *et al.* 2008), the variant of protein used (i.e. the use of wild-type protein or mutant protein) (Smith, D. P. *et al.* 2003), whether seed fibrils are used (i.e. *ex vivo* or *de novo* sourced) (Myers, S. L. *et al.* 2006), ionic strength of buffer (Smith, D. P. *et al.* 2003), the use of ultrasonication (Ohhashi, Y. *et al.* 2005), and with a variety of additives, eg. SDS, TFE, heparin and serum amyloid P component (Yamamoto, S. *et al.* 2004; Myers, S. L. *et al.* 2006). Most of these techniques also require agitation, which also affects the rate, yield and morphology of amyloid fibrils produced (Ohhashi, Y. *et al.* 2005). The differences observed in the morphology of β2-microglobulin fibrils is also reflected in the internal fibrillar structure, with curly fibrils displaying differing FTIR spectra from fibrils which are straight, although the latter had been produced in a variety of ways (Smith, D. P. *et al.* 2003; Jahn, T. R. *et al.* 2008). The variations observed in morphology, and also in the lag-time and speed of fibril formation (Esposito, G. *et al.*), highlight the importance of microscopic analysis of nanofibre formation processes.

The ability of R3A β2-microglobulin to form amyloid-like fibrils has been postulated based upon its close similarity, both in sequence and protein stability to the wild type protein. Protein aggregation and precipitation of R3A β2-microglobulin at pH 6.6 over time in ammonium acetate has been monitored and its interaction with the chaperone protein αB-crystallin established (Pettirossi, F. *et al.* Unpublished data). Under these conditions, R3A β2-microglobulin protein precipitation occurred within 100 hours (~ 4 days); however phosphate buffer (even at low ionic strengths) significantly slows the rate of R3A β2-microglobulin

precipitation. Other research has demonstrated that αB-crystallin still provides chaperone protection against wild type β2-microglobulin fibril formation even at low pH (Raman, B. *et al.* 2005).

4.3 R3A β2-microglobulin nanofibre formation

R3A β2-microglobulin formed protein nanofibres upon incubation at physiological temperature with orbital shaking at 700 rpm in 0.1 M sodium phosphate, 20 mM ThT, pH 7.4. Figure 4.2 shows a lag phase of up to 4 days, followed by an increase in fluorescence (indicating an increase in β-sheet structure) and a plateau after 14 days. Variations in ThT fluorescence readings increase markedly after 12 days, as seen in the large range in standard error beyond this time point (from ~ 40 AU at 12 days to ~ 200 AU at 16 days). No fluorescence was observed from 20 mM ThT in 0.1M sodium phosphate buffer, pH 7.4 after 16 days incubation with shaking.

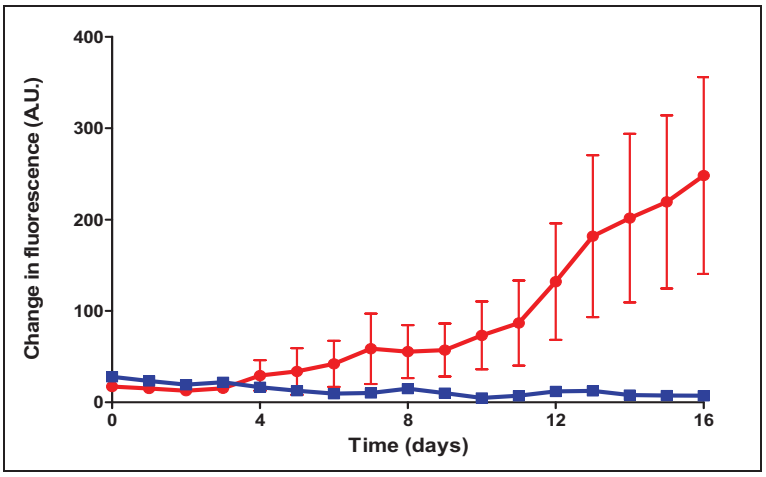

Figure 4.2: ThT fluorescence of R3A β2-microglobulin (●) or ThT alone (■), incubated at 37°C in 0.1 M phosphate buffer, 10 mM ThT, pH 7.4 with orbital shaking at 700 rpm. Results are mean ± SE from 3 experiments.

Light scatter measurements were also acquired, using R3A β2-microglobulin in buffer alone, to assess whether the presence of ThT altered nanofibre formation by this protein. In some situations, β2-microglobulin mutants produce small amounts of fibrillar matter which are undetectable by ThT fluorescence (Myers, S. L. *et al.* 2006), making light scatter analysis an important tool for aggregation monitoring of this protein and its variants. In this set of analyses, no difference was observed in the lag phase or rate of fibril formation in the presence or absence of ThT, except that the plateau phase after day 14 was more marked using light

scatter (Figure 4.3). The increase in standard error after day 12 was still observable by light scatter, indicating that this is variation in the fibril formation.

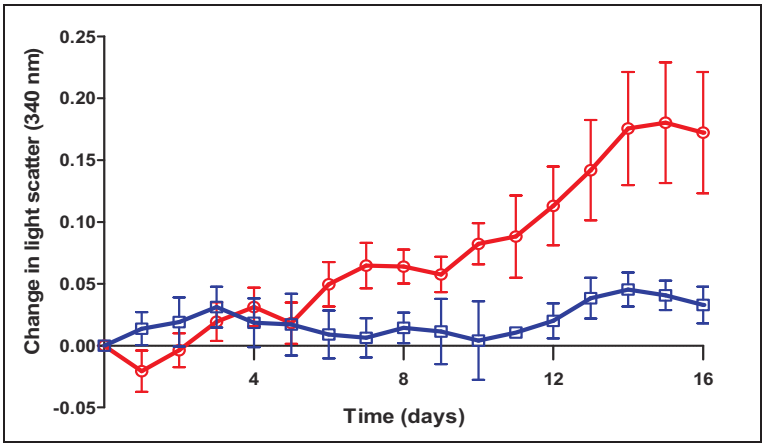

Figure 4.3: Light scatter at 340 nm of R3A β2-microglobulin (○) or buffer alone (□), incubated at 37 °C in 0.1 M sodium phosphate buffer, pH 7.4 with orbital shaking at 700 rpm. Results are mean ± SE from 3 experiments.

TEM was used to confirm nanofibre formation, and showed the presence of protofibrils and fibrils over the 16 day incubation (Figure 4.4). Limited numbers of individual fibrils were observed in all samples. At 8 days, the fibrils appeared similar to seed fibrils or protofibrils, being short in length and frequently curved, which may indicate a high degree of flexibility (Knowles, T. P. *et al.* 2007), and showed a marked tendency to aggregate (Figure 4.4A). They were approximately 10 nm in diameter and developed in length over time, from curly fibrils of up to 50 nm in length (Figure 4.4A and B, 8 and 12 days, respectively) to longer straighter fibrils of up to 300 nm in length (Figure 4.4C, 16 days).

As part of experimental procedure for investigation into inhibitors into amyloid fibril formation (§ 7.3.4), R3A β2-microglobulin was incubated in the presence of immobilised bovine serum albumin (BSA) for 12 days. In the presence of immobilised BSA, amyloid-like fibril formation by R3A β2-microglobulin was enhanced and straight fibrils of up to 300 nm, composed of twisting filaments were visible (Figure 4.4D). No difference was observed in ThT fluorescence between R3A β2-microglobulin alone or in the presence of immobilised BSA (§ 7.3.4). Further, immobilised BSA would not form fibrils under the stated conditions, as it is covalently immobilised to an FEP surface and thus unable to undergo extreme structural rearrangement (§ 7.2.2). The fibrils observed at 12 and

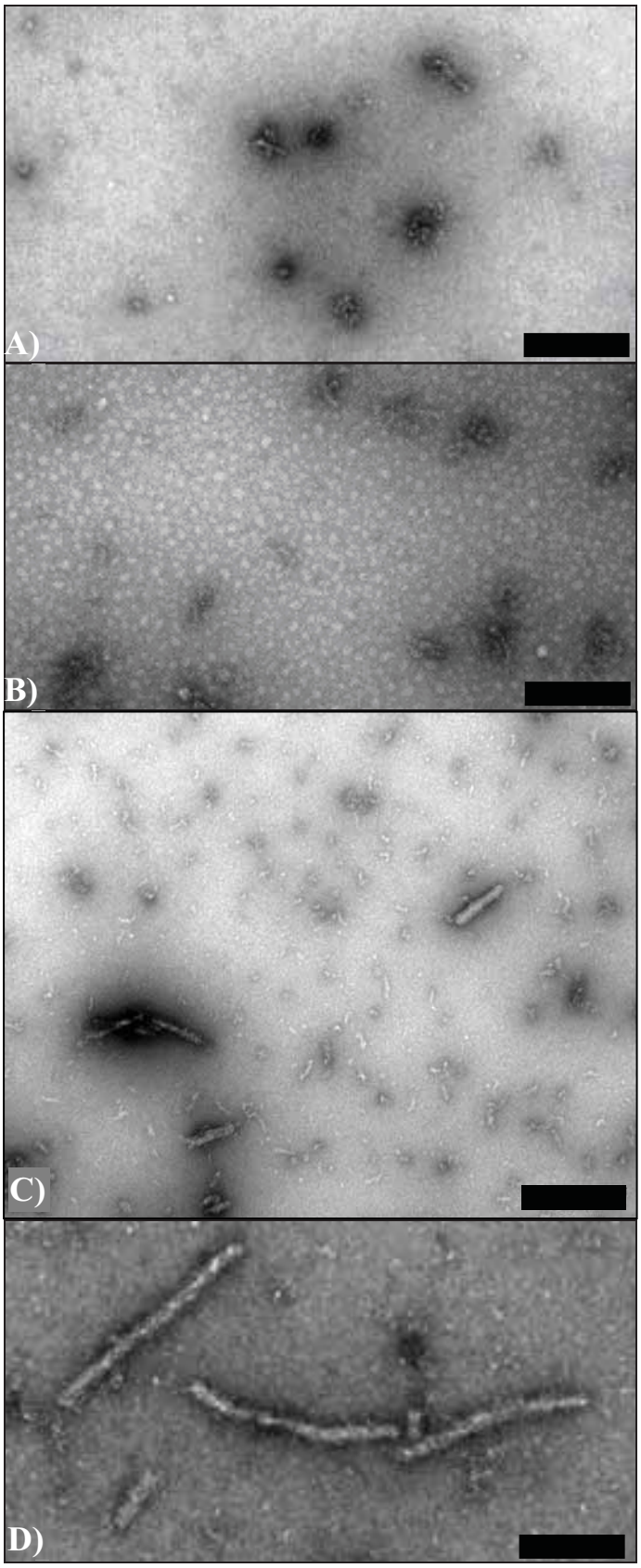

Figure 4.4: TEM of R3A β2-microglobulin amyloid fibrils produced over time at 37°C in 0.1 M Phosphate, 10 mM ThT, pH 7.4 with orbital shaking at 700 rpm after A) 8 days; B) 12 days; C) 16 days; and D) 12 days in the presence of immobilised BSA. All scale bars are 200 nm.

16 days (Figure 4.4C and D) are characteristic of *ex vivo* and *in vitro*, neutral pH-formed β2-microglobulin amyloid fibrils (Jahn, T. R. *et al.* 2008). Short curly aggregates were also observed in all three samples, which may be either protofibrillar species (Knowles, T. P. *et al.* 2007) or the curled morphology fibrils β2-microglobulin is known to form at intermediate pH ranges (Jahn, T. R. *et al.* 2008). If the latter, these may have arisen due to changes in pH stability (observed *via* the lower isoelectric point) from the R3A mutation compared to wild type β2-microglobulin.

Despite the clear ThT fluorescence changes, there was a low yield of visible R3A β2-microglobulin fibrils by TEM, with the majority of images from all samples being similar to that seen in Figure 4.5A. This finding is characteristic of β2-microglobulin proteins (wild type and mutant) at physiological pH (Jones, S. *et al.* 2003), with the majority of studies on this protein being performed at low pH to increase yield (Jahn, T. R. *et al.* 2006). For the investigation of amyloid fibril formation inhibitor molecules, low pH assays are of limited use due to the requirement of physiological conditions for therapeutic strategies. Instead, *in vitro* amyloid-like fibril formation assays must be designed which are effective at as close to physiological conditions as possible.

R3A β2-microglobulin seed fibrils were used to induce native β2-microglobulin fibril formation (§ 4.3.1). β2-microglobulin fibrils are known to be pH sensitive and can become unstable at neutral pH, it is thus common to stabilise β2-microglobulin fibrils prior to seed formation (Jahn, T. R. *et al.* 2008). Seed fibrils were formed by taking a sample at a 16 day time-point, stabilising the fibrils with 20 % TFE then breaking the fibrils into small seeds by sonication for 10 mins (§ 2.3.2.1.2). Figure 4.5B shows the successful breaking up of the semi-fibrillar masses characteristically observed in R3A β2-microglobulin nanofibre-containing samples.

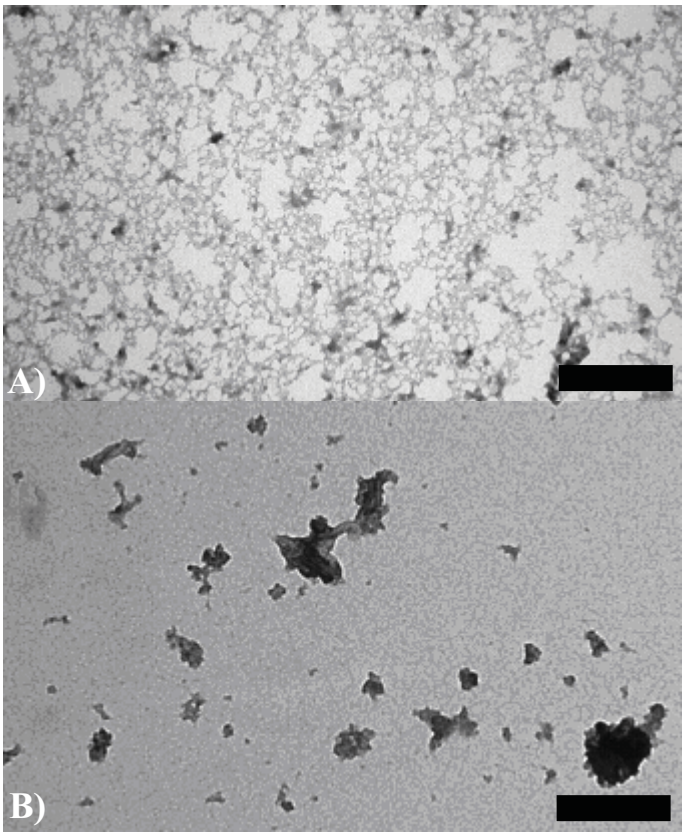

Figure 4.5: TEM of R3A β2-microglobulin nanofibre species produced over time at 37 °C in 0.1 M sodium phosphate, pH 7.4 with orbital shaking at 700 rpm after A) 16 days and B) 16 days stabilised with 20 % TFE followed by sonication for 10 minutes (seed fibrils). Scale bars are 200 nm.

4.3.1 β2-microglobulin nanofibre formation

β2-Microglobulin formed nanofibres after the addition of 20 % v/v R3A β2-microglobulin seed fibrils. Solutions were incubated at 37 °C under orbital shaking at 700 rpm in the presence of 20 mM ThT and the fluorescence measured approximately twice every 24 hours for 16 days (Figure 4.6). No fibril formation, as monitored by ThT fluorescence, occurred for between 4 and 8 days, followed by an increase in fluorescence. Large variation was observed in both the lag time and end-points of seeded fibril formation in samples which were prepared identically and run simultaneously (e.g. β2-microglobulin samples 1 and 2, Figure 4.6). Kinetic variation is quite characteristic of β2-microglobulin protein aggregation and precipitation (Corazza, A. *et al.* 2004). There may also be some variation in amyloid fibril formation from seeding if there are differences in amyloid seed size, due to the role that fibril seeds have on the rate-limiting steps in the nucleation-dependent amyloid fibril forming pathway (Ecroyd, H. and Carver, J. A. 2008a).

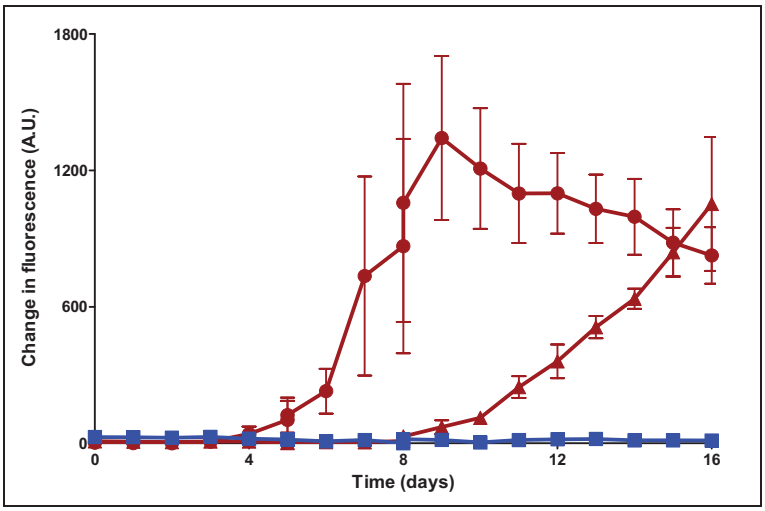

Figure 4.6: ThT fluorescence of β2-microglobulin with 20 % v/v seed fibrils (samples 1: ● and 2: ▲) or ThT alone (■), incubated at 37°C in 0.1 M phosphate buffer, 10 mM ThT, pH 7.4 with orbital shaking at 700 rpm. Results are mean ± SE from 3 experiments.

As with R3A β2-microglobulin, light scatter was tested as a second method of monitoring nanofibre formation. Unlike R3A β2-microglobulin results, there was no correlation between the light scattering results and those observed for ThT fluorescence (Figures 4.6 and 4.7). This may be due to the formation of early non-ThT-binding aggregates, which have been previously observed for β2-microglobulin amyloid fibril formation (Kad, N. M. *et al.* 2003). Light scattering does not discriminate between the formation of amyloid fibrils and amorphous aggregates. In this situation, the presence of large non-fibrillar aggregates, such as were previously observed, could mask the fibril formation kinetics. It has been postulated that these aggregates provide a potential, but not essential, scaffold from which β2-microglobulin can form into nanofibres (Kad, N. M. *et al.* 2003; Ohhashi, Y. *et al.* 2005). These aggregates when examined by TEM were too large for clear imaging (data not shown).

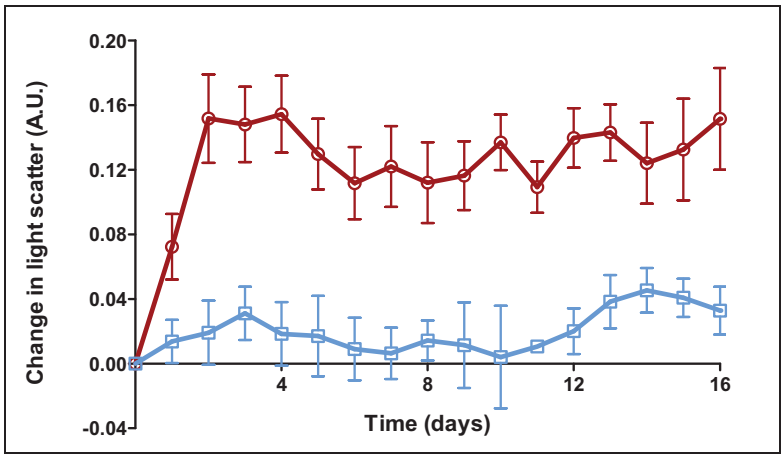

Figure 4.7: Light scatter at 340 nm of β2-microglobulin with 20 % v/v seed fibrils (○) or sodium phosphate buffer alone (□), incubated at 37 °C in 0.1 M sodium phosphate buffer, pH 7.4 with orbital shaking at 700 rpm. Results are mean ± SE from 3 experiments.

To assess whether nanofibres were produced both with and without ThT, β2-microglobulin fibrils were assessed by TEM. Semi-fibrillar material was observed in samples of seeded β2-microglobulin incubated without ThT (Figure 4.8A). This semi-fibrillar material was also the predominant matter observed in seeded β2-microglobulin (with ThT) incubated samples (Figure 4.8B), although some distinct fibrils were visible in these latter samples. Such web-like material is often seen during fibril formation (§ 5.2.5), and has been acceptably referred to as fibrillar matter by this laboratory in the past (Meehan, S. *et al.* 2004) and by other workers (Appel, T. R. *et al.* 2005; Lundmark, K. *et al.* 2005). However, the lack of clear fibrils in the images, combined with the presence of a high ratio (20 % v/v) of fibril-seeds in the original sample, makes it difficult to determine whether new (seeded) fibril formation occurred over incubation.

4.4 Discussion of nanofibre formation by R3A β2-microglobulin and seeded wild-type β2-microglobulin

Amyloid-like fibrils were successfully prepared from two sources, the mutated protein R3A β2-microglobulin and β2-microglobulin initiated with R3A β2-microglobulin amyloid fibril seeds.

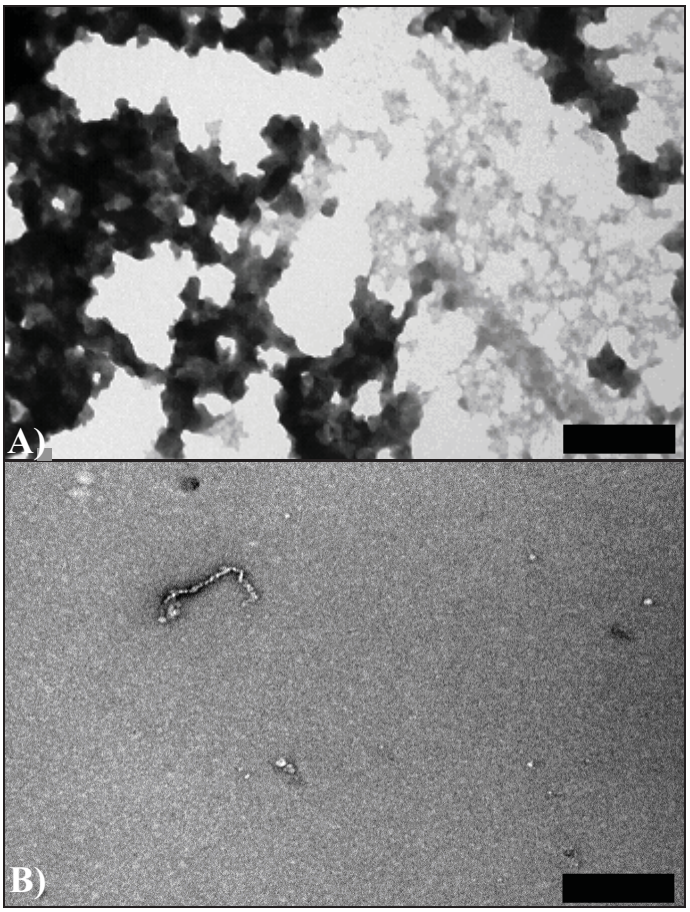

Figure 4.8: TEM of β2-microglobulin nanofibres produced over 16 days incubation at 37°C in 0.1 M sodium phosphate, pH 7.4 with orbital shaking at 700 rpm after the addition of A) 20 % v/v seeds, or B) 20 % v/v seeds and 20 mM ThT. Scale bars are 200 nm.

Fibril formation by R3A β2-microglobulin was achieved at physiological pH and temperature, in 0.1 M sodium phosphate buffer. Nanofibre formation was observed to display reproducible kinetics by both ThT fluorescence and light scatter at 340 nm. Thus R3A β2-microglobulin aggregation, under these conditions, is an amyloid-like fibril formation assay which could be followed by either technique. Fibrils with characteristics typical for physiologically formed (initiated using fibril seeds or mutation) β2-microglobulin fibrils were seen in samples after 12 and 16 days of incubation. These fibrils are similar in morphology to those observed by other researchers, derived at pH 2.5, which are characteristically ~12 nm in diameter with a straight morphology and may show helical twisting (Esposito, G. *et al.* 2000; Jahn, T. R. *et al.* 2006; Jahn, T. R. *et al.* 2008). Shorter fibrils of a curly morphology, were also present in these samples. These fibril structures are more characteristic of β2-microglobulin fibrils formed at intermediate pH (3.5) or under high ionic conditions (Smith, D. P. *et al.* 2003;

Jahn, T. R. *et al.* 2008). Curly amyloid fibrils similar to these have been argued to be a protofibrillar structure on the path to complete amyloid fibril formation (§ 1.2.2.2, Knowles, T. P. *et al.* 2007). R3A β2-microglobulin incubated under physiological conditions forms nanofibres with characteristic amyloid morphology and features within a 14 day timeframe. The formation of these nanofibres may be followed using light scatter or ThT fluorescence and can be confirmed using TEM. From these results, R3A β2-microglobulin nanofibre formation would be an effective model system for *in vitro* assessment of β2-microglobulin amyloid fibril formation inhibitors.

Addition of R3A β2-microglobulin seed fibrils successfully induced amyloid fibril formation by β2-microglobulin, when incubated at physiological pH and temperature for 16 days. ThT fluorescence demonstrated a high variability of fibril formation under these conditions. In particular, a variation of up to 4 days was observed in the lag phase of fibril formation. Such a variation reduces the reliability of this system for use in assessing amyloid fibril formation inhibitors. Light scattering was deemed unreliable to monitor β2-microglobulin seeded nanofibre formation as it is unable to differentiate between amorphous and amyloid-fibrillar aggregation. Instead light scattering provided further evidence of the presence of non-fibrillar aggregate species from early in the β2-microglobulin incubation, potentially correlating to amorphous structures observed by other researchers (Kad, N. M. *et al.* 2003). Fibril structures observed after 16 days of seeded β2-microglobulin incubation appeared as a fibrillar mesh, with very few discrete fibrils observed. From these results it appears that β2-microglobulin seeded with R3A β2-microglobulin fibril seeds is an unreliable model system for *in vitro* assessment of β2-microglobulin fibril formation inhibitors. The high variability of nanofibre formation lag time and inability to reliably follow fibril formation by TEM means that control amyloid fibril formation would be difficult to quantify, thus providing too much scope for error in monitoring the inhibition of β2-microglobulin amyloid fibril formation.

Dialysis-related amyloidosis is known to be greatly enhanced, if not specifically caused, by haemodialysis, the standard treatment for renal disease (Farrell, J. and

Bastani, B. 1997). Prevention of DRA is thus of great interest, due to the accessible nature of a major causative factor (i.e. the haemodialysis membrane) and the recognition of the foremost associated protein (β2-microglobulin). Reliable assay conditions for β2-microglobulin amyloid fibril formation under physiological conditions *in vitro* are widely acknowledged to be challenging (Pettirossi, F. *et al.*; Jones, S. *et al.* 2003; Jahn, T. R. *et al.* 2006). This research characterises the amyloid-like fibril formation kinetics and morphology of the R3A mutant of β2-microglobulin. This mutant is extremely similar in structure to β2-microglobulin, but forms amyloid-like nanofibres within a short timescale (i.e. under 16 days) that can be easily monitored by multiple techniques. This establishes R3A β2-microglobulin amyloid-like fibril formation as a reliable assay for examining inhibitor substances to β2-microglobulin amyloid formation, and thus potential therapeutic strategies for the prevention of DRA.

CHAPTER 5

Protein nanofibres of defined morphology prepared by structural modification of crude lens crystallin mixtures

Amyloid fibrils, in addition to their role in disease processes, are a form of protein nanofibre with potential biotechnological applications (§ 1.2.2.4). Amyloid and amyloid-like fibrils display a number of common properties desirable to the bionanotechnology industry (MacPhee, C. E. and Woolfson, D. N. 2004), including a high level of stability, resistance to enzymatic degradation, strength and a long fibrous morphology (Makin, O. S. and Serpell, L. C. 2005; Smith, J. F. *et al.* 2006; Knowles, T. P. *et al.* 2007). These features are a result of the characteristic structure of amyloid fibrils, where β-sheets are arranged in a 'cross-β' conformation (§ 1.2.2.2) that is distinct from the structure adopted by the amyloidogenic protein in its native state (Zandomeneghi, G. *et al.* 2004). However, if protein nanofibres are to find commercial use then cheap and readily available sourced protein will be required. This chapter aims to form and characterise nanofibres from an inexpensive protein source (lens crystallin proteins) for potential use as a nanomaterial.

5.1 Amyloid-like fibrils as bionanomaterials

The potential role for amyloid-like fibrils in the bionanotechnology industry is a topic of growing interest. The ability of proteins to self-assemble into nanofibrillar structures, which can feature a range of functions, including strength and functionality, provides a new and exciting area of exploration (Zhang, S. 2003). As research continues into the structure of amyloid and amyloid-like fibrils and whether their fibrillar form can be successfully exploited for a variety of nanotechnological uses (Hamada, D. *et al.* 2004), it is important to explore the feasibility of large-scale protein nanofibre production outside of the medical or research laboratory.

The roles of carbon nanotubes within the nanotechnology industry continue to emerge, particularly in the fields of drug delivery (both vaccine and gene) and bioelectronics (Pagona, G. and Tagmatarchis, N. 2006). Protein nanofibres, such as amyloid fibrils, have the potential to supersede carbon nanotubes in many of these roles, as they offer advantages for certain applications due to their readily functionalisable surface and compatibility with aqueous environments (Hamada, D. *et al.* 2004; Waterhouse, S. H. and Gerrard, J. A. 2004; Graveland-Bikker, J. F. and De Kruif, C. G. 2006; Gras, S. L. 2007; Gras, S. L. *et al.* 2008). It has been

shown that amyloid and amyloid-like fibrils can successfully be used as viscosifiers, gelation agents, encapsulators, connectors, templates and scaffolds, as well as being a base for the creation of functionalised fibres (Graveland-Bikker, J. F. and De Kruif, C. G. 2006). In some of these applications, amyloid-like nanofibres can be viewed as an improvement on previous materials, due to the specialised way in which they form, degrade and interact with other molecules (Son, S. J. *et al.* 2007).

One of the benefits of amyloid and amyloid-like fibrils is their ability to self assemble, which provides an attractive feature for material manufacturers (Rajagopal, K. and Schneider, J. P. 2004). This is of particular advantage in the nanotechnological field due to the limitations of 'top-down' assembly methods (creating end-products from large initial products) when fabricating materials on the nanoscale (Aggeli, A. *et al.* 1997). Amyloid-like nanofibres potentially avoid such limitations as they can be produced by the self-association of peptides or proteins (§ 1.2.2.3). This association is a result of non-covalent interactions, rather than covalent bonds (Gazit, E. 2002), which introduces a level of control *via* ready manipulation of fibril formation conditions through pH and temperature variation and chemical modification (Zhang, S. 2003).

The self-assembly of amyloid and amyloid-like fibrils has a second level of external control, as a result of the selection of peptide (or protein) building blocks which contain specific characteristics to be incorporated into the final nanomaterial. There is the potential to design peptides to fill specific needs, a technique which allows for the creation of selectively functionalised amyloid-like fibrils (Deechongkit, S. *et al.* 2005). Due to the extreme structural rearrangement necessary for the formation of nanofibres from native proteins, the original biological functionality is usually lacking in the resultant amyloid fibril (Jiménez, J. L. *et al.* 2002). However, in recent years this image of non-functional amyloid fibrils is being progressively superseded, both by the increasing recognition of biologically driven amyloidin (functional amyloid, § 1.2.2) (Fowler, D. M. *et al.* 2006) and by innovative design and use of selected peptides to create amyloid and amyloid-like fibrils with specific characteristics and functionality (Baldwin, A. J. *et al.* 2006; Cherny, I. and Gazit, E. 2008; Gras, S. L. *et al.* 2008).

The design and manufacture of peptides for the specific purpose of protein nanofibre manufacture open many possibilities within the field of functional nanofibres. However, many of the potential uses of fibrils require only a basic nanofibrillar β-sheet structure. For these materials, the most desirable base substance is a readily available and inexpensively sourced protein (Waterhouse, S. H. and Gerrard, J. A. 2004). The amyloid fibril structure is argued to be an energetically stable state available to all proteins (Chiti, F. and Dobson, C. M. 2006) since it is reliant on the polypeptide backbone, common to all peptides and proteins (§ 1.1). The relative propensity, however, of individual proteins to self-assemble into specific forms is dependent on the stability of their native state and also the physico-chemical properties of their specific sequence (Dubay, K. F. *et al.* 2004). Thus sourcing a supply of protein that readily forms protein nanofibres for commercial manufacture requires careful consideration. Particular care is needed to establish the pH, temperature and solution conditions that will provide an intermediary structure able to lead to amyloid-like fibril formation, as opposed to amorphous aggregation (Uversky, V. N. and Fink, A. L. 2004). The vast majority of amyloid and amyloid-like fibrils reported to form *in vitro* to date, have been generated from small (laboratory scale) quantities of purified proteins. The cost, in both time and consumables, of purifying proteins would hinder the large-scale manufacture of amyloid-like fibrils for nanomaterials. As noted by Kane and Stroock (2007) 'important challenges remain, such as scaling up the manufacture of nanomaterials and protein… creation of standard building blocks and linkages to allow for the rapid development of new assemblies…'. Thus if amyloid-like fibrils are to be used in the nanotechnology industry, then mechanisms will be required for their manufacture that utilise inexpensive, crude mixtures of protein.

5.1.1 Sourcing protein nanofibres

The ability of proteins within crude mixtures to form into amyloid fibrils is incontestable, particularly when one considers the prevalence of amyloidoses *in vivo* amongst different species. Studies into the composition of amyloid plaques found in Alzheimer's disease within humans have shown that a single amyloid fibril forming protein can associate (while on its fibril forming pathway) with nearly 500 different proteins (in native and non-fibrillar states), all of which can be co-isolated with a plaque and that the plaque core itself can consist of up to 26

proteins (Liao, L. *et al.* 2004). Thus, the goal of finding cheap heterogeneous protein sources that can be transformed into amyloid-like fibrils should be achievable, if the right combination of protein source and conditions are found.

To date, *in vitro* studies into amyloid and amyloid-like fibril formation have focused almost exclusively on fibril formation from pure preparations of peptides or proteins, rather than composite mixtures, even when examining disease related peptides and proteins (Chiti, F. and Dobson, C. M. 2006; Munishkina, L. A. and Fink, A. L. 2007; Murphy, R. M. 2007). Where mixed fibrils containing more than one polypeptide sequence have been formed, it has been from solutions containing a combination of highly purified peptides or proteins (MacPhee, C. E. and Dobson, C. M. 2000; Gras, S. L. *et al.* 2008). Crude egg products have been used to form amyloid-like structures (Pearce, F. G. *et al.* 2007); however, the low yield makes this source unsuitable for industrial purposes using current methods. Pure proteins from cheap sources have also been examined for inexpensive nanofibre production purposes. Bovine serum albumin (BSA) has been shown to form aggregates with amyloid-like characteristics within a very short timeframe, but these aggregates do not feature the protease resistant characteristics of true mature amyloid-like fibrils (Holm, N. K. *et al.* 2007). The casein milk proteins are another potential source from which to make amyloid fibrils (§ 6.2), although with current methods a high level of purification is essential due to the molecular chaperone capabilities of some casein proteins within this composite mixture (Thorn, D. C. *et al.* 2005; Thorn, D. C. *et al.* 2008).

In this chapter, the manufacture of protein nanofibres from crude extracts of industrial waste proteins is described, using the crystallin proteins of mammalian eye lenses sourced from abattoirs. This protein source was selected because mammalian eye lenses are a rich source of well structured β-sheet proteins. As discussed previously (§ 1.3.1), mammalian eye lenses are composed almost entirely of proteins, predominantly α, β and γ crystallin (Siezen, R. J. and Argos, P. 1983). The supramolecular arrangement of these crystallin proteins is responsible for the refraction of light and therefore lens transparency (Harrington, V. *et al.* 2007). Mutant γ-crystallin proteins have been associated with

amyloidoses *in vivo* (Sandilands, A. *et al.* 2002) and all crystallin proteins form amyloid fibrils *in vitro* (Meehan, S. *et al.* 2004). Furthermore, the use of simple changes to buffer conditions to alter the morphology of the resulting amyloid fibrils is described, demonstrating the feasibility of using inexpensive proteins to form amyloid fibrils with a variety of different morphologies and open up the possibility of efficient and cheap nanofibre production. This work forms the basis of an invited submission to the International Journal of Nanotechnology (IJNT): Garvey M, Gras SL, Meehan S, Meade SJ, Carver JA and Gerrard JA. "Protein nanofibres of defined morphology prepared from mixtures of crude crystallins". *Int. J. Nanotechnol.,* Vol. 6, Nos. 3/4, 2009; 258-273.

5.2 Protein nanofibres formed from crude crystallin mixtures

5.2.1 Extraction of crystallin proteins

Cow, sheep and deer lenses were homogenised and the crystallin proteins extracted (§ 2.2.1.1). Each lens yielded approximately 20 mL of mixed crystallin protein solution at a concentration of 10.01 mg/mL (± 0.42 mg/mL) per lens, as measured using a Bradford assay with BSA standards (Figure 5.1). This equates to ~200 mg (± 42 mg) of crystallin protein within each bovine lens (20 mL x 10 mg/mL / 1 lens). This finding is within error of previous estimations of crystallin protein concentration, found to be within 230 and 440 mg/mL for human (Fagerholm, P. P. *et al.* 1981) and bovine lenses (Delaye, M. and Tardieu, A. 1983). The slightly lower observed protein concentration isolated from the lens is most likely due to isolation techniques, with previous estimates based on X-ray analysis on the intact lens or after freeze-dry sectioning.

5.2.2 Separation and purification of crystallin proteins

Extracted crystallin proteins from cow, sheep and deer lenses were separated *via* SEC (§ 2.2.1.2). Chromatographs and SDS analysis showed that there was very high similarity of protein composition and their respective concentrations between the three species (Figures 5.2, 5.3 and 5.4, for cow, sheep and deer respectively). All three species showed high molecular weight (HMW) species, the HMW peak is composed mainly of α-crystallin subunits (A and B). In cow and sheep lenses these HMW were separated into two peaks, while in deer lenses these formed one large peak (with a slight shoulder) corresponding to the first peak of the other

species. This difference is likely to be due to the age of the animal lenses (< 1 year for cow, unknown for sheep and deer) as HMW proteins have been observed to increase in amount with age in a manner that is thought to be related to increased light scatter in the lens and possibly cataract (Jedziniak, J. A. *et al.* 1975; Carver, J. A. *et al.* 1996).

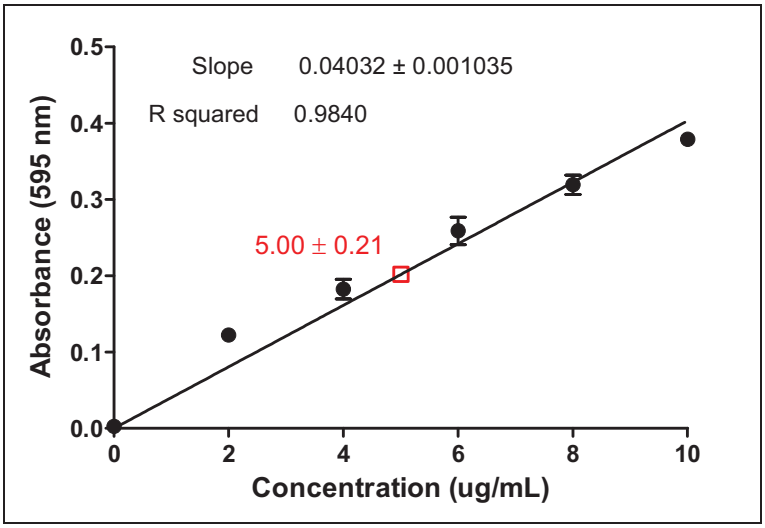

Figure 5.1: Concentration of crystallin protein homogenate (●), extracted from bovine eye lenses (□ , diluted 1:2,000), as assessed by Bradford assay using BSA protein standards.

α-Crystallin proteins from all three species eluted at the same elution volume in the profile and showed almost identical size characteristics upon SDS PAGE analysis, predominantly consisting of two bands near 20 kDa (i.e. αA- ~19.9 and αB- ~20.1 kDa). In cow and deer samples, slight contamination of the HMW and β-crystallins is evident. Two minor bands, at 25 kDa and 17 kDa, are present in the SDS gels. As the sheep SDS-PAGE sample was more diluted, it is possible such contaminant proteins are also present in this sample but are not visible. As described, where pure samples were required SEC sample collection was altered to avoid such contamination (§ 5.2.3).

The β- and γ-crystallin peaks showed only slight variation between the three species. In both sheep and deer lenses the βH-crystallin fraction (composed of hexamers and octomers of the β-crystallins, as isolated by size-exclusion chromatography) made up a larger percentage of the total crystallin protein content (Bloemendal, H. *et al.* 2004). Deer lenses contain a β-fraction which

makes up ~49 % of total crystallin protein and is composed of ~51 % βH- and ~49 % βL-crystallins (dimers and intermediately sized species of β-crystallin subunits) (Chiou, S. H. *et al.* 1988). This trend is observed in the current study, where both deer and sheep lenses were observed to display similar β-crystallin elution profiles. In cow lenses the βL-crystallin peak is seen to be larger than the βH-crystallin peak. This is potentially due to the prevalence of βB2-crystallin, the predominant β-crystallin for both bovines and humans, in this fraction (Horwitz, J. *et al.* 1986; Slingsby, C. and Bateman, O. A. 1990). The β-crystallins, when viewed by SDS-PAGE, had very similar characteristics between the three species. The only variant was a weak band at ~50 kDa, which was observed in the βL-crystallin fractions of sheep and deer, but not cow lenses. This band could be a result of *in vivo* cross-linking of β-crystallin proteins or may be related to a crystallin variant, τ-crystallin which is observed in many vertebrate lenses and has a molecular mass ~47 kDa (Bloemendal, H. *et al.* 2004).

As discussed previously (§ 1.3.3.2), there are seven recognised γ-crystallin proteins in mammalian tissues; γA-F and γS. For ease of reference within this thesis, the γ-crystallins have been classified into three subgroups (as they are separated *via* SEC, Figures 5.2 - 5.4): γS-, γH- and γL- crystallin; with γS-crystallin containing that subunit alone, γH-crystallin containing predominantly γC- with also γA- and γB-crystallins, and γL-crystallin containing predominantly γD- and also γE- and γF-crystallins (Siezen, R. J. *et al.* 1988). Only in the cow lens sample were three γ-crystallin peaks observable during protein separation. The γ-crystallin proteins showed the most variation between the three species, as has been observed previously (Chiou, S. H. *et al.* 1988). The γS-crystallin peak was observed by SEC in the cow lens only, with no separate peak visible for deer or sheep lenses. SDS-PAGE analysis of samples taken at the same elution volume for lenses from all three species, showed a strong γS-crystallin peak for cow and deer lenses, although no visible peak for sheep lenses. Later γ-crystallin peaks (γH- and γL-) were observed for all species by SEC. γ-Crystallins constituted a higher proportion of total crystallin content for deer lens samples than for either cow or sheep lenses, which is in agreement with the findings of Chiou and co-

workers (1988) who found that deer lenses had almost one third higher yield of γ-crystallins than other vertebrate species.

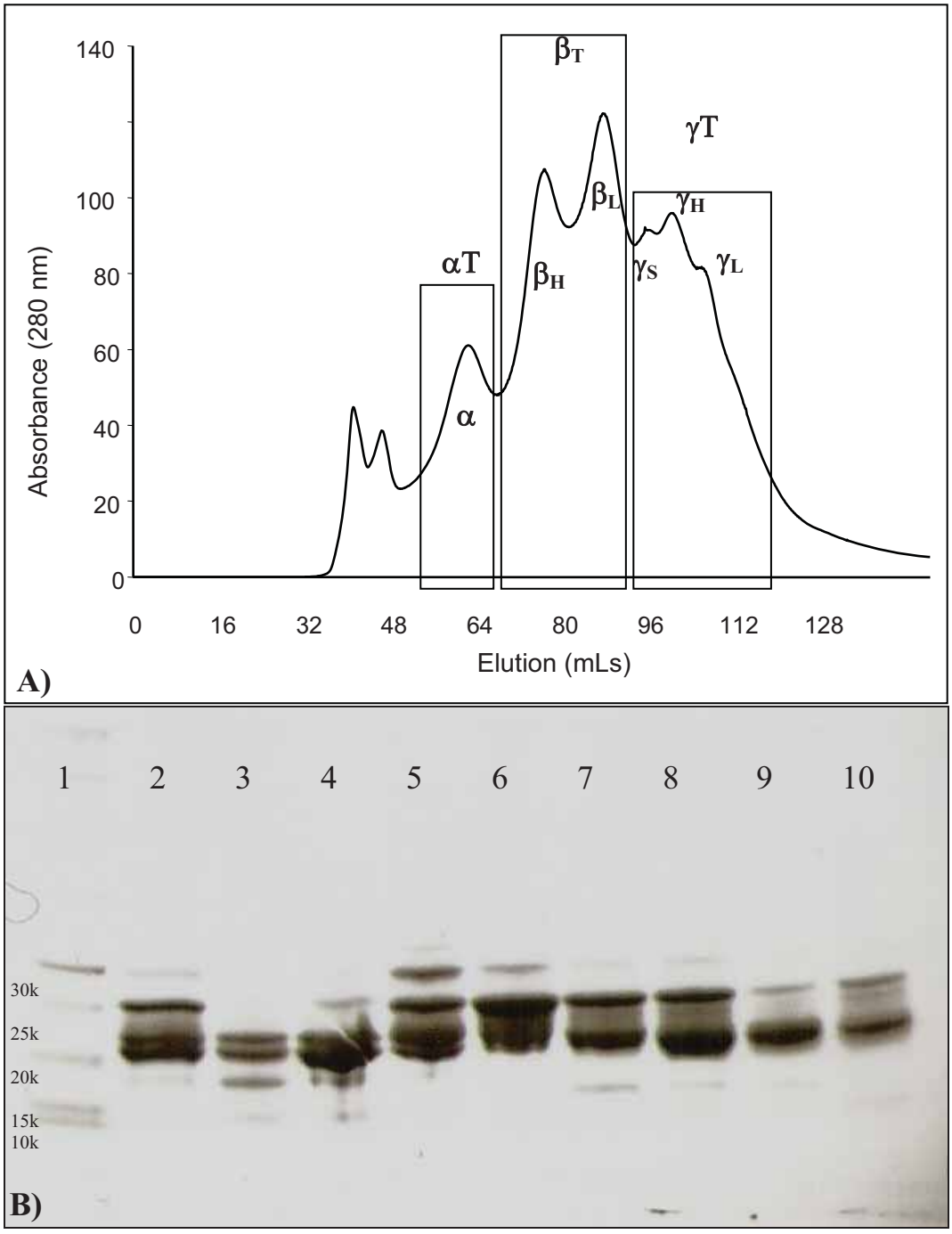

Figure 5.2: Separation of crystallin proteins extracted from bovine eye lenses, A) size exclusion chromatograph showing labelled crystallin fractions. Protein eluting before the α-crystallins were named the high molecular weight (HMW) fraction, and B) SDS-PAGE gel showing crystallin proteins in bovine lens extracts after SEC: 1) molecular weight markers (Fermentas PageRuler unstained protein standard); 2) crude eye lens extract; 3) high molecular weight fraction; 4) α fraction; 5) βH fraction; 6) βL fraction; 7) γS fraction; 8) γH fraction; 9) γL fraction; and 10) second γL fraction (120 ml).

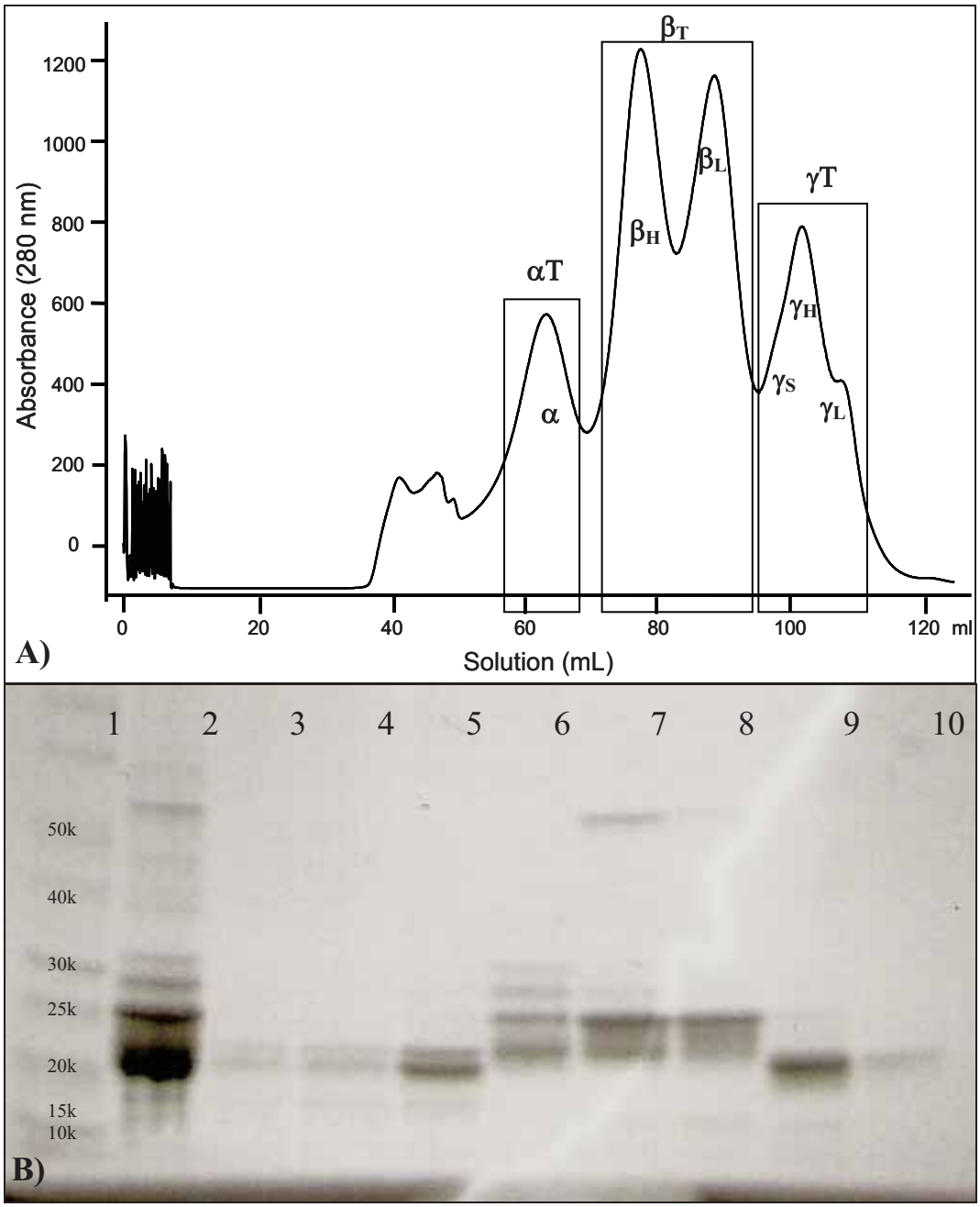

Figure 5.3: Separation of crystallin proteins extracted from ovine eye lenses, A) size exclusion chromatograph showing labelled crystallin fractions. Protein eluting before the α-crystallins were named the high molecular weight (HMW) fraction, and B) SDS-PAGE gel showing crystallin proteins in ovine lens extracts after SEC: 1) molecular weight markers (Fermentas PageRuler unstained protein standard); 2) diluted crude eye lens extract; 3) high molecular weight fraction peak 1; 4) high molecular weight fraction peak 2; 5) α fraction; 6) βH fraction; 7) βL fraction; 8) γS fraction (slight shoulder visible); 9) γH fraction; and 10) γL fraction.

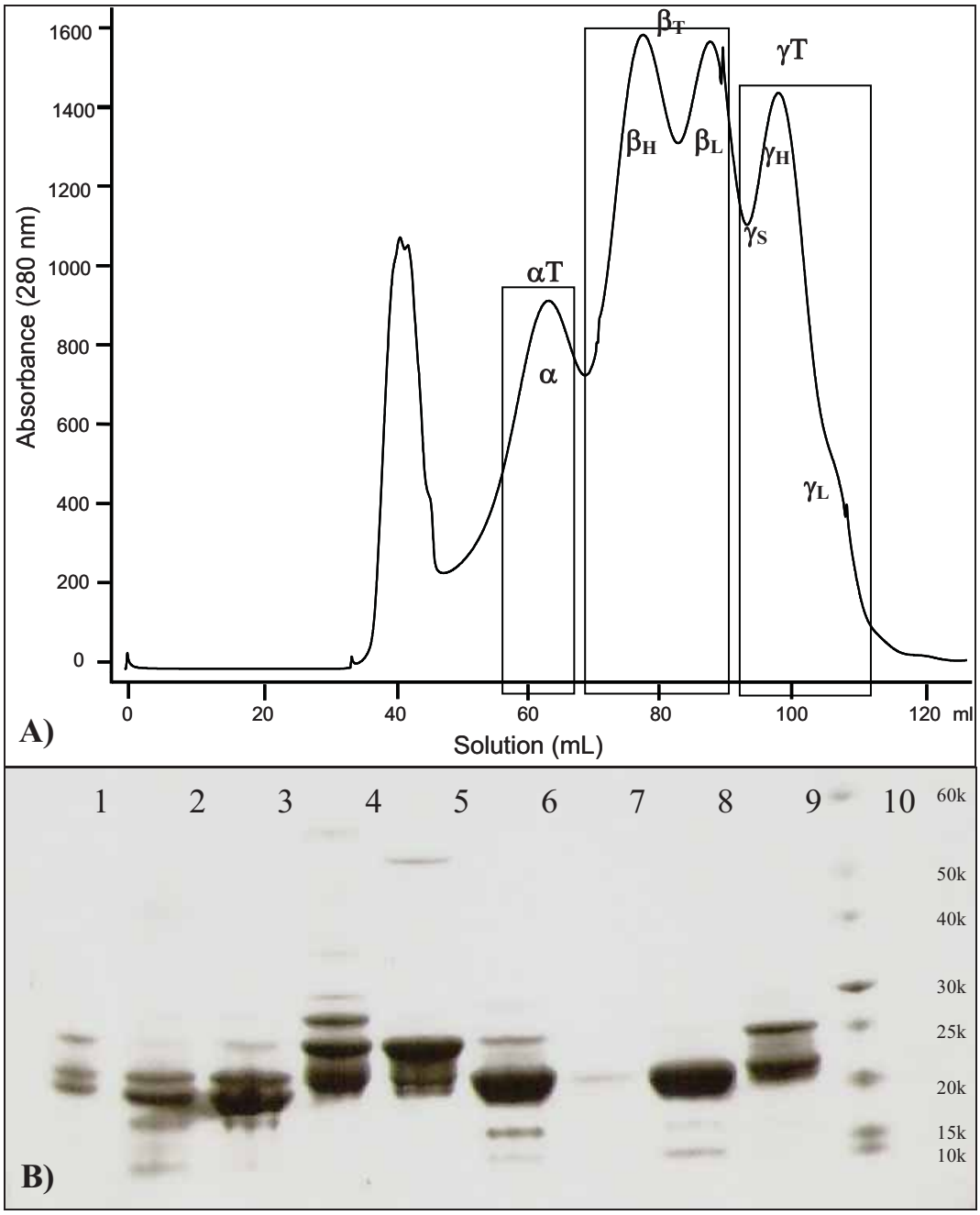

Figure 5.4: Separation of crystallin proteins extracted from cervine eye lenses, A) size exclusion chromatograph showing labelled crystallin fractions. Protein eluting before the α-crystallins were named the high molecular weight (HMW) fraction, and B) SDS-PAGE gel showing crystallin proteins in cervine lens extracts after SEC; 1) very dilute crude eye lens extract; 2) high molecular weight fraction; 3) α fraction; 4) βH fraction; 5) βL fraction; 6) γS fraction (no shoulder visible, sample taken where shoulder seen in bovine and ovine lenses); 7) contaminated lane; 8) γH fraction; 9) γL fraction; and 10) molecular weight markers (Fermentas PageRuler unstained protein standard).

5.2.3 Formation of nanofibres from pure crystallin proteins

Pure crystallin stocks were prepared by collecting the protein corresponding to a single peak from the SEC. Concentrated solutions of three pure crystallins, αT-,

βL- and γL-crystallins (§ 2.2.1.2), were used for nanofibre formation. Only samples with two discrete bands for 19 and 21 kDa for αT-crystallin and a single band at 20 kDa for γL-crystallin (as assessed by SDS-PAGE, § 2.2.4) were used for fibril formation. Protein nanofibres were formed from pure bovine crystallin proteins in H_2O using a mixture of low pH (pH 2), addition of 10 % TFE and thermal destabilisation at 60 °C (§ 2.3.2.1, methods adapted from Meehan, S. *et al.* 2004).

Transmission electron micrographs confirmed the presence of nanofibres in treated samples of pure (αT-, βL-, or γL-) bovine crystallin preparations, as shown in Figure 5.5. Bovine crystallin amyloid fibrils display two distinct morphologies, i.e. long and straight or short and curly in character, and have been demonstrated to contain all characteristics of amyloid fibrils (Meehan, S. *et al.* 2004). These morphologies were observed in the current work, with the αT-crystallin fraction transformed into long, straight, un-branching fibrils (Figure 5.5A) and the βL- and γL-crystallin fractions transforming into short, curly amyloid fibrils (Figure 5.5B and C, respectively). The variable morphology of crystallin-based nanofibres is a potentially desirable characteristic in the bionanotechnology industry, where multiple uses may be required from a single crude protein source.

5.2.4 Formation of nanofibres from semi-pure crystallin mixtures

Semi-purified crystallin stocks were prepared by combining multiple SEC peaks (§ 2.2.1.2), where all peaks in the α-region, β-region or γ-region of the SEC profile were collectively referred to as αT, βT and γT, respectively. Protein collection volume was preferred to protein purification, so some overlap of peaks (i.e. contamination by other crystallin subgroups) was allowed. Combined solutions (semi-purified crystallin stocks) were assessed using SDS-PAGE (§ 2.2.4; Figure 5.6). Contamination is visible in the α_T-crystallin fraction which, in addition to the two α-crystallin bands at 19.8 and 20.1 kDa, shows clear bands at 29, 24 and 14 kDa. These are likely to be due to either HMW or β-crystallin proteins, thus proteins other than those found in pure αT-crystallin (Figure 5.3). Multiple bands are also

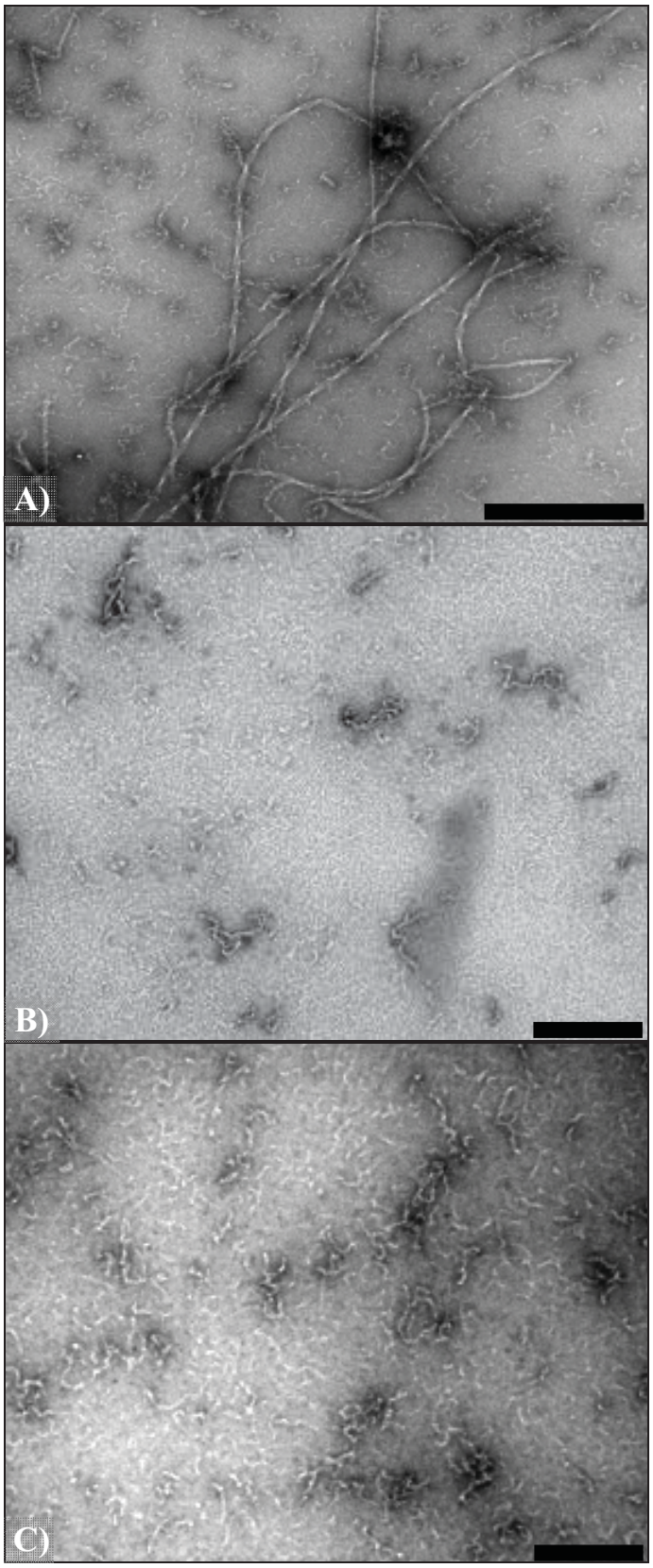

Figure 5.5: Transmission electron micrographs of nanofibres formed from pure crystallin protein stocks, after incubation in H_2O at pH 2 with 10 % TFE, for 18 hours at 60°C: A) αT-crystallin; B) βL-crystallin; and C) γL-crystallin. The scale bars are 1 μm (A) and 200 nm (B and C) in length.

visible in the γT-crystallin fraction, where pure γ-crystallin proteins exist as discrete peaks ~20 kDa, indicating contamination by β-crystallin proteins has occurred. The purity of the βT-crystallin sample is difficult to determine due to the similarity in mass of some β-crystallin proteins and the α- and γ-crystallin proteins (§ 1.3.2). Nanofibres were formed from these semi-purified bovine crystallin proteins (αT, βT or γT) immediately following SEC in 0.1 M Tris, 1 mM EDTA buffer, using a mixture of low pH, TFE addition and thermal destabilisation (§ 2.3.2.1). Fibril formation was assessed by TEM as outlined below.

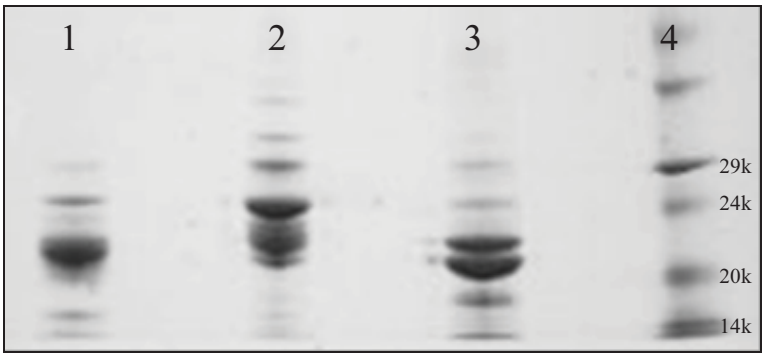

Figure 5.6: SDS-PAGE gel showing the purity of the crystallin proteins in semi-purified crystallin mixtures: 1) α_T fraction; 2) β_T fraction; 3) γ_T fraction; and 4) molecular weight markers (Sigma MWM 14000-66000).

Transmission electron micrographs confirmed the presence of nanofibres in treated samples of semi-pure (αT, βT or γT) bovine crystallin preparations as shown in Figure 5.7. The purification process was found to influence the morphology of αT-crystallin fibrils. In semi-pure preparations (i.e. those still in elution buffer and containing minor contaminants) αT-crystallin fibrils were shorter and more curly (Figure 5.7A) compared to the long straight fibrils observed in pure preparations (Figure 5.6A). In contrast, the morphology of fibrils in the β- and γ-crystallin samples was similar for semi-pure (βT and γT) and pure samples (βL, or γL) (Figures 5.7 and 5.6, B and C). The change in α-crystallin fibril morphology suggests that small quantities of other proteins in the semipurified αT-crystallin fraction (Figure 5.6, § 5.2.2), such as HMW aggregates and β-crystallin proteins, can modify the fibril assembly process.

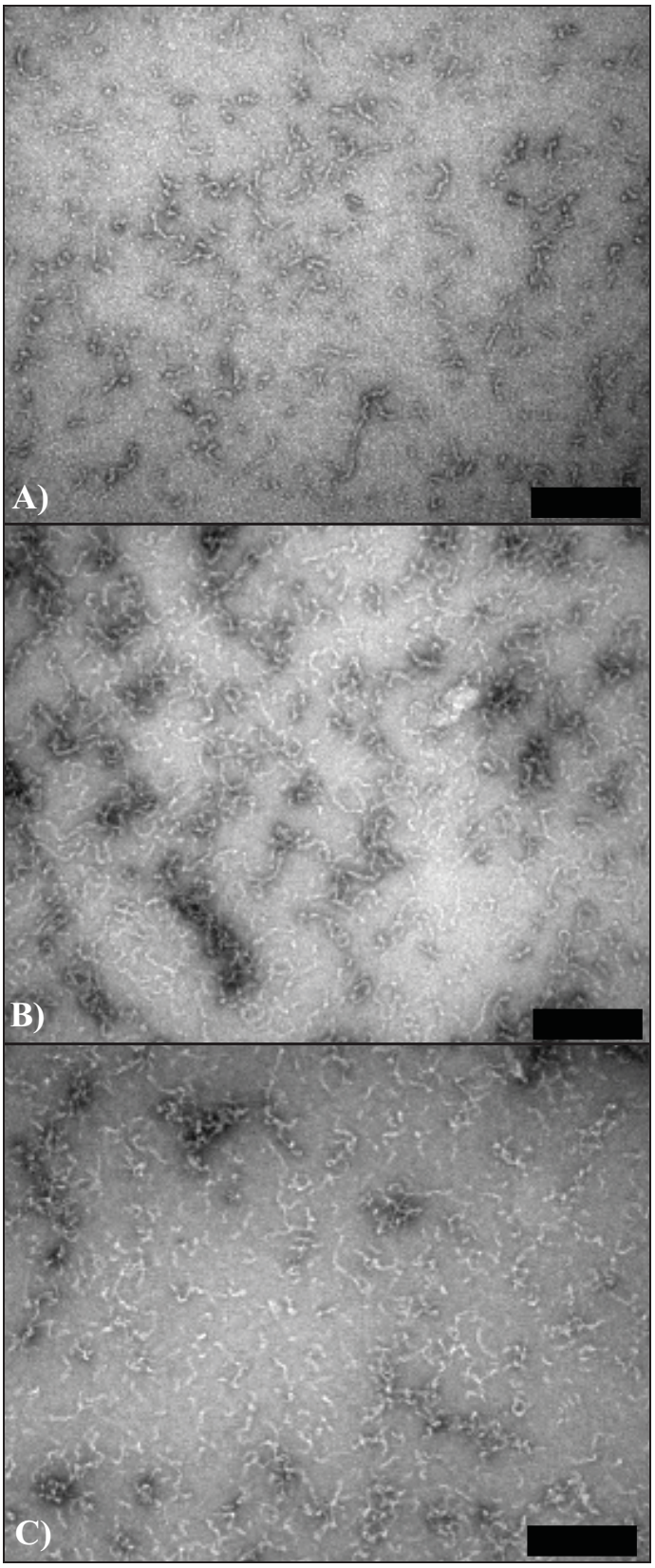

Figure 5.7: Transmission electron micrographs of nanofibres formed from mixtures of crystallin proteins in 50 mM Tris, 1 mM EDTA, pH 2 with 10 % TFE incubated at 60 °C for 18 hours: A) αT-crystallin; B) βT-crystallin; and C) γT-crystallin. Scale bars are 200 nm in length.

The successful formation of nanofibres from these heterogeneous protein mixtures indicates that crystallin proteins have the ability to form into nanofibres while still in the presence of other crystallin proteins. In the case of α-crystallin, despite the presence of the unrelated β-crystallin subunits, fibril formation still occurs. This is a highly desirable characteristic for commercial production within the field of bionanotechnology. Protein homology is likely to be a key factor in the formation of nanofibres from protein mixtures. Indeed, polypeptide sequence similarity influences the efficiency of fibril seeding for both peptides and proteins (O'nuallain, B. *et al.* 2004; Wright, C. F. *et al.* 2005), although dissimilar polypeptides can be incorporated within a single fibril if their rate of self-assembly is matched (MacPhee, C. E. and Dobson, C. M. 2000). The crystallin proteins have high structural homology within their different classes. There is also significant sequence and structural similarity between the β- and γ-crystallin proteins (Siezen, R. J. and Argos, P. 1983), and enough similarity between their domains to facilitate domain swapping between these crystallins (Wright, G. *et al.* 1998). The phenomenon of domain swapping is postulated to be associated with amyloid fibril formation in other proteins (Carey, J. *et al.* 2007). The change in morphology of α-crystallin nanofibres in this study may indicate that sequence similarity within the crystallins allows for the presence of multiple proteins within crystallin nanofibres.

5.2.5 Formation of nanofibres from crude crystallin mixtures

Given the successful formation of protein nanofibres from heterogeneous crystallin mixtures, crude mixtures of bovine crystallin proteins were examined to see if they could form nanofibres without prior purification. Amyloid-like fibril characteristics were examined in detail, including their dye-binding capacity, structural characteristics, proteolytic resistance and their ability to display different morphologies under different assembly conditions.

5.2.5.1 Nanofibres with clumping morphology formed from crude crystallin mixtures

Nanofibres were formed directly from crude mixtures of crystallins after extraction and centrifugation, by diluting one part crude crystallin stock into ten parts 0.05 M Tris, 0.04 % NaN_3 and using the same combination of low pH,

addition of TFE and thermal destabilisation (§ 2.3.2.1). This nanofibre production process was used for crude solutions of bovine, deer and sheep crystallins. Protein nanofibre formation was initially assessed by TEM.

Transmission electron micrographs of treated crude crystallin preparations revealed the presence of nanofibres from all three mammalian lens mixtures, i.e. cow, deer and sheep (Figure 5.8). The morphology of these fibrils was difficult to assess, due to the high rate of clumping observed in the fibril product. These clumps are a common feature of crystallin fibril morphology, and have been previously classified as fibrillar in nature due to associated XRD, Congo red and ThT results (Meehan, S. *et al.* 2004; Meehan, S. *et al.* 2007). Clearly visible in the deer eye lens fibril sample are long curly nanofibres within the fibrillar clumps. Samples such as this may or may not have potential uses in the bionanotechnology industry. These structures may still retain many amyloid fibril characteristics, allowing them to bind amyloid specific dyes and give 'cross-β' diffraction patterns; however, they would be of limited use to markets which require the fibrous aspects (such as for nanowire templating) of amyloid fibrils (Reches, M. and Gazit, E. 2003). To increase the potential product viability, a range of optimizing conditions were investigated using crude bovine lens mixtures to promote individual fibril formation (as opposed to clumps of nanofibres).

5.2.5.2 Nanofibres with individual fibril morphology formed from crude crystallin mixtures

Nanofibre formation from crude bovine crystallin mixtures was trialled at a range of temperatures and with various additives. These alterations were selected due to their potential to affect (i.e. stabilise) particular intermediate species in the off-pathway folding or amyloid fibril formation pathway, thus allowing for the formation of individual fibrils. Table 5.1 outlines the solution conditions trialled for fibril formation from crude bovine lens mixtures.

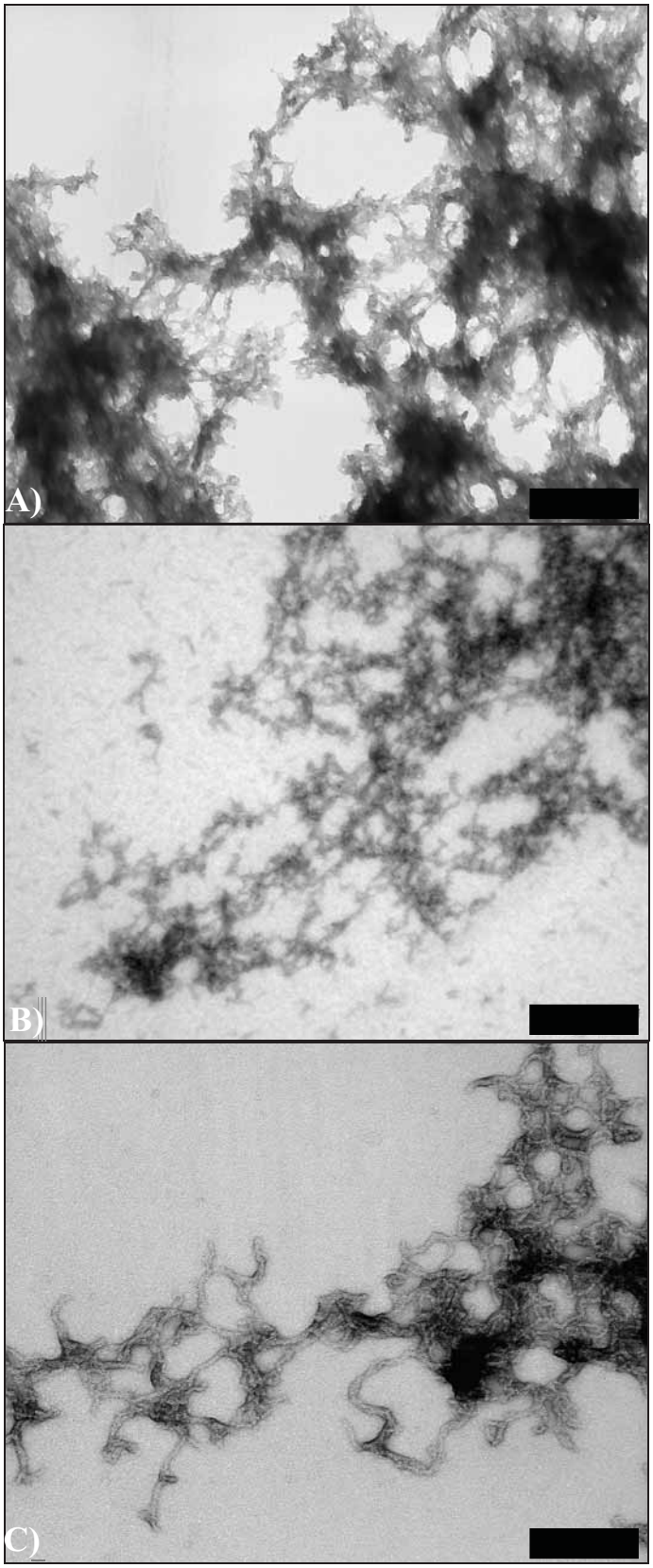

Figure 5.8: Nanofibres with clumping morphology, made at 60°C for 2 hours from solutions diluted 1:10 into 50 mM Tris, pH 2 with 10 % TFE: A) crude bovine crystallins, containing both straight and curly fibrils; B) crude sheep crystallins and C) crude deer crystallins, containing long curly fibrils. Scale bars are 200 nm in length.

Table 5.1: Nanofibre formation conditions trialled with crude bovine lens mixtures, changing one variable each time from the method: 1:10 dilution of multiple bovine lens homogenate, H_2O with 10 % TFE at pH 2, 60 °C for 18 hours.

Altered variable	Reason altered	Nanofibres	Fibril morphology
Lens mixture			
Homogenate from a single lens	Reduce post-translational modification variation	Yes	Clumps
Destabilant			
1 M GdnHCl	Alter intermediate species	No	-
Temperature			
50 °C	Slow off-pathway folding	Yes	Clumps
pH of solution			
pH 7	Slow off-pathway folding	Yes	Clumps
Buffer			
0.1 M Phosphate	Alter intermediate species	Yes	Clumps
0.02 M Tris		Yes	Clumps
0.02 M Tris, 1 mM EDTA		Yes	Individual fibrils

As fibril formation had already been achieved, the trialled optimising conditions were selected as variables that would only minimally effect the nanofibre formation by bovine lens mixtures. As a result most alterations had no obvious effect on fibril morphology. Variations to the homogenate source, incubation temperature and solution pH produced nanofibre clumps identical to those obtained by the original method. Changing the destabilant from TFE to GdnHCl resulted in no fibril formation, implying that the required intermediate species are not present when crystallin protein mixtures are unfolded using this chemical. Whilst GdnHCl has been used to form amyloid fibrils from α-crystallin (Meehan, S. *et al.* 2007), it has been shown that GdnHCl does not produce nanofibres from β- and γ-crystallins, instead inducing amorphous aggregation (S. Meehan, PhD thesis).

Addition of buffer salts to the incubation solution, including 0.1 M sodium phosphate or 0.2 M Tris, also had little effect on nanofibre formation of bovine lens mixtures, again resulting in clumps of fibrils. However, the addition of 1 mM EDTA to a 0.2 M Tris solution led to a significant reduction in clumps of fibrils (after altered pH, TFE and thermal destabilisation), with TEM images showing a preponderance of individual nanofibres. Metal salts are often implicated in amyloid fibril formation, and are thought to increase fibril-fibril interactions for some disease-related amyloidogenic peptides and proteins (Munishkina, L. A. *et al.* 2004; Karr, J. W. and Szalai, V. A. 2008). The addition of EDTA (a known

metal chelator) to the bovine crystallin mixture may have slowed the rate of fibril formation by these proteins, leading to a reduced number of nanofibre clumps. TEM of nanofibres produced in the presence of EDTA revealed the presence of nanofibres of both long and straight morphology and short, curly morphology (Figure 5.9). This finding is interesting given the change in α-crystallin fibril morphology, from straight to curly fibrils, when α-crystallin is mixed with other proteins in semi-pure crystallin preparations (Figures 5.6A and 5.7A). It may indicate that the relative concentration of crystallin proteins in pure, semi-pure and crude mixtures is an important factor that influences fibril assembly and morphology.

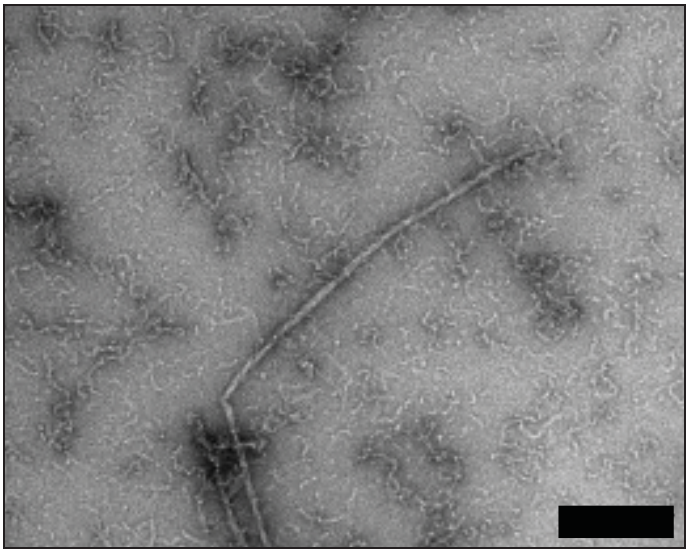

Figure 5.9: Nanofibres, including both straight and curly fibrils, made from homogenate solutions of crude bovine crystallins diluted 1:10 into 50 mM Tris and 1 mM EDTA at pH 2 with 10 % TFE, incubated at 60 °C for 18 hrs. Scale bars are 200 nm in length.

Nanofibres were also produced from crude homogenates of sheep and deer lenses (Figure 5.10A and B, respectively). Finally, nanofibres were produced from a mixture containing equal parts of all three homogenates (cow, sheep and deer), made and incubated under the same conditions as used for bovine crude fibrils (Figure 5.10C). The nanofibres produced from the mixture of lenses had identical morphological characteristics to those observed for each individual species. Thus, it is possible to produce nanofibres from crude mixtures of eye lens proteins from cow, sheep and deer lenses, as well as from a combined mixture of lenses from all three species.

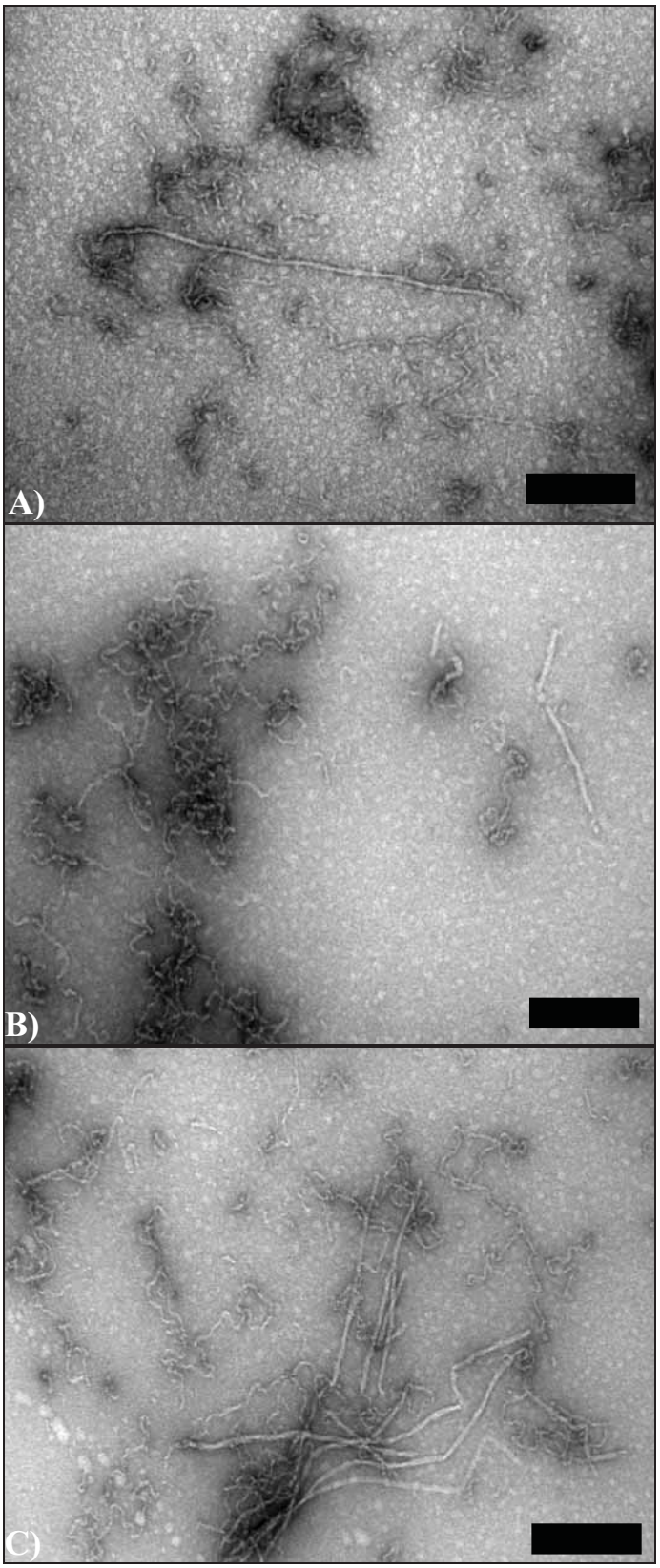

Figure 5.10: Nanofibres, including both straight and curly fibrils, made from homogenate solutions of crude crystallins diluted 1:10 into 50 mM Tris and 1 mM EDTA at pH 2 with 10 % TFE, incubated at 60 °C for 18 hrs: A) sheep homogenate; B) deer homogenate; and C) an equal mixture of cow, sheep and deer homogenates. Scale bars are 200 nm in length.

As discussed below, ThT binding ability, resistance to proteosomal degradation and X-ray fibre diffraction were selected as methods to confirm the production of amyloid fibrils in the above samples. Nanofibres from bovine homogenate, produced in the presence of EDTA as described above were selected as representative of all three species and were used for all further testing.

5.2.5.3 Nanofibres with curly and loop morphology from crude mixtures of bovine crystallins

Fibrils with an altered morphology were formed from bovine crystallin mixtures that had been pre-incubated. βB2-crystallin is a highly heat stable protein, which can remain in solution even at temperatures of 90 °C (Horwitz, J. *et al.* 1986). After heat treatment at 75 °C, following the methods of Horwitz and co-workers (1986) βB2-crystallin was the predominant subunit remaining in the crystallin mixture (§ 2.2.1.2). However, via the chaperone activity of α-crystallin, these samples also contain amounts of other proteins, including as significant ammount of αT-crystallin. In comparison, when only βL-crystallin is heat-treated in this fashion a pure band of βB2-crystallin is observed (Figure 5.11).

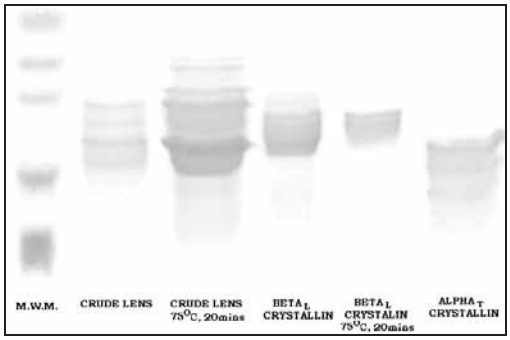

Figure 5.11: SDS-PAGE of crystallin proteins, showing crude lens (dilute), crude lens after heat treatment (75 °C for 20 minutes in the presence of 1mm DTT), βL-crystallin, βL-crystallin after heat treatment (75 °C for 20 minutes in the presence of 1mm DTT) and αT-Crystallin.

Samples incubated for 20 minutes at 75°C in the presence of 1 mM DTT, prior to fibril formation, formed curly fibrils and loop structures with no visible straight fibrils (Figure 5.12). This finding is consistent with the idea of α-crystallin being responsible for the formation of long straight fibrils. α-Crystallin is a molecular chaperone that associates with other crystallin proteins when heated (Reddy, G. B. *et al.* 2000). Heat treatment would cause α-crystallin to associate with other

crystallin proteins, reducing its availability for self-association and the formation of straight protein fibres.

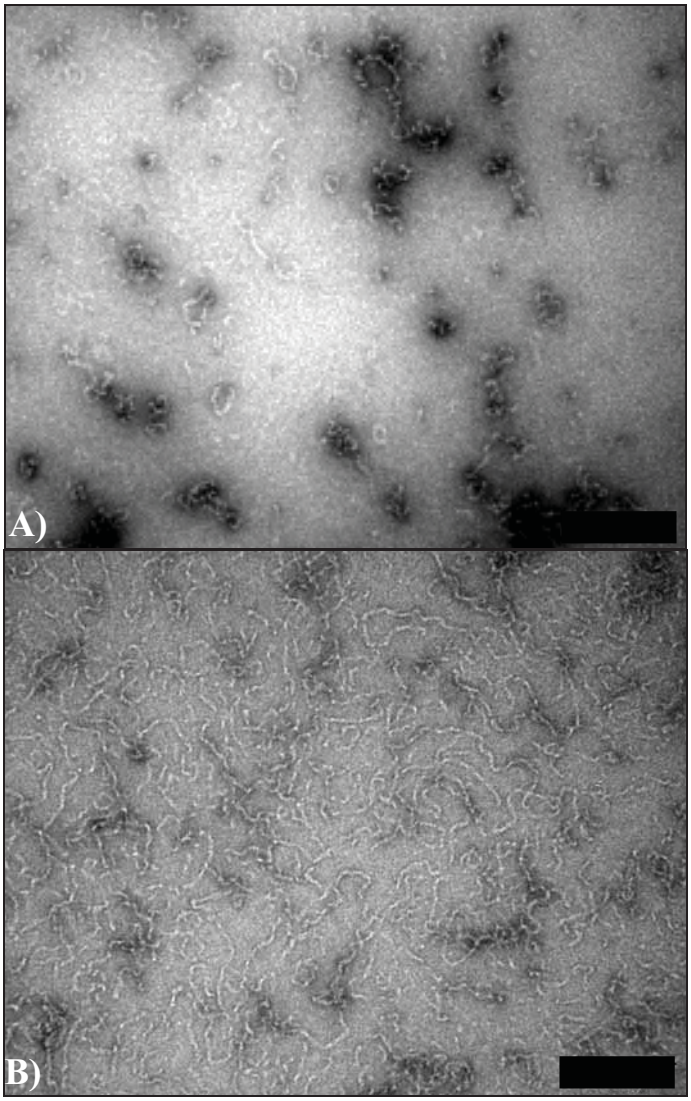

Figure 5.12: Nanofibres made from solutions of crude bovine crystallins diluted 1:10 into 0.02 M Tris, 1 mM EDTA, 1 mM DTT and heat treated (75 °C for 20 minutes) prior to protein nanofibre formation containing curly and loop fibrils, after incubation at 60 °C with 10 % TFE, for A) 1 hour and B) 18 hours. Scale bars are 200 nm in length.

5.2.5.4 Thioflavin t assessment of nanofibres formed from crude bovine mixtures

ThT results on crystallin proteins should be interpreted with caution, as the native crystallin structure contains a high proportion of β-sheet structure (§ 1.3.2). As a result, crystallin proteins can interact significantly with ThT in their native state (Meehan, S. *et al.* 2004). In this research, a high level of background fluorescence was observed for crude mixtures of crystallin proteins. However, a significant (P

< 0.05) increase in ThT fluorescence of over 25 % was observed following incubation (Figure 5.13). In conjunction with the TEM showing fibril structures, this increase in ThT implies that amyloid fibrils formed in these samples.

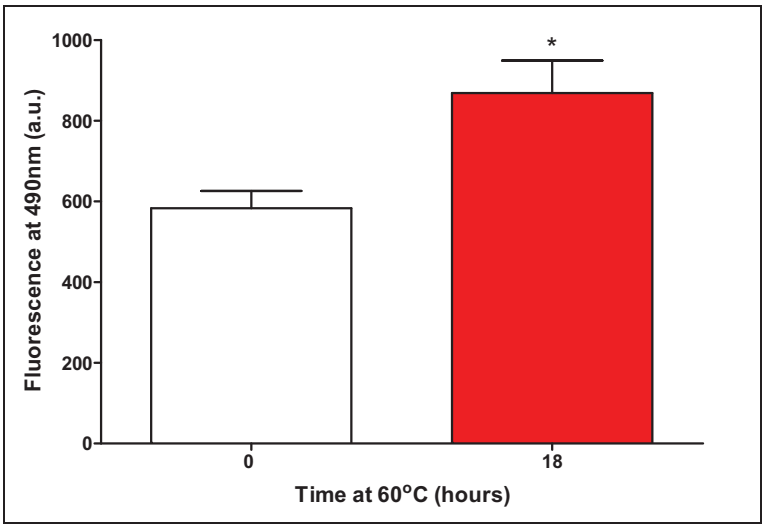

Figure 5.13: Thioflavin T dye binding of crude bovine crystallin preparations before and after incubation diluted 1:10 into 0.02 M Tris, 1 mM EDTA, pH 2 with 10 % TFE at 60 °C for 18 hours. Significance values from student t-test are: * = P < 0.05.

5.2.5.5 Protease resistance of nanofibres formed from crude mixtures of bovine crystallins

Protease resistance is a frequent, although not a definitive, characteristic of amyloid and amyloid-like fibrils. Protease treatment has thus been used by researchers to assess potential amyloid structures (Nilsson, M. R. 2004). The susceptibility of fibrils to proteolytic digestion was also examined by exposing fibrils formed by the standard method to the enzyme pepsin (§ 2.3.2.2.4). Crystallin nanofibres with both straight and curly morphologies were found to resist proteolysis with pepsin at low pH, as determined by examination by TEM after protease treatment. Non-fibrillar crystallin protein was effectively digested by an equal concentration of pepsin, as assessed by mass spectrometric characterisation (data not shown). Figure 5.14 shows there was no change in fibril morphology after this treatment (compared to Figure 5.9). The resistance of crude crystallin fibres to proteolytic enzymes, together with the fibril morphology observed by TEM and the capacity to increase ThT fluorescence, confirms that these fibres have classic amyloid fibril characteristics.

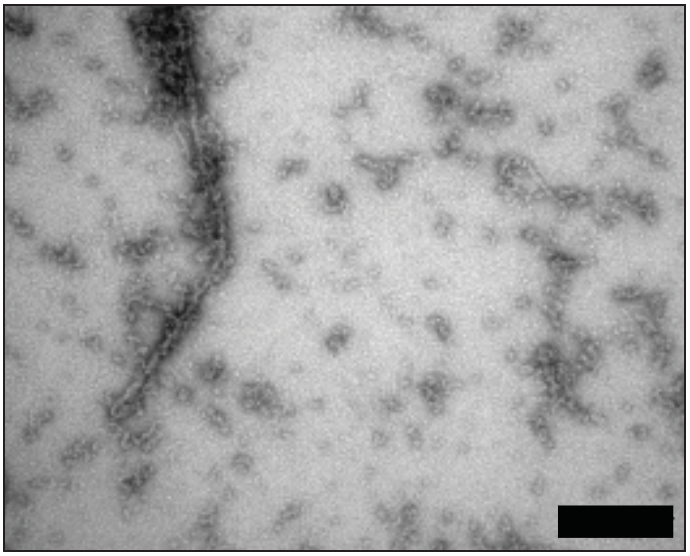

Figure 5.14: Nanofibres including both straight and curly fibrils, made from solutions of crude bovine crystallins (diluted 1:10 in 50 mM Tris, 1 mM EDTA, pH 2, 10 % TFE at 60 °C for 18 hours) treated with pepsin (1:200 w/w pepsin:crystallin at 37°C for 1 hr in 50 mM Tris and 1 mM EDTA at pH 2). Scale bars are 200 nm in length.

5.2.5.6 X-ray fibre diffraction of nanofibres from crude mixtures of bovine crystallin

Native crude bovine crystallin solutions and fibril structures from crude bovine crystallin solutions, produced with or without EDTA (§ 5.2.5.2 and § 5.2.5.1, respectively), were examined to reveal their protein structures (Figure 5.15). Extremely similar diffraction patterns were observed for all three solutions, which all showed reflections at 4.7 Å and 10.0 Å. Whilst these reflections are in positions consistent with the traditional meridional and equatorial reflections produced by amyloid fibrils, the reflections were isotropic in all three samples. This result indicates high levels of β-sheet structure, but does not confirm the presence of amyloid fibrils. The high proportion of ordered β-sheet (51-68 %) in native crystallin proteins (Siezen, R. J. and Argos, P. 1983) explains the resemblance between the diffraction patterns for native and treated crystallin samples. This similarity indicates that the β-sheet structure of the crystallin proteins may be largely unperturbed during fibril formation, certainly there is no indication of anisotropy in the two reflections that may indicate amyloid fibril

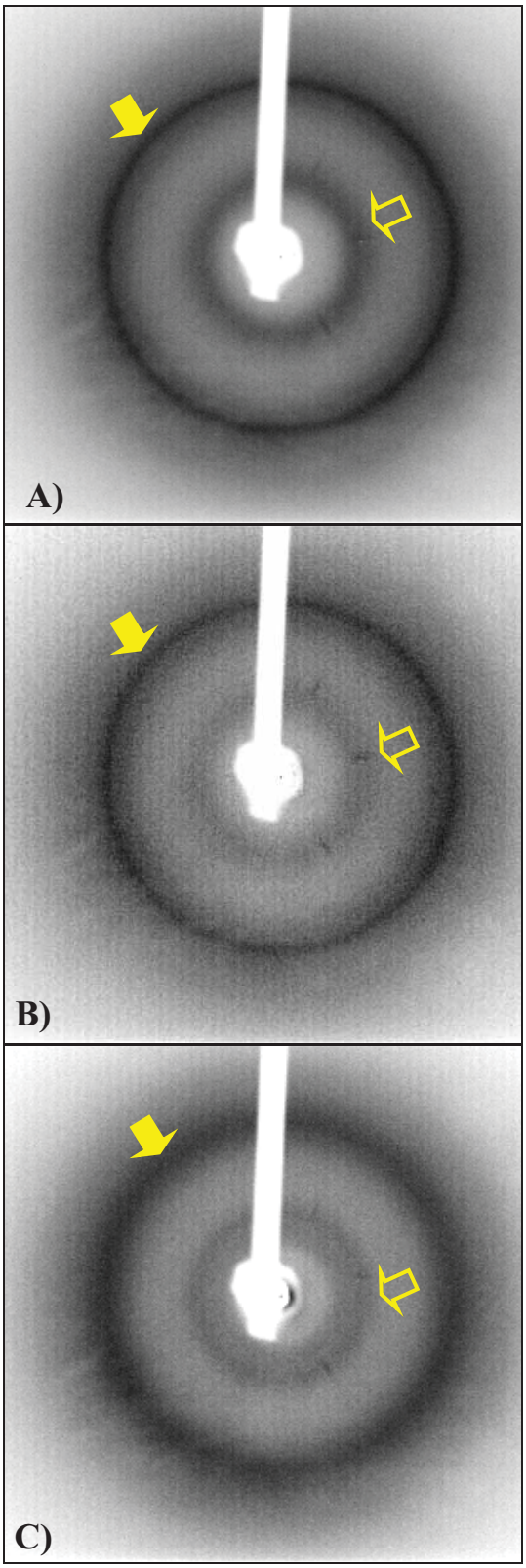

Figure 5.15: **Wide angle X-ray fibre diffraction pattern of A) crude bovine crystallin mixture, B) crude bovine crystallin nanofibres formed in 50 mM Tris with 10 % TFE, pH 2 at 60 °C for 18 hours (clumping fibril morphology) and C) crude bovine crystallin amyloid fibrils formed in 50 mM Tris, 1mM EDTA with 10 % TFE, pH 2 at 60 °C for 18 hours (non-clumping fibril morphology). Open arrows indicate meridional reflection at 4.7 Å and closed arrows the equatorial reflection at 10.0 Å.**

structures in alignment (Sunde, M. *et al.* 1997). However, isotropic reflections in these regions have also be observed in unaligned amyloid fibril samples (Eanes, E. D. and Glenner, G. G. 1968). These results confirm that there are high levels of ordered β-sheet structures in all samples (native and with amyloid fibril morphology and characteristics), and are consistent with the high level of initial ThT fluorescence observed for crystallin mixtures.

5.3 Discussion of nanofibre formation by lens crystallin proteins and protein mixtures

During mammalian life, the supramolecular order of lens crystallin proteins plays an important role in focusing light and maintaining lens transparency (Horwitz, J. 2003). In the meat industry, however, these proteins have little value, being counted among the animal waste products. The ready propensity of native crystallin proteins to rearrange and form amyloid fibrils, a situation which has been implicated in the formation of cataract (Meehan, S. *et al.* 2004), makes them an apt choice for the formation of inexpensive protein nanofibres. Crude eye lens homogenates contain a mixture of the α-, β- and γ-crystallin proteins (Kapphahn, R. J. *et al.* 2003). The ability of the different crystallin proteins to each form morphologically different nanofibres adds to their usefulness as model fibril formation targets.

The goal of this chapter was to prepare nanofibres from a cheap source of waste protein with minimal processing. The feasibility of forming protein nanofibres from pure, semi-pure and crude samples of crystallin proteins was thus examined. Individual classes of crystallin proteins (αT, βT or γT) were separated from this crude mixture using SEC**.** Crystallins to be purified were subjected to a further processing step where proteins were concentrated and buffer salts removed. SEC fractions were also combined; creating larger quantities of semi-pure samples (αT, βT or γT) that contain two or more structurally similar proteins. Further purification removed minor contaminants and produced ‘pure’ crystallin fractions. A summary of the components of each protein solution is given in Table 5.2. Previously, only pure crystallin preparations have been used for nanofibre formation (Meehan, S. *et al.* 2004; Meehan, S. *et al.* 2007).

Table 5.2: A summary of the components of each crystallin protein solution used to form nanofibres in this chapter. In all cases protein nanofibres were formed by the addition of 10 % TFE, at a pH of 2 for 18 hours.

Protein solution	Components	Solution
'Pure' crystallin fractions		
Bovine:		
α-crystallin	Concentrated α–crystallin	H_2O
βL-crystallin	Concentrated βL-crystallin	
γL-crystallin	Concentrated γL-crystallin	
Semi-pure crystallin mixtures		
Bovine:		
αT-crystallins	All α crystallins	50mM Tris, 1mM EDTA, pH 2
βT-crystallins	All β crystallins	
γT-crystallins	All γ crystallins	
Crude crystallin mixture		
Bovine:		
Diluted crude mixture	All HMW, α, β and γ crystallins	H_2O, pH 2
Diluted crude mixture	All HMW, α, β and γ crystallins	50mM Tris, 1mM EDTA, pH 2
Boiled crude mixture	Heat-stable HMW, α, β and γ crystallins	
Ovine:		
Diluted crude mixture	All HMW, α, β and γ crystallins	
Cervine:		
Diluted crude mixture	All HMW, α, β and γ crystallins	
Mixed species:		
Combined mixture of diluted crude bovine, ovine and cervine lenses	All HMW, α, β and γ crystallins	

All crystallin solutions were able to form protein nanofibres, although morphological variations were observed between solutions. The image of amyloid fibrils as consisting only of long, ribbon-like structures has, in recent years, been undergoing a revision. The identification of curly or loop fibrils, and research into their properties (Hatters, D. M. *et al.* 2003; Meehan, S. *et al.* 2007) provides greater understanding of the possibilities presented by amyloid and amyloid-like fibrils as protein nanofibres, with potential uses in many different areas of nanotechnology. Further research is currently underway to establish methods for the formation of protein nanofibres with individual morphologies directly from crude crystallin mixtures, potentially through the introduction of amyloid seeds displaying the desired characteristics (Griffin, M. D. *et al.* 2008). The research shown in this chapter indicates that a single source of crude proteins may be used as the major ingredient for the formation of a range of nanofibre products, each with different characteristics. Further, waste products would not require separation by species, as nanofibres can still be produced from crude protein sources that contain a combination of mammalian lenses (i.e. cow, sheep and deer

lens proteins in one mixture). A final important point is that, while sourced from mammalian waste products, there is no chance of prion transmission (such as occurs to cause the transmissible spongiform encephalopathies). The lens acts to diffract light into the eye-cup where it is collected and transmitted via the optic nerves (Land, M. F. and Fernald, R. D. 1992) and thus the lens tissue is without nerves or nervous tissue (responsible for transmissible spongiform encephalopathy transmission).

This study has shown that crude crystallin protein mixtures are a potential industrial source for protein nanofibres. In summary, it has been demonstrated for the first time that protein nanofibres can be created from an inexpensive crude protein source (the crystallin proteins of mammalian eye lenses) using a simple method, without time consuming and expensive protein purification. Such heterogenous mixtures, composed primarily of short, flexible fibrils, have potential uses as effective scaffolds to support other functional molecules, and preliminary trials into their effectiveness as such have shown promising results (J. Gerrard, 2009 personal communication). Future work should examine the protein composition of the nanofibres formed from such protein mixtures, and further explore the structure, function and applications of the different morphological forms.

CHAPTER 6

Retention of biological chaperone activity of α-crystallin after modification into amyloid fibrillar structures

The previous chapter (§ 5) explored the ability of crystallin proteins to form into amyloid fibrils when destabilised. Amyloid fibril formation is typically associated with a loss of protein function, as the native structure of a protein undergoes extreme structural changes to form into amyloid fibrils (a highly ordered β-sheet array). The ability of protein nanofibres, including amyloid fibrils, to be functionalised (i.e. to have biofunctional regions incorporated within or attached to the nanostructure) is one reason protein nanotubes have the potential to become widely used as a nanomaterial (Hamada, D. *et al.* 2004). The increasing recognition of amyloidin (§ 1.2.2), has lead to increased interest in the potential of amyloid fibrils that may retain native function (Fowler, D. M. *et al.* 2006). As discussed below, α-crystallin proteins display enhanced chaperone ability under conditions of structural stress, including thermal and chemical destabilisation. This chapter explores the ability of αT- and αB-crystallin to retain their molecular chaperone activity under conditions of extreme structural change, in particular as amyloid fibril structures.

6.1 Structure and function of α-crystallin

The structure and function of mammalian lens crystallin proteins and their roles in lenticular tissue have been extensively researched over the previous decades. As discussed in § 1.3, crystallin proteins are primarily found within the mammalian eye lens where they form part of the protein array that focuses light onto the retina *via* a supramolecular liquid-like order (Bloemendal, H. *et al.* 2004). Crystallin proteins are required to be highly stable, as there is very limited protein turn-over in the lens (Meehan, S. *et al.* 2004). αT-Crystallin, the predominant chaperone protein of the lens, is normally present as a heterogenous multimer, comprising two closely related subunits, αA- and αB-crystallin, in a ratio of 3:1, respectively (Abgar, S. *et al.* 2000). αT-Crystallin multimers are composed of between 15 and 50 of these two subunits and have an average mass of approximately 700 kDa (Horwitz, J. *et al.* 2004). Horwitz (1992) described the molecular chaperone activity of αT-crystallin. It is a sHSP and in the eye lens this chaperone action is important in maintaining the stability and solubility of other proteins in this tissue, in particular due to the high protein concentration. αB-crystallin, a subunit of αT-crystallin, is also found throughout the body and thus potentially has many further chaperone roles (Kato, K. *et al.* 1991; Ecroyd, H. and Carver, J. A. 2008a).

The identification of αB-crystallin in amyloid fibril deposits associated with a number of diseases, e.g. Alzheimer's disease, suggests that it may play a part in these diseases by acting to prevent the protein aggregation leading to amyloid fibril formation (Groenen, P. J. *et al.* 1994; Ecroyd, H. and Carver, J. A. 2008a). These findings have led to research into the activity of αA- and αB-crystallin, both as homogeneous and heterogenous multimers. One common aim of such research is to delineate ways in which the chaperone activity may be modified, in particular to be enhanced, as this could have significant potential for use in therapeutic interventions.

Chaperone activity is argued to mainly involve hydrophobic interactions, which generally occur when a target protein partially unfolds (during the off-pathway folding) and its hydrophobic core becomes revealed (Augusteyn, R. C. 2004a). The exact role hydrophobicity plays in chaperone-related binding of target proteins, particularly with regard to α-crystallin, is currently unclear, but it has been shown to be involved in the binding interaction (Kumar, M. S. *et al.* 2005). Potential binding sites have been established for both αA- and αB-crystallin, through selective point mutation studies and pin arrays of small peptide regions of the proteins (Sharma, K. K. *et al.* 2000; Ghosh, J. G. *et al.* 2005; Bhattacharyya, J. *et al.* 2006; Ghosh, J. G. *et al.* 2007; Treweek, T. M. *et al.* 2007). These regions, discussed in more detail in § 6.3, are areas where α-crystallin proteins are able to interact with partially folded proteins (proteins in an intermediate state, whether on the normal folding pathway or undergoing off-pathway folding). This interaction stablilises the partially folded proteins (referred to in this text as target proteins), preventing their aggregation and precipitation and, when occurring *in vivo*, potentially preventing disease states that may occur due to the misfolding of such proteins.

As can be discerned from their name, sHSPs act in times of cellular stress (Haslbeck, M. *et al.* 2005). Under thermal stress, the structure of αT-crystallin is altered due to partial unfolding and a subsequent enhancement in chaperone activity can be observed. αA-Crystallin, in particular, acts with increased efficiency at elevated temperature (Datta, S. A. and Rao, C. M. 1999; Reddy, G.

B. *et al.* 2000). This increase in chaperone activity is postulated to be linked to an increase in exposed hydrophobicity within a stable structure of αA-crystallin formed at temperatures above 50 °C (Abgar, S. *et al.* 2000; Reddy, G. B. *et al.* 2000). αB-Crystallin, whilst not exhibiting an increased chaperone activity, also retains its ability to act as a chaperone even at high temperatures (i.e. above 60 °C) (Datta, S. A. and Rao, C. M. 1999; Reddy, G. B. *et al.* 2000). αT-Crystallin, being composed of predominantly heat-stable αA-crystallin, can thus remain stable under thermal stress and acts as an enhanced molecular chaperone under such situations. Thermal stress is not the only situation that may lead to increased chaperone activity. Das and Liang (1997) demonstrated that α-crystallin, when unfolded by guanidine hydrochloride (GdnHCl), forms a molten globule (intermediate) state with enhanced chaperone ability. They argue that such intermediate forms of α-crystallin would occur *in vivo* due to post-translational modifications such as glycation, oxidation and mixed disulfide formation. In its activity as a sHSP, α-crystallin would be relied upon to act effectively especially under conditions of cellular stress (i.e. during heat-shock), thus the ability to retain activity when disrupted or partially unfolded is essential to α-crystallin's biological function (Carver, J. A. and Lindner, R. A. 1998).

Concomitant with α-crystallin's thermally increased activity is an increase in aggregate size of α-crystallin multimers upon heating. Electron micrographs show that the size of the αT-crystallin oligomers increases from 14.7 ± 2.7 nm at 35 °C to 26.8 ± 4.3 nm at 60 °C (Burgio, M. R. *et al.* 2000). The increase in chaperone activity is thought to be associated with increased hydrophobicity of α-crystallin multimers under thermal stress, rather than to be linked to aggregate size (Kumar, M. S. *et al.* 2005). The increase in subunit dynamics (i.e. subunit exchange of dimeric species) is also thought to be a significant factor in the enhanced activity of αT-crystallin at higher temperature (Liu, L. *et al.* 2006). The hydrophobicity theory is supported by the ability of urea denatured α-crystallin to refold into smaller aggregates which exhibit an increased chaperone activity (Saha, S. and Das, K. P. 2007). Further, studies done on crosslinked αT-crystallin show that it retains chaperone activity, although significantly less against some target proteins, even when highly crosslinked (Sharma, K. K. and Ortwerth, B. J. 1995;

Augusteyn, R. C. 2004b). This latter study implies that the dissociated (probably dimeric) form of αT-crystallin is not entirely responsible for the chaperone action of the protein, i.e. the aggregated form is also chaperone active. However, a systematic study of the impact of aggregation on chaperone ability had not previously been completed.

6.2 αT-Crystallin amyloid fibril chaperone assessment

6.2.1 αT-Crystallin amyloid fibril formation

αT-Crystallin was extracted and purified as described previously (§ 2.2.1). SEC separation produced distinct peaks for each class of crystallin protein, as shown previously (§5.2.2). αT-Crystallin amyloid fibrils were formed (§ 2.3.2.1.7) and the transformation from native to fibrillar state confirmed by TEM (Figure 6.1). The fibrils ranged in length from 20 nm to 1 μM and showed the characteristic morphologies previously described for αT-crystallin amyloid fibrils formed under these conditions (§ 5.2.3, Meehan, S. *et al.* 2007). A number of smaller aggregates, potentially either protofibrils or amorphous aggregates, were also present after incubation.

6.2.2 Chaperone activity assessment of native and fibrillar αT-crystallin against amorphous aggregation

Disordered protein aggregation is commonly induced and monitored *in vitro* as a technique to learn more about the aggregation potential of different proteins and the activity of potential chaperone molecules (Carver, J. A. *et al.* 1996). The specific qualities of a protein influence the state under which it can be induced to aggregate, and even how it will aggregate (either amorphously or into amyloid fibrils). Throughout this research, a range of target proteins and destabilisation techniques were used, providing a more comprehensive picture of the activity of the chaperone proteins of interest. Temperature, agitation, protein concentration and buffer salts all alter the rate of target protein aggregation, so the end point of protein aggregation in all cases was assessed individually based on the aggregation profile.

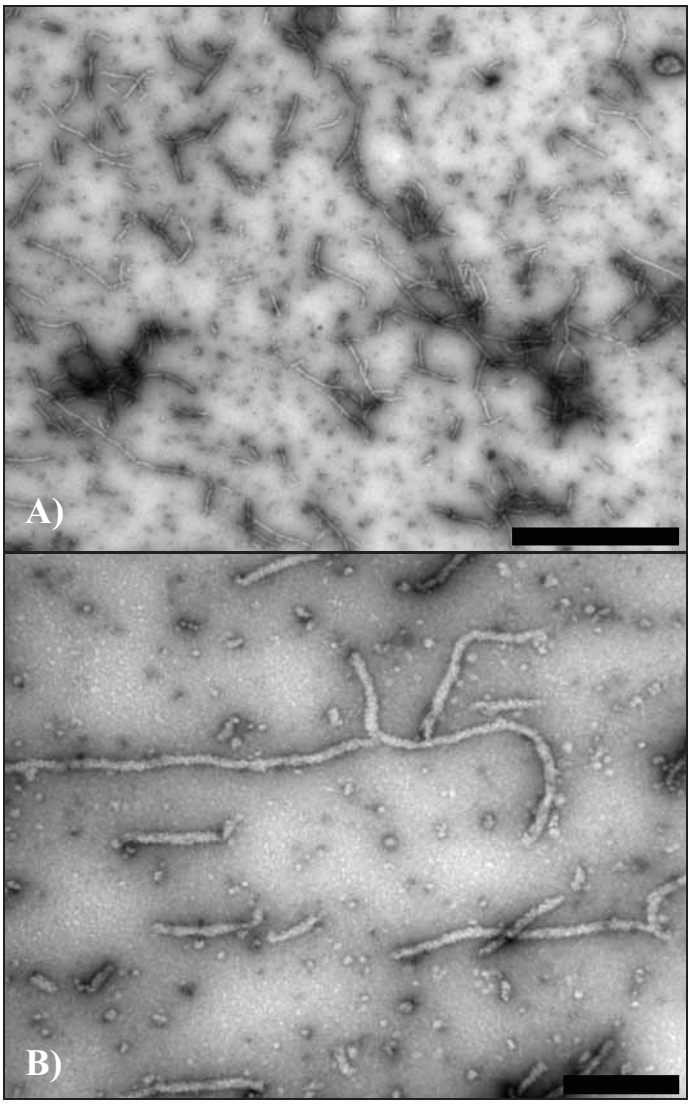

Figure 6.1: αT-crystallin in 1 M GdnHCl, 0.1 M sodium phosphate, pH 7.4 at 60 °C for 2 hours, with scale bars at: A) low magnification; and B) high magnification. Scale bars are 1 µM and 200 nm, respectively.

Assessment of αT-crystallin chaperone activity in native and amyloid fibril structural states was made against two target proteins: catalase destabilised by high temperature (60 °C) and insulin destabilised by reduction (37 °C). Both these target proteins are commonly used in our laboratory as reliable aggregating target proteins, characteristic of their forms of aggregation induction and which α-crystallin effectively chaperones (Ecroyd, H. *et al.* 2007). Amorphous aggregation, similarly to amyloid fibril formation (§ 3.1.2), occurs in three main stages: a lag stage during which target protein unfolding and association occurs; an exponential stage, where protein aggregates become large enough to precipitate from solution; and a plateau stage, where target protein precipitation is judged to

have finished (Horwitz, J. *et al.* 1998). Precipitation of protein was monitored *via* light scattering (§ 2.3.1.1). Both insulin and catalase reached a plateau of light scatter, indicative of the completion of precipitation, after 40 minutes. The percentage of protection afforded by the chaperone is visible in the reduction of target protein precipitation, and was quantified for further statistical analysis using Equation 1 (§ 2.3.3). The chaperone activity results are given below in Figures 6.2 and 6.3 (target proteins are insulin and catalase respectively).

Native αT-crystallin provided chaperone protection against thermally induced amorphous aggregation of catalase (Figure 6.2). At low concentrations (50 μg/mL) fibrillar αT-crystallin provided significantly less protection against heat-induced amorphous aggregation of catalase, compared to an equivalent concentration of native αT-crystallin. At 100 to 150 μg/mL there was a non-significant trend toward lessened activity of αT-crystallin fibrils, while at 200 μg/mL, no significant difference between the activity of native and fibrillar αT-crystallin was observed, with catalase being protected to a degree of 70 ± 7 % and 66 ± 13 % respectively.

Native αT-crystallin also protected insulin B chain from reduction induced amorphous aggregation in a concentration dependent manner. Fibrils formed from αT-crystallin protected against insulin amorphous aggregation in a manner comparable to native αT-crystallin (Figure 6.3). There was an observable trend of reduced protection by fibrillar αT-crystallin; however, there was no statistical difference between the percentage of protection provided by equivalent concentrations of native versus fibrillar αT-crystallin: for example, no statistical difference was observed between the protection given by 800 μg/mL of native αT-crystallin (83 ± 0.3 %) or fibrillar αT-crystallin (71 ± 5 %).

The plot of light scattering from insulin aggregation over time (Figure 6.3A) illustrates that fibrillar αT-crystallin causes a slightly faster rate of insulin aggregation (lessened lag phase) than native αT-crystallin. This finding is not characteristically seen in chaperone proteins. Instead, this is likely to be the result

of trace amounts (under 0.1 M) of GdnHCl being present in samples of fibrillar αT-crystallin.

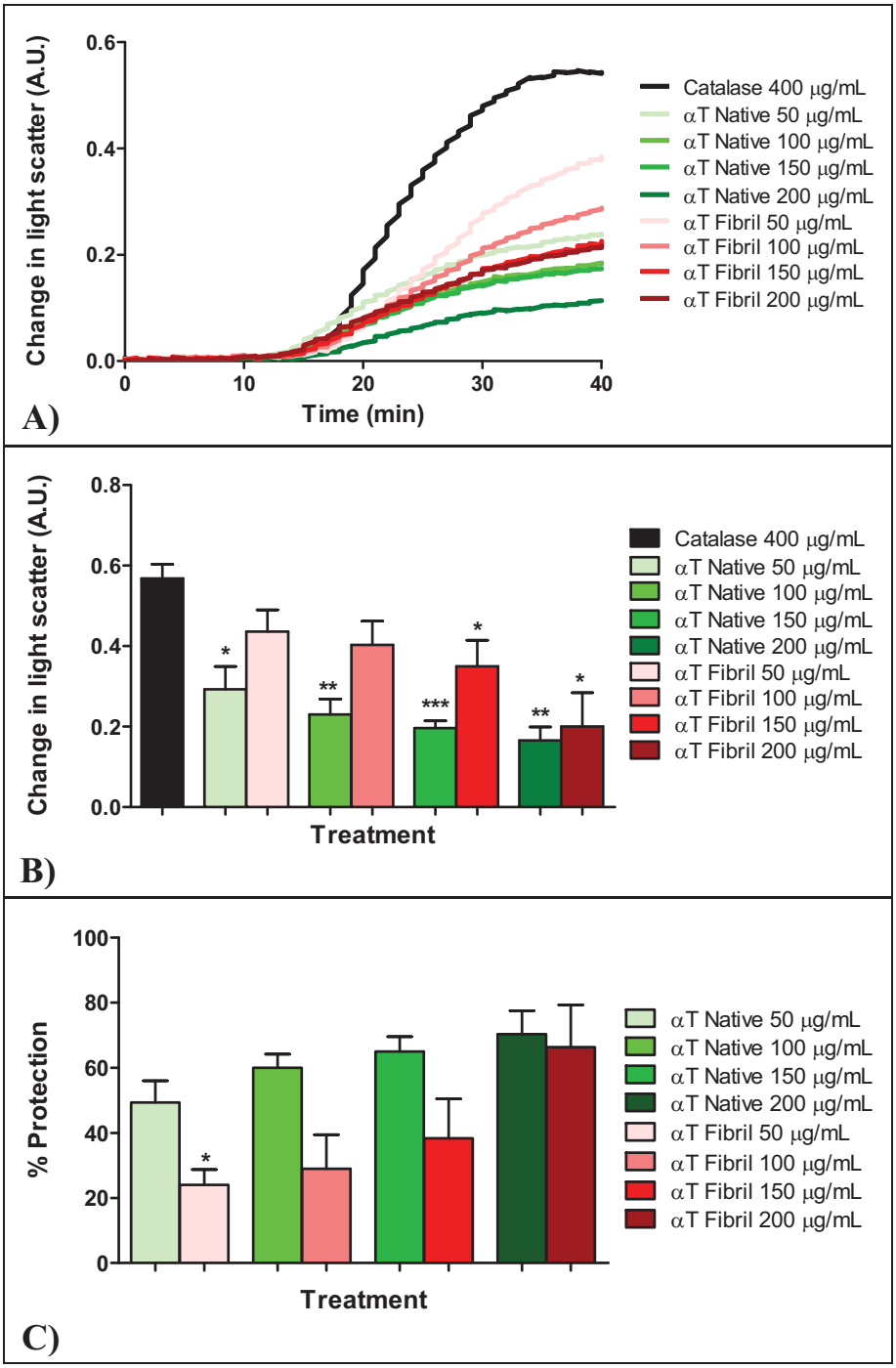

Figure 6.2: Native and fibrillar αT-crystallin chaperone protection of catalase at 400 µg/mL in 0.1 M sodium phosphate buffer at pH 7.4, undergoing thermal destabilisation at 60 °C: A) representative light scatter profile; B) maximum light scatter for all replicates, significance values are given against maximum light scatter for catalase at 400 µg/mL; and C) the percentage of protection provided by each potential chaperone, significance values are against Native sample of equal concentration (B and C: means ± SE of 3 separate experiments, P values indicating significant difference from student t-tests are: * < 0.05, **<0.01, *<0.001).**

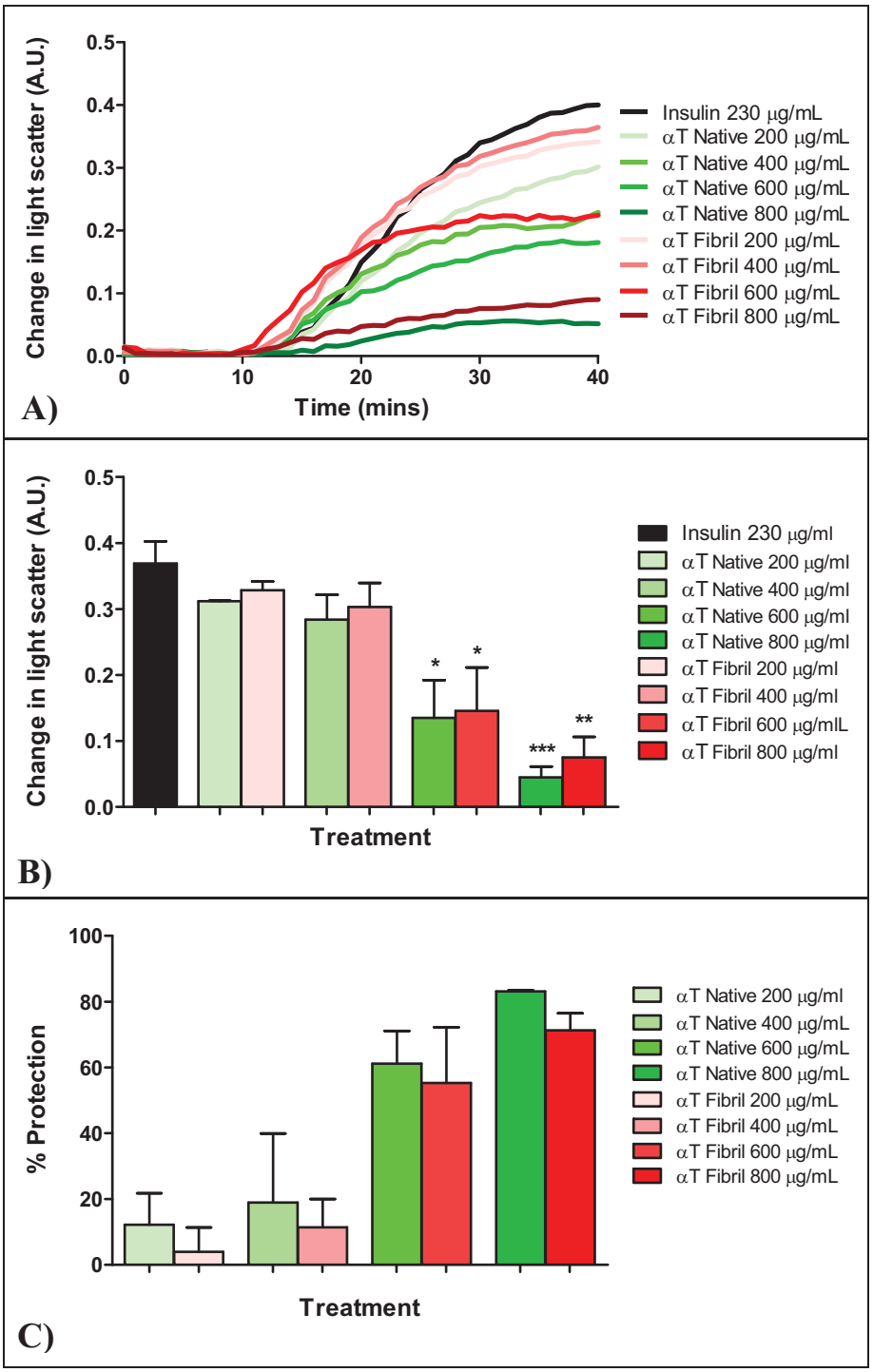

Figure 6.3: Native and fibrillar αT-crystallin chaperone protection of reduced insulin, 230 µg/mL in 0.1M sodium phosphate buffer pH 7.4, at 37 °C in the presence of 10 mM DTT: A) representative light scatter profile; B) maximum light scatter for all replicates, significance values are given against maximum light scatter for insulin at 230 µg/mL; and C) the percentage of protection provided by each potential chaperone, significance values are against Native sample of equal concentration (B and C: means ± SE of 3 separate experiments, P values indicating significant difference from student t-tests are: * < 0.05, **<0.01, *<0.001).**

GdnHCl destabilises proteins, and may have acted in an additive manner with DTT to increase the rate of insulin amorphous aggregation. In the current assays

GdnHCl was present in insulin with fibrillar αT-crystallin samples, and not in insulin alone, or insulin and native αT-crystallin samples. Even with GdnHCl potentially increasing the rate of insulin aggregation, fibrillar αT-crystallin still acts as an equivalent chaperone to native αT-crystallin (Figure 6.3B and C).

6.2.3 Amorphous aggregate and βH-crystallin amyloid fibril controlled assays of αT-crystallin fibril chaperones

To investigate the chaperone ability of fibrillar αT-crystallin further, a stock of native αT-crystallin was prepared with an equal amount of GdnHCl as was used to prepare the fibrillar form. This stock was stored at 4 °C for use in assays ('αT GdnHCl Native', § 2.3.1.1.3) or fibrils were prepared as described above ('αT Fibril', § 2.3.2.1.7). TEM examination showed no observable difference in morphology between native αT-crystallin and GdnHCl treated native αT-crystallin. Both these samples (Figure 6.4A and B) appear as roughly spherical multimeric structures of approximately 15 nm in diameter, as observed by other researchers (Haley, D. A. *et al.* 2000). Following sample incubation, all samples used in this assay were spin-filtered (§ 2.3.4) to remove any GdnHCl (where present). Samples with no GdnHCl were subjected to the same treatment to produce equivalent conditions in all samples and thus allow for comparison between all samples. αT-Crystallin amyloid fibrils appeared no different after spin filtering to those produced earlier (§ 6.2.1) and were equivalent to non-spun αT-crystallin fibrils in length and concentration (Figures 6.1B and 6.4C).

To examine whether the activity of aggregated αT-crystallin was specific for the fibrillar form, an amorphous aggregated form of αT-crystallin was also prepared by incubation in 0.1 M sodium phosphate buffer with 1 M GdnHCl at 90 °C for 2 hours ('αT Amorphous', § 2.3.1.1.4). The amorphous aggregates of αT-crystallin appeared as larger, mostly spherical, aggregates with some clumps of protein present (Figure 6.5A). This is consistent with the findings of Burgio *et al.* (2000) and previous findings of this laboratory (S. Meehan, PhD Thesis) who demonstrated both increased size of αT-crystallin aggregates under high temperatures and a tendency to clump into beads or strings where individual aggregates were still observable.

To test whether the chaperone activity was specific to αT-crystallin amyloid fibrils, amyloid fibrils were formed from a non-chaperone active protein, βH-crystallin ('βH Fibrillar', § 2.3.2.1.4). βH-Crystallin has previously been demonstrated to form amyloid fibrils under low pH, addition of TFE and thermal stress conditions (§ 5.2.3, Meehan, S. *et al.* 2004). These fibrils are short and curled in nature, as seen in Figure 6.5B. Finally, amorphous aggregates of aldehyde dehydrogenase (ADH), a non-chaperone amorphously aggregating protein, were prepared to examine the generic chaperone ability of this form of protein aggregates. Thus ADH was incubated in 0.1M sodium phosphate, pH 7.4 with 1 M GdnHCl at 90 °C for 2 hours ('ADH Amorphous', § 2.3.1.1.4). Figure 6.5C shows clumps of amorphously aggregated ADH with no fibrillar characteristics and in which no individual species can be observed.

Table 6.1 outlines the proteins and formation conditions used to prepare the above chaperone treatments and the morphology of each observed by TEM (Figure 6.4 and 6.5). All samples, following incubation (at 4, 60 or 90 °C), were dialysed to remove GdnHCl prior to chaperone assessment (§2.3.1.1.3). For ease of reference, the treatment names in Table 6.1 will be used throughout this section.

Table 6.1: αT-Crystallin species formed for chaperone assessment of structural variation

Treatment	Protein	Incubation conditions				Morphology
		Buffer	pH	Temp (°C)	Time (Hr.)	
αT Native	αT-crystallin	0.1M sodium phosphate	7.4	4	2	Spherical aggregates ~15nm in diameter
αT GdnHCl Native	αT-crystallin	1M GdnHCl, 0.1M sodium phosphate	7.4	4	2	Spherical aggregates ~15nm in diameter
αT Fibril	αT-crystallin	1M GdnHCl, 0.1M sodium phosphate	7.4	60	2	Long fibrils, (20nm – 1μm in length), plus short fibrils and/or spherical aggregates
αT Amorphous	αT-crystallin	1M GdnHCl, 0.1M sodium phosphate	7.4	90	2	Larger spherical aggregates ~ 30nm in diameter singly and in clumps
βH Fibril	βH-crystallin	H_2O with 10 % TFE	2	60	18	Short, curly fibrils, 20nm to 200nm in length
ADH Amorphous	ADH	1M GdnHCl, 0.1M sodium phosphate	7.4	90	2	Large non-fibrillar protein clumps

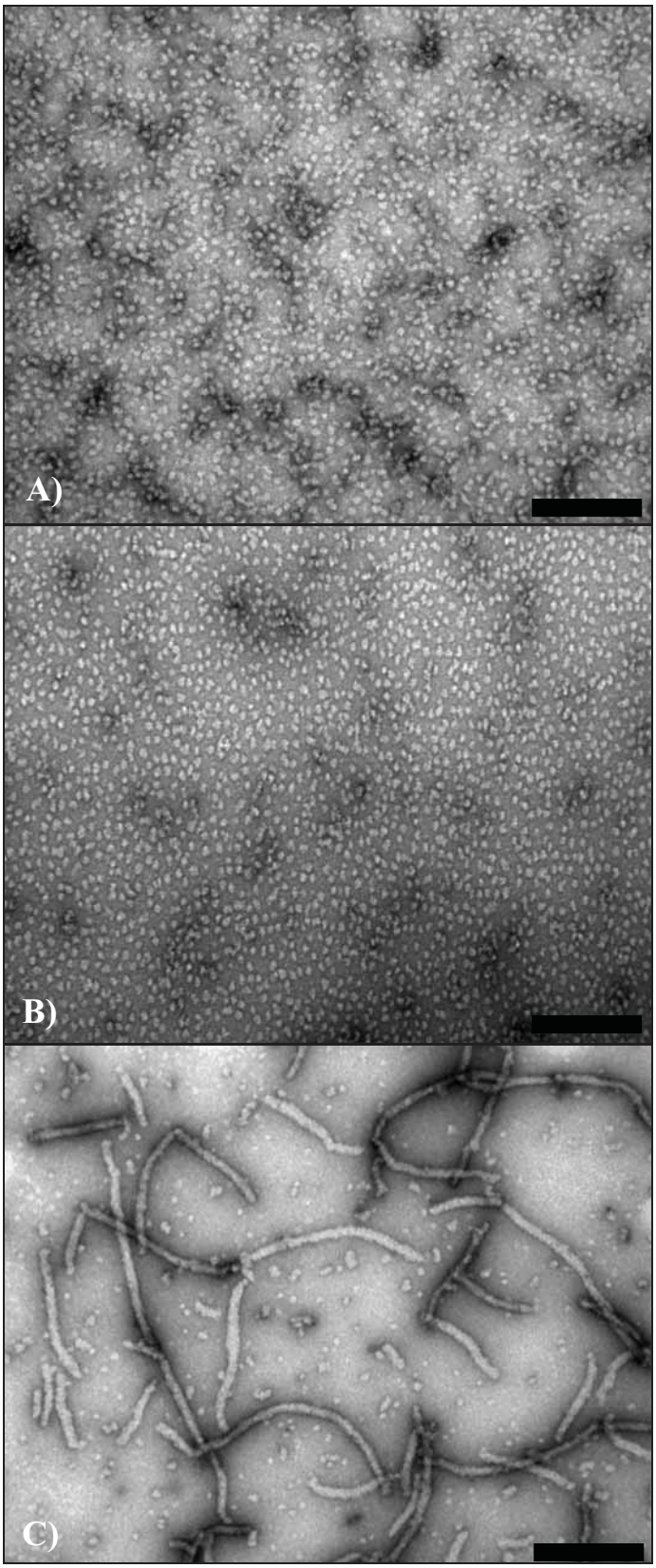

Figure 6.4: TEM of αT-crystallin samples formed to assess the effects of structural variation on chaperone activity: A) αT Native; B) αT GdnHCl Native; C) αT Fibril. All samples were prepared as described in Table 1. Scale bars are 200nm.

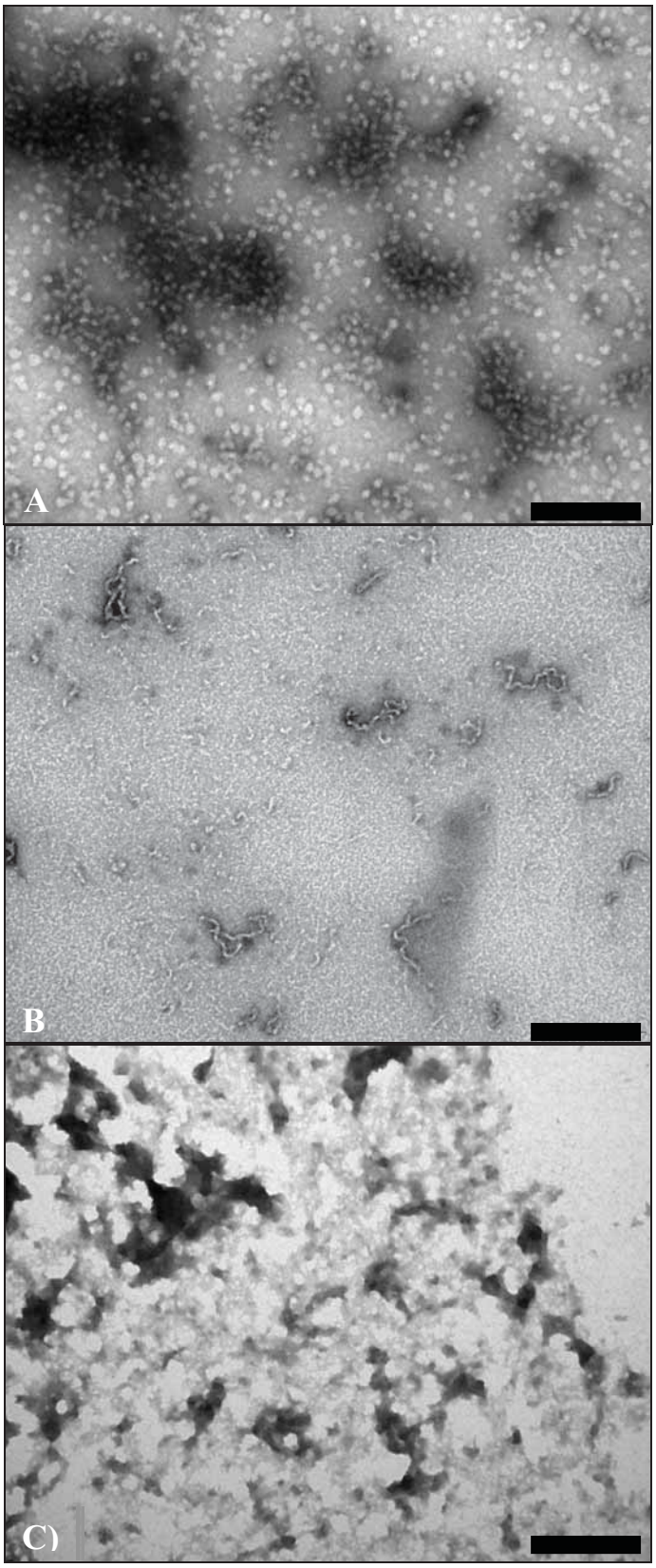

Figure 6.5: TEM of samples formed to assess the effects of structural variation on chaperone activity: A) αT Amorphous; B) βH Fibril; and C) ADH Amorphous. All samples were prepared as described in Table 1. Scale bars are 200nm.

Within one hour of preparation, samples were used in light scatter chaperone activity assays against insulin and catalase amorphous aggregation (§ 2.3.1.1). Figure 6.6 illustrates the activity of each species against thermally destabilised catalase at 60 °C (A) and reduction destabilised insulin at 37 °C (B).

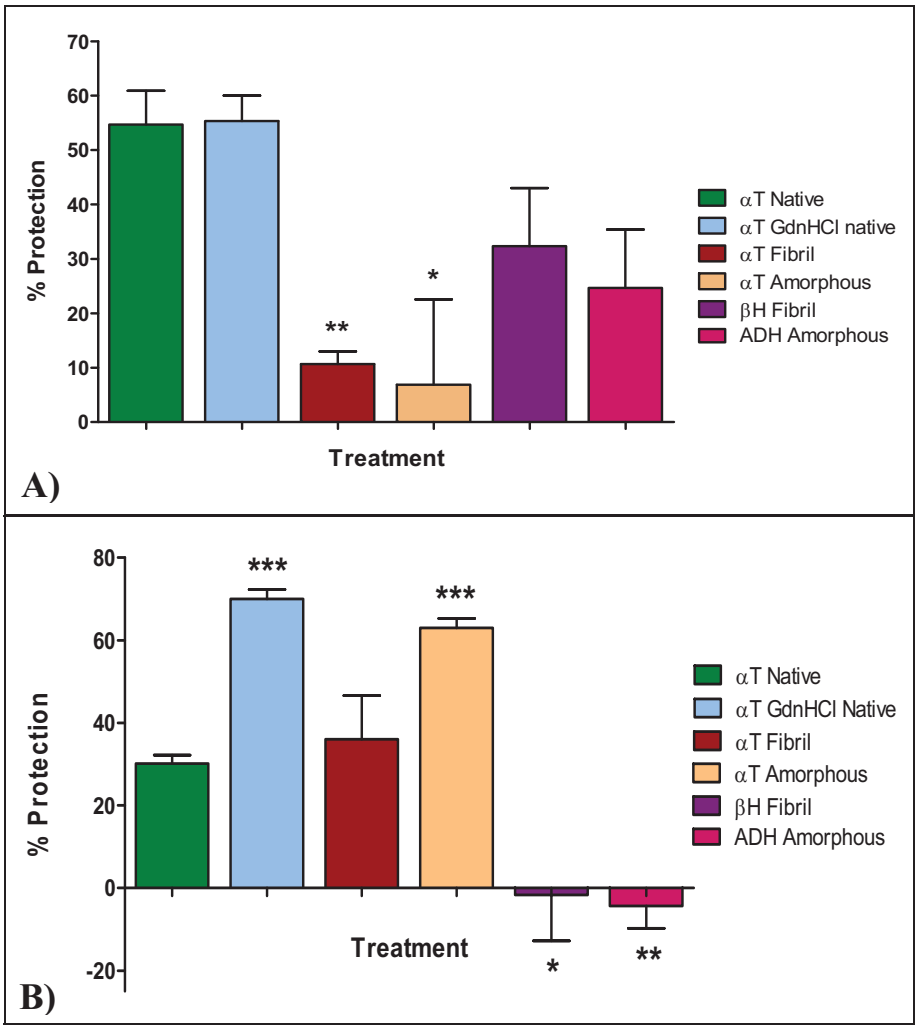

Figure 6.6: Chaperone protection provided by various native, fibrillar and amorphous species against amorphous aggregation of: A) catalase, 400 µg/mL in 0.1 M sodium phosphate, pH 7.4 at 60°C (chaperones at 200 µg/mL); and B) reduced insulin, 250 µg/mL in 0.1 M sodium phosphate, pH 7.4 and 20 mM DTT at 37°C (chaperones at 800 µg/mL). All results show means ± SE of 3 separate experiments. P values, derived by student t-tests, indicate a significant difference against αT Native, and equal: * < 0.05, **<0.01, *<0.001.**

The above assays highlight the abilities of αT-crystallin to act as a chaperone under a range of conditions. They further show that differences in target proteins and/or aggregation conditions lead to increased or decreased activity of each chaperone species, i.e. that some chaperones work more effectively against catalase at 60 °C than they do against insulin at 37 °C, or *vise versa*. Against

thermally induced catalase amorphous aggregation, αT Native and αT GdnHCl Native acted with equivalent chaperone activity. αT Fibril acted with some chaperone activity, but significantly less than αT Native. This is in contrast to earlier findings (§ 6.2.2) and provides further evidence that GdnHCl was playing an additive role in catalase aggregation in the previous assays. The chaperone activity observed for the αT Fibril sample was significantly lower than that of αT Native; however, it was not statistically significantly different to that of βH Fibril sample, although a non-significant trend to greater protection by βH Fibrils was observed. This indicates that the chaperone activity observed may not be attributable to the action of αT Fibrils specifically, but instead a result of inherent hydrophobicity in the amyloid fibril structure. αT Amorphous species acted with equivalent chaperone activity to αT Fibril samples, i.e. significantly less than αT Native. Further, the activity of αT Amorphous was equivalent to that observed for ADH Amorphous species indicating that, as with the fibrillar samples, the chaperone activity may be a result of the presence of aggregates with hydrophobic regions (as opposed to the activity of a specific region within the αT-crystallin species).

Against insulin aggregation at 37 °C, without any GdnHCl present in the assay, αT Native and αT Fibril species act with equivalent chaperone activity, as observed earlier (Figures 6.3 and 6.6B). The overall chaperone activity for all treatments was consistently lower compared to earlier assays (§ 6.2.2), most likely as a result of protein loss during the spin filter process (used for all samples to remove GdnHCl where present). αT GdnHCl Native and αT Amorphous both acted with significantly enhanced chaperone activity, as compared to αT Native. Both βH Fibrils and ADH Amorphous treatments demonstrated no chaperone activity, and as such acted significantly less effectively than αT Native. αT Amorphous exhibited enhanced chaperone activity, compared to αT Native, and may therefore be responsible for the chaperone activity of the αT Fibril sample, which contained both amyloid fibrils and amorphous aggregates (Figure 6.4C). The enhanced activity of αT-crystallin in the presence of GdnHCl has been demonstrated (Das, B. K. and Liang, J. J. 1997), when an intermediate structure

was deemed to have enhanced chaperone activity. It has also been demonstrated that after urea denaturation, αT-crystallin can refold into aggregates with increased chaperone activity, concomitant with an increased surface hydrophobicity of the resulting aggregate species (Saha, S. and Das, K. P. 2007).

The findings from these assays indicate a difference in activity of the various αT-crystallin species against varying target proteins (insulin or catalase) and/or under different assay conditions (reduction at 37 °C or heating at 60 °C). The differences observed between the data for each species in Figures 6.6A and 6.6B may be related to the different stresses involved by the alterations in assay conditions. This has been observed previously and the chaperone ability of αB-crystallin is recognised to be stress-dependent (Horwitz, J. 1992; Ecroyd, H. and Carver, J. A. 2008b). It is probable that the various crystallin species used in this research share this stress-dependency, and are thus displaying varying activity dependent on the assay conditions employed.

To further examine this, potentially stress-dependent, variation in activity, a third target protein was examined. Milk protein κ-casein has been shown to have a high amyloidogenic propensity once isolated from other casein proteins (Farrell, H. M., Jr. *et al.* 2003). This propensity can be further enhanced by reduction and carboxymethylation of the protein (§ 2.2.3), leading to formation of amyloid fibrils under physiological temperature and pH conditions, which can be monitored by ThT fluorescence (§ 2.3.2.2.1) (Thorn, D. C. *et al.* 2005). This provides a model aggregation assay (§ 2.3.2.1.8) that can be performed at 37 °C (the same as insulin), but which is different to insulin in that it involves an amyloid fibril forming target protein (as opposed to the amorphous aggregating systems thus far examined). For the following assays, all chaperone samples were prepared as described above (Table 6.1) to ensure no GdnHCl remained in the samples for chaperone assessment. Results of ThT fluorescence assessment and percentages of chaperone protection are provided in Figures 6.7 and 6.8.

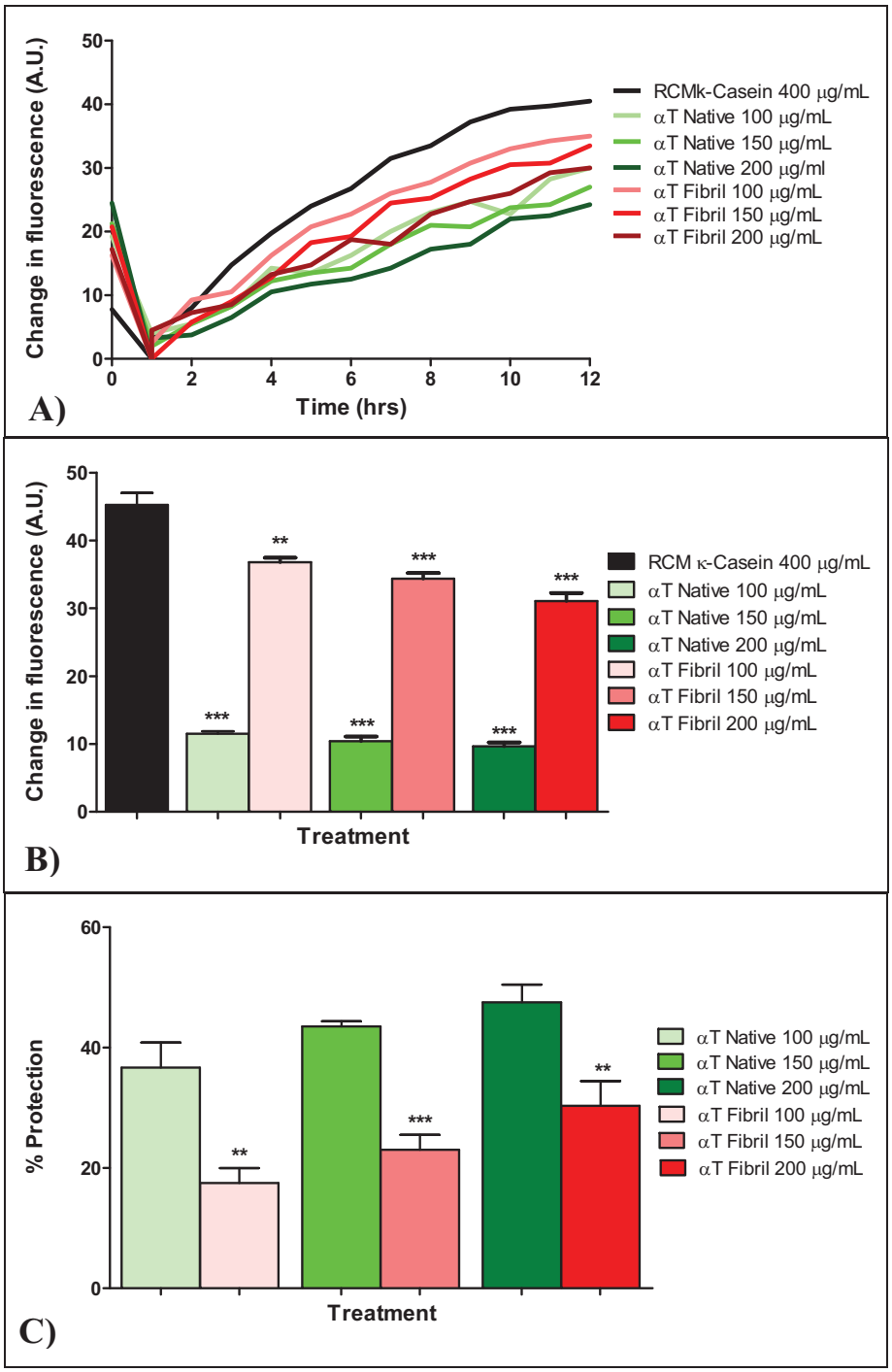

Figure 6.7: RCMκ-Casein 400 µg/mL incubated at 37 °C, in 0.1 M sodium phosphate, 10 µM ThT for 12 hours in the presence of various chaperone species, showing A) representative fluorescent profile (ex. 420 nm, em. 490 nm); B) maximal change in fluorescence after 12 hours (significances are against maximum RCM κ-casein fluorescence); and C) percent of protection given against amyloid fibril formation of RCM κ-casein by αT Native and αT Fibril (significances are against equivalent concentration of αT Native). For B and C results are mean ± SE of 3 separate experiments. P values determined by student t-test are: *<0.05, **<0.01, *<0.001.**

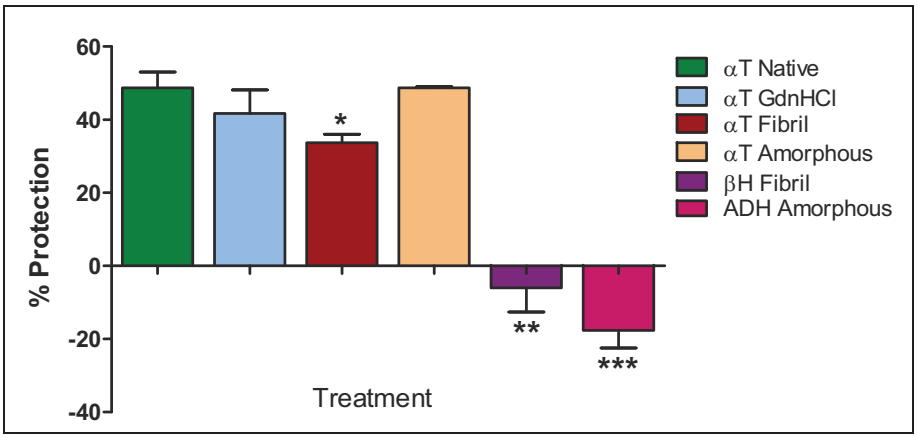

Figure 6.8: RCM κ-Casein 400 µg/mL incubated at 37 °C for 22 hours in the presence of various native, amorphous and fibrillar chaperone species (200 µg/mL) and monitored *via* ThT fluorescence. Results are mean ± SE of the percentage protection given by chaperones over 3 experiments. P values, derived by student t-test, are given against αT Native and are *<0.05, **<0.01, *<0.001.**

Native and fibrillar αT-crystallin both protected RCMκ-casein from amyloid fibril formation in a concentration dependent manner. The αT Fibril sample was significantly less effective than αT Native (200 µg/mL of chaperone protected 48 ± 2 % and 37 ± 1 % respectively). Other αT-crystallin species (αT GdnHCl Native and αT Amorphous) acted with similar efficiency to αT Native. There was no chaperone activity exhibited by aggregates of non-chaperone proteins, including βH Fibrils and ADH Amorphous. In fact both non-chaperone species led to a slight increase in ThT fluorescence associated with fibril formation. This has been observed previously (Lindner, R. A. *et al.* 1998) and may be an effect of molecular crowding, where the addition of extra protein leads to increased assembly of amyloid fibrils by increasing the rate of self association between subunits of the amyloidogenic protein.

The interaction between αT-crystallin species and RCM κ-casein reveals that all αT-crystallin species (native, previously destabilised, amyloid fibrils and amorphous aggregates) retain chaperone activity against this amyloid fibril forming protein. Unlike the activity of αT-crystallin species against amorphous insulin aggregation, there is no increased protection given by the previously destabilised and amorphous aggregated αT-crystallin species. The fibrillar species of αT-crystallin is less effective as a molecular chaperone than the native or other species; however, it is unclear whether this chaperone activity is the effect of the

amyloid fibrils or amorphous aggregates present in the αT Fibril sample. Similar to amorphous aggregation at 37 °C, there was no chaperone activity from non-chaperone aggregates (fibrillar or amorphous). This indicates that the chaperone activity exhibited by aggregated αT-crystallin species is a true chaperone action and not the result of randomly exposed hydrophobicity from aggregated species.

The ability of destabilised and amorphously aggregated species of αT-crystallin to act as chaperones makes it unclear whether αT-crystallin fibrils actually retain chaperone activity. It is possible that the observed chaperone activity of samples containing αT-crystallin fibrils is in fact due to the, in some cases heightened (e.g. against reduced insulin), activity of αT-crystallin amorphous aggregates which are also present within these samples (Figure 6.4C). While the ability of amorphously aggregated αT-crystallin to act so effectively as a molecular chaperone is of interest in itself, and will be discussed in detail below (§ 6.3), a clearer understanding of whether α-crystallin amyloid fibrils can act as molecular chaperones is desired.

6.2.4 Chaperone activity of αB-crystallin fibrils and other species

αT-Crystallin is composed of two subunits, αA- and αB-crystallin, in a ratio of approximately 3:1 (§ 1.3.3.1). Human αB-crystallin is found throughout the body, although it is in its highest concentration in the eye lens (Kato, K. *et al.* 1991; Bloemendal, H. *et al.* 2004). αB-Crystallin acts throughout the body (in many tissues) as a molecular chaperone and acts *in vitro* at 37 °C as a molecular chaperone with similar efficaciousness to αT-crystallin. Genetic recombination involves the insertion of one gene into a separate genetic carrier (plasmid) which may then allow that protein to be expressed in bacteria. It effectively produces an exact replica of the wild type protein and is a conventionally acceptable way to obtain pure human proteins that would otherwise be difficult to acquire, particularly in non-disease related situations (Johnson, I. S. 1983). Recombinant wild type αB-crystallin has been used over the last decade by a number of research groups and has been shown to be a stable and reliable protein with the same characteristics of αB-crystallin purified from mammalian sources. Previous work in our laboratory has shown that amyloid fibrils formed from αB-crystallin

contain significantly less (under 5 % of the sample) amorphously aggregated species than are present in αT-crystallin fibril samples (Meehan, S. *et al.* 2007). For this reason αB-crystallin was selected for use in duplicate assays to those already performed on αT-crystallin, as the low percentage of native protein remaining in the 'fibrillar' sample will help to clarify how much chaperone effect is due to remnant native protein. Thus, when only low levels of chaperone activity occur this may be due solely to remnant native species. However, when equivalent or higher chaperone activity occurs, some (though not necessarily all) of this must be attributable to the fibrillar or amorphous species, due to the very low levels of remnant native protein in this sample.

Native and amyloid fibril species of αB-crystallin were used to examine the effect of α-crystallin amyloid fibrils, without the interference of amorphous aggregates. For comparison, identical samples to αT-crystallin (§ 6.2.3) were prepared from αB-crystallin: αB Native; αB GdnHCl Native (§ 2.3.1.1.3); αB Fibril (§ 2.3.2.1.7); αB Amorphous (§ 2.3.1.1.4); βH Fibril (§ 2.3.2.1.4); and ADH Amorphous (§ 2.3.1.1.4), as described in Table 6.2.

Table 6.2: αB-Crystallin species formed for chaperone assessment of structural variation

Treatment	Protein	Incubation conditions				Morphology
		Buffer	pH	Temp (°C)	Time (Hr.)	
αB Native	αB-crystallin	0.1M sodium phosphate	7.4	4	2	Spherical aggregates ~15 nm in diameter
αB GdnHCl Native	αB-crystallin	1M GdnHCl, 0.1M sodium phosphate	7.4	4	2	Spherical aggregates ~15 nm in diameter
αB Fibril	αB-crystallin	1M GdnHCl, 0.1M sodium phosphate	7.4	60	2	Long fibrils, (> 1 μm in length)
αB Amorphous	αB-crystallin	1M GdnHCl, 0.1M sodium phosphate	7.4	90	2	Larger spherical aggregates ~ 30 nm in diameter, singly or in row-like clumps
βH Fibril	βH-crystallin	H_2O with 10 % TFE	2	60	18	Short, curly fibrils, 20 nm to 200 nm in length
ADH Amorphous	ADH	1M GdnHCl, 0.1M sodium phosphate	7.4	90	2	Large non-fibrillar protein clumps

Spin filtering to remove GdnHCl (where present) was again performed on all samples (§ 2.3.4). All new species were examined by TEM prior to chaperone assessment (Figure 6.9). αB-Crystallin species were almost identical to those seen for αT-crystallin (Figures 6.4 and 6.5), with the exception of the αB-crystallin

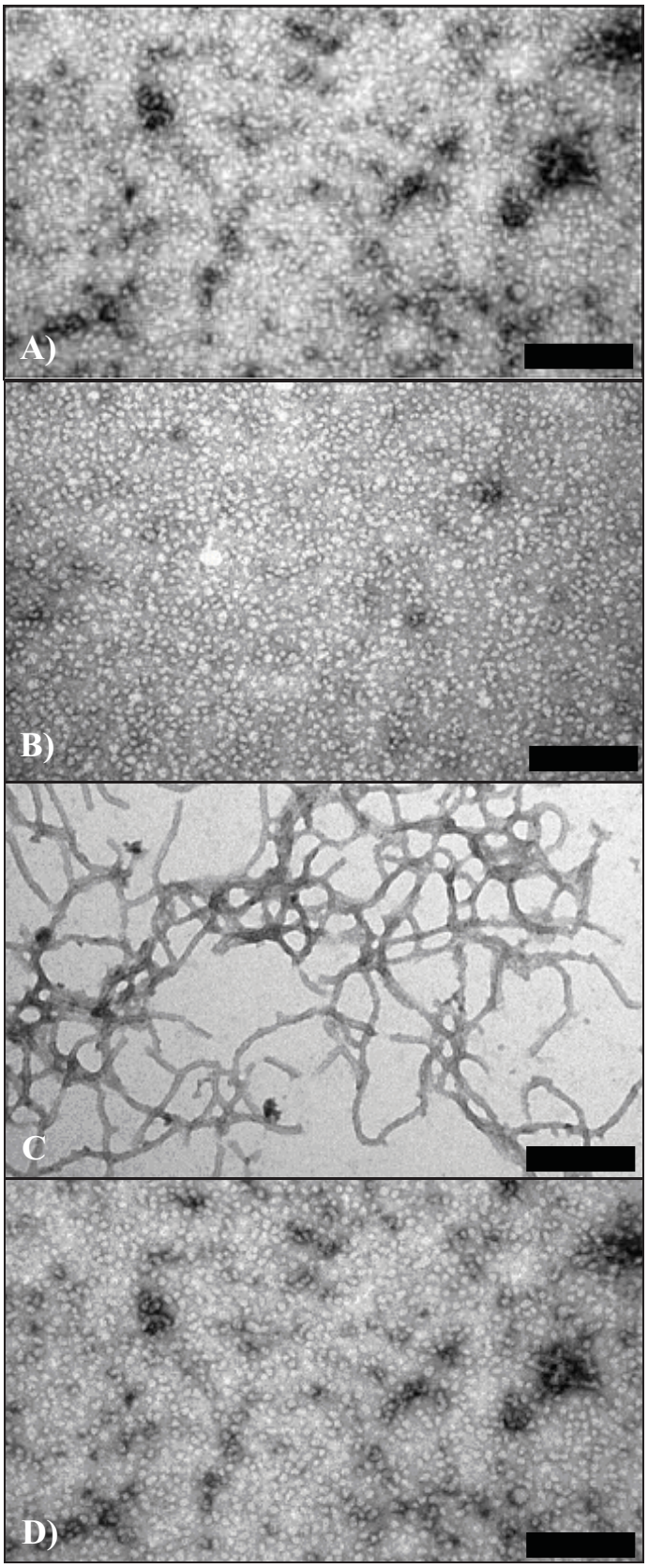

Figure 6.9: TEM of αB-crystallin species formed to assess the effects of structural variation on chaperone activity: A) αB Native; B) αB GdnHCl Native; C) αB Fibril; D) αB Amorphous. All samples were prepared as described in Table 62. Scale bars are 200 nm.

amyloid fibril sample, which showed amyloid fibrils over 1 μm in length and almost no amorphous aggregates (Figures 6.4C and 6.9C). Chaperones were assessed against insulin amorphous aggregation and RCM κ-casein amyloid fibril aggregation (as described previously, § 6.2.3), as assays at this temperature previously showed no chaperone activity by general non-chaperone based amyloid fibril and amorphous aggregate structures (such as that seen at 60 °C).

Destabilised forms of αB-crystallin, including GdnHCl treated native protein and both fibrillar and amorphous aggregates, act as successful chaperones to prevent both insulin amorphous aggregation and RCMκ-casein amyloid fibril formation (Figure 6.10). For both target proteins, there was a statistically significant increase in chaperone activity of αB Fibril compared to αB Native (although only minor in the case of RCM κ-casein fibril formation). There was also a non-significant trend towards increased activity by the αB GdnHCl Native (compared to αB Native) evident against both insulin and RCMκ-casein aggregation (amorphous and fibrillar, respectively). Similarly to αT-crystallin amorphous aggregates, the αB Amorphous sample acted significantly more effectively against insulin amorphous aggregation (over three times as effective as αB Native), yet acted with equivalent activity to native αB-crystallin against RCMκ-casein amyloid fibril formation. The increased activity against insulin aggregation thus appears specific to that target protein. Further, it is unlikely to be an effect of the enhanced exposed hydrophobicity of this species, as ADH amorphous aggregates and βH-crystallin amyloid fibrils exhibited no chaperone activity against these target proteins under these conditions (Figure 6.10).

6.3 Discussion of chaperone activity by α-crystallin aggregate species

α-Crystallin maintains its ability to chaperone even under considerable structural stress. A number of researchers have demonstrated that α-crystallin not only acts as a chaperone but that its chaperone ability is increased when it is structurally perturbed, i.e. under conditions of increased temperature or GdnHCl exposure α-crystallin becomes partially unfolded and has an enhanced chaperone ability

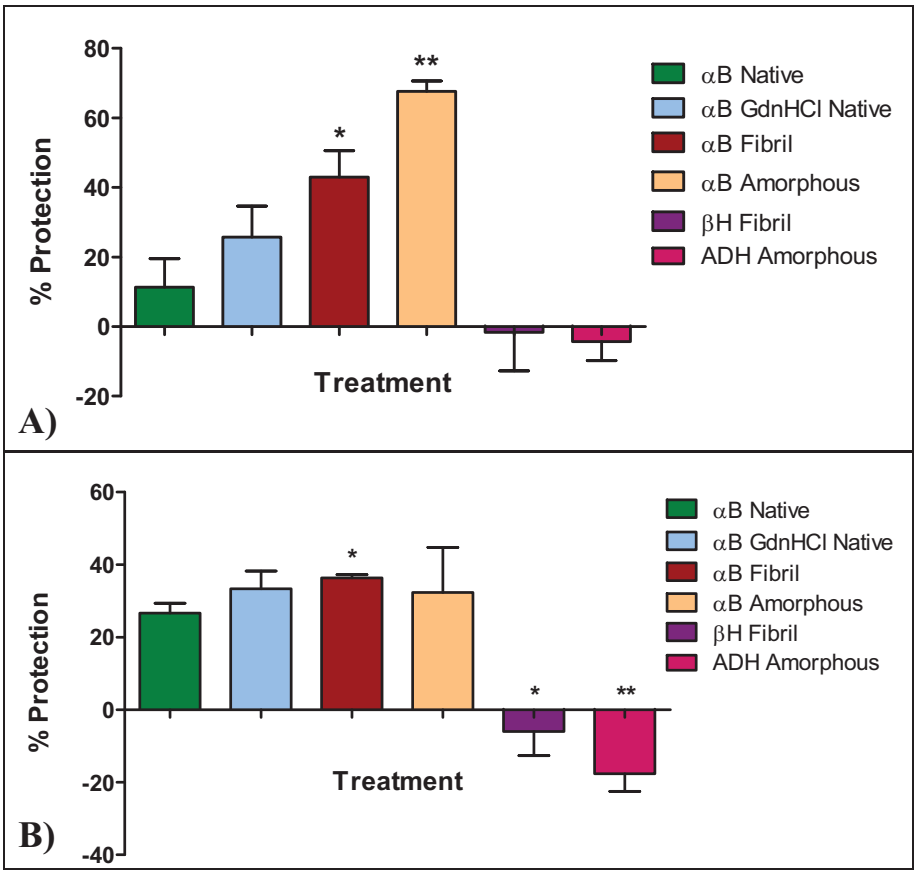

Figure 6.10: Chaperone protection of various native, fibrillar and amorphous species against: A) amorphous aggregation of insulin, 250 µg/mL at 37 °C in 0.1 M sodium phosphate, 20 mM DTT, pH 7.4 (chaperone at 800 µg/mL); and B) amyloid fibril aggregation of RCM κ-casein, 400 µg/mL, 10 µM ThT at 37 °C, pH 7.4 (chaperone at 200 µg/mL). P values, derived by student t-tests, indicate a significant difference against αB Native and equal: * < 0.05, ** < 0.01, * < 0.001.**

(Das, B. K. and Liang, J. J. 1997; Raman, B. and Rao, C. M. 1997; Datta, S. A. and Rao, C. M. 1999; Reddy, G. B. *et al.* 2000; Spinozzi, F. *et al.* 2006). Further, a range of other treatments and conditions have also been shown to enhance the activity of α-crystallin, including pressure treatment, various small molecules, metal effects and some post-translational modifications, e.g. phosphorylation (Bode, C. *et al.* 2003; Ganadu, M. L. *et al.* 2004; Srinivas, V. *et al.* 2005; Ecroyd, H. *et al.* 2007; Ecroyd, H. and Carver, J. A. 2008b). Finally, α-crystallin retains some of its chaperone activity even when fully unfolded at low pH (S. Buckley unpublished data, Raman, B. *et al.* 2005).

As discussed earlier (§ 6.1), there is a link between hydrophobicity and chaperone activity. Thus, an increase in the exposed hydrophobicity of a chaperone protein would be expected to result in increased chaperone ability. Such a mechanism

may also account for the generic chaperone activity observed in this study from amorphous and fibrillar forms of proteins in high temperature assays (60 °C). Amyloid fibrils from specific proteins may, due to the structural changes undergone during fibril formation, have accessible hydrophobic regions and, as a result, some inherent chaperone activity under appropriate conditions. The ability of non-chaperone based amyloid fibrils and amorphous aggregates (derived from βH-crystallin and ADH, respectively) to act as chaperones to prevent catalase amorphous aggregation at 60 °C is likely to be an example of exposed hydrophobic regions acting in a chaperone manner. Interestingly, under these conditions both amorphous and amyloid fibrillar aggregates of αT-crystallin were significantly less effective chaperones than native αT-crystallin and showed a non-significant trend of lower chaperone activity than their non-chaperone amyloid fibril or amorphous aggregate counterparts.

The current project has demonstrated that even after undergoing the extreme structural rearrangement necessary to convert α-crystallin into amyloid fibrils or amorphous aggregates, significant chaperone activity is retained. Whilst some of this chaperone activity may de due to remnant native protein, which may be acting with an increased activity due to structural destabilisation, the high levels of chaperone activity which occur, particularly with αB-crystallin (in which little native protein is found in fibrillar samples) argues that some of this chaperone activity is due to the amorphous and fibrillar species present. Against both amorphous insulin aggregation and RCM κ-casein amyloid fibril formation (both at 37 °C) α-crystallin amyloid fibrils and amorphous aggregate species act as effective chaperones. Under these conditions, non-chaperone based amyloid fibrils and amorphous aggregates do not exhibit chaperone activity. This indicates that the chaperone activity of α-crystallin amyloid fibril and amorphous aggregate species is due to the specific chaperone properties of α-crystallin being retained, as opposed to the activity of general exposed hydrophobic regions (as was observed in high temperature assays).

Table 6.3 summarises the chaperone activity results for αT- and αB-crystallin species and clearly shows that there is significant variation in the chaperone

activity of the different forms of α-crystallin. Altered chaperone activity is evident against different target proteins, as well as for the different types of aggregation and assay conditions. As a result of these variations, it is difficult to draw generalised conclusions about the effects of α-crystallin aggregated species. Nevertheless, it is certain that even after α-crystallin has undergone the major structural rearrangement necessary to produce amorphous aggregates or amyloid fibrils it still retains, against all target proteins and under all conditions tested, a significant degree of its chaperone ability.

Table 6.3: Chaperone results for αT- and αB-crystallin species, showing percent protection values from § 6.2.3 and § 6.2.4. Symbols show difference in activity compared to native sample for each target protein.

	Native	GdnHCL Native	Fibrillar	Amorphous
αT-crystallin:				
Insulin amorphous aggregation	30 ± 2	70 ± 2 ↑	36 ± 11 —	63 ± 2 ↑
Catalase amorphous aggregation*	55 ± 6	55 ± 5 —	11 ± 2 ↓	7 ± 15 ↓
RCMκ-casein amyloid fibril formation	49 ± 4	42 ± 6 —	34 ± 11 ↓	49 ± 1 —
αB-crystallin:				
Insulin amorphous aggregation	11 ± 8	25 ± 9 —	43 ± 8 ↑	68 ± 3 ↑
RCMκ-casein amyloid fibril formation	27 ± 3	33 ± 5 —	36 ± 1 ↑	32 ± 12 —

* Non-chaperone amyloid fibril and amorphous aggregate controls acted as chaperones against this target protein under these conditions

At high temperatures, i.e. 60 °C, all amyloid fibril and amorphous species tested demonstrated some chaperone activity, including those derived from proteins that possess no native chaperone activity. However, in assays at 37 °C, against two target proteins each aggregating in a different way (insulin aggregating amorphously and RCM κ-casein forming into amyloid fibrils) α-crystallin species retained chaperone activity whilst non-chaperone based amyloid fibrils and amorphous aggregates provided no chaperone protection to the aggregating proteins. This indicates that for both αT- and αB-crystallin the structural changes that occur in amyloid fibril formation do not necessarily result in a loss of protein function. This is very unusual in the process of fibril formation, and may be the first recorded instance of the retention of biological functionality within a fibrillar

form. However, further examination will be required to establish the extent to which native α-crystallin acts within these samples, and thus exactly how much activity is due solely to α-crystallin fibrillar species.

In the case of α-crystallin, and possibly other chaperones, this preservation of chaperone activity may be seen as a natural progression from the increase in chaperone ability when α-crystallin is structurally destabilised. For molecular chaperones to work most effectively in these conditions, when they are most needed, they must be able to maintain their chaperone activity under conditions which cause structural perturbation (Carver, J. A. and Lindner, R. A. 1998). For α-crystallin, a conserved region in the C-terminal domain has been identified as one of the putative chaperone binding sites (Ghosh, J. G. *et al.* 2005). This may remain exposed to solution for potential interaction with target proteins even after fibril formation (Meehan, S. *et al.* 2007), allowing the α-crystallin fibril to exhibit comparable levels of chaperone activity to the protein in its native conformation.

Putative regions involved in amyloid fibril formation from αB-crystallin and αA-crystallin have been previously studied using aggregation profile prediction software (Tartaglia, G. G. *et al.* 2008). For both profiles, the C-terminal extension remains external to the proposed fibrillar core (Figure 6.11, adapted from Meehan, S. *et al.* 2007). This finding is supported by NMR studies of fibrillar αB-crystallin, which indicate that the extension retains its flexibility upon fibril formation (Meehan, S. *et al.* 2007). Many regions have been listed as potential chaperone active sites, and these may vary depending on the type of aggregation being examined, i.e. amorphous or fibrillar (Ecroyd, H. and Carver, J. A. 2008a). Residues 131-134 in αB-crystallin are potentially involved in αB-crystallin chaperone activity against amorphously aggregating targets (Ghosh, J. G. *et al.* 2005). This region, according to protein aggregation predictions (Figure 6.11), would be situated external to the fibrillar core (Meehan, S. *et al.* 2007). As would a second region, further into the C-terminal region, in which mutation has been shown to have effects on both chaperone activity and the oligomerisation of αB-crystallin (Treweek *et al.* 2007). These sequences differ from the proposed chaperone active site on αA-crystallin (residues 70-88) which equates to a second

proposed chaperone active site on αB-crystallin (residues 73-92) (Sharma, K. K. *et al.* 2000; Bhattacharyya, J. *et al.* 2006), both of which would be incorporated into a proposed α-crystallin fibrillar state. If αB-crystallin fibrillar aggregates retain a chaperone region external to the fibrillar core, this may explain the increased chaperone activity observed by these species against insulin amorphous aggregation and RCM κ-casein fibril formation. In addition, regions external to the fibrillar core would, most likely, be in extended conformations and/or conformationally mobile (Meehan, S. *et al.* 2007) which may facilitate its interaction with target proteins during chaperone action.

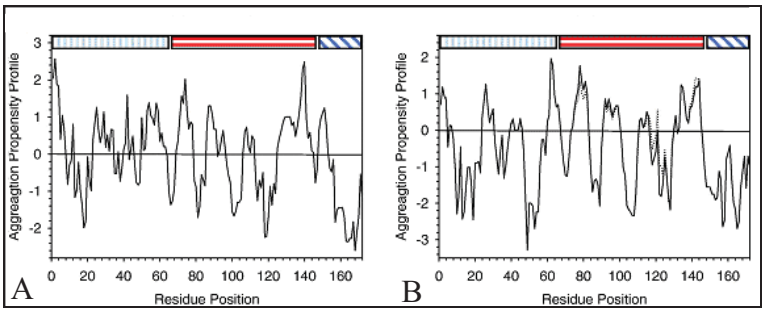

Figure 6.11: Amyloid aggregation profile for α-crystallin species, adapted from Meehan *et al.* (2007)[12], indicating aggregation profiles generated for: (A) αA-crystallin at pH 7.4; (B) αB-crystallin (continuous line) and an αB-crystallin mutant, R120G αB-crystallin (dotted line) at pH 7.4. Indicated on the panels as rectangular boxes are the N-terminal domain (vertical line pattern), the central "α-crystallin" domain (horizontal line pattern), and C-terminal domain (diagonal line pattern) encompassing the flexible C-terminal region. Aggregation propensity is shown, with the higher the aggregation propensitiy score the more liable a region is self associate into β-sheeted structure.

The ability of αB-crystallin fibrillar aggregates to act as molecular chaperones is a surprising finding. For most proteins, the formation into amyloid fibrils requires a significant change in protein structure. It is rare that biological function is retained after such structural perturbation, and this situation is generally only observed in biologically active amyloid fibrils, the amyloidins (Chiti, F. and Dobson, C. M. 2006; Fowler, D. M. *et al.* 2006; Gras, S. L. *et al.* 2008). Unlike αT-crystallin fibrils, which occur as a mixed population of amyloid fibrils and amorphous aggregates, αB-crystallin amyloid fibrils are formed with very limited quantities of amorphous aggregates present. Further, against RCM κ-casein amyloid fibril

[12] Reprinted with permission from Elsevier.

formation, αB-crystallin amyloid fibrils acted with enhanced activity, while amorphous aggregates of αB-crystallin acted in an equivalent manner to native αB-crystallin. This indicates that αB-crystallin amyloid fibrils not only retain the chaperone activity of the native protein, but that it may have an enhanced function due to the structural rearrangement that has occurred. Enhanced biological activity has previously been observed in the attachment of catalytic enzymes to peptide nanotubes, and is thought to be related to stabilisation of more bioactive structural forms of the active molecule (Yu, L. *et al.* 2005).

For over 15 years, α-crystallin has been recognised as a molecular chaperone of great importance in the prevention of cataract and other protein aggregation disorders (Horwitz, J. 1992; Ecroyd, H. and Carver, J. A. 2008a). This research has established that both αT-crystallin and αB-crystallin can each retain chaperone activity following destabilisation by GdnHCl and the formation of amorphous aggregates and amyloid fibrils. Further, αB-crystallin has enhanced chaperone activity after structural modification into amyloid fibrils. Thus, α-crystallin's role as a molecular chaperone *in vivo* is likely to be maintained even under conditions wherein the protein cannot sustain its native conformation.

α-Crystallin's role as a molecular chaperone is to inhibit protein aggregation under conditions of cellular stress. As a result, α-crystallin's ability to work with enhanced activity when structurally perturbed is a desirable biological quality that assists the successful function of this protein. The results presented in this chapter provide further support for such a hypothesis. In fact, it may be proposed that nature has engineered α-crystallin to act as an effective chaperone under all potential protein states, i.e. when the protein is in normal, stressed (perturbed) and fibrillar states. If true, this would establish αB-crystallin as one of the small family of amyloidin, amyloid with biological functions which play important roles in the cellular environment. Further, αB-crystallin would be the only protein in that family which acts with the same native biological function in both its native and fibrillar state.

CHAPTER 7

Structural modification of αB-crystallin by immobilisation onto a solid carrier leads to enhanced chaperone activity

αB-Crystallin plays an important role in the prevention of amorphous aggregation and amyloid fibril formation throughout the body. As such, it has the potential to be used for therapeutic intervention for various amyloidoses where it is known to interact with the relevant fibril forming protein or peptide (Ecroyd, H. and Carver, J. A. 2008a). As discussed in the previous chapter (§ 6) structural modifications to α-crystallin may affect its chaperone capability, and in certain cases enhance α-crystallin's chaperone activity. To further the examination into the effect of structural modifications on α-crystallin, the effect of immobilising αB-crystallin onto a solid carrier has been investigated. This research is of particular relevance due to the potential use of immobilised αB-crystallin to prevent dialysis-related amyloidosis (DRA).

7.1 Structure of αB-crystallin

The biological activity of αB-crystallin owes much to its structural features. There is no crystal structure of αB-crystallin, due to the inherent flexibility and variable oligomeric characteristics of this protein (§ 1.3.3.1). However, it is possible to propose certain features of the protein structure from comparison with other sHSPs, such as *Methanococcus jannaschii* HSP-16.5 and wheat HSP-16.9, whose crystal structures are available (Kim, K. K. *et al.* 1998; Berengian, A. R. *et al.* 1999; Haley, D. A. *et al.* 2000; Van Montfort, R. L. *et al.* 2001; Augusteyn, R. C. 2004a; Ghosh, J. G. and Clark, J. I. 2005; Stamler, R. *et al.* 2005). αB-Crystallin, in common with all the sHSP family, contains an 'α-crystallin domain' (§ 1.3.3.1.1) to which is ascribed, at least in part, the chaperone activity of this class of proteins (De Jong, W. W. *et al.* 1998). Comparisons of tertiary structures and features in the regions conserved between sHSPs, as well as structural studies by techniques including NMR spectroscopy, mass spectrometry and surface plasmon resonance, have led to an increased understanding of the structure of αB-crystallin (Lindner, R. A. *et al.* 1998; Carver, J. A. 1999; Aquilina, J. A. *et al.* 2004; Liu, L. *et al.* 2006). Figure 7.1 outlines the polypeptide sequence and putative secondary features of αB-crystallin. It also highlights the position of lysine residues in this protein (in red) (adapted from: Carver, J. A. *et al.* 1992; Carver, J. A. *et al.* 1994; Carver, J. A. and Lindner, R. A. 1998; Augusteyn, R. C. 2004a; Ghosh, J. G. *et al.* 2005). The presence of accessible lysines, particularly in the C-terminal extension

of αB-crystallin (underlined), provides a platform for immobilisation *via* Schiff-based chemistry as will be discussed in § 7.2.2.

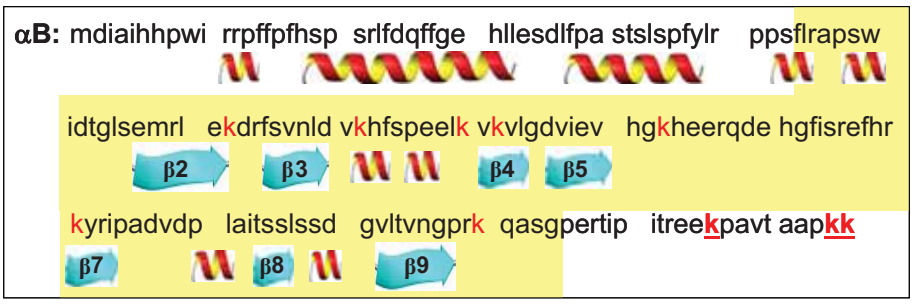

Figure 7.1: Primary sequence of αB-crystallin, with the crystallin domain highlighted in yellow. Putative secondary features (α-helices and β-strands, based on the X-ray crystal structure of two non-mammalian sHSPs, wheat HSP 16.9 and *Methanococcus jannaschi* HSP 16.5) are indicated (Ghosh, J. G. and Clark, J. I. 2005). Lysine residues are labeled in red and solvent exposed lysine residues underlined (Carver, J. A. *et al.* 1992).

Due to the importance of αB-crystallin's chaperone abilities, wherein it acts as a first line of defence against protein misfolding and aggregation in many cells throughout the body (Ecroyd, H. and Carver, J. A. 2008a), various studies have been undertaken into ways to increase αB-crystallin's chaperone activity (§ 6.3). These have included investigation into the effects of temperature, small molecules, post-translational modifications, cross-linking and other structural modifiers (Koretz, J. F. *et al.* 1998; Datta, S. A. and Rao, C. M. 1999; Bode, C. *et al.* 2003; Aquilina, J. A. *et al.* 2004; Kumar, M. S. *et al.* 2005; Ecroyd, H. and Carver, J. A. 2008b). Many of these modifications have been shown to effectively alter αB-crystallin's chaperone activity *in vitro* against one or two misfolding (target) proteins, and they are thought to be reflections of processes which would up-regulate chaperone protection and activity *in vivo* (Haslbeck, M. et al. 2005).

While αT-crystallin is traditionally associated primarily with chaperoning against amorphous aggregation, for example in the mammalian eye lens (Augusteyn, R. C. *et al.* 2002), αB-crystallin has been shown, in recent years, to also protect against fibrillar forms of protein aggregation (Rekas, A. *et al.* 2004; Ecroyd, H. *et al.* 2007; Ghosh, J. G. *et al.* 2007). Of particular relevance to this study, αB-crystallin has been shown to protect β2-microglobulin from aggregation into amyloid fibrils *in vitro*, when in conditions that cause αB-crystallin to exist in a molten globule state, i.e. in solution at pH 2.5 (Raman, B. *et al.* 2005).

This chapter further explores the nature of the αB-crystallin's chaperone activity by examining how α-crystallin interacts with a range of misfolding proteins *in vitro* when immobilised on a polymerised aldehyde surface. Protein immobilisation has become an area of research focus over the last decades due to its potential uses in a range of fields, including biosensing, protein fouling prevention, protein structure studies and tissue outgrowth (McArthur, S. L. *et al.* 2001). During this research, all immobilisation was achieved via plasma polymerisation followed by Schiff-based covalent linkage, as discussed below (§ 7.2). The interactions produced following covalent immobilisation of αB-crystallin onto this surface are characterised by XPS, AFM and QCM-D analysis. The chaperone activity of native and immobilised αB-crystallin were then investigated against amorphous (insulin and catalase) and amyloid fibril (RCM κ-casein and R3A β2-microglobulin) aggregation.

7.2 Protein immobilisation

7.2.1 Aldehyde polymerisation onto solid carriers

Thin polymer coatings are increasingly used to modify the interfacial properties of base substances (Blattler, T. M. *et al.* 2006). Plasma generated aldehyde polymers can be instigated on a wide range of solid supports, including thick and thin fluorinated ethylene propylene copolymers (FEP), silicon wafer and gold coated surfaces, all of which were used in this research. Plasma coating of solid carriers with aldehyde polymer layers was achieved following the method of Blättler *et al.* (2006). Plasma treatment proceeded at 50 watts for 2 minutes, followed by treatment at 20 watts for a further 2 minutes (§ 2.4.1.1).

X-ray photoelectron spectroscopy is a technique used for characterisation of the composition of surfaces, providing quantitative information on the elements within the surface layer or adlayer (Griesser, H. J. *et al.* 2004). XPS is based upon photoelectron emissions, which differ dependent on which element they originate from. Thus, by using X-rays to excite molecules the emitted photoelectrons can be measured and used to establish the elemental composition of the surface, up to a depth of 10 nm (Griesser, H. J. *et al.* 2003). XPS analysis (§ 2.4.2.1) indicated a confluent polymer aldehyde layer was produced on FEP, completely coating the surfaces to a thickness of over 10 nm. Prior to aldehyde polymerisation the

fluorine peak on FEP had been 67 % but decreased to less than 3 % after treatment. This drop in fluorine availability indicates that this species is now buried under the polymer aldehyde layer by the treatment. The associated increase in the peaks of carbon and oxygen represents those aldehydes and will be discussed in detail below (§ 7.2.2.1). Plasma polymerisation, has previously been demonstrated to be equally effective on FEP, silicon wafer and other solid materials (Vermette, P. *et al.* 2003; Thissen, H. *et al.* 2006).

Surface topography of silicon wafer coated with aldehydes or with surface immobilised αB-crystallin (§ 7.2.2.2) was examined using AFM, performed by Dr. M. Nussio (Flinders University, Australia). Liquid tapping mode AFM (§ 2.4.2.2) topographical images of the aldehyde polymer layer on silica wafer (selected as representative of all 3 surfaces) revealed a flat surface, with a Z-range of 8.0 nm ± 2.6nm (Figure 7.2). This indicates the creation of a smooth surface that does not significantly vary in roughness to silicon wafer alone (Mueller, H. *et al.* 1999). Occasional granular material was observed and assumed to be experimental atmospheric contamination prior to plasma treatment. These granular features were variable in size, with diameters ranging from 4.4 nm to 61.1 nm. They were found on surfaces before and after protein immobilisation and were never observed to constitute more than 3.5 % of any AFM image.

7.2.2 Covalent immobilisation of proteins to aldehyde polymer layers on solid carriers

Covalent immobilisation provides a strong and reliable attachment of peptides or proteins to selected substrates, and as such is highly desirable (Vermette, P. *et al.* 2003). Schiff-based chemistry is a well characterised technique which is known to create covalent bonds between amine groups and aldehyde groups, *via* the formation of imines. Sodium cyanoborohydrate is a commonly used catalyst due to its unique properties in preferentially reacting with the amine groups of lysine residues, whilst not affecting arginine or asparagine residues. αB-Crystallin contains 10 lysine residues (Figure 7.1). They are found primarily within the putative β-strand regions and the C-terminal extension, with no lysine residues contained in the N-terminal extension (Augusteyn, R. C. 2004a; Ghosh, J. G. *et al.* 2005) which is hypothesised to be relatively buried and inaccessible to solvent

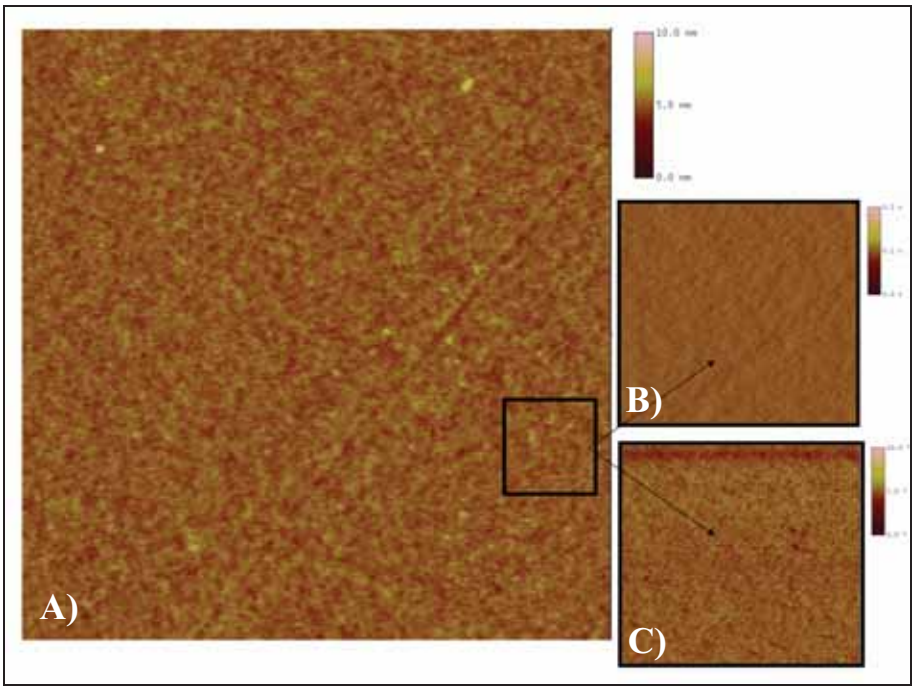

Figure 7.2: Atomic force micrograph images of aldehyde coated silicon wafer: A) AFM topographic image (2 x 2 µm^2, 512 x 512 lines), scale bar shows height variation (Z-scale: 0 - 10 nm); B) amplitude image at higher magnification (300 x 300 nm^2, 512 x 512 lines), scale bar shows volts (scale: 0 - 10 v); and C) phase contrast image, dual of amplitude, scale bar shows degree of viscoelasticity (scale: 0 - 10 °). All images are representative of 3 separate immobilisation experiments.

(Carver, J. A. *et al.* 1994). αB-Crystallin and BSA were immobilised onto aldehyde polymers produced on FEP and silicon wafer *via* sodium cyanoborohydrate reductive deamination (§ 2.4.1.2). Aldehyde-coated QCM-D crystals underwent protein covalent immobilisation during QCM experiments, as described below (§ 7.2.2.3). The success of protein immobilisation was characterised by XPS and AFM.

7.2.2.1 Assessment of protein immobilisation by X-ray Photoelectron Spectroscopy

Protein immobilisation on the FEP and silicon wafer was evidenced by the production of nitrogen peaks, quantified by XPS (Figure 7.3). A very similar level of nitrogen was observed for both FEP and silicon wafer, indicating the consistency of this immobilisation technique across a range of surfaces. Table 7.1 displays the composition of each surface prior and post protein immobilisation.

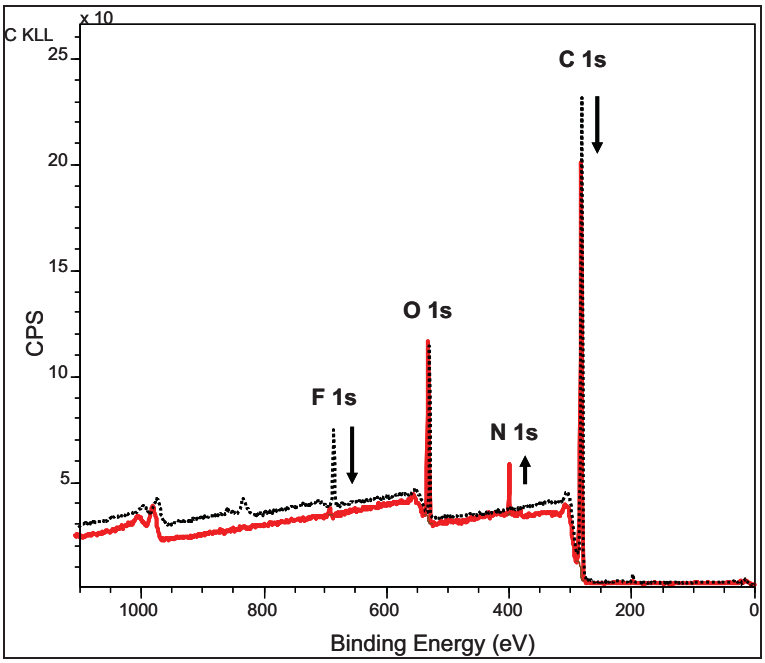

Figure 7.3: XPS chromatograph of aldehyde coated FEP (dashed black line) and FEP with αB-crystallin immobilised (solid red line), arrows indicate changes in elemental composition after αB-crystallin immobilisation. Image is representative of 3 separate immobilisation experiments.

Nitrogen content can be used as a means to determine the specific density of a protein present on a given surface using multilayer XPS algorithms, as described previously (Chatelier, R. C. *et al.* 1997; Thissen, H. *et al.* 2006). The use of XPS N signal from multiple integrated spectra to estimate the quantity of adsorbed protein with minimal random error was achieved using software designed by Chatelier, John et al. (1997). αB-Crystallin has a nitrogen composition of 8.9 %, as calculated from the atomic composition (Gasteiger E., H. C., Gattiker A., Duvaud S., Wilkins M.R., Appel R.D., Bairoch A. 2005). From this it can be estimated that 300 ng/cm^2 of protein was immobilised onto all surfaces (working not shown, provided by Professor H. Griesser, Ian Wark Research Institute, University of South Australia).

Table 7.1: XPS % atomic concentration for aldehyde-coated FEP with or without αB-crystallin immobilised (*n*=3).

Surface	% C	% O	% N	% F	% Other
Aldehyde-coated FEP	86 ± 1	12 ± 0	0 ± 0	2 ± 2	0 ± 0
Immobilised αB-crystallin on FEP	63 ±21	23 ± 11	7 ± 2	1 ± 1	0 ± 0

7.2.2.2 Atomic Force Microscopic analysis of protein immobilisation

Liquid phase tapping mode AFM (§ 2.4.2.2) confirmed that there was a significant increase in surface roughness of all topological images after αB-crystallin immobilisation on the surfaces. Figure 7.4 illustrates the surface topography, with the inset showing a closer (314 nm^2) subset of the surface-attached protein clearly showing granule-like structures. Grain analysis of these granules (§ 2.4.2.2), for 2 x 2 μm micrographs, revealed particles ranging in size between 8.8 nm and 31.5 nm, with a mean diameter of 16.0 nm ± 0.5 nm. Particle diameter was selected for analysis over height data due to the potentially uneven base surface produced by plasma deposition. Assuming a finite dimension of lateral convolution due to tip width (tip radius curvature of 15 nm) the data obtained from AFM topographical images indicates immobilisation of oligomeric species of αB-crystallin. The measured dimensions are in good agreement with those of αB-crystallin determined in solution *via* cryo EM, where a modal diameter of 15 nm for αB-crystallin assemblies, and a range between 8 and 18 nm was observed (Haley, D. A. *et al.* 1998).

The immobilised αB-crystallin oligomeric species were imaged in a stable and reproducible form. They occupied over 60 % of the imaged surface in all samples, withstood repetitive scanning and were able to be imaged at high resolution with no evidence of subunit exchange. These factors indicate a robust binding of αB-crystallin oligomers onto the solid carrier, as would be expected due to covalent attachment.

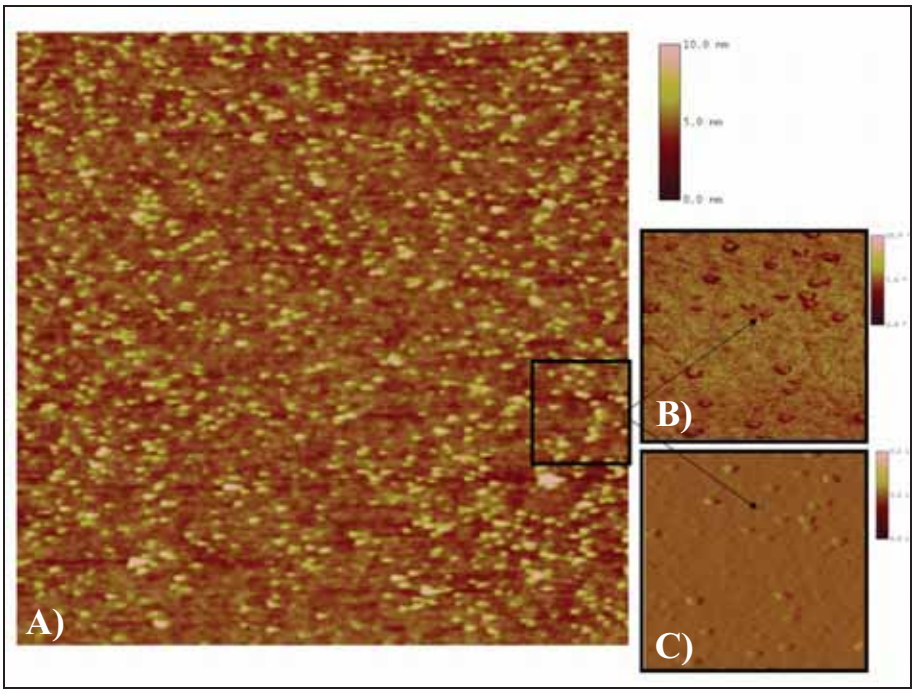

Figure 7.4: Atomic force micrograph images of silicon wafer with immobilised αB-crystallin: A) AFM topographic image (2 x 2 μm^2, 512 x 512 lines), scale bar shows height variation (Z-scale: 0 - 10 nm); B) amplitude image at higher magnification (300 x 300 nm^2, 512 x 512 lines), scale bar shows volts (scale: 0 - 10 v); and C) phase contrast image, dual of amplitude, scale bar shows degree of viscoelasticity (scale: 0 - 10 °). All images are representative of 3 separate immobilisation experiments.

7.2.2.3 Quartz crystal microbalance assessment of protein immobilisation

QCM-D is a technique used to accurately measure molecular mass on a surface and obtain information about its structural properties (Janshoff, A. *et al.* 2000). Quartz-crystal microbalance with dissipation measurements were performed with the assistance of Dr B. Thierry (University of South Australia, Australia). Quartz crystal microbalance with dissipation (QCM-D) measurements, were used to more accurately quantify the amount of αB-crystallin immobilised onto surfaces. Plasma treatment (as described above, § 7.2.1) was used to coat the gold surface of QCM sensors. This process produces an aldehyde plasma polymer layer with equivalent surface chemistry to that already observed on FEP and Silcon wafer (Vermette, P. *et al.* 2003; Thissen, H. *et al.* 2006). Covalent immobilisation of αB-crystallin *via* Schiff-linkage of lysine residues was then performed (§ 2.4.2.3).

Frequency shifts measured by the QCM-D technique can be converted to the mass of protein immobilised on the plasma functionalised QCM chips using the

Sauerbrey equation (Janshoff, A. *et al.* 2000). Although this equation underestimates the adsorbed mass for viscoelastic layers measured in liquids, for thin protein layers the difference is estimated to be less than 10 % (Voinova, M. V. *et al.* 2002). Importantly, the obtained mass is the wet mass, i.e. the mass of the adsorbed protein and the water coupled to the proteinaceous film which is associated with, or within, the immobilised layer (Rodahl, M. *et al.* 1997). As seen in Figure 7.5A, there was a frequency shift of -35 Hz (± 6 Hz) due to αB-crystallin immobilisation. The observed changes correspond (after taking the characteristics of the QCM chip into consideration) to a mass change of 616 ± 39 ng/cm^2 (§ 2.4.2.3). When compared with the mass of αB-crystallin determined by XPS (300 ng/cm^2), this result indicates that about 50 % of the mass obtained from QCM correspond to water coupled to the protein layer, in good agreement with a previously reported study (Voros, J. 2004).

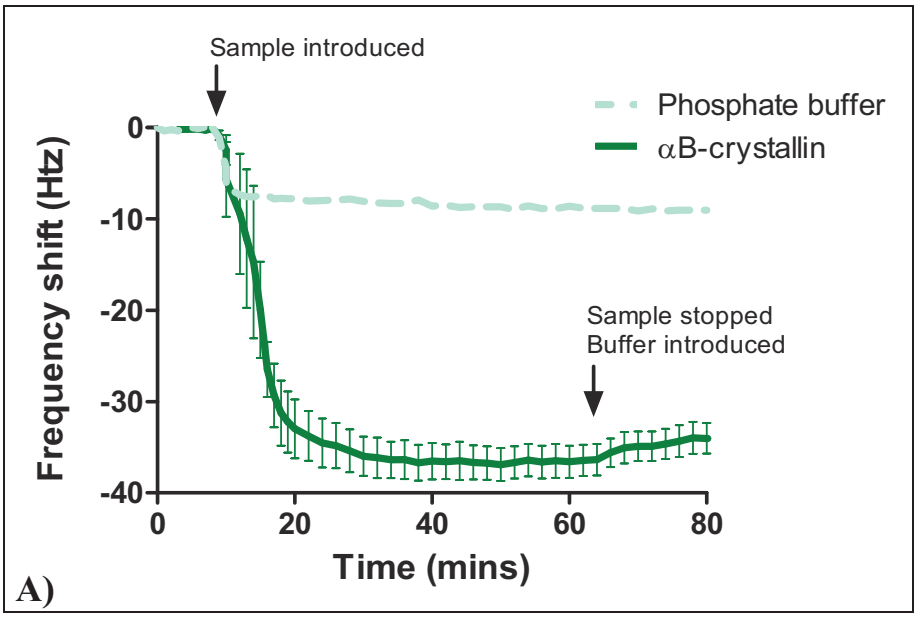

Figure 7.5: QCM-D results of αB-Crystallin immobilisation on Au-coated quartz crystals A) frequency plot showing change in Hz due to protein layer formation. Results are mean ± SE of three separate immobilisation experiments.

7.3 Chaperone activity of immobilised αB-crystallin

Chaperone activity of immobilised αB-crystallin was compared to that of αB-crystallin in solution against a range of target proteins, aggregating either amorphously or into amyloid fibrils, measured *via* light scattering or turbidity, as described previously (§ 2.3.1.1). Chaperone solution stocks were prepared a day prior to assay (immediately prior to immobilisation) and stored at 4 °C, as per

immobilisation procedure. Assay conditions were altered to include a sample volume of 100 µl in each well, increasing the ratio of immobilised protein to solution volume (as a finite amount of protein could be immobilised *via* the technique outlined above). FEP pieces were pre-cut to exactly cover the well base of a 96 well plate (6 mm diameter). Each assay included an aldehyde-coated FEP piece, to control against any spectroscopic impairment or interaction by the aldehyde-coated FEP alone. Chaperone protection was determined as a percentage using Eq.1 (§2.3.3).

7.3.1 Reduction-induced amorphous aggregation

Insulin (400 µg/mL) with or without αB-crystallin in solution, αB-crystallin covalently immobilised on FEP or aldehyde-coated FEP (with no protein immobilised) was incubated at 37 °C with 10 mM DTT and constant linear shaking at 115 rpm. The turbidity of the solution at 340 nm was measured every 60 seconds for 40 minutes, when a plateau was reached in the turbidity profile (Figure 7.6A), indicating that protein precipitation was complete (§ 2.3.1.1.2). The presence of aldehyde-coated FEP did not significantly alter insulin aggregation or impair turbidity measurements. A significant decrease in insulin aggregation was observed in the presence of αB-crystallin immobilised on FEP, as compared to insulin alone or insulin with aldehyde-coated FEP (Figures 7.6A and B). No significant difference of insulin aggregation was observed in the presence of BSA immobilised on FEP (data not shown). Immobilised αB-crystallin reduced the amount of light scatter due to the aggregation and precipitation of insulin by 35 ± 8 %, which was significantly more than the activity of an equivalent amount (850 ng/mL, which is a 1:0.0006 molar ratio of insulin:αB-crystallin) of αB-crystallin in solution (Figure 7.6C). To achieve a similar chaperone effect to that of immobilised αB-crystallin (on FEP), a 5,000-fold higher concentration of αB-crystallin in solution was necessary (Figure 7.6C, Table 7.2).

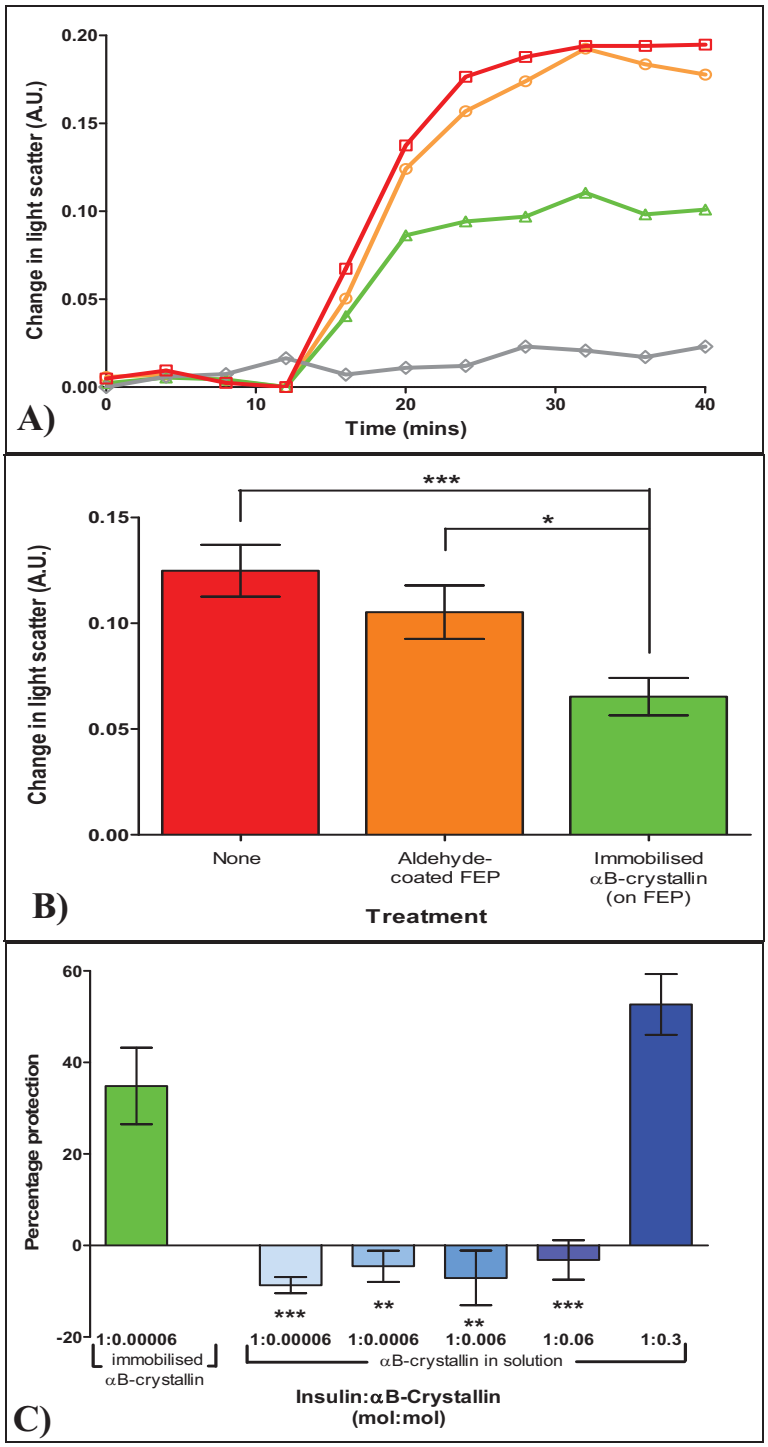

Figure 7.6: Protection by αB-crystallin of insulin amorphous aggregation induced by reduction of its disulfide bonds (mean ± SE of 4 separate immobilisation experiments; P values indicating significant difference from student t-tests are * <0.05, **<0.01, *<0.001): A) turbidity of buffer with DTT ◇, insulin alone □, and in the presence of aldehyde-coated FEP ○ or immobilised αB-crystallin (on FEP) △ ; B) showing maximum light scatter at 40 minutes; and C) amount of protection immobilised αB-crystallin (on FEP) provides against insulin aggregation compared with increasing amounts of αB-crystallin in solution until an equal rate of chaperone activity is observed (significance values are given against immobilised αB-crystallin activity, all ratios are mol insulin:mol αB-crystallin).**

7.3.2 Thermally induced amorphous aggregation

Catalase underwent amorphous aggregation and precipitation upon heating at 55 °C (§ 2.3.1.1.1). Catalase (200 μg/mL) with or without αB-crystallin in solution, αB-crystallin covalently immobilised on FEP or aldehyde-coated FEP (with no protein immobilised) was incubated at 55 °C and with constant linear shaking at 115 rpm. The turbidity of the solution at 340 nm was measured every 2 minutes and precipitation was judged complete (i.e. a plateau was reached) after 50 minutes.

The presence of aldehyde-coated FEP did not significantly alter catalase aggregation or impair turbidity measurements. A significant decrease in catalase aggregation (turbidity) was observed in the presence of immobilised αB-crystallin (on FEP), as compared to both catalase alone and catalase in the presence of aldehyde-coated FEP (Figure 7.7A). In total, the small amount of immobilised αB-crystallin (850 ng/mL) decreased the amount of light scattering due to the aggregation and precipitation of catalase by 39 ± 8 %. In contrast, an equivalent concentration αB-crystallin in solution caused significantly different behaviour, leading to a significant increase in catalase aggregation (Figure 7.7B), an effect we have observed before with the addition of low levels of chaperone and which is discussed in more detail below. Immobilised αB-crystallin works much more effectively as a chaperone than when it is in solution. In fact, a 1,000-fold higher concentration of αB-crystallin in solution was needed to achieve the same amount of protection as immobilised αB-crystallin (Figure 7.7C, Table 7.2).

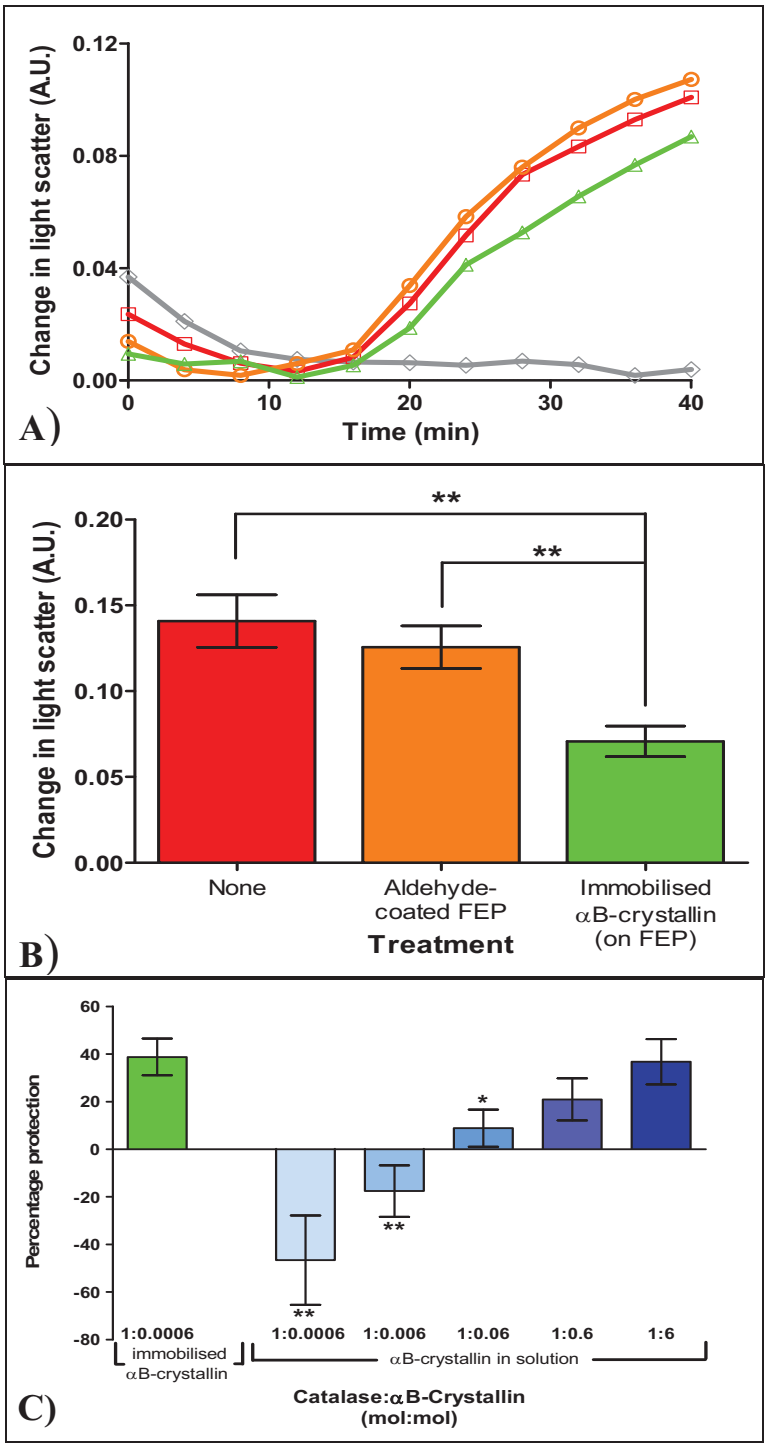

Figure 7.7: Protection of catalase against thermally induced amorphous aggregation by αB-crystallin (mean ± SE of 3 separate immobilisation experiments; P values indicating significant difference from student t-tests are * <0.05, **<0.01, *<0.001): A) turbidity of buffer alone ◇, catalase alone □, and in the presence of aldehyde-coated FEP ○ or immobilised αB-crystallin (on FEP) △; B) showing maximum fluorescence at 50 minutes; and C) amount of protection immobilised αB-crystallin (on FEP) provides against catalase aggregation compared to increasing amounts of αB-crystallin in solution until an equal rate of chaperone activity is observed (significance values are given against immobilised αB-crystallin activity, all ratios are mol catalase:mol αB-crystallin).**

7.3.3 Amyloid fibrillar aggregation of κ-casein

Reduced and carboxymethylated κ-Casein (§ 2.2.3) was incubated at 37 °C and amyloid fibril formation was monitored *in situ* by measuring ThT fluorescence (§ 2.3.2.1.8), with a plateau in fluorescence, indicating completion of fibril formation, reached within 12 hours (Figure 7.8A). The presence of aldehyde-coated FEP did not significantly alter RCM κ-casein aggregation. A significant decrease in RCM κ-casein fibril formation was observed in the presence of immobilised αB-crystallin (on FEP) when compared to RCM κ-casein fibril formation alone and in the presence of aldehyde-coated FEP (Figure 7.8A and B). No significant difference of RCM κ-casein fibril formation was observed in the presence of BSA immobilised on FEP (data not shown). Immobilised αB-crystallin decreased the maximum ThT fluorescence of RCM κ-casein by 15 ± 4 %, while at an equivalent concentration αB-crystallin in solution showed no alteration in ThT fluorescence associated with RCMκ-casein fibril formation (Figure 7.8C). To achieve a similar chaperone effect to that of immobilised αB-crystallin, 5,000 times more αB-crystallin in solution was required (Figure 8C, Table 7.2).

7.3.4 Mutation induced amyloid-like fibrillar aggregation of β2-microglobulin

A disease-linked protein, β2-microglobulin, was also assessed as a physiologically relevant amyloid forming target protein. Destabilisation of this target protein was achieved as described previously (§ 4.1.1), by prior mutation of an arginine (R3) to an alanine (A), which disrupts β2-microglobulin's stability (Esposito, G. *et al.* 2005; Corazza, A. *et al.* 2004). Fibrils were formed at physiological pH and temperature, with all solutions agitated in an orbital manner (700 rpm) throughout the fibril formation process (§ 2.3.2.1.2; § 4.3) until formation was judged complete at 13 days.

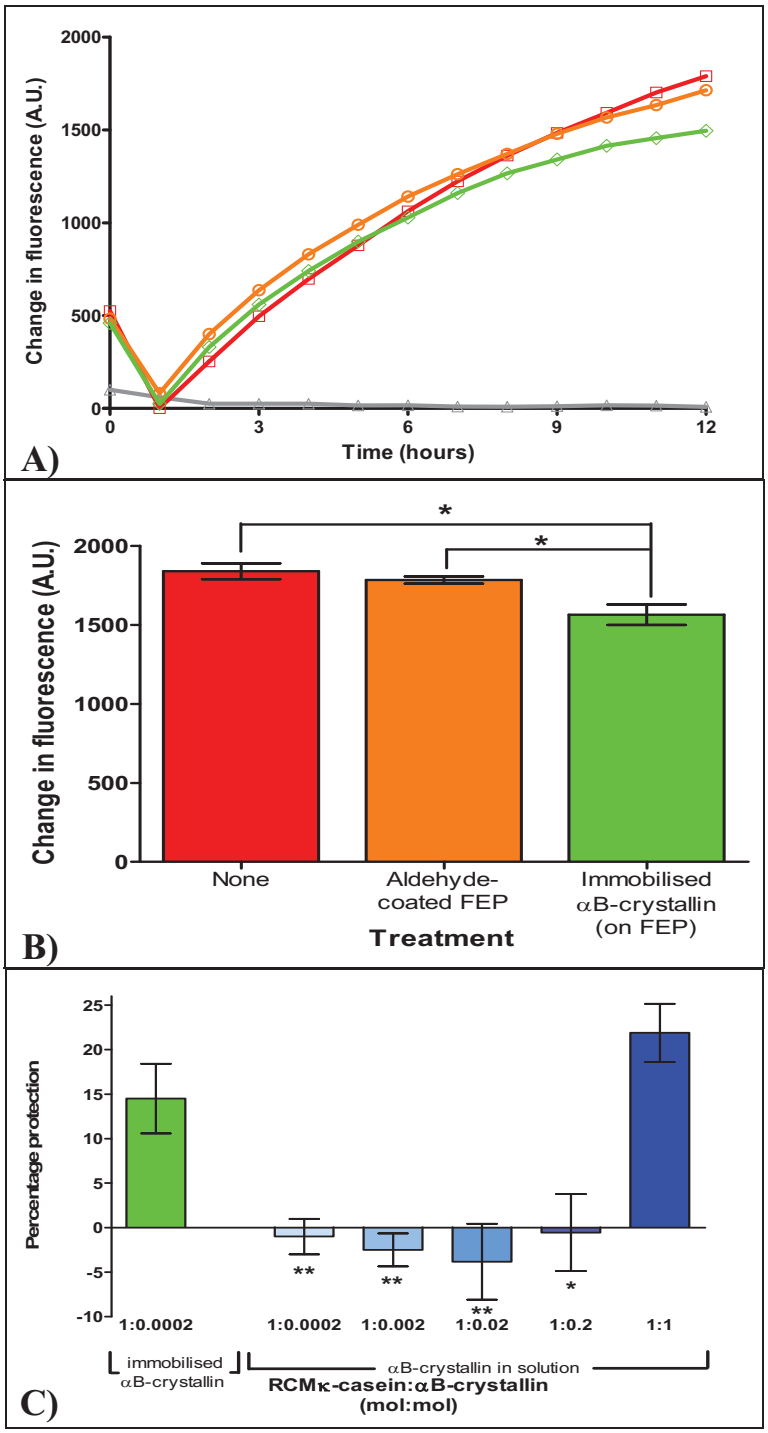

Figure 7.8: Protection by αB-crystallin of RCM κ-casein fibril formation (mean ± SE of 3 separate immobilisation experiments; P values indicating significant difference from student t-tests are * <0.05, **<0.01): A) ThT fluorescence of ThT buffer ◇, RCM κ-casein alone □, and in the presence of aldehyde-coated FEP ⬡ or immobilised αB-crystallin (on FEP) △; B) showing maximum fluorescence at 12 hours; and C) amount of protection immobilised αB-crystallin (on FEP) provides against RCM κ-casein fibril formation compared to increasing amounts of αB-crystallin in solution until an equal rate of chaperone activity is observed (significance values are given against immobilised αB-crystallin activity, all ratios are mol RCM κ-casein:mol αB-crystallin).

The presence of aldehyde-coated FEP did not significantly alter R3A β2-microglobulin fibril formation. A significant lowering of R3A β2-microglobulin fibril formation was observed in the presence of immobilised αB-crystallin (on FEP), decreasing maximum fluorescence of ThT by 53 ± 8 % (Figure 7.9A). At an equivalent concentration αB-crystallin in solution (850 ng/mL) an increase in fibril formation of R3A β2-microglobulin fibril formation was observed (Figure 7.9B). αB-Crystallin in solution acts as a very effective chaperone against slowly aggregating target proteins (Carver, J. A. and Ecroyd, H. 2008), such as R3A β2-microglobulin, and was therefore observed to effectively chaperone this target protein at much lower concentrations in solution than the other target proteins studied. However, immobilised αB-crystallin was still found to be as effective at preventing fibril formation of R3A β2-microglobulin as a 100-times greater amount of αB-crystallin in solution (Figure 7.9C, Table 7.2).

Immobilised BSA (on FEP) was also used in this assay to examine whether covalent immobilisation of proteins leads to a general decrease in the aggregation of target proteins, rather than an enhancement of αB-crystallin's chaperone activity specifically. However, immobilised BSA (on FEP) had no statistically significant effect on R3A β2-microglobulin fibril formation and the ThT fluorescence of R3A β2-microglobulin associated with it. TEM was used to confirm the presence of R3A β2-microglobulin fibrils alone, in the presence of aldehyde coated FEP, and in the presence of FEP with either αB-crystallin or BSA immobilised (Figure 7.10). There were noticeably fewer fibrils in the presence of FEP with immobilised αB-crystallin (Figure 7.10C), whilst larger aggregates were observed in the presence of FEP immobilised BSA (Figure 7.10D).

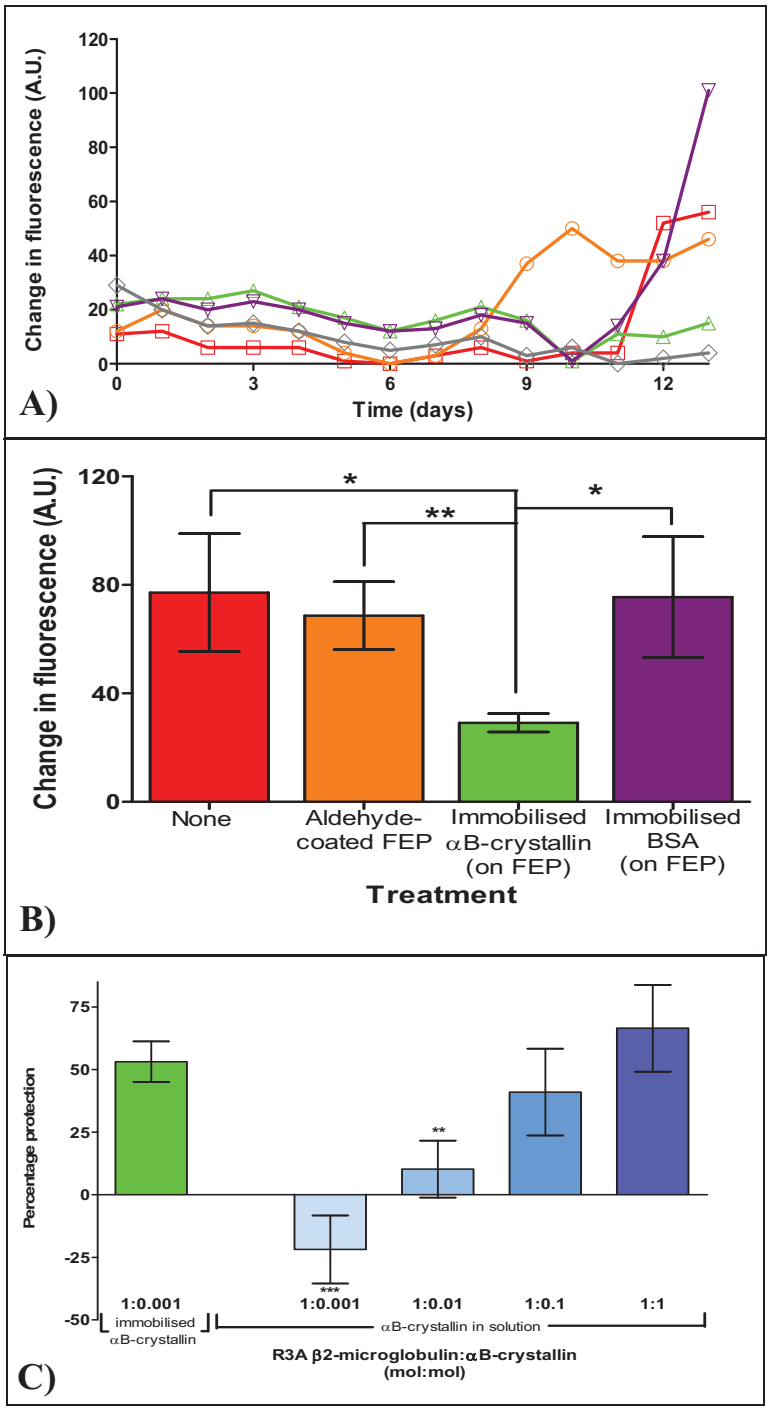

Figure 7.9: Protection by αB-crystallin of R3A β2-microglobulin fibrillar aggregation induced by inherent destabilisation (mean ± SE of 4 separate immobilisation experiments; P values indicating significant difference from student t-tests are * <0.05, **<0.01, *<0.001): A) ThT fluorescence of ThT buffer ◇, R3A β2-microglobulin alone □, and in the presence of aldehyde-coated FEP ⬭, immobilised αB-crystallin (on FEP) △ or immobilised BSA (on FEP) ▽; B) showing maximum fluorescence at 13 days; and b) amount of protection immobilised αB-crystallin (on FEP) provides against R3A β2-microglobulin aggregation compared to increasing concentrations of αB-crystallin in solution until an equal rate of chaperone activity is observed (significance values are given against immobilised αB-crystallin activity, all ratios are mol R3A β2-microglobulin:mol αB-crystallin).**

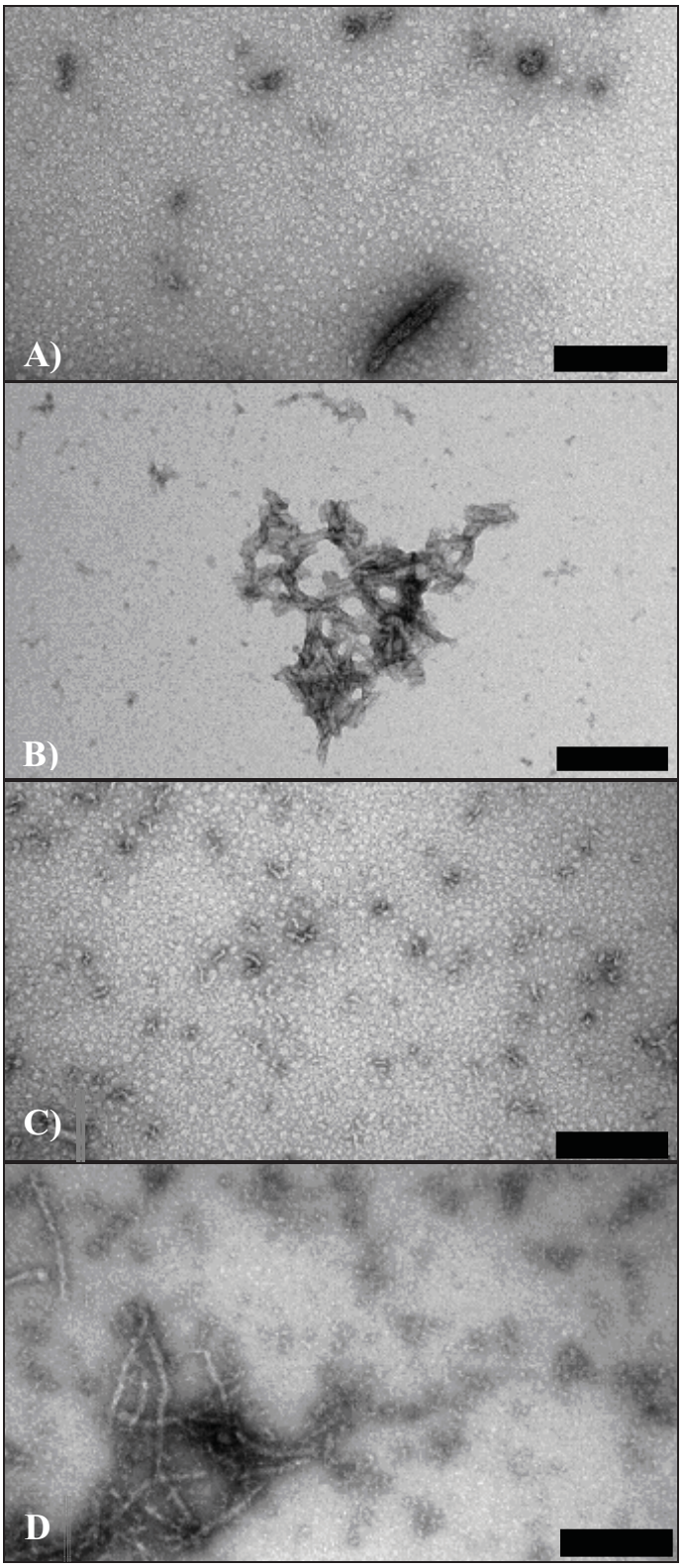

Figure 7.10: Transmission electron micrographs of R3A β2-microglobulin amyloid fibrils, formed after 13 day at 37 °C in the presence of (images representative of 3 separate experiments): A) alone; B) aldehyde-coated FEP; C) immobilised αB-crystallin (on FEP); and D) immobilised BSA (on FEP). Scale bars are 200 nm.

7.4 Discussion of immobilisation of αB-crystallin and its effects on the chaperone activity of this protein

αB-Crystallin acts as a molecular chaperone, acting in an ATP-independent manner to prevent processes of protein aggregation and precipitation, most particularly in the eye lens but potentially throughout the body (Horwitz, J. 2003; Augusteyn, R. C. 2004a). As a result, αB-crystallin is viewed as one of the most primary mammalian defence mechanisms against protein misfolding diseases (Carver, J. A. and Ecroyd, H. 2008). The immobilisation technique used in this research resulted in a significant increase in αB-crystallin's *in vitro* chaperone activity against all target proteins examined. Table 7.2 summarises the results of all αB-crystallin chaperone activity assays, highlighting the differences in chaperone activity between equal amounts of αB-crystallin, when immobilised or in solution, and at what concentration αB-crystallin in solution protected against protein aggregation as effectively as immobilised αB-crystallin (for each target protein). Immobilised αB-crystallin's increase in activity ranged from 100-fold to 5,000-fold, dependent on the target protein and protein destabilisation conditions used. Immobilised αB-crystallin acted in this enhanced manner under physiological temperature (excepting the temperature destabilisation assay) and pH ranges, and was effective to inhibit amyloid-like fibril formation of a variant of disease-related β2-microglobulin (R3A β2-microglobulin). Immobilisation of αB-crystallin thus provides an effective new method for the capture of misfolding proteins.

Table 7.2: Summary of chaperone activity results for αB-crystallin, immobilised and in solution.

	Comparison between equal concentrations of αB-crystallin (850ng/ml)			Comparison between equivalent chaperone protection (target:αB-crystallin)		
Target protein	**Immobilised protection (%)**	**Solution protection (%)**	**Apparent increase in activity**	**Immobilised (mol:mol)**	**In solution (mol:mol)**	**True increase in activity**
Catalase	39	-47	86 %	1:0.0006	1:6	1000 %
Insulin	35	-9	44 %	1:0.00006	1:0.3	5000 %
RCMκ-Casein	15	-1	16 %	1:0.0002	1:1	5000 %
R3A β2-Microglobulin	53	-22	75 %	1:0.001	1:0.1	100 %

It is well recognised that structure is intrinsically linked to function (Banavar, J. R. and Maritan, A. 2007). Most sHsps, including αB-crystallin, are inherently flexible, which is integral for their ability to function as molecular chaperones. The link between this flexibility, and the regions of the protein responsible for it, is a topic of current interest in protein chemistry (Vendruscolo, M. and Dobson, C. M. 2006). Numerous conditions which structurally perturb αB-crystallin (whether affecting the multimeric assembly or the individual subunits) have now been demonstrated to lead to an increase in functionality (Sharma, K. K. and Ortwerth, B. J. 1995; Raman, B. and Rao, C. M. 1997; Koretz, J. F. *et al.* 1998; Horwitz, J. *et al.* 2004; Ecroyd, H. *et al.* 2007), as was further demonstrated in § 6. α-Crystallin oligomers are highly dynamic assemblies which vary in size, due to subunit exchange, under a wide range of conditions, including temperature, pH, ionic changes, protein concentration, and also the age and species of the α-crystallin source (Vanhoudt, J. *et al.* 2000; Horwitz, J. 2003; Aquilina, J. A. *et al.* 2004).

In this chapter, αB-crystallin has been covalently immobilised onto solid surfaces *via* its solvent exposed lysine residues, i.e. in its C-terminal extension. NMR studies have demonstrated how this region of αB-crystallin is highly dynamic and exposed to solution (Carver, J. A. *et al.* 1994; Carver, J. A. 1999). It is also lysine rich (Carver, J. A. *et al.* 1992), making it the most likely region for interaction *via* Schiff based chemistry. AFM showed αB-crystallin oligomers covering the surface post-immobilisation. These oligomers were roughly spherical in size and with an average diameter of 16.0 ± 0.5nm. This is in good agreement with the results of Haley and co-workers (1998), who established a range for αB-crystallin oligomers of from 8 to 18 nm *via* cryoEM, with the most common assembly being 15 nm. The range of particle size is greater in the present work, with the smaller particles being within 2 nm of earlier observations (9.8 ± 1.0 nm) but the larger particles being significantly different (29.7 ± 1.8 nm). These larger particles were few in number and may be similar to those larger oligomers occasionally observed by Aquilina, Benesch *et al.* (2003). Alternatively, these may be the result of two or more oligomers which have been immobilised so that they are inseparable. The presence of oligomers reinforces the hypothesis that it is the C-terminal extension

lysines (K166, K174 and K175) that are involved in the Schiff based immobilisation, as it is primarily the α-crystallin core domain that is involved in the dimer interface between αB-crystallin subunits, the putative building blocks of this protein's higher order assemblies (Ghosh, J. G. and Clark, J. I. 2005).

It has repeatedly been shown that both αT-crystallin and αB-crystallin act as a more efficient chaperones when under slight structural perturbation (Raman, B. and Rao, C. M. 1997; Koretz, J. F. *et al.* 1998; Lindner, R. A. *et al.* 1998; MacRae, T. H. 2000; Bode, C. *et al.* 2003; Kumar, M. S. *et al.* 2005; Ecroyd, H. *et al.* 2007; Rekas, A. *et al.* 2007). Following these results, there have been investigations into the size and structure of αT- and αB-crystallin oligomers, particularly when under stress, to examine the dissociation of the oligomers and the hydrophobicity of α-crystallin assemblies under these conditions. Variations in oligomer size have been observed to be common where αT- and αB-crystallin chaperone activity has been altered, however there has been no definitive link drawn between either oligomer size or hydrophobicity and increased chaperone ability (MacRae, T. H. 2000; Bhattacharyya, J. *et al.* 2002; Augusteyn, R. C. 2004a; Saha, S. and Das, K. P. 2004; Kumar, M. S. *et al.* 2005; Carver, J. A. and Ecroyd, H. 2008). In fact, Augustyn (2004a) demonstrated that crosslinked α-crystallin chaperoned at a slightly increased rate than native α-crystallin, showing that chaperone activity can occur by the oligomer independent of subunit dynamics. Monomeric or dimeric α-crystallin (bovine) also retains chaperone activity, with subunits acting as effective molecular chaperones even at low pH when completely unfolded (Raman, B. *et al.* 2005) or when aggregated into amorphous or amyloid fibril structures (§ 6.3).

Peterson and co-workers (2005) demonstrated that bovine α-crystallin could be immobilised on a gold film and the oligomeric assembly separated by repeated urea washes. The remaining α-crystallin monomer or dimer subunits retained the ability to form non-covalent interactions with other crystallin proteins, as monitored by surface plasmon resonance, although the amount of α-crystallin present was not quantified so comparative activity could not be established. In the current research, the chaperone activity of αB-crystallin when immobilised was

consistently higher on a molar basis than that of αB-crystallin in solution. This finding may be further reinforcement of Augusteyn's findings (2004b) that dissociation is not essential for molecular chaperone activity. However, it must also be observed that the presence of αB-crystallin oligomers does not rule out the concomitant presence of monomers, dimers, or small oligomers, which are too small to observe *via* AFM. Thus the large increase in chaperone activity observed may be due to the greater exposure of the relevant chaperone binding sites upon αB-crystallin's immobilisation and/or due to the presence of small αB-crystallin subunits, such as monomers or dimers, which are the putative active components (Van Montfort, R. L. *et al.* 2001; Aquilina, J. A. *et al.* 2004; Benesch, J. L. *et al.* 2008).

Once immobilised, αB-crystallin acts as a significantly more effective chaperone than when in solution. The results presented in this chapter, have shown that this increase in chaperone activity occurs with a range of target proteins and under a range of stress conditions. In all situations examined immobilised αB-crystallin was greater than a 100-fold more effective chaperone than under solution *in vitro* conditions. This was even apparent under conditions in which αB-crystallin (in solution) is known to act as a chaperone with heightened activity, such as under increased temperature or against slow aggregation target proteins (Rekas, A. *et al.* 2007). This increase in chaperone activity, when combined with the stability and reliability of covalent protein immobilisation *via* this technique, implies that immobilised αB-crystallin has potential use as a non-selective *in vitro* chaperone. In particular it highlights the potential for use in the prevention of DRA, *via* the immobilisation of αB-crystallin onto haemodialysis membranes, especially as immobilised αB-crystallin has now been shown to act as an effective chaperone against amyloid fibril formation by β2-microglobulin.

Covalent immobilisation of αB-crystallin onto a solid substrate resulted in a significant increase of its chaperone action, enhancing its activity by 100- to 5,000-fold. Immobilisation was achieved by covalent bonding to inert aldehyde polymer layers and was achieved on a range of surfaces. Aldehyde polymerisation resulted in a topologically flat covering that had no significant effect on target

protein aggregation. αB-Crystallin was immobilised at a concentration of ~300 ng/cm^2 and was observed to still retain characteristic multimeric features. The significant enhancement of chaperone activity following covalent immobilisation of αB-crystallin indicates this technique has the potential to be an effective tool for capturing misfolding proteins in *in vitro* or *ex vivo* situations, i.e. attached to haemodialysis membranes for the prevention of DRA.

CHAPTER 8

CONCLUSIONS AND FUTURE DIRECTIONS

Amyloid fibril structures are increasingly being recognised for aspects other than their disease associations. The recognition of, and investigations into, amyloidin has sparked new interest in the unique properties of these highly ordered structures (Chiti, F. and Dobson, C. M. 2006; Fowler, D. M. *et al.* 2006; Gras, S. L. 2007). As further insights are developed into their formation, molecular structures, morphologies and biological functions, the potential roles (both positive and negative) of amyloid and particularly amyloid-like fibrils will become evident.

The formation and characterisation of protein nanofibre structures was a major focus of the research described in this thesis. Protein nanofibres, incluing amyloid and amyloid-like fibrils, were formed from proteins and peptides for three differing reasons: to examine the amyloid propensity of bioactive peptides, and explore whether they could be of use in amyloid fibril formation kinetic studies; to establish a disease-related *in vitro* assay for assessment of amyloid fibril formation inhibitors against dialysis-related amyloidosis; and to assess the feasibility of forming inexpensive protein nanofibre structures for industrial purposes.

The formation of amyloid-like fibrils from RsAFP-19 provides a new amyloidogenic peptide, which may be of use in structural or formation studies of amyloid fibrils. RsAFP-19 is of particular interest due to the rapid kinetics of fibril formation in this peptide system at near physiological pH making it a possible target protein for investigation of fibril inhibitors. Investigation into the amyloid-like fibril formation by R3A β2-microglobulin was aimed at creating such a model system, moreover one with disease relevance due to the role of β2-microglobulin in DRA. A reliable amyloid-like fibril forming model, able to be monitored *via* multiple methods, was achieved and used to assess the ability of surface immobilised αB-crystallin as a chaperone to inhibit amyloid fibril formation by this protein. Disease-related amyloid models, such as this, are of importance in the search for therapeutic treatments against amyloidoses, against both specific diseases and the amyloid fibril structure generally (Dobson, C. M. 2001).

To be of practical use in the bionanotechnology industry, protein nanofibres structures would need to be simple, inexpensive and able to be generated in large quantities (Waterhouse, S. H. and Gerrard, J. A. 2004). Crude mixtures of mammalian lens crystallins, a protein source normally destroyed as waste, were examined in this role. It was established that crude mixtures, semi-pure mixtures and pure protein solutions of mammalian lens crystallins can form protein nanofibres after simple buffer treatment with incubation, and that these fibrils could be morphologically varied (dependent upon the protein composition and solution conditions). Most importantly, it was demonstrated that crude protein mixtures from multiple species could be used to form protein nanofibres, indicating that large-scale production of fibrils is feasible.

The second aim of the research in this thesis was the investigation of structural changes on α-crystallin chaperone activity. The negative aspects of protein aggregation and amyloid fibril formation, particularly relating to diseases such as cataract and DRA, remain a central focus of research (Dobson, C. M. 2006; Jahn, T. R. and Radford, S. E. 2008). α-Crystallin species, due to their dual roles in amyloid fibril formation (being able to both inhibit and participate in the process amyloid fibril formation), have a unique place in protein off-pathway folding (Ecroyd, H. and Carver, J. A. 2008). The research presented herein demonstrates that the biological function of α-crystallin is retained under conditions of extreme structural rearrangement.

αB-Crystallin has been shown, in this thesis, to act as a chaperone in multiple structural states, some of which are probably unattainable *in vivo*. The structural states examined included: in its native state; as a refolded oligomer (post-GdnHCl unfolding); as amorphous aggregates; as amyloid fibrils; and covalently immobilised onto a solid carrier. That αB-crystallin developed enhanced activity under the latter two conditions (as amyloid fibrils and due to covalent immobilisation) displays the remarkable tenacity of this protein to maintain its biological role. The ability of αT- and particularly αB-crystallin to act with its biological function as amyloid fibrils introduces the possibility that α-crystallin may be a form of amyloidin, although differing from amyloidins described to date

in that the amyloid fibril structure is not required for the biological function to occur. Further, the enhanced activity of αB-crystallin opens the possibility of novel therapeutic uses for this protein. Covalently immobilised αB-crystallin, in particular, has been demonstrated to act effectively (100-fold more than αB-crystallin in solution) to chaperone R3A β2-microglobulin. In fact, the haemodialysis membrane, important in the development of DRA, with which β2-microglobulin is associated, provides a framework onto which immobilised αB-crystallin could be attached.

Many possibilities for future work have been derived from the research to date. Small peptides are able to be used in many techniques incompatible with larger proteins, making RsAFP-19 an ideal candidate for research into specific details of amyloid-like fibril structure and formation characteristics. Investigations into effect of nanofibre formation on the biological activity of RsAFP-19 would also be of relevance, as this peptide is of potential use in the agricultural industry (as an antifungal and antimicrobial) (Lay, F. T. and Anderson, M. A. 2005).

In the development of industrial methods for protein nanofibre formation, increased usefulness to the nanobiotechnology industry would be achieved if morphological variations were easily controlled during the bottom up self-assembly process (Zhang, S. 2003; Hamada, D. *et al.* 2004; Hamley, I. W. 2007). Further work into alterations of solution conditions for crude crystallin nanofibre formation may help establish ways in which one morphological nanofibre species is preferentially formed. Further research into the interspecies mixtures which formed nanofibres would establish whether this formation still occurs with the addition of new species (including non-mammalian lens proteins, such as from fish). Finally, fluorescence techniques, or protease digestion coupled with mass spectrometry, could be employed to establish whether individual fibrils formed in crude mixtures are composed of homogeneous or heterogeneous proteins.

The recognition of biologically active amyloid fibrils composed of α-crystallin prompts further research to investigate how far ranging this retention of chaperone activity is, i.e. if it occurs against biologically relevant proteins such as other

crystallins, and are there specific aggregation conditions that quench this activity. Investigations are also underway to establish whether this property is consistent enough to categorise amyloid fibrils formed from αB-crystallin as a biologically functional amyloid fibril species, or amyoidin.

Finally, the activity of immobilised αB-crystallin against R3A β2-microglobulin has stimulated further work in this area. Research is being undertaken to establish whether such activity is achievable in serum conditions (i.e. against β2-microglobulin carried within blood). Such studies are the next step to establishing immobilised αB-crystallin as part of a therapeutic treatment for DRA. Further work may also be done to establish how broad ranging is the increase in chaperone activity of αB-crystallin after covalent immobilisation, and whether it may be of use as a therapeutic against other targets.

CHAPTER 9

REFERENCE LIST

Abgar, S., Backmann, J., Aerts, T., Vanhoudt, J. and Clauwaert, J. (2000). "The structural differences between bovine lens αA- and αB-crystallin." *European Journal of Biochemistry* 267: 5916-25.

Aggeli, A., Bell, M., Boden, N., Keen, J. N., Knowles, P. F., Mcleish, T. C., Pitkeathly, M. and Radford, S. E. (1997). "Responsive gels formed by the spontaneous self-assembly of peptides into polymeric β-sheet tapes." *Nature* 386: 259-62.

Andley, U. P. (2007). "Crystallins in the eye: Function and pathology." *Progress in Retinal & Eye Research* 26: 78-98.

Anfinsen, C. B. (1973). "Principles that govern the folding of protein chains." *Science* 181: 223-30.

Appel, T. R., Richter, S., Linke, R. P. and Makovitzky, J. (2005). "Histochemical and topo-optical investigations on tissue-isolated and *in vitro* amyloid fibrils." *Amyloid* 12: 174-83.

Aquilina, J. A., Benesch, J. L., Bateman, O. A., Slingsby, C. and Robinson, C. V. (2003). "Polydispersity of a mammalian chaperone: mass spectrometry reveals the population of oligomers in αB-crystallin." *Proceedings of the National Academy of Sciences of the United States of America* 100: 10611-6.

Aquilina, J. A., Benesch, J. L. P., Ding, L. L., Yaron, O., Horwitz, J. and Robinson, C. V. (2004). "Phosphorylation of αB-crystallin alters chaperone function through loss of dimeric substructure." *Journal of Biological Chemistry* 279: 28675-80.

Augusteyn, R. C. (2004a). "α-Crystallin: a review of its structure and function." *Clinical & Experimental Optometry* 87: 356-66.

Augusteyn, R. C. (2004b). "Dissociation is not required for α-crystallin's chaperone function." *Experimental Eye Research* 79: 781-4.

Augusteyn, R. C., Murnane, L., Nicola, A. and Stevens, A. (2002). "Chaperone activity in the lens." *Clinical & Experimental Optometry* 85: 83-90.

Baldwin, A. J., Bader, R., Christodoulou, J., MacPhee, C. E., Dobson, C. M. and Barker, P. D. (2006). "Cytochrome display on amyloid fibrils." *Journal of the American Chemical Society* 128: 2162-3.

Banavar, J. R. and Maritan, A. (2007). "Physics of proteins." *Annual Review of Biophysics & Biomolecular Structure* 36: 261-80.

Barral, J. M., Broadley, S. A., Schaffar, G. and Hartl, F. U. (2004). "Roles of molecular chaperones in protein misfolding diseases." *Seminars in Cell & Developmental Biology* 15: 17-29.

Bax, B., Lapatto, R., Nalini, V., Driessen, H., Lindley, P. F., Mahadevan, D., Blundell, T. L. and Slingsby, C. (1990). "X-ray-analysis of βB2-crystallin and evolution of oligomeric lens proteins." *Nature* 347: 776-80.

Becker, J. W. and Reeke, G. N. (1985). "Three-dimensional structure of β2-microglobulin." *Proceedings of the National Academy of Sciences of the United States of America* 82: 4225-9.

Bellotti, V., Stoppini, M., Mangione, P., Sunde, M., Robinson, C., Asti, L., Brancaccio, D. and Ferri, G. (1998). "β2-Microglobulin can be refolded into a native state from *ex vivo* amyloid fibrils." *European Journal of Biochemistry* 258: 61-7.

Bely, M. and Apathy, A. (2000). "Histochemical and immunohistochemical differential diagnosis of amyloidosis - a brief illustrated essay and personal experience with Romhanyi's method." *Amyloid* 7: 212-7.

Benedek, G. B. (1971). "Theory of transparency of the eye." *Applied Optics* 10: 459-73.

Benesch, J. L., Ayoub, M., Robinson, C. V. and Aquilina, J. A. (2008). "Small heat shock protein activity is regulated by variable oligomeric substructure." *Journal of Biological Chemistry* 283: 28513-7.

Berengian, A. R., Parfenova, M. and McHaourab, H. S. (1999). "Site-directed spin labeling study of subunit interactions in the α-crystallin domain of small heat-shock proteins. Comparison of the oligomer symmetry in αA-crystallin, HSP 27 and HSP 16.3." *Journal of Biological Chemistry* 274: 6305-14.

Bhattacharyya, J., Padmanabha Udupa, E. G., Wang, J. and Sharma, K. K. (2006). "Mini αB-crystallin: a functional element of αB-crystallin with chaperone-like activity." *Biochemistry* 45: 3069-76.

Bhattacharyya, J., Srinivas, V. and Sharma, K. K. (2002). "Evaluation of hydrophobicity versus chaperonelike activity of bovine αA- and αB-crystallin." *Journal of Protein Chemistry* 21: 65-71.

Binnig, G., Quate, C. F. and Gerber, C. (1986). "Atomic force microscope." *Physical Review Letters* 56: 930-3.

Blattler, T. M., Pasche, S., Textor, M. and Griesser, H. J. (2006). "High salt stability and protein resistance of poly(L-lysine)-g-poly(ethylene glycol) copolymers covalently immobilized *via* aldehyde plasma polymer interlayers on inorganic and polymeric substrates." *Langmuir* 22: 5760-9.

Bloemendal, H., De Jong, W., Jaenicke, R., Lubsen, N. H., Slingsby, C. and Tardieu, A. (2004). "Ageing and vision: structure, stability and function of lens crystallins." *Progress in Biophysical and Molecular Biology* 86: 407-85.

Bloemendal, H., Piatigorsky, J. and Spector, A. (1989). "Recommendations for crystallin nomenclature." *Experimental Eye Research* 48: 465-6.

Brady, J. P., Garland, D., Duglas-Tabor, Y., Robison Jr., W. G., Groome, A. and Wawrousek, E. F. (1997). "Targeted disruption of the mouse αA-crystallin gene induces cataract and cytoplasmic inclusion bodies containing the small heat shock protein αB-crystallin" *Proceedings of the National Academy of Sciences of the United States of America* 94: 884-9.

Brady, J. P., Garland, D., Green, D. E., Tamm, E. R., Giblin, F. J. and Wawrousek, E. F. (2001). "αB-Crystallin in lens development and muscle integrity: a gene knockout approach" *Investigative Opthalmology and Visual Science* 42: 2924-34.

Bode, C., Tolgyesi, F. G., Smeller, L., Heremans, K., Avilov, S. V. and Fidy, J. (2003). "Chaperone-like activity of α-crystallin is enhanced by high-pressure treatment." *Biochemical Journal* 370: 859-66.

Bucciantini, M., Giannoni, E., Chiti, F., Baroni, F., Formigli, L., Zurdo, J., Taddei, N., Ramponi, G., Dobson, C. M. and Stefani, M. (2002). "Inherent toxicity of aggregates implies a common mechanism for protein misfolding diseases." *Nature* 416: 507-11.

Burgio, M. R., Kim, C. J., Dow, C. C. and Koretz, J. F. (2000). "Correlation between the chaperone-like activity and aggregate size of α-crystallin with increasing temperature." *Biochemical & Biophysical Research Communications* 268: 426-32.

Bush, A. I. (2008). "Drug development based on the metals hypothesis of Alzheimer's disease." *Journal of Alzheimer's Disease* 15: 223-40.

Carey, J., Lindman, S., Bauer, M. and Linse, S. (2007). "Protein reconstitution and three-dimensional domain swapping: benefits and constraints of covalency." *Protein Science* 16: 2317-33.

Carulla, N., Caddy, G. L., Hall, D. R., Zurdo, J., Gairi, M., Feliz, M., Giralt, E., Robinson, C. V. and Dobson, C. M. (2005). "Molecular recycling within amyloid fibrils." *Nature* 436: 554-8.

Carver, J. A. (1999). "Probing the structure and interactions of crystallin proteins by NMR spectroscopy." *Progress in Retinal & Eye Research* 18: 431-62.

Carver, J. A., Aquilina, J. A. and Truscott, R. J. (1994). "A possible chaperone-like quaternary structure for alpha-crystallin." *Experimental Eye Research* 59: 231-4.

Carver, J. A., Aquilina, J. A., Truscott, R. J. and Ralston, G. B. (1992). "Identification by 1H NMR spectroscopy of flexible C-terminal extensions in bovine lens α-crystallin." *FEBS Letters* 311: 143-9.

Carver, J. A. and Lindner, R. A. (1998). "NMR spectroscopy of α-crystallin. Insights into the structure, interactions and chaperone action of small heat-shock proteins." *International Journal of Biological Macromolecules* 22: 197-209.

Carver, J. A., Nicholls, K. A., Aquilina, J. A. and Truscott, R. J. (1996). "Age-related changes in bovine α-crystallin and high-molecular-weight protein." *Experimental Eye Research* 63: 639-47.

Chamberlain, A. K., MacPhee, C. E., Zurdo, J., Morozova-Roche, L. A., Hill, H. A., Dobson, C. M. and Davis, J. J. (2000). "Ultrastructural organization of amyloid fibrils by atomic force microscopy." *Biophysical Journal* 79: 3282-93.

Channon, K. J., Devlin, G. L., Magennis, S. W., Finlayson, C. E., Tickler, A. K., Silva, C. and MacPhee, C. E. (2008). "Modification of fluorophore photophysics through peptide-driven self-assembly." *Journal of the American Chemical Society* 130: 5487-91.

Chapman, M. R., Robinson, L. S., Pinkner, J. S., Roth, R., Heuser, J., Hammar, M., Normark, S. and Hultgren, S. J. (2002) "Role of *Escherichia coli* curli operons in directing amyloid fiber formation." *Science* 295: 851-5.

Chatelier, R. C., St John, H. A. W., Gengenbach , T. R., Kingshott, P. and Griesser, H. J. (1997). "Incorporation of surface topography in the XPS analysis of curved or rough samples covered by thin multilayers." *Surface & Interface Analysis* 25: 741-6.

Cherny, I. and Gazit, E. (2008). "Amyloids: not only pathological agents but also ordered nanomaterials." *Angewandte Chemie International Edition* 47: 4062-9.

Chiou, S. H., Chang, W. P., Ting, L. M., Lai, T. A. and Lin, H. K. (1988). "Biochemical characterization of lens crystallins from three mammalian species." *Current Eye Research* 7: 1017-22.

Chiti, F. and Dobson, C. M. (2006). "Protein misfolding, functional amyloid and human disease." *Annual Review of Biochemistry* 75: 333-66.

Cocinero, E. J., Lesarri, A., Sanz, M. E., Lopez, J. C. and Alonso, J. L. (2006). "Conformations of α-aminobutyric acid in the gas phase." *Chemphyschem* 7: 1481-7.

Cooper, P. G., Carver, J. A. and Truscott, R. J. (1993). "1H-NMR spectroscopy of bovine lens β-crystallin. The role of the βB2-crystallin C-terminal extension in aggregation." *European Journal of Biochemistry* 213: 321-8.

Corazza, A., Pettirossi, F., Viglino, P., Verdone, G., Garcia, J., Dumy, P., Giorgetti, S., Mangione, P., Raimondi, S., Stoppini, M., Bellotti, V. and Esposito, G. (2004). "Properties of some variants of human β2-microglobulin and amyloidogenesis." *Journal of Biological Chemistry* 279: 9176-89.

Cornet, B., Bonmatin, J. M., Hetru, C., Hoffmann, J. A., Ptak, M. and Vovelle, F. (1995). "Refined three-dimensional solution structure of insect defensin A." *Structure* 3: 435-48.

Das, B. K. and Liang, J. J. (1997). "Detection and characterization of α-crystallin intermediate with maximal chaperone-like activity." *Biochemical and Biophysical Research Commununications* 236: 370-4.

Datta, S. A. and Rao, C. M. (1999). "Differential temperature-dependent chaperone-like activity of αA- and αB-crystallin homoaggregates." *Journal of Biological Chemistry* 274: 34773-8.

De Jong, W. W., Caspers, G. J. and Leunissen, J. A. (1998). "Genealogy of the α-crystallin small heat-shock protein superfamily." *International Journal of Biological Macromolecules* 22: 151-62.

De Samblanx, G. W., Goderis, I. J., Thevissen, K., Raemaekers, R., Fant, F., Borremans, F., Acland, D. P., Osborn, R. W., Patel, S. and Broekaert, W. F. (1997). "Mutational analysis of a plant defensin from radish (*Raphanus sativus* L.) reveals two adjacent sites important for antifungal activity." *Journal of Biological Chemistry* 272: 1171-9.

Deechongkit, S., Powers, E. T., You, S. L. and Kelly, J. W. (2005). "Controlling the morphology of cross β-sheet assemblies by rational design." *Journal of the American Chemical Society* 127: 8562-70.

Delano, W. L. (2002). The PyMOL molecular graphics system, DeLano Scientific, San Carlos, CA, USA.

Delaye, M. and Tardieu, A. (1983). "Short-range order of crystallin proteins accounts for eye lens transparency." *Nature* 302: 415-7.

Dobson, C. M. (2001). "The structural basis of protein folding and its links with human disease." *Philosophical Transactions of the Royal Society of London Series B Biological Sciences* 356: 133-45.

Dobson, C. M. (2002). "Getting out of shape." *Nature* 418: 729-30.

Dobson, C. M. (2003). "Protein folding and misfolding." *Nature* 426: 884-90.

Dobson, C. M. (2004). "Principles of protein folding, misfolding and aggregation." *Seminars in Cell & Developmental Biology* 15: 3-16.

Dobson, C. M. (2006). "Protein aggregation and its consequences for human disease." *Protein & Peptide Letters* 13: 219-27.

Domike, K. R. and Donald, A. M. (2007). "Thermal dependence of thermally induced protein spherulite formation and growth: Kinetics of β-lactoglobulin and insulin." *Biomacromolecules* 8: 3930-7.

Dubay, K. F., Pawar, A. P., Chiti, F., Zurdo, J., Dobson, C. M. and Vendruscolo, M. (2004). "Prediction of the absolute aggregation rates of amyloidogenic polypeptide chains." *Journal of Molecular Biology* 341: 1317-26.

Eanes, E. D. and Glenner, G. G. (1968). "X-ray diffraction studies on amyloid filaments." *Journal of Histochemistry and Cytochemistry* 16: 673-7.

Ecroyd, H. and Carver, J. A. (2008a). "Crystallin proteins and amyloid fibrils." *Cell & Molecular Life Sciences*. 66: 62-81.

Ecroyd, H. and Carver, J. A. (2008b). "The effect of small molecules in modulating the chaperone activity of αB-crystallin against ordered and disordered protein aggregation." *FEBS Journal* 275: 935-47.

Ecroyd, H. and Carver, J. A. (2008c). "Unraveling the mysteries of protein folding and misfolding." *IUBMB Life*. 60: 769-74.

Ecroyd, H., Koudelka, T., Thorn, D. C., Williams, D. M., Devlin, G., Hoffmann, P. and Carver, J. A. (2008). "Dissociation from the oligomeric state is the rate-limiting step in fibril formation by κ-casein." *Journal of Biological Chemistry* 283: 9012-22.

Ecroyd, H., Meehan, S., Horwitz, J., Aquilina, J. A., Benesch, J. L., Robinson, C. V., MacPhee, C. E. and Carver, J. A. (2007). "Mimicking phosphorylation of αB-crystallin affects its chaperone activity." *Biochemical Journal* 401: 129-41.

Elgersma, R. C., Meijneke, T., Posthuma, G., Rijkers, D. T. and Liskamp, R. M. (2006). "Self-assembly of amylin(20-29) amide-bond derivatives into helical ribbons and peptide nanotubes rather than fibrils." *Chemistry* 12: 3714-25.

Esposito, G., Corazza, A., Viglino, P., Verdone, G., Pettirossi, F., Fogolari, F., Makek, A., Giorgetti, S., Mangione, P., Stoppini, M. and Bellotti, V. (2005). "Solution structure of β(2)-microglobulin and insights into fibrillogenesis." *Biochimica et Biophysica Acta* 1753: 76-84.

Esposito, G., Michelutti, R., Verdone, G., Viglino, P., Hernandez, H., Robinson, C. V., Amoresano, A., Dal Piaz, F., Monti, M., Pucci, P., Mangione, P., Stoppini, M., Merlini, G., Ferri, G. and Bellotti, V. (2000). "Removal of the N-terminal hexapeptide from human β2-microglobulin facilitates protein aggregation and fibril formation." *Protein Science* 9: 831-45.

Fagerholm, P. P., Philipson, B. T. and Lindstrom, B. (1981). "Normal human lens - the distribution of protein." *Experimental Eye Research* 33: 615-20.

Fandrich, M. and Dobson, C. M. (2002). "The behaviour of polyamino acids reveals an inverse side chain effect in amyloid structure formation." *Embo Journal* 21: 5682-90.

Fant, F., Vranken, W., Broekaert, W. and Borremans, F. (1998). "Determination of the three-dimensional solution structure of *Raphanus sativus* antifungal protein 1 by 1H NMR." *Journal of Molecular Biology* 279: 257-70.

Farahbakhsh, Z. T., Huang, Q. L., Ding, L. L., Altenbach, C., Steinhoff, H. J., Horwitz, J. and Hubbell, W. L. (1995). "Interaction of α-crystallin with spin-labeled peptides." *Biochemistry* 34: 509-16.

Farrell, H. M., Jr., Cooke, P. H., Wickham, E. D., Piotrowski, E. G. and Hoagland, P. D. (2003). "Environmental influences on bovine κ-casein: reduction and conversion to fibrillar (amyloid) structures." *Journal of Protein Chemistry* 22: 259-73.

Farrell, J. and Bastani, B. (1997). "β2-Microglobulin amyloidosis in chronic dialysis patients: a case report and review of the literature." *Journal of the American Society of Nephrology* 8: 509-14.

Feder, M. E. and Hofmann, G. E. (1999). "Heat-shock proteins, molecular chaperones and the stress response: evolutionary and ecological physiology." *Annual Review Physiology* 61: 243-82.

Fernandez-Escamilla, A. M., Rousseau, F., Schymkowitz, J. and Serrano, L. (2004). "Prediction of sequence-dependent and mutational effects on the aggregation of peptides and proteins." *Nature Biotechnology* 22: 1302-6.

Fezoui, Y., Hartley, D. M., Walsh, D. M., Selkoe, D. J., Osterhout, J. J. and Teplow, D. B. (2000). "A *de novo* designed helix-turn-helix peptide forms nontoxic amyloid fibrils." *Nature Structural Biology* 7: 1095-9.

Fleming, B. D., Praporski, S., Bond, A. M. and Martin, L. L. (2008). "Electrochemical quartz crystal microbalance study of azurin adsorption onto an alkanethiol self-assembled monolayer on gold." *Langmuir* 24: 323-7.

Floege, J., Schaffer, J. and Koch, K. M. (2001). "Scintigraphic methods to detect β2-microglobulin associated amyloidosis (β2-microglobulin amyloidosis)." *Nephrology Dialysis & Transplantation* 16 s4: 12-6.

Fowler, D. M., Koulov, A. V., Alory-Jost, C., Marks, M. S., Balch, W. E. and Kelly, J. W. (2006). "Functional amyloid formation within mammalian tissue." *PLoS Biology* 4: 6.

Ganadu, M. L., Aru, M., Mura, G. M., Coi, A., Mlynarz, P. and Kozlowski, H. (2004). "Effects of divalent metal ions on the αB-crystallin chaperone-like activity: spectroscopic evidence for a complex between copper(II) and protein." *Journal of Inorganic Biochemistry* 98: 1103-9.

Gasteiger E., H. C., Gattiker A., Duvaud S., Wilkins M.R., Appel R.D., Bairoch A. (2005). Protein Identification and Analysis Tools on the ExPASy Server. *The Proteomics Protocols Handbook, Humana Press*. J. M. Walker 571-607.

Gazit, E. (2002). "A possible role for π-stacking in the self-assembly of amyloid fibrils." *FASEB Journal* 16: 77-83.

Ghosh, J. G. and Clark, J. I. (2005). "Insights into the domains required for dimerization and assembly of human αB-crystallin." *Protein Science* 14: 684-95.

Ghosh, J. G., Estrada, M. R. and Clark, J. I. (2005). "Interactive domains for chaperone activity in the small heat shock protein, human αB-crystallin." *Biochemistry* 44: 14854-69.

Ghosh, J. G., Houck, S. A. and Clark, J. I. (2007). "Interactive sequences in the molecular chaperone, human αB-crystallin modulate the fibrillation of amyloidogenic proteins." *International Journal of Biochemistry and Cell Biology* 39:1804-15.

Glomm, W. R., Halskau, O., Jr., Hanneseth, A. M. and Volden, S. (2007). "Adsorption behavior of acidic and basic proteins onto citrate-coated Au surfaces correlated to their native fold, stability, and pI." *Journal of Physical Chemistry B* 111: 14329-45.

Gras, S. L. (2007). "Amyloid fibrils: from disease to design. New biomaterial applications for self-assembling cross-β fibrils." *Australian Journal of Chemistry* 60: 333-42.

Gras, S. L., Tickler, A. K., Squires, A. M., Devlin, G. L., Horton, M. A., Dobson, C. M. and MacPhee, C. E. (2008). "Functionalised amyloid fibrils for roles in cell adhesion." *Biomaterials* 60: 333-342.

Graveland-Bikker, J. F. and De Kruif, C. G. (2006). "Unique milk protein based nanotubes: Food and nanotechnology meet." *Trends in Food Science & Technology* 17: 196-203.

Griesser, H. J., Kingshott, P., McArthur, S. L., Mclean, K. M., Kinsel, G. R. and Timmons, R. B. (2004). "Surface-MALDI mass spectrometry in biomaterials research." *Biomaterials* 25: 4861-75.

Griesser, H. J., McArthur, S. L., Wagner, M. S., Castner, D. G., Kingshott, P. and Mclean, K. M. (2003). "XPS, ToF-SIMS and MALDI-MS for Characterizing Adsorbed Protein Films." *Biopolymers at Interfaces*. Ed. M. Malmsten, Marcel Dekker Inc 641-69.

Griffin, M. D., Mok, M. L., Wilson, L. M., Pham, C. L., Waddington, L. J., Perugini, M. A. and Howlett, G. J. (2008). "Phospholipid interaction induces molecular-level polymorphism in apolipoprotein C-II amyloid fibrils via alternative assembly pathways." *Journal of Molecular Biology* 375: 240-56.

Groenen, P. J., Merck, K. B., De Jong, W. W. and Bloemendal, H. (1994). "Structure and modifications of the junior chaperone α-crystallin. From lens transparency to molecular pathology." *European Journal of Biochemistry* 225: 1-19.

Groenning, M., Norrman, M., Flink, J. M., Van De Weert, M., Bukrinsky, J. T., Schluckebier, G. and Frokjaer, S. (2007). "Binding mode of Thioflavin T in insulin amyloid fibrils." *Journal of Structural Biology* 159: 483-97.

Gsponer, J. and Vendruscolo, M. (2006). "Theoretical approaches to protein aggregation." *Protein & Peptide Letters* 13: 287-93.

Haley, D. A., Bova, M. P., Huang, Q. L., Mchaourab, H. S. and Stewart, P. L. (2000). "Small heat-shock protein structures reveal a continuum from symmetric to variable assemblies." *Journal of Molecular Biology* 298: 261-72.

Haley, D. A., Horwitz, J. and Stewart, P. L. (1998). "The small heat-shock protein, αB-crystallin, has a variable quaternary structure." *Journal of Molecular Biology* 277: 27-35.

Hamada, D., Yanagihara, I. and Tsumoto, K. (2004). "Engineering amyloidogenicity towards the development of nanofibrillar materials." *Trends in Biotechnology* 22: 93-7.

Hamley, I. W. (2007). "Peptide fibrillization." *Angewandte Chemie International Edition* 46: 8128-47.

Hammersley, A. P. (1995). FIT2D V5.18 Reference Manual V1.6.

Hanson, S. R., Smith, D. L. and Smith, J. B. (1998). "Deamidation and disulfide bonding in human lens γ-crystallins." *Experimental Eye Research* 67: 301-12.

Harding, J. J. and Dilley, K. J. (1976). "Structural proteins of the mammalian lens: a review with emphasis on changes in development, aging and cataract." *Experimental Eye Research* 22: 1-73.

Harrington, V., Srivastava, O. P. and Kirk, M. (2007). "Proteomic analysis of water insoluble proteins from normal and cataractous human lenses." *Molecular Vision* 13: 1680-94.

Hartl, F. U. and Hayer-Hartl, M. (2002). "Molecular chaperones in the cytosol: from nascent chain to folded protein." *Science* 295: 1852-8.

Haslbeck, M., Franzmann, T., Weinfurtner, D. and Buchner, J. (2005). "Some like it hot: the structure and function of small heat-shock proteins." *Nature Structural & Molecular Biology* 12: 842-6.

Hatters, D. M., Macraild, C. A., Daniels, R., Gosal, W. S., Thomson, N. H., Jones, J. A., Davis, J. J., MacPhee, C. E., Dobson, C. M. and Howlett, G. J. (2003). "The circularization of amyloid fibrils formed by apolipoprotein C-II." *Biophysical Journal* 85: 3979-90.

Hermans, E., Dubbelman, M., Van Der Heijde, R. and Heethaar, R. (2007). "The shape of the human lens nucleus with accommodation." *Journal of Vision* 7: 1-10.

Hoang, T. X., Marsella, L., Trovato, A., Seno, F., Banavar, J. R. and Maritan, A. (2006). "Common attributes of native-state structures of proteins, disordered proteins and amyloid." *Proceedings of the National Academy of Sciences of the United States of America* 103: 6883-8.

Holm, N. K., Jespersen, S. K., Thomassen, L. V., Wolff, T. Y., Sehgal, P., Thomsen, L. A., Christiansen, G., Andersen, C. B., Knudsen, A. D. and Otzen, D. E. (2007). "Aggregation and fibrillation of bovine serum albumin." *Biochimica et Biophysica Acta* 1774: 1128-1138.

Horwitz, J. (1992). "α-Crystallin can function as a molecular chaperone." *Proceedings of the National Academy of Sciences of the United States of America* 89: 10449-53.

Horwitz, J. (2003). "α-Crystallin." *Experimental Eye Research* 76: 145-53.

Horwitz, J., Huang, Q. and Ding, L. (2004). "The native oligomeric organization of α-crystallin, is it necessary for its chaperone function?" *Experimental Eye Research* 79: 817-21.

Horwitz, J., Huang, Q. L., Ding, L. and Bova, M. P. (1998). "Lens α-crystallin: chaperone-like properties." *Methods in Enzymology* 290: 365-83.

Horwitz, J., Mcfall-Ngai, M., Ding, L. and Yaron, O. (1986). Thermal stability of lens crystallins. *The Lens: Transparency and Cataract*. Ed. G. Duncan, Eurage.

Ingolia, T. D. and Craig, E. A. (1982). "Four small *Drosophila* heat shock proteins are related to each other and to mammalian α-crystallin." *Proceedings of the National Academy of Sciences of the United States of America* 79: 2360-4.

Jahn, T. R., Parker, M. J., Homans, S. W. and Radford, S. E. (2006). "Amyloid formation under physiological conditions proceeds via a native-like folding intermediate." *Nature Structural & Molecular Biology* 13: 195-201.

Jahn, T. R. and Radford, S. E. (2008). "Folding versus aggregation: polypeptide conformations on competing pathways." *Archives of Biochemistry & Biophysics* 469: 100-17.

Jahn, T. R., Tennent, G. A. and Radford, S. E. (2008). "A common β-sheet architecture underlies *in vitro* and *in vivo* β2-microglobulin amyloid fibrils." *Journal of Biological Chemistry* 283: 17279-86.

Janshoff, A., Galla, H. J. and Steinem, C. (2000). "Piezoelectric mass-sensing devices as biosensors - an alternative to optical biosensors?" *Angewandte Chemie International Edition* 39: 4004-32.

Jedziniak, J. A., Kinoshita, J. H., Yates, E. M. and Benedek, G. B. (1975). "The concentration and localization of heavy molecular weight aggregates in aging normal and cataractous human lenses." *Experimental Eye Research* 20: 367-9.

Jimenez, J. L., Guijarro, J. I., Orlova, E., Zurdo, J., Dobson, C. M., Sunde, M. and Saibil, H. R. (1999). "Cryo-electron microscopy structure of an SH3 amyloid fibril and model of the molecular packing." *Embo Journal* 18: 815-21.

Jimenez, J. L., Nettleton, E. J., Bouchard, M., Robinson, C. V., Dobson, C. M. and Saibil, H. R. (2002). "The protofilament structure of insulin amyloid fibrils." *Proceedings of the National Academy of Sciences of the United States of America* 99: 9196-201.

Jin, L. W., Claborn, K. A., Kurimoto, M., Geday, M. A., Maezawa, I., Sohraby, F., Estrada, M., Kaminsky, W. and Kahr, B. (2003). "Imaging linear birefringence and dichroism in cerebral amyloid pathologies." *Proceedings of the National Academy of Sciences of the United States of America* 100: 15294-8.

Jobby, M. K. and Sharma, Y. (2007). "Calcium-binding to lens βB2- and βA3-crystallins suggests that all β-crystallins are calcium-binding proteins." *FEBS Journal* 274: 4135-47.

Johnson, I. S. (1983). "Human insulin from recombinant DNA technology." *Science* 219: 632-7.

Jones, S., Smith, D. P. and Radford, S. E. (2003). "Role of the N and C-terminal strands of β2-microglobulin in amyloid formation at neutral pH." *Journal of Molecular Biology* 330: 935-41.

Kad, N. M., Myers, S. L., Smith, D. P., Smith, D. A., Radford, S. E. and Thomson, N. H. (2003). "Hierarchical assembly of β2-microglobulin amyloid *in vitro* revealed by atomic force microscopy." *Journal of Molecular Biology* 330: 785-97.

Kammerer, R. A., Kostrewa, D., Zurdo, J., Detken, A., García-Echeverría, C., Green, J. D., Müller, S. A., Meier, B. H., Winkler, F. K., Dobson, C. M. and Steinmetz, M. O. (2004). "Exploring amyloid formation by a *de novo* design." *Proceedings of the National Academy of Sciences of the United States of America* 101: 4435-40.

Kane, R. S. and Stroock, A. D. (2007). "Nanobiotechnology: protein-nanomaterial interactions." *Biotechnology Progress* 23: 316-9.

Kapphahn, R. J., Ethen, C. M., Peters, E. A., Higgins, L. and Ferrington, D. A. (2003). "Modified αA-crystallin in the retina: altered expression and truncation with aging." *Biochemistry* 42: 15310-25.

Karr, J. W. and Szalai, V. A. (2008). "Cu(II) binding to monomeric, oligomeric, and fibrillar forms of the Alzheimer's Disease amyloid-β peptide." *Biochemistry* 47: 5006-16.

Kato, K., Shinohara, H., Kurobe, N., Inaguma, Y., Shimizu, K. and Ohshima, K. (1991). "Tissue distribution and developmental profiles of immunoreactive αB-

crystallin in the rat determined with a sensitive immunoassay system." *Biochimica et Biophysica Acta* 1074: 201-8.

Kelly, J. W. (2002). "Towards an understanding of amyloidogenesis." *Nature Structural Biology* 9: 323-5.

Kim, K. K., Kim, R. and Kim, S. H. (1998). "Crystal structure of a small heat-shock protein." *Nature* 394: 595-9.

Knowles, T. P., Fitzpatrick, A. W., Meehan, S., Mott, H. R., Vendruscolo, M., Dobson, C. M. and Welland, M. E. (2007). "Role of intermolecular forces in defining material properties of protein nanofibrils." *Science* 318: 1900-3.

Kodoma, H., Matsumura, S., Yamashita, T and Mihara, H. (2004) "Construction of a protein array on amyloid-like fibrils using co-assembly of designed peptides." *Chemical Communications* 2876 - 2877.

Koretz, J. F., Doss, E. W. and Labutti, J. N. (1998). "Environmental factors influencing the chaperone-like activity of α-crystallin." *International Journal of Biological Macromolecules* 22: 283-94.

Krebs, M. R., MacPhee, C. E., Miller, A. F., Dunlop, I. E., Dobson, C. M. and Donald, A. M. (2004). "The formation of spherulites by amyloid fibrils of bovine insulin." *Proceedings of the National Academy of Sciences of the United States of America* 101: 14420-4.

Kumar, M. S., Kapoor, M., Sinha, S. and Reddy, G. B. (2005). "Insights into hydrophobicity and the chaperone-like function of αA- and αB-crystallins: an isothermal titration calorimetric study." *Journal of Biological Chemistry* 280: 21726-30.

Laemmli, U. K. (1970). "Cleavage of structural proteins during the assembly of the head of bacteriophage T4." 227: 680-5.

Land, M. F., and Fernald, R. D. (1992) *Annual Review of Neuroscienc* 15: 1-29.

Lashuel, H. A., Labrenz, S. R., Woo, L., Serpell, L. C. and Kelly, J. W. (2000). "Protofilaments, filaments, ribbons and fibrils from peptidomimetic self-assembly: Implications for amyloid fibril formation and materials science." *Journal of the American Chemical Society* 122: 5262-77.

Lay, F. T. and Anderson, M. A. (2005). "Defensins - components of the innate immune system in plants." *Current Protein & Peptide Science* 6: 85-101.

Lay, F. T., Brugliera, F. and Anderson, M. A. (2003a). "Isolation and properties of floral defensins from ornamental tobacco and petunia." *Plant Physiology* 131: 1283-93.

Lay, F. T., Schirra, H. J., Scanlon, M. J., Anderson, M. A. and Craik, D. J. (2003b). "The three-dimensional solution structure of NaD1, a new floral defensin

from *Nicotiana alata* and its application to a homology model of the crop defense protein alfAFP." *Journal of Molecular Biology* 325: 175-88.

Liao, L., Cheng, D., Wang, J., Duong, D. M., Losik, T. G., Gearing, M., Rees, H. D., Lah, J. J., Levey, A. I. and Peng, J. (2004). "Proteomic characterization of postmortem amyloid plaques isolated by laser capture microdissection." *Journal of Biological Chemistry* 279: 37061-8.

Lindner, R. A., Kapur, A., Mariani, M., Titmuss, S. J. and Carver, J. A. (1998). "Structural alterations of α-crystallin during its chaperone action." *European Journal of Biochemistry* 258: 170-83.

Liu, L., Ghosh, J. G., Clark, J. I. and Jiang, S. (2006). "Studies of αB-crystallin subunit dynamics by surface plasmon resonance." *Anals of Biochemistry* 350: 186-95.

Lucas, R. M., McMichael, A. J., Armstrong, B. K. and Smith W. T. "Estimating the global disease burdan due to ultraviolet radiation exposure." *International Journal of Epidemiology* (2008), 37: 654-667.

Lundmark, K., Westermark, G. T., Olsén, A. and Westermark, P. (2005). "Protein fibrils in nature can enhance amyloid protein A amyloidosis in mice: Cross-seeding as a disease mechanism." *Proceedings of the National Academy of Sciences of the United States of America* 102: 6098-102.

Ma, B. and Nussinov, R. (2003). "Molecular dynamics simulations of the unfolding of β2-microglobulin and its variants." *Protein Engineering* 16: 561-75.

MacPhee, C. E. and Dobson, C. M. (2000). "Chemical dissection and reassembly of amyloid fibrils formed by a peptide fragment of transthyretin." *Journal of Molecular Biology* 297: 1203-15.

MacPhee, C. E. and Woolfson, D. N. (2004). "Engineered and designed peptide-based fibrous biomaterials." *Current Opinion in Solid State & Materials Science* 8: 141-9.

MacRae, T. H. (2000). "Structure and function of small heat shock/α-crystallin proteins: established concepts and emerging ideas." *Cell & Molecular Life Sciences* 57: 899-913.

Makin, O. S. and Serpell, L. C. (2005). "Structures for amyloid fibrils." *FEBS Journal* 272: 5950-61.

Marchant, R. E., Kang, I., Sit, P. S., Zhou, Y., Todd, B. A., Eppell, S. J. and Lee, I. (2002). "Molecular views and measurements of hemostatic processes using atomic force microscopy." *Current Protein & Peptide Science* 3: 249-74.

Massa, M., Mangione, P., Pignatti, P., Stoppini, M., Zanotti, G., Arcidiaco, P., Merlini, G., Ferri, G. and Bellotti, V. (2000). "Conformational dynamics of the

β2-microglobulin C-terminal in the cell-membrane-anchored major histocompatibility complex type I." *Cell & Molecular Life Sciences* 57: 675-83.

McArthur, S. L., Mclean, K. M., St. John, H. A. W. and Griesser, H. J. (2001). "XPS and surface-MALDI-MS characterisation of worn HEMA-based contact lenses." *Biomaterials* 22: 3295-304.

McClellan, A. J., Tam, S., Kaganovich, D. & Frydman, J. (2005). "Protein quality control: chaperones culling corrupt conformations" *Nature Cell Biology* 7: 736-41.

McFalngai, M., Horwitz, J. and Ding, L. L. (1986). "Age-dependent changes in the heat-stable crystallin, βBp, of the human lens." *Current Eye Research* 5: 387-94.

Meehan, S., Berry, Y., Luisi, B., Dobson, C. M., Carver, J. A. and MacPhee, C. E. (2004). "Amyloid fibril formation by lens crystallin proteins and its implications for cataract formation." *Journal of Biological Chemistry* 279: 3413-9.

Meehan, S., Knowles, T. P., Baldwin, A. J., Smith, J. F., Squires, A. M., Clements, P., Treweek, T. M., Ecroyd, H., Tartaglia, G. G., Vendruscolo, M., MacPhee, C. E., Dobson, C. M. and Carver, J. A. (2007). "Characterisation of amyloid fibril formation by small heat-shock chaperone proteins human αA-, αB- and R120G αB-crystallins." *Journal of Molecular Biology* 372: 470-84.

Mueller, H., Butt, H. J. and Bamberg, E. (1999). "Force measurements on myelin basic protein adsorbed to mica and lipid bilayer surfaces done with the atomic force microscope." *Biophysical Journal* 76: 1072-9.

Munishkina, L. A., Cooper, E. M., Uversky, V. N. and Fink, A. L. (2004). "The effect of macromolecular crowding on protein aggregation and amyloid fibril formation." *Journal of Molecular Recognition* 17: 456-64.

Munishkina, L. A. and Fink, A. L. (2007). "Fluorescence as a method to reveal structures and membrane-interactions of amyloidogenic proteins." *Biochimica et Biophysica Acta* 1768: 1862-85.

Muranov, K., Poliansky, N., Winkler, R., Rieger, G., Schmut, O. and Horwath-Winter, J. (2004). "Protection by iodide of lens from selenite-induced cataract." *Graefes Archive of Clinical and Experimental Ophthalmology* 242: 146-51.

Murphy, R. M. (2007). "Kinetics of amyloid formation and membrane interaction with amyloidogenic proteins." *Biochimica et Biophysica Aacta* 1768: 1923-34.

Musialik, D. (1989). "Urinary excretion of β2-microglobulin in patients with active metabolic stone disease." *International Urology & Nephrology* 21: 381-7.

Myers, S. L., Jones, S., Jahn, T. R., Morten, I. J., Tennent, G. A., Hewitt, E. W. and Radford, S. E. (2006). "A systematic study of the effect of physiological

factors on β2-microglobulin amyloid formation at neutral pH." *Biochemistry* 45: 2311-21.

Naiki, H., Hashimoto, N., Suzuki, S., Kimura, H., Nakakuki, K. and Gejyo, F. (1997). "Establishment of a kinetic model of dialysis-related amyloid fibril extension *in vitro*." *Amyloid* 4: 223-32.

Naiki, H., Yamamoto, S., Hasegawa, K., Yamaguchi, I., Goto, Y. and Gejyo, F. (2005). "Molecular interactions in the formation and deposition of β2-microglobulin-related amyloid fibrils." *Amyloid* 12: 15-25.

Nielsen, L., Khurana, R., Coats, A., Frokjaer, S., Brange, J., Vyas, S., Uversky, V. N. and Fink, A. L. (2001). "Effect of environmental factors on the kinetics of insulin fibril formation: elucidation of the molecular mechanism." *Biochemistry* 40: 6036-46.

Nilsson, M. R. (2004). "Techniques to study amyloid fibril formation in vitro." *Methods* 34: 151-60.

Nelson, R., Sawaya, M. R., Balbirnie, M., Madsen, A. O., Reikel, C., Grothe, R. and Eisenberg, D. (2005) "Structure of the cross-β spine of amyloid-like fibrils." *Nature* 435: 773-8.

Nordstedt, C., Naslund, J., Tjernberg, L. O., Karlstrom, A. R., Thyberg, J. and Terenius, L. (1994). "The Alzheimer Aβ-peptide develops protease resistance in association with its polymerization into fibrils." *Journal of Biological Chemistry* 269: 30773-6.

Ohhashi, Y., Kihara, M., Naiki, H. and Goto, Y. (2005). "Ultrasonication-induced amyloid fibril formation of β2-microglobulin." *Journal of Biological Chemistry* 280: 32843-8.

O'nuallain, B., Williams, A. D., Westermark, P. and Wetzel, R. (2004). "Seeding specificity in amyloid growth induced by heterologous fibrils." *Journal of Biological Chemistry* 279: 17490-9.

Ouderaa, F. J., De Jong, W. W. and Bloemendal, H. (1973). "The Amino Acid Sequence of the αA_2 Chain of Bovine α-Crystallin." *European Journal of Biochemistry* 39: 207-22.

Ouderaa, F. J., De Jong, W. W., Hilderink, A. A. and Bloemendal, H. (1974). "The Amino Acid Sequence of the αB_2 Chain of Bovine α-Crystallin." *European Journal of Biochemistry* 49: 157-68.

Pagona, G. and Tagmatarchis, N. (2006). "Carbon nanotubes: materials for medicinal chemistry and biotechnological applications." *Current Medicinal Chemistry* 13: 1789-98.

Pearce, F. G., Mackintosh, S. H. and Gerrard, J. A. (2007). "Formation of amyloid-like fibrils by ovalbumin and related proteins under conditions relevant to food processing." *Journal of Agricultural & Food Chemistry* 55: 318-22.

Peterson, J., Radke, G. and Takemoto, L. (2005). "Interaction of lens α- and γ-crystallins during aging of the bovine lens." *Experimental Eye Research* 81: 680-9.

Peterson, J. J., Young, M. M. and Takemoto, L. J. (2004). "Probing α-crystallin structure using chemical cross-linkers and mass spectrometry." *Molecular Vision* 10: 857-66.

Petkova, A. T., Ishii, Y., Balbach, J. J., Antzutkin, O. N., Leapman, R. D., Delaglio, F. and Tycko, R. (2002). "A structural model for Alzheimer's beta-amyloid fibrils based on experimental constraints from solid state NMR", *Proceedings of the National Academy of Sciences of the United States of America* 99: 16742-7.

Pettirossi, F., Esposito, G. and Carver, J. A. Unpublished data.

Rajagopal, K. and Schneider, J. P. (2004). "Self-assembling peptides and proteins for nanotechnological applications." *Current Opinion in Structural Biology* 14: 480-6.

Raman, B., Ban, T., Sakai, M., Pasta, S. Y., Ramakrishna, T., Naiki, H., Goto, Y. and Rao, C. M. (2005). "αB-Crystallin, a small heat-shock protein, prevents the amyloid fibril growth of an amyloid β-peptide and β2-microglobulin." *Biochemical Journal* 392: 573-81.

Raman, B. and Rao, C. M. (1997). "Chaperone-like activity and temperature-induced structural changes of α-crystallin." *Journal of Biological Chemistry* 272: 23559-64.

Reches, M. and Gazit, E. (2003). "Casting metal nanowires within discrete self-assembled peptide nanotubes." *Science* 300: 625-7.

Reddy, G. B., Das, K. P., Petrash, J. M. and Surewicz, W. K. (2000). "Temperature-dependent chaperone activity and structural properties of human αA- and αB-crystallins." *Journal of Biological Chemistry* 275: 4565-70.

Rekas, A., Adda, C. G., Aquilina, J. A., Barnham, K. J., Sunde, M., Galatis, D., Williamson, N. A., Masters, C. L., Anders, R. F., Robinson, C. V., Cappai, R. and Carver, J. A. (2004). "Interaction of the molecular chaperone αB-crystallin with α-synuclein: effects on amyloid fibril formation and chaperone activity." *Journal of Molecular Biology* 340: 1167-83.

Rekas, A., Jankova, L., Thorn, D. C., Cappai, R. and Carver, J. A. (2007). "Monitoring the prevention of amyloid fibril formation by alpha-crystallin. Temperature dependence and the nature of the aggregating species." *FEBS Journal* 274: 6290-304.

Rochet, J. C. and Lansbury, P. T., Jr. (2000). "Amyloid fibrillogenesis: themes and variations." *Current Opinion in Structural Biology* 10: 60-8.

Rodahl, M., Hook, F., Fredriksson, C., Keller, C. A., Krozer, A., Brzezinski, P., Voinova, M. and Kasemo, B. (1997). "Simultaneous frequency and dissipation factor QCM measurements of biomolecular adsorption and cell adhesion." *Faraday Discuss*: 229-46.

Ruth, L., Eisenberg, D. and Neufeld, E. F. (2000). "α-$_L$-iduronidase forms semi-crystalline spherulites with amyloid-like properties." *Acta Crystallographica Section D - Biological Crystallography* 56: 524-8.

Sackewitz, M., Von Einem, S., Hause, G., Wunderlich, M., Schmid, F. X. and Schwarz, E. (2008). "A folded and functional protein domain in an amyloid-like fibril." *Protein Science* 17: 1044-54.

Saha, S. and Das, K. P. (2004). "Relationship between chaperone activity and oligomeric size of recombinant human alphaA- and alphaB-crystallin: a tryptic digestion study." *Proteins* 57: 610-7.

Saha, S. and Das, K. P. (2007). "Unfolding and refolding of bovine α-crystallin in urea and its chaperone activity." *Protein Journal* 26: 315-26.

Sandilands, A., Hutcheson, A. M., Long, H. A., Prescott, A. R., Vrensen, G., Loster, J., Klopp, N., Lutz, R. B., Graw, J., Masaki, S., Dobson, C. M., MacPhee, C. E. and Quinlan, R. A. (2002). "Altered aggregation properties of mutant γ-crystallins cause inherited cataract." *Embo Journal* 21: 6005-14.

Schaaper, W. M., Posthuma, G. A., Plasman, H. H., Sijtsma, L., Fant, F., Borremans, F. A., Thevissen, K., Broekaert, W. F., Meloen, R. H. and Van Amerongen, A. (2001). "Synthetic peptides derived from the β2-β3 loop of *Raphanus sativus* antifungal protein 2 that mimic the active site." *Journal of Peptide Research* 57: 409-18.

Schechter, Y., Patchornik, A. and Burstein, Y. (1973). "Selective reduction of cystine 1-8 in α-lactalbumin." *Biochemistry* 12: 3407-13.

Serpell, L. C., Sunde, M., Benson, M. D., Tennent, G. A., Pepys, M. B. and Fraser, P. E. (2000). "The protofilament substructure of amyloid fibrils." *Journal of Molecular Biology* 300: 1033-9.

Shao, Z., Yang, J. and Somlyo, A. P. (1995). "Biological atomic force microscopy: from microns to nanometers and beyond." *Annual Review of Cell & Developmental Biology* 11: 241-65.

Sharma, K. K., Kumar, R. S., Kumar, G. S. and Quinn, P. T. (2000). "Synthesis and characterization of a peptide identified as a functional element in αA-crystallin." *Journal of Biological Chemistry* 275: 3767-71.

Sharma, K. K. and Ortwerth, B. J. (1995). "Effect of cross-linking on the chaperone-like function of α-crystallin." *Experimental Eye Research* 61: 413-21.

Sherman, M. Y. and Goldberg, A. L. (2001). "Cellular defenses against unfolded proteins: a cell biologist thinks about neurodegenerative diseases." *Neuron* 29: 15-32.

Siezen, R. J. and Argos, P. (1983). "Structural homology of lens crystallins. III. Secondary structure estimation from circular dichroism and prediction from amino acid sequences." *Biochimica et Biophysica Acta* 748: 56-67.

Siezen, R. J., Wu, E., Kaplan, E. D., Thomson, J. A. and Benedek, G. B. (1988). "Rat lens gamma-crystallins. Characterization of the six gene products and their spatial and temporal distribution resulting from differential synthesis." *Journal of Molecular Biology* 199: 475-90.

Slingsby, C. and Bateman, O. A. (1990). "Rapid separation of bovine β-crystallin subunits βB1, βB2, βB3, βA3 and βA4." *Experimental Eye Research* 51: 21-6.

Slingsby, C. and Clout, N. J. (1999). "Structure of the crystallins." *Eye* 13: 395-402.

Smith, D. P., Jones, S., Serpell, L. C., Sunde, M. and Radford, S. E. (2003). "A systematic investigation into the effect of protein destabilisation on β2-microglobulin amyloid formation." *Journal of Molecular Biology* 330: 943-54.

Smith, J. F., Knowles, T. P., Dobson, C. M., MacPhee, C. E. and Welland, M. E. (2006). "Characterization of the nanoscale properties of individual amyloid fibrils." *Proceedings of the National Academy of Sciences of the United States of America* 103: 15806-11.

Son, S. J., Bai, X. and Lee, S. B. (2007). "Inorganic hollow nanoparticles and nanotubes in nanomedicine. Part 1. Drug/gene delivery applications." *Drug Discovery Today* 12: 650-6.

Spinozzi, F., Mariani, P., Rustichelli, F., Amenitsch, H., Bennardini, F., Mura, G. M., Coi, A. and Ganadu, M. L. (2006). "Temperature dependence of chaperone-like activity and oligomeric state of αB-crystallin." *Biochimica et Biophysica Acta* 1764: 677-87.

Squires, A. M., Devlin, G. L., Gras, S. L., Tickler, A. K., MacPhee, C. E. and Dobson, C. M. (2006). "X-ray scattering study of the effect of hydration on the cross-β structure of amyloid fibrils." *Journal of the American Chemical Society* 128: 11738-9.

Srinivas, V., Raman, B., Rao, K. S., Ramakrishna, T. and Rao, C. M. (2005). "Arginine hydrochloride enhances the dynamics of subunit assembly and the chaperone-like activity of α-crystallin." *Molecular Vision* 11: 249-55.

Stamler, R., Kappe, G., Boelens, W. and Slingsby, C. (2005). "Wrapping the α-crystallin domain fold in a chaperone assembly." *Journal of Molecular Biology* 353: 68-79.

Stone, M. J. (1990). "Amyloidosis: a final common pathway for protein deposition in tissues." *Blood* 75: 531-45.

Sunde, M., Serpell, L. C., Bartlam, M., Fraser, P. E., Pepys, M. B. and Blake, C. C. (1997). "Common core structure of amyloid fibrils by synchrotron X-ray diffraction." *Journal of Molecular Biology* 273: 729-39.

Takahashi, Y., Ueno, A. and Mihara, H. (2002). "Amyloid architecture: complementary assembly of heterogeneous combinations of three or four peptides into amyloid fibrils." *Chembiochem* 3: 637-42.

Tardieu, A. (1988). "Eye lens proteins and transparency: from light transmission theory to solution X-ray structural analysis." *Annual Review of Biophysics & Biophysical Chemistry* 17: 47-70.

Tartaglia, G. G., Pawar, A. P., Campioni, S., Dobson, C. M., Chiti, F. and Vendruscolo, M. (2008). "Prediction of aggregation-prone regions in structured proteins." *Journal of Molecular Biology* 380: 425-36.

Thierry, B., Zimmer, L., Mcniven, S., Finnie, K., Barbe, C. and Griessert, H. J. (2008). "Electrostatic self-assembly of PEG copolymers onto porous silica nanoparticles." *Langmuir* 24: 8143-50.

Thissen, H., Johnson, G., Hartley, P. G., Kingshott, P. and Griesser, H. J. (2006). "Two-dimensional patterning of thin coatings for the control of tissue outgrowth." *Biomaterials* 27: 35-43.

Thomas, P. J., Qu, B. H. and Pedersen, P. L. (1995). "Defective protein folding as a basis of human disease." *Trends in Biochemical Sciences* 20: 456-9.

Thomma, B. P., Cammue, B. P. and Thevissen, K. (2002). "Plant defensins." *Planta* 216: 193-202.

Thorn, D. C., Ecroyd, H., Sunde, M., Poon, S. and Carver, J. A. (2008). "Amyloid fibril formation by bovine milk αS2-casein occurs under physiological conditions yet is prevented by its natural counterpart, αS1-casein." *Biochemistry* 47: 3926-36.

Thorn, D. C., Meehan, S., Sunde, M., Rekas, A., Gras, S. L., MacPhee, C. E., Dobson, C. M., Wilson, M. R. and Carver, J. A. (2005). "Amyloid fibril formation by bovine milk κ-casein and its inhibition by the molecular chaperones αS- and β-casein." *Biochemistry* 44: 17027-36.

Tjernberg, L. O., Callaway, D. J., Tjernberg, A., Hahne, S., Lilliehöök, C., Terenius, L., Thyberg, J. and Nordstedt, C. (1999). "A molecular model of

Alzheimer amyloid β-peptide fibril formation." *Journal of Biological Chemistry* 274: 12619-25.

Treweek, T. M., Ecroyd, H., Williams, D., Meehan, S., Carver, J. A. and Walker, M. J. (2007). "Site-directed mutations in the C-terminal extention of human αB-crystallin affect chaperone function and block amyloid fibril formation." *PLoS One* 10: 1046.

Trinh, C. H., Smith, D. P., Kalverda, A. P., Phillips, S. E. V. and Radford, S. E. (2002). "Crystal structure of monomeric human β2-microglobulin reveals clues to its amyloidogenic properties." *Proceedings of the National Academy of Sciences of the United States of America* 99: 9771-6.

True, H. L. and Lindquist, S. L. (2000). "A yeast prion provides an exploratory mechanism for genetic variation and phenotypic diversity." *Nature* 407: 477-83.

Tycko, R. (2006) "Solid state NMR as a probe of amyloid structure." *Protein and Peptide Letters* 13: 229-34

Uversky, V. N. and Fink, A. L. (2004). "Conformational constraints for amyloid fibrillation: the importance of being unfolded." *Biochimica et Biophysica Acta* 1698: 131-53.

Van Montfort, R. L., Basha, E., Friedrich, K. L., Slingsby, C. and Vierling, E. (2001). "Crystal structure and assembly of a eukaryotic small heat shock protein." *Nature Structural Biology* 8: 1025-30.

Vanhoudt, J., Abgar, S., Aerts, T. and Clauwaert, J. (2000). "Native quaternary structure of bovine α-crystallin." *Biochemistry* 39: 4483-92.

Vendruscolo, M. and Dobson, C. M. (2006). "Structural biology. Dynamic visions of enzymatic reactions." *Science* 313: 1586-7.

Veretout, F., Delaye, M. and Tardieu, A. (1989). "Molecular-basis of eye lens transparency - osmotic-pressure and X-ray-analysis of α-crystallin solutions." *Journal of Molecular Biology* 205: 713-28.

Vermette, P., Gengenbach, T., Divisekera, U., Kambouris, P. A., Griesser, H. J. and Meagher, L. (2003). "Immobilization and surface characterization of NeutrAvidin biotin-binding protein on different hydrogel interlayers." *Journal of Colloid & Interface Science* 259: 13-26.

Vinckier, A., Gervasoni, P., Zaugg, F., Ziegler, U., Lindner, P., Groscurth, P., Pluckthun, A. and Semenza, G. (1998). "Atomic force microscopy detects changes in the interaction forces between GroEL and substrate proteins." *Biophysical Journal* 74: 3256-63.

Voinova, M. V., Jonson, M. and Kasemo, B. (2002). "Missing mass effect in biosensor's QCM applications." *Biosensors & Bioelectronics* 17: 835-41.

Voros, J. (2004). "The density and refractive index of adsorbing protein layers." *Biophysical Journal* 87: 553-61.

Waterhouse, S. H. and Gerrard, J. A. (2004). "Amyloid fibrils in bionanotechnology." *Australian Journal of Chemistry* 57: 519-23.

Westermark, P., Benson, M.D., Buxbaum, J.N., Cohen, A.S., Frangione, B., Ikeda, S. I., Masters, C. L., Merlini, G., Saraiva, M. J. and Sipe, J. D. (2007) "A primer of amyloid nomenclature" *Amyloid* 14: 179-183.

WHO. World Health Report 2001 - Mental Health: New understanding, new hope. (2001) Geneva: World Health Organization.

Wright, C. F., Teichmann, S. A., Clarke, J. and Dobson, C. M. (2005). "The importance of sequence diversity in the aggregation and evolution of proteins." *Nature* 438: 878-81.

Wright, G., Basak, A. K., Wieligmann, K., Mayr, E. M. and Slingsby, C. (1998). "Circular permutation of βB2-crystallin changes the hierarchy of domain assembly." *Protein Science* 7: 1280-5.

Yamamoto, S., Hasegawa, K., Yamaguchi, I., Tsutsumi, S., Kardos, J., Goto, Y., Gejyo, F. and Naiki, H. (2004). "Low concentrations of sodium dodecyl sulfate induce the extension of β2-microglobulin-related amyloid fibrils at a neutral pH." *Biochemistry* 43: 11075-82.

Yang, H., Fung, S. Y., Pritzker, M. and Chen, P. (2007). "Surface-assisted assembly of an ionic-complementary peptide: controllable growth of nanofibers." *Journal of the American Chemical Society* 129: 12200-10.

Yu, L., Banerjee, I. A., Gao, X., Nuraje, N. and Matsui, H. (2005). "Fabrication and application of enzyme-incorporated peptide nanotubes." *Bioconjugate Chemistry* 16: 1484-7.

Zandomeneghi, G., Krebs, M. R., McCammon, M. G. and Fandrich, M. (2004). "FTIR reveals structural differences between native β-sheet proteins and amyloid fibrils." *Protein Science* 13: 3314-21.

Zhang, S. (2003). "Fabrication of novel biomaterials through molecular self-assembly." *Nature Biotechnology* 21: 1171-8.

Zurdo, J., Guijarro, J. I. and Dobson, C. M. (2001). "Preparation and characterization of purified amyloid fibrils." *Journal of the American Chemical Society* 123: 8141-2.